

Climatic Reliability of Electronics:

Prediction of PCB Failure under Humidity using Predictive Analytics

A thesis submitted to the technical University of Denmark for the degree of doctor of philosophy in the department of mechanical engineering

By

Sajjad Bahrebar



Technical University of Denmark

Department of Civil and Mechanical Engineering

Section of Materials and Surface Engineering

Center for Electronic Corrosion

July 2022

Climatic Reliability of Electronics: Prediction of PCB Failure under Humidity using Predictive Analytics

A doctoral thesis by

Sajjad Bahrebar
sajbahr@mek.dtu.dk
Technical University of Denmark
Department of Civil and Mechanical Engineering
Building 425, 2800 Kgs. Lyngby, Denmark

Principal Supervisor

Professor Rajan Ambat
ram@mek.dtu.dk
Technical University of Denmark
Department of Civil and Mechanical Engineering
Building 425, 2800 Kgs. Lyngby, Denmark

Co-Supervisors

Associate Professor Morten Stendahl
Jellesen
msj@mek.dtu.dk
Technical University of Denmark
Department of Civil and Mechanical
Engineering
Building 425, 2800 Kgs. Lyngby, Denmark

Associate Professor Murat Kulahci
muku@dtu.dk
Technical University of Denmark
Department of Applied Mathematics and
Computer Science
Building 321, 2800 Kgs. Lyngby, Denmark

Copyright: Reproduction of this publication in whole or in part must be include the customary bibliographic citation.

Published by: Technical University of Denmark, Department of Mechanical Engineering, Materials and Surface Engineering, Center for Electronic Corrosion, Building 425, 2800 Kgs, Lyngby, Denmark.

*Dedicate to my dear parents, my cherished brother, my adored sister
and my beloved wife...*

Preface

This doctoral thesis is submitted in partial fulfilment of the requirements for achieving the degree of PhD at the Department of Mechanical Engineering at the Technical University of Denmark (DTU). The project was funded by ELMAC Project and CreCon Industrial Consortium and carried out at the Department of Mechanical Engineering, Section of Materials and Surface Engineering, Center for Electronic Corrosion, during the period from May 1st 2019 to July 31th 2022. The project was supervised by Professor Rajan Ambat, and Senior Researcher Morten Stendahl Jellesen from the Department of Mechanical Engineering, Section of Materials and Surface Engineering, Center for Electronic Corrosion, and Associate Professor Murat Kulahci from Department of Applied Mathematics and Computer Science at the Technical University of Denmark (DTU).

Sajjad Bahrebar
Lyngby, Denmark
July 2022

Abstract

This PhD project is supported by the IFD (Innovation Fund Denmark) through the ELMAC (Electronic Systems Manufactured for Climate) and by CELCORR (Centre for Electronic Corrosion) via the CreCon (Consortium for Climatically Reliable Electronics) at DTU. Humidity caused corrosion failures in electronics is an important contributor to the robustness and reliability issues due to several external and inherent factors related to electronics. External factors include wide-spread use of electronics today exposing them to all climatic conditions, while inherent factors include the multi-material use in electronics, miniaturization, and manufacturing process related contributions. Corrosion occurrence in electronics under humid conditions is a multi-parameter effects involving many factors. Hence, it is important to understand combined effects of various parameters and their relative importance in relation to the failure mechanisms. The motivation of this project is to investigate the possibility of using predictive analytics approaches based on statistical, probabilistic, and ML (machine learning) techniques to forecast PCB failures based on multiparameter experimental test data. Such approach not only provide models based on multi-parameters effects, but also can determine the relative contribution of different factors or multiple factors based on the statistical analysis. The research in this thesis also focused on the investigation of critical factor effects such as pitch distance, contamination level, voltage, temperature, humidity, contamination type, and their interactions on SIR (Surface Insulation Resistance) reduction and LC (Leakage Current), besides dendrite formation and ECM (Electrochemical Migration) on PCB surfaces under various corrosive conditions created of a combination of diverse factors/ levels.

Chapter 1 provides a background to the climatic reliability of electronics, the motivation and research objectives for this PhD project, and the structure of the current PhD thesis. Chapter 2 reviews critical factors influencing climatic reliability issues and failures on PCB surfaces and literature review. Additionally, PCB testing with common failure mechanisms and data analytics focusing on predictive analytics is described. Chapter 3 summarizes the materials, experimental works done in this thesis, and predictive methods are employed in the PhD project. Chapter 4 contains a summary of appended papers with highlights and important outcomes. The research results of investigations and predictions are brought in chapters 5-7 from research papers published in peer-reviewed journals or in the form of a

draft for publication in the journals. The first paper (chapter 5) investigates the critical factors' effect and their interactions to forecast leakage current (LC) and time to failure (TTF) due to ECM on PCB surfaces under humidity conditions with a focus on the first branch of predictive analytics, i.e., statistical analysis. The second paper (chapter 6) focuses on TTF prediction on PCBs under humidity conditions using probabilistic analysis as the second branch of predictive analytics. The third paper (chapter 7) concentrates on using ML algorithms as the third branch of predictive analytics and creating a comprehensive ML investigation for forecasting PCB failure and LC values based on the training input conditions mixed from five numerical and one categorical factor of experimental data results. Eventually, chapters 9-10 provide the overall discussion, conclusions, and suggestions for future works.

Overall, the principal results of this PhD project are categorized into three types of empirical investigations in three individual papers, each focusing on a separate branch of predictive analytics. Based on the advantages and disadvantages of each predictive model, one can select all or one of them according to the experimental dataset, which includes; the number of factors/levels/conditions, and also responses, limitations, and accuracy of prediction models. In addition, the investigations of this project thoroughly explained the mathematical simulation of the general leak current behavior, the importance and numerical influence of each changeable factor and their interactions on numerical responses (LC and TTF values), and the correlation of the responses at various corrosive conditions on PCB surfaces. An overall analysis of three approaches are provided in overall discussion section.

Resumé

Dette PhD projekt er finansieret af (IFD) Innovations fonden Danmark gennem ELMAC (electronic systems manufactured for climate) og af CELCORR (Centre for electronic corrosion) via CreCon (Consortium for clamatically reliable electronics) på DTU. Fugtrelaterede korrosionsfejl i elektronik er en vigtig faktor i robustheds og pålideligheds problemer pga. flere eksterne og integrerede faktorer relaterede til elektronik. Eksterne faktorer inkluderer den udbredte brug af elektronik hvor de bliver eksponeret til alle slags klima tilstande, imens integrerede faktorer inkluderer brugen af multi-materiale i elektronik, miniaturisering, og bidrag fra fremstillingsprocesser. Korrosion i elektronik i et fugtigt klima er en multiparameter effekt der involverer mange faktorer. Derfor er det vigtigt at forstå de kombinerede effekter fra flere parametre og deres relative vigtighed i relation til fejlmekanismer. Motivationen bag projektet er at undersøge muligheden for at bruge en fremgangsmåde med forudsigende analyser baseret på statistiske, probabilistisk og automatisk læringsmetoder til at forudsige PCB fejl baseret på multiparameter eksperimentelt testdata. Sådant en fremgangsmåde giver ikke kun modeller baseret på multiparametre, men kan også bestemme de relative bidrag fra forskellige faktorer eller flere faktorer baseret på statistisk analyse. Forskningen i denne afhandling er også fokuseret på at undersøge effekten af kritiske faktorer som pitch afstand, forureningsniveau, temperatur, luftfugtighed, spænding, forureningstype og deres interaktioner på SIR (overflade insuleringsmodstand) reducering og LC (lækage strøm), udover dendritformation og ECM (elektrokemisk migration) på PCB overflader under forskellige korrosive betingelser lavet af en kombination af diverse faktorer/niveauer.

Kapitel 1 giver en baggrund til den klimaafhængige pålidelighed af elektronik, motivationen og strukturen for dette PhD projekt og afhandling. Kapitel 2 kigger på kritiske faktorer der påvirker klimarelaterede pålidelighedsproblemer og fejl på PCB overflader, samt en litteraturgennemgang. Udover dette, beskrives der PCB tests med gængse fejlmekanismer og data analyser med et fokus på forudsigende analyser. Kapitel 3 giver et resumé af materialerne, det eksperimentelle arbejde i afhandlingen, og de forudsigende metoder brugt i PhD projektet. Kapitel 4 indeholder et resumé af vedlagte artikler med fremhævelser og vigtige pointer. Forskningsresultaterne af undersøgelser og forudsigelser er bragt i kapitlerne 5-7 fra videnskabelige artikler publiceret i 'peer-reviewed' tidsskrifter

eller i form af kladder til publicering i tidsskrifter. Den første artikel (kapitel 5) undersøger de kritiske faktorerers effekt og deres interaktioner for at forudsige lækage strøm og tid før der opstår fejl pga. ECM på PCB overflader i et fugtigt miljø med fokus på den første del af forudsigende analyser, fx statistisk analyse. Den anden artikel (kapitel 6) fokuserer på at forudsige tid til fejl på PCB i fugtigt miljø ved brug af probabilistisk analyser som den anden del af forudsigende analyser. Den tredje artikel (kapitel 7) er koncentreret omkring brug af ML-algoritmer som den tredje del af forudsigende analyser og på at lave en generaliseret ML-model til at forudsige PCB fejl og LC værdier baseret på træningsinput og betingelser der kombinerer seks kritiske faktorer. Til sidst, bidrager kapitel 9-10 til den samlede diskussion, konklusion og forslag til fremtidigt arbejde.

Samlet set er hovedresultaterne fra dette projekt kategoriseret i 3 typer af eksperimentelle studier i 3 individuelle artikler, der hver fokuserer på en separat del af forudsigende analyser. Baseret fordele og ulemper for hver model, kan man udvælge alle eller en model afhængigt af det eksperimentelle dataset, hvilket inkluderer; antallet af faktorer/niveauer/tilstande med tilhørende reaktioner, begrænsninger og nøjagtigheden af de forudsigende modeller. Herudover forklarede undersøgelserne i dette projekt grundigt den matematiske simulation af hvordan den generelle strøm opførte sig, vigtigheden af hver varierende faktor og den numeriske effekt heraf, samt deres interaktioner ved numeriske responser (LC og TTF værdier), og korrelationen mellem reaktionerne ved forskellige korrosive miljøer på PCB overflader. En overordnet analyse af tre fremgangsmåder er givet i den samlede diskussions sektion.

Acknowledgements

Firstly, I would like to express my sincere gratitude to my main supervisor Professor Rajan Ambat for the guidance, continuous support, and invaluable advice throughout the project. I appreciate his dedication to the project, the time spent on fruitful discussions, and the given freedom to explore and apply different approaches for achieving the set goals. Thanks for always being available even out of working hours and for understanding my personal life issues during my study.

I am very grateful to my co-supervisors, Associate Professor Morten Stendahl Jellesen and Associate Professor Murat Kulahci, for their invaluable support. I am very thankful to Max Peter Spooner for his contribution and co-author Sajad Homayoun for his valuable comments and for supporting me in the present research project.

I would like to acknowledge the CreCon member companies; Grundfos, Danfoss, Vestas, Widex, Volvo, Inventec, and Wevo, as well as the ELMAC project member companies; Cadaminds, Circle consult, Force Technonology, Danfoss, Eltek, Grundfos, Vestas for their generous funding and overall support in this Ph.D. project. Special thanks to global lead engineer Jesper Kjærnulf Konge, senior reliability specialists Kim Albert Storbacka Schmidt, and Peter De Place Rimmen for their fruitful meetings and discussions over this Ph.D. project. Many thanks also go to Professor Frede Blaabjerg, Professor Francesco Lannuzzo, and Associate Professor Amir Sajjad Bahman at Aalborg University for their contribution and support during my research on the ELMAC project.

I would like to acknowledge Dr. Victoria Zimmermann, Dr. Michael Jank, and Weiyi Chen for experimental suggestions and support during my research stay abroad at Fraunhofer Institute for Integrated Systems and Device Technology (Fraunhofer IISB) in Germany.

I further express my thanks to all my colleagues and friends in the Section of Materials and Surface Engineering and the CELCORR group for their support and for creating a positive working environment; special thanks to Kamila Piotrowska, Helene Virginie Conseil Gudla, Vadimas Verdingovas, Feng Li, Saber Haratian, Ioannis Mantis, Nikolaj Gersager Henriksen, Markus Kalle Santeri Asikainen, Kapil Kumar Gupta, Anish Rao Lakkaraju, Jyothsna Murli Rao, Peter Jacob Schwencke Westermann, and Gitte Salomon.

My deepest love and gratitude goes to my patient wife, Sima Rastayesh, for his boundless emotional support and enormous scientific insight, and motivation, and for standing by my side with unconditional endless love, giving me the power and confidence to bear the rough times and reminding me to never give up on things I truly believe during this academic endeavor.

Last but not least, I wish to express my love and sincerest appreciation to my mother for her unconditional love, continuous invaluable support, and encouragement in any way possible, especially after passing my dear father. I am also thankful to my sister and brother for their friendships, trust, and backing me up throughout my life.

List of articles and conference contributions in chronological order

Peer-reviewed articles included in this thesis:

1. **S. Bahrebar**, R. Ambat, “Investigation of critical factors effect to predict leakage current and time to failure due to ECM on PCB under humidity”, *Microelectronics Reliability*, (2021), doi: [10.1016/j.microrel.2021.114418](https://doi.org/10.1016/j.microrel.2021.114418). **(Published)**
2. **S. Bahrebar**, R. Ambat, “Time to Failure Prediction on a Printed Circuit Board Surface under Humidity Using Probabilistic Analysis”, *Journal of Electronic Materials*, (2022), doi: [10.1007/s11664-022-09668-7](https://doi.org/10.1007/s11664-022-09668-7). **(Published)**
3. **S. Bahrebar**, S. Homyoun and R. Ambat, “Using Machine Learning Algorithms to Predict Failure on the PCB Surface under Corrosive Conditions”, *Corrosion Science*, (2022), doi: [10.1016/j.corsci.2022.110500](https://doi.org/10.1016/j.corsci.2022.110500). **(Published)**

Conference contributions and oral presentations:

1. **S. Bahrebar**, R. Ambat, ‘Corrosion Reliability of Electronic Devices: Effect of Contamination Levels and Pitch Distance on PCBA’, International conference of the Microelectronics Packaging (IMAPS Nordic 2019), Lyngby, Denmark, 11-13 June 2019. **(Oral presentation)**
2. **S. Bahrebar**, R. Ambat, ‘Climatic Reliability of Electronic Devices: Failure Risk Prediction on PCBA Using Probabilistic Model’, 445th International conference of the European Corrosion Congress (EUROCORR 2019), Seville, Spain, 9-13 September 2019. **(Oral presentation)**
3. **S. Bahrebar**, M. Kulahci, R. Ambat, ‘PCBA Failure Estimation by Analysis of Leakage Current Behavior’, 446th International conference of the European Corrosion Congress (EUROCORR 2020), Brussels, Belgium, 7-11 September 2020. **(Oral presentation)**
4. M. S. Jellesen, I. Mantis, H. V. C. Gudla, F. Li, **S. Bahrebar**, R. Ambat, ‘Methods for Evaluation of Contamination Levels on Electronics’, 447th International conference of the European Corrosion Congress (EUROCORR 2021), Budapest, Hungary, 20-24 September 2021. **(Oral presentation)**
5. **S. Bahrebar**, M. S. Jellesen, R. Ambat, ‘Probabilistic Graphical Approach for PCBA Corrosion Failure Risk Prediction’, 447th International conference of the European Corrosion Congress (EUROCORR 2021), Budapest, Hungary, 20-24 September 2021. **(Oral presentation)**
6. R. Ambat, **S. Bahrebar**, ‘Some Effects of PCBA Cleanliness on Humidity Robustness and Use of Probabilistic Models for Prediction (Predictive analytics)’, Electronics in Harsh Environments Conference (SMTA 2022), Amsterdam, Netherlands, 17-19 May 2022. **(Oral presentation)**
7. **S. Bahrebar**, R. Ambat, ‘Tree-Based Machine Learning Methods to PCB Failure and Leakage Current Prediction’, 448th International conference of the European Corrosion Congress (EUROCORR 2022), Berlin, Germany, 28th August-1st September 2022. **(Accepted)**

List of abbreviations and symbols

Units

μm	Micro meter
$\mu\text{g}/\text{cm}^2$	Micro gram per square centimeter
$^{\circ}\text{C}$	Degree of centigrade
V	Volt
ppm	Parts per million (mg/l)
mg/l	Milligram per liter
%RH	Relative humidity percent
s	Second
min	Minute
h	Hour
n	Nano

Abbreviations

P	Pitch distance
C	Contamination level
T	Temperature
V	Voltage
H	Humidity
CT	Contamination type
No.	Number
LC	Leakage current
DT	Decision tree
RF	Random forest
DC	Direct current
ML	Machine learning
TTF	Time to failure
ECM	Electrochemical migration
SMD	Surface mount device
k-NN	K-nearest neighbors
ERH	Efflorescence relative humidity
DRH	Deliquescent relative humidity
SVM	Support vector machines
DNN	Deep neural network
ANN	Artificial neural network
WOA	Weak organic acid
PCB	Printed circuit board
MSE	Mean squared error
MAE	Mean absolute error
DTU	Technical University of Denmark
MEK	Department of Mechanical Engineering
RMSE	Root mean square error
MAPE	Mean absolute percentage error
PCBA	Printed circuit board assembly

Table of contents

Preface.....	iii
Abstract.....	iv
Resumé.....	vi
Acknowledgements.....	viii
List of abbreviations and symbols	xi
Table of contents.....	xii
1 Introduction	1
1.1 Background	1
1.2 Motivation and research objectives.....	3
1.3 Scope and structure of the thesis	4
2 Literature review.....	9
2.1 Climatic reliability of electronics.....	9
2.2 Factors influencing climatic reliability of electronics.....	10
2.2.1 External climatic conditions	12
2.2.2 Important PCBA characteristics for humidity effects.....	13
2.2.2.1 Contamination on PCBA.....	14
2.2.2.2 Importance of PCBA design on humidity effects	18
2.2.2.3 PCBA materials.....	20
2.3 PCBA failures due to climatic conditions.....	23
2.3.1 Surface insulation resistance reduction and LC.....	24
2.3.2 Electrochemical migration and short circuit	25
2.4 Testing PCBA under humidity and current measurement	27
2.4.1 Design of Experiment Methodology.....	29
2.5 Data analytics framework.....	30

2.5.1	Predictive analytics for PCBA failure prediction	31
2.5.1.1	Statistical analysis	32
2.5.1.2	Probabilistic approaches.....	34
2.5.1.3	Machine learning algorithms.....	38
2.5.1.3.1	k-Nearest Neighbors	40
2.5.1.3.2	Decision Tree.....	40
2.5.1.3.3	Random Forest.....	40
2.5.1.3.4	Support Vector Machine.....	41
2.5.1.3.5	Artificial Neural Networks	41
2.6	Literature on the use of data analytics for corrosion data analysis and objective of present thesis	42
3	Materials and methods.....	59
3.1	SIR PCB specimens	59
3.2	Specimens preparation	60
3.3	SIR DC testing and equipment.....	61
3.4	Statistical analysis	62
3.5	Probabilistic analysis.....	62
3.6	Machine learning algorithms.....	63
4	Summary of appended papers.....	64
4.1	Investigation of critical factors effect to predict leakage current and time to failure due to ECM on PCB under humidity	64
4.2	Time to failure prediction on printed circuit board surface under humidity using probabilistic analysis	65
4.3	Using machine learning algorithms to predict failure on the PCB surface under corrosive conditions	66
5	Manuscript I.....	67
5.1	Introduction	68
5.2	Materials and methods	70

5.2.1	Experimental setup.....	71
5.2.1.1	Interdigitated SIR test PCB used for experiments	71
5.2.1.2	Preparation of the SIR Patterns	72
5.2.1.3	Humidity testing	72
5.2.2	Experimental conditions	73
5.2.2.1	Pitch distance on SIR PCB.....	74
5.2.2.2	Contamination	74
5.2.2.3	Climate conditions.....	74
5.2.2.4	Voltage	75
5.2.3	Typical response from testing and failure modes	75
5.3	Results and discussion.....	76
5.3.1	Leak current profiles from testing and microscopic analysis	76
5.3.2	Distribution of LC and TTF.....	80
5.3.3	ANOVA models for LC and TTF.....	83
5.3.4	Model validation	85
5.3.5	Model interpretation.....	86
5.3.6	Overall discussion.....	87
5.4	Conclusion.....	89
6	Manuscript II	97
6.1	Introduction	98
6.2	Material and methods	101
6.2.1	Method and experiment design.....	101
6.2.2	Specimens, preparations, and test equipment	103
6.2.3	Multivariate regression model	105
6.2.4	Probabilistic distribution analysis	105
6.2.5	CART analysis	106

6.3	Results and discussion.....	106
6.3.1	LC and TTF study for each factor.....	106
6.3.2	Investigation of vertical experimental conditions.....	111
6.3.3	Investigation of horizontal experimental conditions.....	114
6.3.4	Comparison of pitch distance and temperature as two significant factor ..	116
6.3.5	CART and Multivariate regression analysis	118
6.3.6	Models validation and interpretation	121
6.3.7	Perspectives on modelling result in relation to humidity effects on electronics.....	123
6.3.7.1	Effect of pitch distance and temperature.....	124
6.3.7.2	Effect of contamination and voltage	125
6.3.7.3	Combined effect of pitch distance, contamination, and temperature.....	125
6.4	Conclusion.....	126
7	Manuscript III.....	133
7.1	Introduction	134
7.2	Materials and methods	137
7.2.1	Experimental data conditions.....	137
7.2.1.1	Pitch Distance.....	137
7.2.1.2	Voltage	138
7.2.1.3	Climatic Conditions.....	138
7.2.1.4	Contamination	138
7.2.2	Experimental setup.....	139
7.2.2.1	SIR PCB Specimen	139
7.2.2.2	SIR PCB preparation for testing	140
7.2.2.3	Climatic chamber for testing and electrochemical system for LC measurement	140
7.2.2.4	ML algorithms and designation of their hyperparameters	140
7.2.2.5	Evaluation metrics for ML algorithms	142

7.3	Results and Discussion.....	143
7.3.1	Results of humidity testing: leak current data and electrochemical migration failure.....	143
7.3.2	Validation and hyperparameters tuning of ML algorithms.....	147
7.3.3	ML algorithms setup	147
7.3.4	Evaluation of trained ML algorithms for classifying PCB failures	149
7.3.5	Evaluation of trained ML algorithms for estimating LC values	151
7.3.6	Selection of the best trained ML models	152
7.3.7	Evaluating the best-trained models	153
7.3.8	Overall discussion.....	157
7.4	Conclusion.....	159
8	Overall discussion.....	174
9	Overall conclusion.....	177
10	Suggestions for further work	180

1 Introduction

1.1 Background

Nowadays, climatic reliability and humidity robustness of electronic devices has become a significant issue for both consumer and industrial electronics due to various reasons. One reason for this increased problem is due to the widespread use of electronics. Typical examples are the application of power electronics in the electrification of vehicles, information technology and renewable energy [1]. Similar situation exists for consumer electronics, where the users demand higher portability and device functionalities, while it is expected to work in different climatic environments [2], [3]. Demand for smaller devices causes an increase in the assembly design density or miniaturization of the printed circuit board assemblies (PCBAs) [4], [5]. Printed circuit board (PCB) surface is one of the main parts of electronics that gets affected by humidity due to water layer formation under transient climate conditions such as temperature and humidity further, due to several inherent factors of the PCB surface itself [6], [7]. Among various electronics/electrical components in a power electronics system, PCBAs are the weakest link when it comes to climatic effects.

Exposure of a PCBA surface to varying humidity and temperature conditions due to exposed climate creates a thin water layer on the PCBA surface, whether the conditions are conducive [8], [9]. This water film has a limited conductivity, however dissolution of residues on the PCBA surface provide enough conductivity and act as electrolyte medium between biased points [10]. The electrical property of the water layer is mainly determined by the electrochemical aspects of the microcell formed on the PCB surface when water film connects between neighboring biased points such as soldered connections or legs of components [10], [11]. The thickness of the water layer formed under humid conditions can vary from nanometer to hundredths, depending on the temperature, humidity, hygroscopic residues, and PCB parameters [12], [13]. Failure of electronics is specified by the interaction of these electrochemical sequences resulting in a parasitic circuit of diverse capacities interfering with the electrical aspects of the PCB surface [14], [15]. Therefore, understanding and controlling the water film build-up and predicting knowledge on subsequent variations in the electrochemical facets leading to a critical level of electrical current are vital in controlling the critical conditions related to failures in electronics [5],

Introduction

[16]. Figure 1.1 schematically shows different important factors causing surface insulation resistance (SIR) reduction and leakage current (LC) followed by electrochemical migration (ECM) and short circuit failure on PCBAs. Among these factors, metals and alloys are part of all electrical contacts on PCBA. A potential bias also exists on PCBA, while it is under function. Contamination is usually arising from process related residues, and humidity from exposure atmosphere.

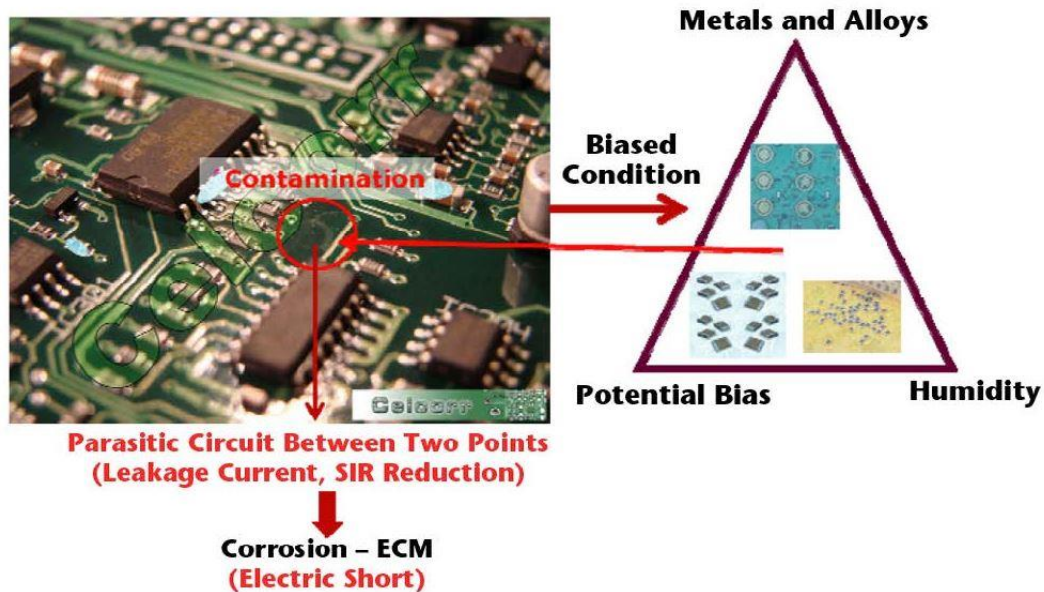


Figure 1.1 Schematic of critical influencing factors related to PCBA failures, adapted from [17].

Overall statistics related to electronics corrosion show a considerable percentage of the cost of the annual industrialized countries, around 3% to 4% of gross domestic product (GDP), attributed to electronics corrosion. Moreover, this anticipated percentage increases more due to the increased demand for electronics in almost all aspects and applications [18]. Figure 1.2 (a) illustrates electric components failure distribution, with PCB failure in high level of failure risk, and (b) significant overstresses and factors impacts on electronics failure with major effect of climatic conditions i.e. humidity and temperature influences [18], [19], [20]. In general, effect of changes in the climate conditions, as well as contaminations cause water film formation on PCBs, which is an important aspect for reliability of electronic devices [5], [16].

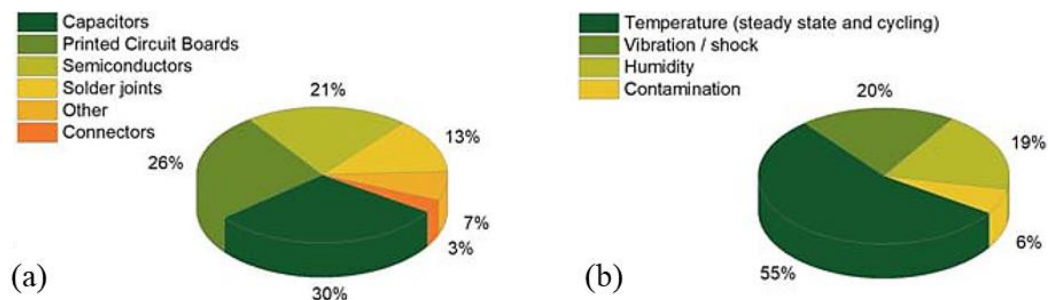


Figure 1.2 (a) Electronic component failure percentage distribution, (b) Percentage of important stresses and factors effect on electronic failures, adapted from [18].

Overstressed mechanisms on electronics refer to the conditions that exceed the strength of components and give a short product lifetime. The mechanisms corresponding to climatic effects usually cause abrupt electrical failures such as SIR reduction and LC, which is the precursor for the ECM and short circuit on PCBAs. Electrical failure mechanisms like LC and ECM can occur once environmental conditions with the combination of critical factors for instance humidity, temperature, as well as contamination create overstress conditions [5]. There are some studies on LC or ECM analysis that does not consider the failure time and its dependency between LC and ECM, besides commonly separate parameters are analyzed instead of multi-parameter effects and their dependencies [21], [22], [23], [24]. In addition, the mechanistic approach and the physics of failure models because of the reason that the electrical failure mechanisms process is complex and involves many parameters could not reasonably predict the multi-parameter effect and resulting failure. Hence, it is substantial to understand the impacts of various factors and their interactions on the PCB failure mechanisms. As well as investigation of the possible appropriate predictive models to forecast PCB failures based on multi-parameter experimental data results operating predictive analytics approaches as the main purpose of this thesis are very influential to improve reliability and reduce risk of electronics failure.

1.2 Motivation and research objectives

This PhD project is part of CreCon industrial consortium and ELMAC (Electronics Manufactured for Climate) project under the center for electronic corrosion (CELCORR) on climatically reliable electronics. The highlight of the studies focused in this PhD project is related to understanding the interplay between electrochemical mechanisms and the failure of PCBs due to changes in electrical functionality under humid conditions and how

Introduction

to use predictive analytics. The detailed investigation of the project is carried out by using predictive analytics models based on critical factors and interactions analyses to define failure prediction models and risk condition prediction, which can be used for industrial applications and customers. The PhD outputs are evaluated the excessive use of predictive analytics, which is a type of data analytics framework that uses a mixture of statistical analysis, probabilistic approaches, and machine learning algorithms to predict the different states of failure processes (SIR reduction and LC to dendrite formation and ECM) based on input datasets of various conditions combined of critical factors/ levels from the experimental lab results. This PhD these is presented the most suitable approach and prediction model based on the input datasets that could provide better perspective of PCB reliability and helps to reduce the electronic waste due to failure. Besides, a proper understanding of various factors/levels effect in a fitted prediction model could help make robust electronics design. The main investigation carried out in this thesis include:

- Investigation of critical factors' effect and interactions to predict failure on PCB surface under humidity.
- Detailed recognition of current behavior under various conditions as well as estimation of the correlation between dependent and independent parameters on PCB failure.
- Implementation of comprehensive predictive analytics, by using a combinations of statistical analysis, probabilistic approaches, and machine learning algorithms to predict leakage current, time to failure, failure state, and high risky conditions.

1.3 Scope and structure of the thesis

Figure 1.3 presents a bird view diagram of this doctoral thesis structured into ten individual chapters. Chapter 1 introduces the motivation and research objectives as well as provides the scope and structure of the thesis. In chapter 2, relevant literature on climatic reliability of electronics, factors influencing climatic reliability, PCB failures due to humidity, testing electronics for humidity effects and use of predictive analytics for PCB failure prediction with many details are reviewed. In chapter 3, the experimental procedure and design of experiments with various conditions combined with different controllable factors/levels and predictive analytics approaches utilized in this project are addressed. A summary of the main research findings and appended papers are provided in chapter 4. Chapters 5-7 are in the form of manuscripts, which provide detailed descriptions and discussions of the

experimental results. The PhD thesis is completed with an overall discussion in chapter 8, and an overall conclusion in chapter 9, followed by remarks on future works and suggestions in chapter 10.

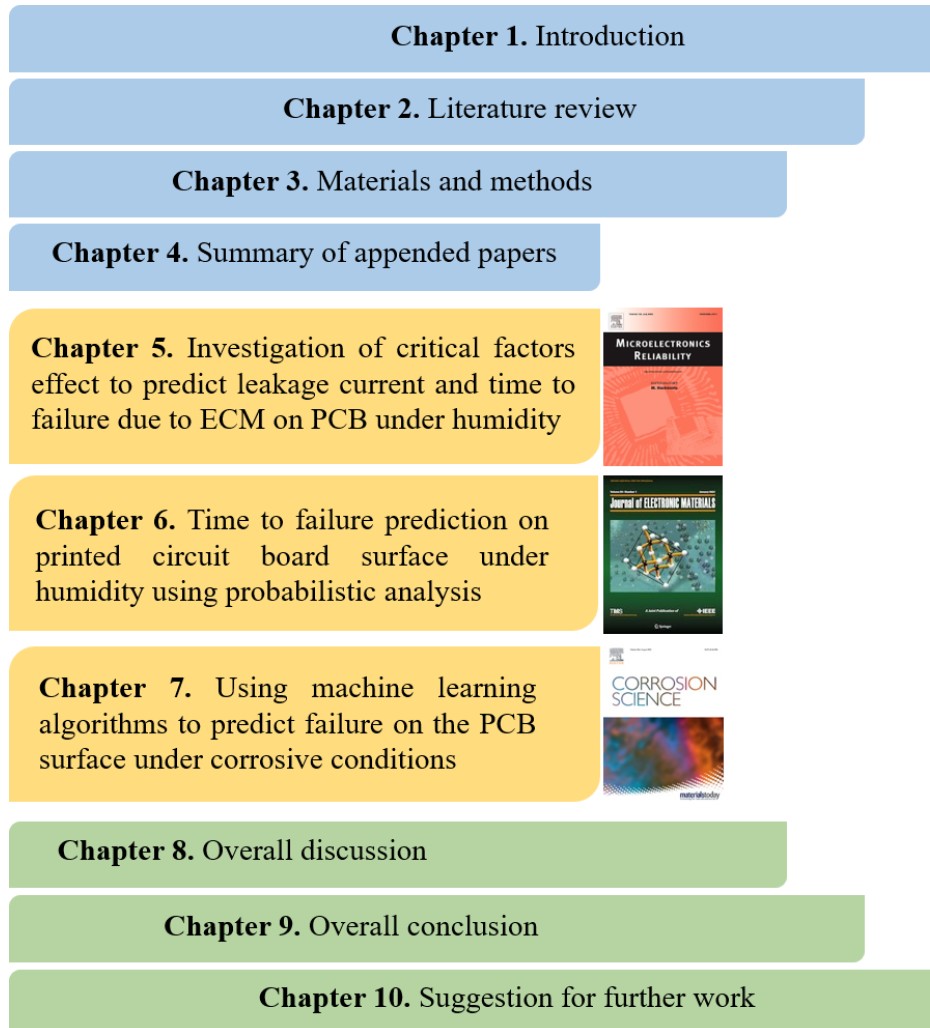


Figure 1.3 Brid view diagram showing structure of the PhD thesis.

Introduction

References

- [1] S. Bahrebar, S. Homayoun, R. Ambat, Using Machine Learning Algorithms to Predict Failure on the PCB Surface under Corrosive Conditions, *Corros. Sci.* (2022) 110500. <https://doi.org/10.1016/J.CORSCI.2022.110500>.
- [2] R.A. Ambat, Climatic Reliability of Electronic Devices and Electrochemical Migration, *ECS Meet. Abstr. MA2011-01* (2011) 1097–1097. <https://doi.org/10.1149/ma2011-01/15/1097>.
- [3] J.B. Jacobsen, J.P. Krog, L. Rimestad, A. Riis, A.H. Holm, Climate-Protective Packaging: Using Basic Physics to Solve Climatic Challenges for Electronics in Demanding Applications, *IEEE Ind. Electron. Mag.* 8 (2014) 51–59. <https://doi.org/10.1109/MIE.2014.2330912>.
- [4] V. Verdingovas, Climatic Reliability of Electronics: Early Prediction and Control of Contamination and humidity effects, Technical University of Denmark (DTU), 2015.
- [5] S. Bahrebar, R. Ambat, Investigation of critical factors effect to predict leakage current and time to failure due to ECM on PCB under humidity, *Microelectron. Reliab.* 127 (2021) 114418. <https://doi.org/10.1016/j.microrel.2021.114418>.
- [6] K. Piotrowska, V. Verdingovas, R. Ambat, Humidity-related failures in electronics: effect of binary mixtures of weak organic acid activators, *J. Mater. Sci. Mater. Electron.* 29 (2018) 17834–17852. <https://doi.org/10.1007/s10854-018-9896-0>.
- [7] M.S. Jellesen, D. Minzari, U. Rathinavelu, P. Møller, R. Ambat, Corrosion in Electronics at Device Level, *ECS Trans.* 25 (2019) 1–14. <https://doi.org/10.1149/1.3321952>.
- [8] R. Ambat, K. Piotrowska, Importance of PCBA cleanliness in humidity interaction with electronics, in: *Humidity Electron.*, Elsevier, 2022: pp. 141–196. <https://doi.org/10.1016/b978-0-323-90853-5.00005-0>.
- [9] K. Piotrowska, R. Ambat, Residue-Assisted Water Layer Build-Up Under Transient Climatic Conditions and Failure Occurrences in Electronics, *IEEE Trans. Components, Packag. Manuf. Technol.* 10 (2020) 1617–1635. <https://doi.org/10.1109/TCPMT.2020.3005933>.
- [10] R. Ambat, K. Piotrowska, Factors determining water film buildup on surfaces and relevance to corrosion in electronics, in: *Humidity Electron.*, Elsevier, 2022: pp. 93–140. <https://doi.org/10.1016/B978-0-323-90853-5.00003-7>.
- [11] K. Piotrowska, M.S. Jellesen, R. Ambat, Water film formation on the PCBA surface and failure occurrence in electronics, in: *2018 IMAPS Nord. Conf. Microelectron. Packag.*, IEEE, 2018: pp. 72–76. <https://doi.org/10.23919/NORDPAC.2018.8423854>.
- [12] K. Piotrowska, M. Grzelak, R. Ambat, No-Clean Solder Flux Chemistry and Temperature Effects on Humidity-Related Reliability of Electronics, *J. Electron. Mater.* 48 (2019) 1207–1222. <https://doi.org/10.1007/s11664-018-06862-4>.
- [13] K. Piotrowska, F. Li, R. Ambat, Thermal decomposition of binary mixtures of organic activators used in no-clean fluxes and impact on PCBA corrosion reliability, *Solder. Surf. Mt. Technol.* 32 (2019) 93–103. <https://doi.org/10.1108/SSMT-05-2019-0020>.

- [14] V. Verdingovas, M.S. Jellesen, R. Ambat, Colorimetric visualization of tin corrosion: A method for early stage corrosion detection on printed circuit boards, *Microelectron. Reliab.* 73 (2017) 158–166. <https://doi.org/10.1016/j.microrel.2017.05.005>.
- [15] R. Ambat, H. Conseil-Gudla, V. Verdingovas, Corrosion in Electronics, in: *Encycl. Interfacial Chem.*, Elsevier, 2018: pp. 134–144. <https://doi.org/10.1016/B978-0-12-409547-2.13437-7>.
- [16] S. Bahrebar, R. Ambat, Time to Failure Prediction on a Printed Circuit Board Surface Under Humidity Using Probabilistic Analysis, *J. Electron. Mater.* (2022) 1–19. <https://doi.org/10.1007/s11664-022-09668-7>.
- [17] R. Ambat, Climatic reliability of electronic devices and components, *SMT Surf. Mt. Technol. Mag.* 29 (2014) 12–28.
- [18] R. Ambat, K. Piotrowska, Humidity and Electronics: Corrosion Reliability Issues and Preventive Measures, Elsevier, 2021. <https://doi.org/10.1016/B978-0-323-90853-5.00010-4>.
- [19] H. Wang, D. Zhou, F. Blaabjerg, A reliability-oriented design method for power electronic converters, in: *Conf. Proc. - IEEE Appl. Power Electron. Conf. Expo. - APEC*, IEEE, 2013: pp. 2921–2928. <https://doi.org/10.1109/APEC.2013.6520713>.
- [20] E. Wolfgang, Examples for failures in power electronics systems, presented at ECPE tutorial on reliability of power electronic systems, Nuremberg, Ger. 16 (2007).
- [21] X. He, L. Zhou, J. Shen, A study for a typical leakage failure of PCBA with no-cleaning process, in: *2016 17th Int. Conf. Electron. Packag. Technol.*, IEEE, 2016: pp. 53–56. <https://doi.org/10.1109/ICEPT.2016.7583088>.
- [22] V. Verdingovas, M.S. Jellesen, R. Ambat, Effect of pulsed voltage on electrochemical migration of tin in electronics, *J. Mater. Sci. Mater. Electron.* 26 (2015) 7997–8007. <https://doi.org/10.1007/s10854-015-3454-9>.
- [23] B.I. Noh, S.B. Jung, Behaviour of electrochemical migration with solder alloys on printed circuit boards (PCBs), *Circuit World.* 34 (2008) 8–13. <https://doi.org/10.1108/03056120810918060>.
- [24] H. Conseil-Gudla, M.S. Jellesen, R. Ambat, Printed Circuit Board Surface Finish and Effects of Chloride Contamination, Electric Field, and Humidity on Corrosion Reliability, *J. Electron. Mater.* 46 (2017) 817–825. <https://doi.org/10.1007/s11664-016-4974-7>.

2 Literature review

2.1 Climatic reliability of electronics

Climatic reliability of electronics is attributed to the interaction of external climatic conditions and electronic system, which compromise the performance due to electrochemical failure modes. Electronic systems depending on the place of use are exposed to all climatic conditions. For various applications, they must be highly reliable and robust under extreme climatic conditions. Climatic conditions can cause reliability issues in electronics resulting in intermittent or permanent failures. Many of the failures are due to transient water film formation on PCB surfaces or other assembly components under diverse climatic exposure [1]. This trigger electrochemical process between closely spaced biased points on the PCBA surface causing leak current (surface insulation resistance drop) and finally electric short due to electrochemical migration (ECM) [2]. However, ECM is only one corrosion failure mode, while depending on the materials and environmental conditions, other corrosion failure modes are possible. Therefore, knowledge-based design for climatic reliability prediction and developing preventive strategies are essential [3]. Regardless of whether the system is a low or high power, fundamental mechanisms operating under climatic conditions have many similarities. Based on prediction methods, there are several possibilities for preventive measures using extrinsic strategies like changing in the exposed environment using conformal coating as barrier protection [4], and the special enclosure to keep the low effect of climatic conditions [5], as well as internal strategies like changing PCBA characteristics using different material, design, and soldering processes in production [6], [7].

The most significant feature connected to the climatic reliability of electronics is corrosion failure at PCBAs in contact with various influencing factors from external climatic conditions and inherent PCBA characteristics such as factors related to PCBA design, PCBA contamination, and PCBA materials. Figure 2.1 as an instance, schematically presents the important factors that can affect corrosion failure on electronic devices. The detailed description of each factor given in the following sections.

Literature review

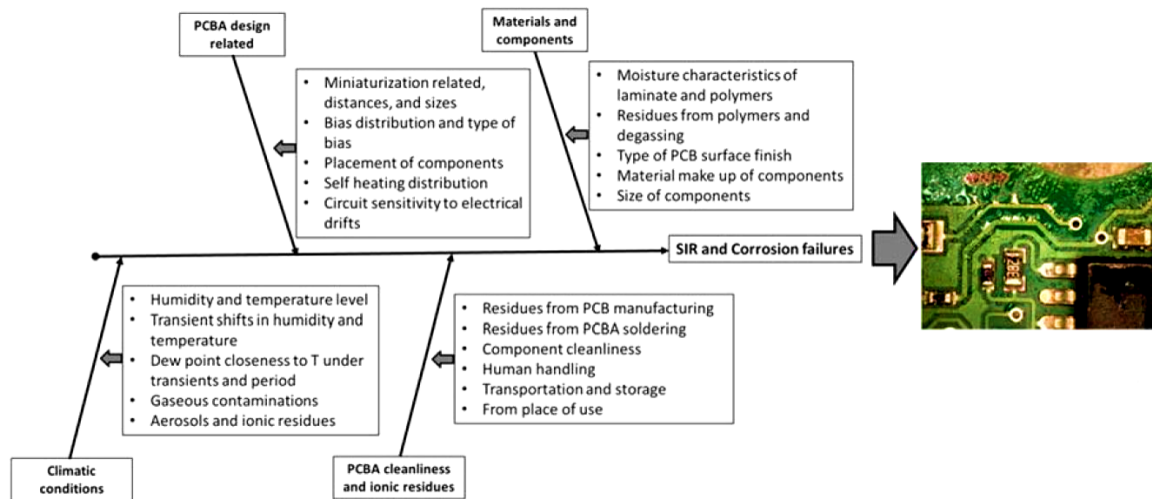


Figure 2.1 Schematic of intrinsic and extrinsic effective factors in electronic corrosion, adapted from [8].

Corrosion failure refer to degradation and destruction of the material's structure in different environment [9], [10]. In electronics, the potential risk of metal corrosion in PCBAs is due to existing conductive metals and alloys as the electrical connection like copper traces, besides polymer or ceramic corrosion is due to existing of the mixture of polymer/ceramic material as the dielectric and resistive properties for preserving the desired electrical performance, is important [11]. Corrosion in electronics is an electrochemical process, which induced the electrolytic and galvanic corrosion cells formation with a combination of many materials, residues from the PCBA manufacturing process and water condensation due to deliquescence and climatic conditions on the PCBA surface. Generally, the electronic corrosion problems are related to the existence of the combinations of multi-material comprising in the PCBAs, and the combination of multi-factors that make corrosive conditions for PCBA failures in different environments. Hence, from many parts in electronics systems that can cause corrosion issues, the focus of this thesis is only on PCBA, and especially on PCB surfaces as a substrate because of its important effect (the high percentage effect) in the failure distribution of electronic components (Figure 1.2 (a)).

2.2 Factors influencing climatic reliability of electronics

In order to improve the reliability of electronics, it requires a detailed understanding of the synergetic and interaction effects of various controllable factors. Finding the effect of single factor has limited applicability since in application multiple factors together are causing the problem, as well as interaction between factors. Moreover, it is crucial for reliability assessment to understand the relative importance of factors and their levels to take remedial

action at an earlier stage based on selecting the best PCBA material, soldering process, and optimizing the design in desired tasks for particular applications and climatic conditions. Figure 2.2 presents an overview of two main factors as part of the climatic reliability issues focussing on PCBA namely: (i) the external climate conditions and (ii) the substrate for corrosion i.e. PCBA characteristics. Climatic conditions from the testing point of view corresponds to various controllable factors such as humidity and temperature that can be set inside the climatic chamber for different tests. Besides, uncontrollable factors such as environmental radiation, environmental electric/electromagnetic fields, and air pressure on PCBAs are not easy to control or change in usual laboratories for investigating their effect. The PCBA characteristics also have different aspects regarding the cleanliness due to various contaminations, design of electrical components and overall assembling on PCB, and type of materials that are used on PCBs substrate, surface, connectors, and assembles components. More explanations of each category and the influencing factors are given in the following subsections of 2.2.

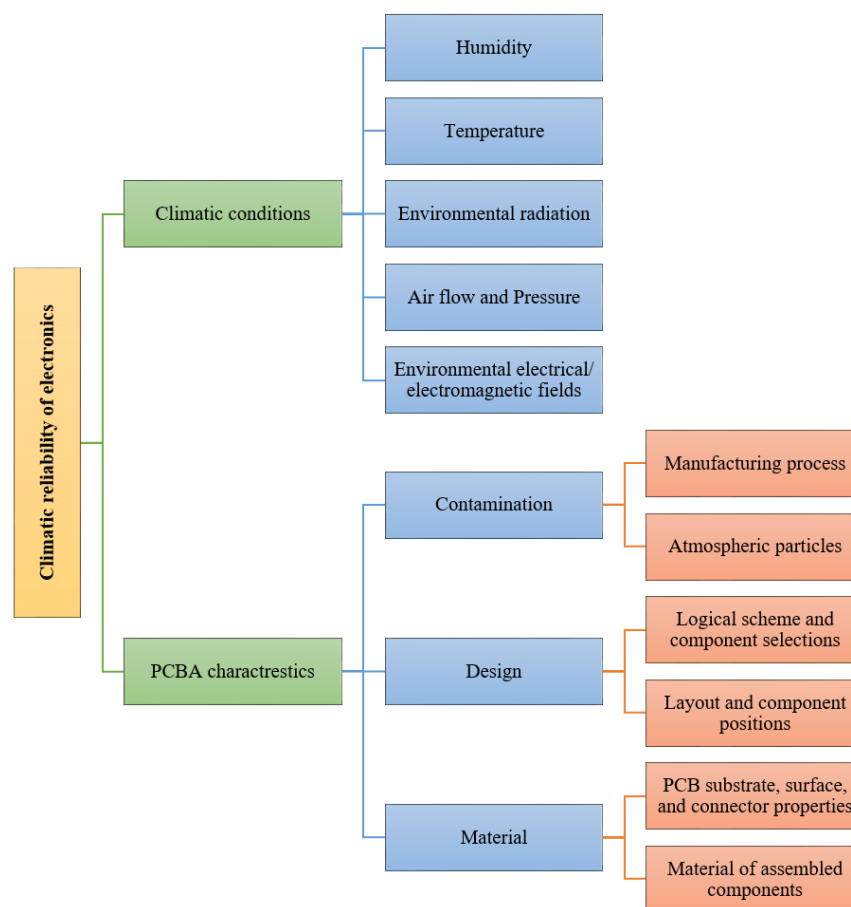


Figure 2.2 Overall categories and factors that affect climate reliability issues of electronics.

Literature review

2.2.1 External climatic conditions

The exposure of PCBAs to external climatic conditions consist of several factors for instance humidity, temperature, pressure, environmental radiation, and electrical/electromagnetic fields. Among these, humidity and temperature are the key factors leading to the water film formation on the PCBA surface that can lead to corrosion failure by acting as electrolyte layer for electrochemical processes. Fluctuation in the humidity and temperature is another factor, and the parameter connected to this is the dew point temperature, which represents the temperature to which a surface needs to be cooled in order to get condensation. DP temperature is a function of absolute humidity and temperature. However, water film on a PCBA surface can also form under constant humidity conditions due to the hygroscopic nature of the PCBA surface. This aspect will be discussed later.

Related to the humidity in the air, presence of diffused water vapor in the air is described in two ways, namely (i) Absolute humidity (AH), which is defined as the water vapor density in the air expressed as g/m³, and (ii) Relative humidity (RH) described as the ratio (percentage) of the partial pressure of the water vapor to the saturation vapor pressure and expressed as a percentage [12], [13]. AH is a function of temperature, while RH value is independent of temperature as it is expressed as a ratio to saturation vapour pressure. However, same RH value at two temperatures does not mean that the absolute humidity level in the air is same. Two places with same RH level with different temperatures will have higher AH for the place with higher temperature. RH can be easily measured using a sensor and it is usually used commonly for engineering applications as it is expressed as a percentage to saturation level. The changes of water vapor in the air to the state of liquid on the PCB surface are referred to as condensation phenomena [14]. The temperature at which condensation transpires and differs with the RH is named the dew point. Figure 2.3 illustrates the temperature, RH, and dew point relationship based on the Magnus formula to create condensation [15]. The Magnus approximation is described by equation [16], [17]:

$$T_{DP} = \frac{A[\ln(RH/100) + (B \cdot T/A + T)]}{B - \ln(RH/100) - (B \cdot T/A + T)}$$

Where T_{DP} is the DP temperature of the air (°C), T is the temperature (°C), RH is relative humidity (%), which only these two parameters (T and RH) of the air have to be measured,

and A and B are constant parameters with the values of 243.04, and 17.625, respectively [17], [18]. RH and T fluctuations are different throughout the day (different times) and for different locations. In the same RH condition for the condensation on a PCBA surface, the difference between ambient temperature (T) and dew point temperature (T_{DP}) is required. The temperature difference needed for condensation is small at high levels of humidity. For instance, at an ambient of 20°C and 60%RH, the dew point is around 12°C; however, when there is 90%RH, the dew point is around 18°C.

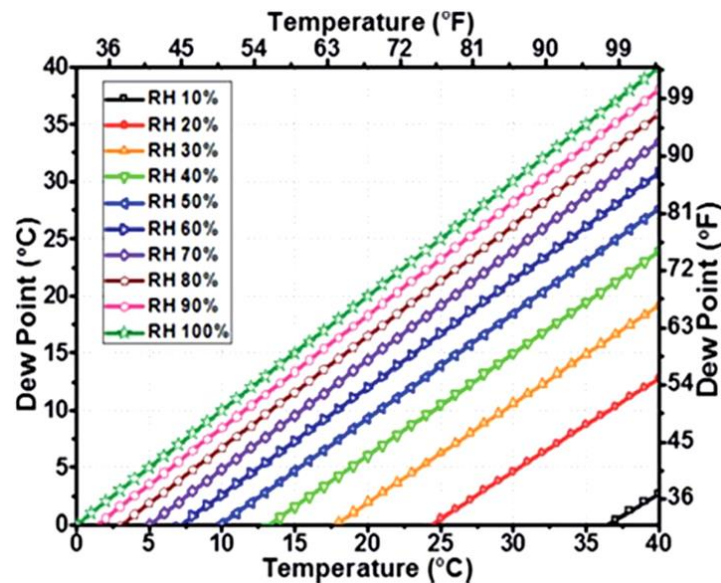


Figure 2.3 Dew point versus temperature relationship for different levels of RH, adapted from [15].

2.2.2 Important PCBA characteristics for humidity effects

As PCBs are the most important part of all electronic devices as it is the connecting substrate with conductive tracks, which also act as mechanical support for the whole assembly. When components are placed on the PCB and soldered, the final assembly is called PCBA [19]. The electric components are placed using different soldering process for instance wave soldering, reflow soldering and hand soldering, which have explained more in the next section [20]. Soldering process is important for the climatic reliability because of the application of no-clean flux systems to activate the soldering surfaces, while the flux leaves tiny levels of hygroscopic residues contributing to the humidity related corrosion issues [20]. Level and placement of flux residue left depends on the automated soldering process and PCBA design aspects, while the type of flux residue depends on the chemistry of the flux used. Some no-clean flux chemistries are more prone to humidity absorption on

Literature review

PCBA surface compared to others due to their hygroscopic behavior. Therefore, these factors could influence the corrosion failure and act in three ways; (i) chemistry and nature of contamination (ii) changing the PCBA design and thermal characteristics while soldering, and (iii) changing the humidity absorption behavior. Figure 2.4 depicts the factors influencing PCBAs characteristics and their robustness properties under various climatic conditions, which have incrementally improved for specific systems in enhancing climatic reliability of electronics point of view.

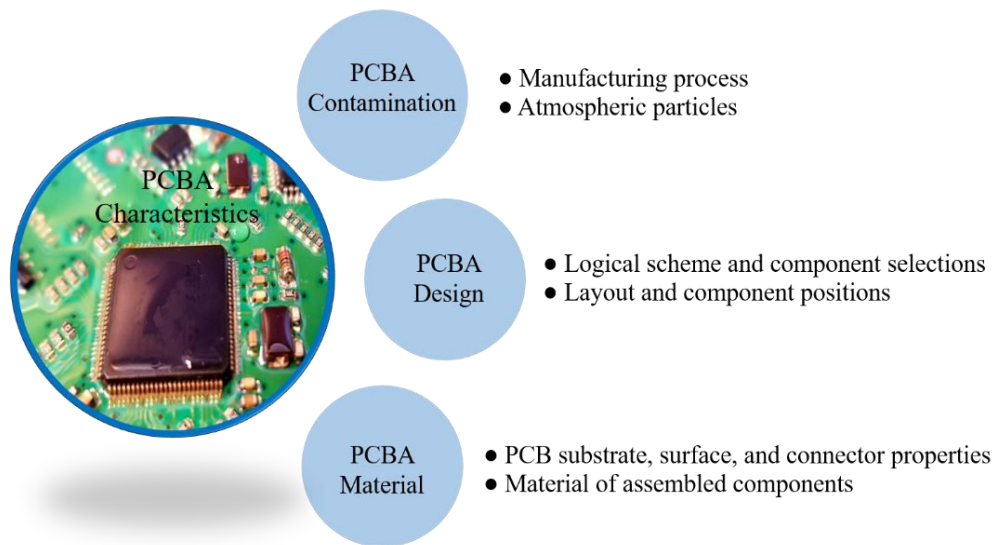


Figure 2.4 Various factors related to PCBA and process important for humidity issues.

Following sections discuss on how some of the factors above namely the contamination, material and PCBA design including bias level etc. contribute to the humidity related corrosion issues.

2.2.2.1 Contamination on PCBA

The creation of the water film and possible corrosion creation is specified using the PCBA cleanliness due to their hygroscopic nature assisting water layer formation [21], [22]. The contamination typically found inside the electronic devices originates either from the PCBA manufacturing process, handling during manufacturing and service life, and the environment [23], [24], [25]. However, process related contamination inherent on the PCBA surface is most important as in most cases external contamination entry to the PCBA surface is avoided by proper packaging. Figure 2.5 shows more details of the origination of residual contaminants on PCBAs.

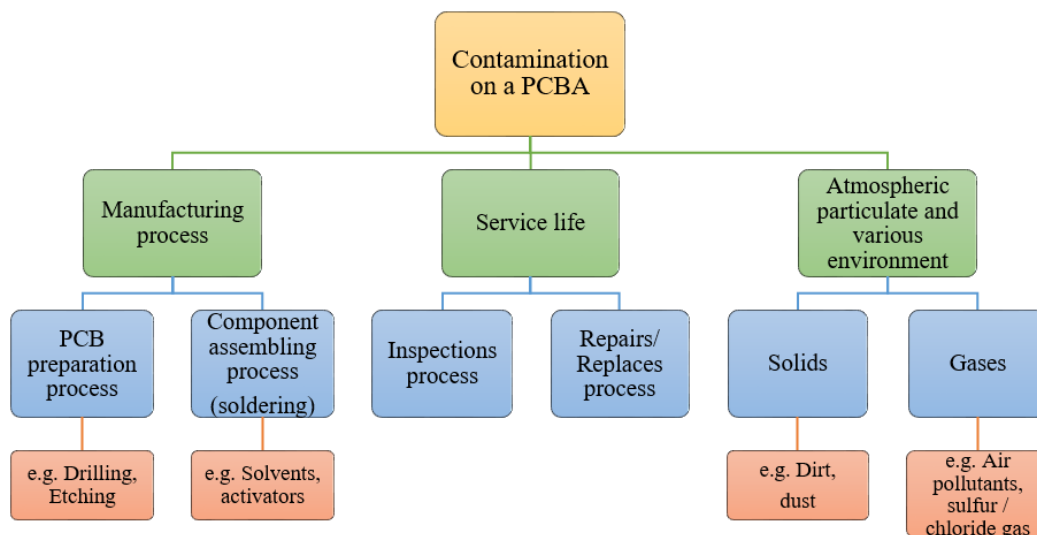


Figure 2.5 Different sources of contamination on PCBA surface.

Generally, the electronic devices with PCBAs are well packaged with a properly designed enclosure to avoid any aerosols entering the device. Moreover, chloride-related chemicals are totally avoided in the production process. Therefore, major hygroscopic residues causing problems on the PCB surface are arising from the solder flux residue resulting from the manufacturing process. For most applications today, no-clean solder flux technology conveys no need for cleaning after the soldering process with the thinking that a minimal amount of residues is left [20]. The certain amounts of residues remaining on a PCBA surface due to its hygroscopic nature attract humidity from the surrounding environment and build up water layer, act as corrosion accelerated factors, and contribute to deterioration in the electronic device's functionality and increase of LC [26], [27]. Solder flux systems depend on the soldering process, is generally divided into three kinds; wave soldering, a liquid type of flux is utilized; reflow soldering, a paste type of flux is utilized; hand soldering, a wire type of flux is used [20]. Figure 2.6 displays the main steps of the reflow soldering process, which uses a solder paste, and electrical components are directly mounted on the pasts, upon the surface of PCBA. For this process, paste is first printed on the PCB pad followed by mounting of components and then passing through the oven for the soldering process. Hence, the flux residue in this case is localized to below the components.

Literature review

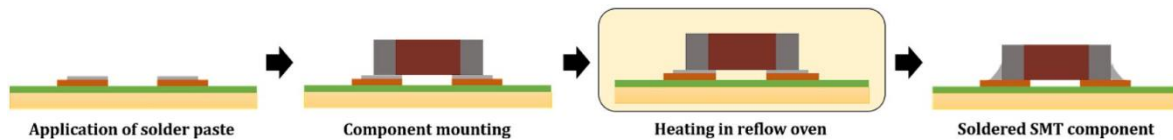


Figure 2.6 Main steps of the reflow soldering process, adapted from [28].

Most of the no-clean flux systems today are based on weak organic acid (WOA) activators. Typically, these acids can be adipic, succinic, glutaric, or malic acids to name a few. Similar to sodium chloride, these acids are hygroscopic, and deliquescent relative humidity (DRH) and efflorescence relative humidity (ERH) levels are different for different activators [29]. Typical flux chemistry also contains other ingredients such as solvents and resins; however, they have minimal effect in relation to humidity issues. The soldering process, especially wave soldering because of the use of liquid flux by spraying process introduces ionic residues on the PCBA surface during the manufacturing process, which along with other factors, affects the corrosion failures related to humidity on the PCB surface [29].

Wave soldering processing is the most common method to assemble electronics components onto PCBs [30]. It is mostly used for through-hole (TH) components assembly, but can also be used for surface mounting on PCBs [31]. Figure 2.7 illustrates the main process of the wave soldering, including; component mounting on PCB, PCB flux coating, warm-up and passing through a molten solder wave, soldered TH component, and cool-down steps, respectively.

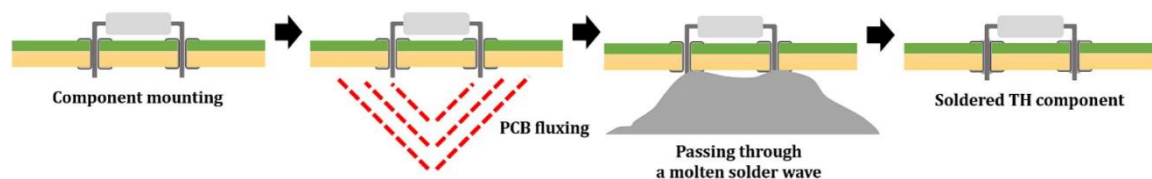


Figure 2.7 Main steps of the wave soldering process, adapted from [28].

From liquid solder flux system (PCB fluxing) for wave soldering, activators like weak organic acids (WOAs) with a high hygroscopic nature act as an etching agent for the oxide layer from the metallic surfaces and allow the molten solder to rigid stick to the metal connections [32]. Figure 2.8 displays the details of the liquid solder flux system with different components and why there are, include in the flux chemistry.

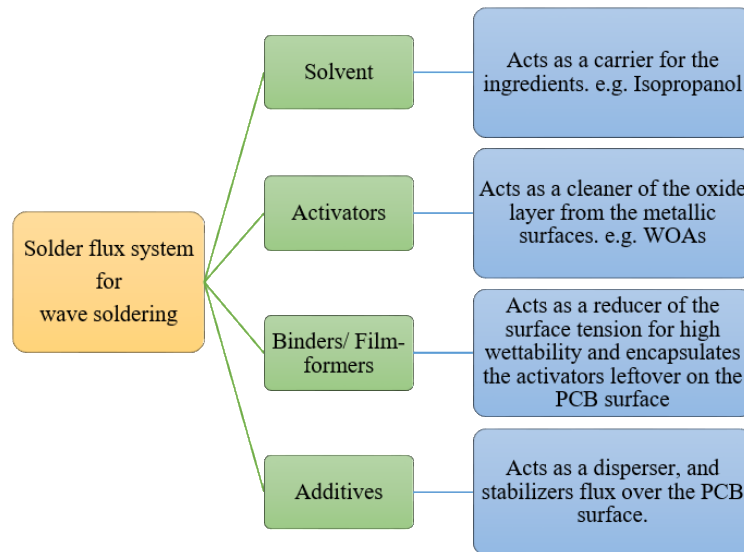
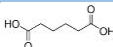
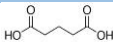
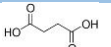
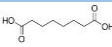
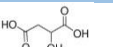
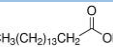


Figure 2.8 Liquid solder flux system for wave soldering.

Table 2.1 illustrate the most commonly found weak organic acid in solder flux systems, with different DRH and ERH levels depending on the chemical structure and properties [33], [34], [35], [36], [37]. Most of the contaminations on PCBs due to having hygroscopic properties are also extremely soluble in water, which can uptake humidity and enrich the formation of a layer with some electrical conductivity on the on the PCB surfaces, causing different failures. Besides, both WOAs solubility and WOAs strength have defined the conductivity of the water layer that has made on the PCBA, which the high conductivity has shown a high LC value and a high increase in the corrosion failure on PCBAs [29]. The WOAs solubility has specified the amount of the solvability of the residue at a temperature, and WOAs strength determines the dissociability of the acids (determined by the pKa values).

Literature review

Table 2.1 Most usual WOAs are found in soldering flux systems with selected properties [14], [20].

	Adipic acid	Glutaric acid	Succinic acid	Suberic acid	DL-Malic acid	Palmitic acid
Chemical structure						
Mol. Formula	C ₆ H ₁₀ O ₄	C ₅ H ₈ O ₄	C ₄ H ₆ O ₄	C ₈ H ₁₄ O ₄	C ₄ H ₆ O ₅	C ₁₆ H ₃₂ O ₂
Melting point	151-154°C	95- 98°C	185-189°C	140-144°C	130-132°C	61- 63°C
Boiling point	337°C	304°C	235°C	345.5°C	150°C	352°C
Solubility in water at 25°C [g/l]	24	1400	83.5	2.43	1440	0.007
RH for deliquescence at 25°C	~ 99%	~ 87%	~ 98%	~ 99.9%	~ 78%	

Three factors connected to the ionic contamination on the PCBA in relation to the humidity effects are (Figure 2.9) (i) type of contamination or chemistry of contamination due to the difference in DRH, ERH, and pKa values, (ii) amount of contamination (contamination level) on the PCBA surface, and (iii) position of the contamination on a PCB surface for example whether it is present near or underneath a sensitive component (this aspect is more dependent on PCBA design as discussed below).

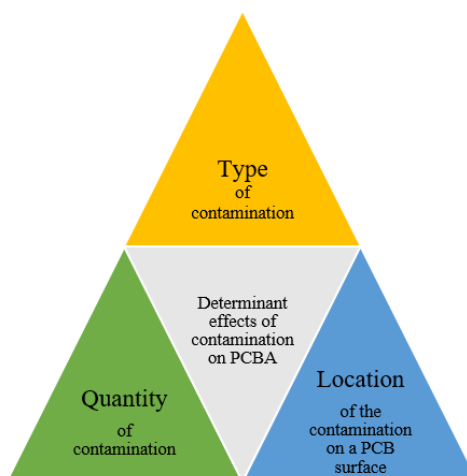


Figure 2.9 Factors contributing to the detrimental effect of the contamination on PCB surfaces.

2.2.2.2 Importance of PCBA design on humidity effects

The design of PCBAs goes through two main steps namely base PCB manufacturing with required layout (places for component mounting and connecting tracks) followed by assembling of component and soldering. Base PCB surface finish can be of different types depending on the requirements of the PCBA for e.g. ENIG type, HASL (Hot Air Solder Leveling) type, Immersion silver, Immersion Tin etc. Surface finish means the coating on

the external exposed tracks of the PCB where the components will be mounted and soldered. Surface finish used in this thesis for testing is HASL (See next section). In PCB manufacturing, the layout, surface finish, and definition of positions for all components and tracks for linking components together are considered. Then for the mounting assemblies and soldering process, the logical scheme, which defines the electronic components with different properties and their interconnections with proper application potential bias, is deliberated [38]. Spacing between the opposite potential bias of electrodes on a component and between two different components, as well as the range of applying a potential bias between two electrodes, are very important features in the PCBA design [22]. Other important factors influencing PCBA design are component placement/orientation, the size of the components, and gap sizes where residues can trap as well as water trap during condensation [8]. Besides, heat distribution on the PCBA surface is another important factor in PCBA design. Based on it, if there is any component that provides heat, then the hot part is less prone to humidity effects [8], [39]. It means the soldering process could depend on the placement of the heat-absorbing and heavy components, and it could affect the flux decomposition causing a heterogeneous distribution of the contamination on the PCBA [20]. For instance, the WOAs in the solder flux are more probable for residue decomposition depending on the thermal treatment whether the PCBA temperature attain a specified level, which interaction with humidity determines their effect on the PCBA corrosion failure [20].

The pitch distance is a significant issue due to the various demands of users for the portability of electronic devices, as well as their use of them in different climatic environments [40]. This issue causes an increase in the miniaturization or assembly design density of the PCBAs [29], [41]. The compact device has caused the space reduction of different components and between the various components on the PCB surfaces. This distance decreasing causes increasing the electric field, in which the electric field strength has a direct relationship with potential bias (voltage) and reverse relationship with the distance between conducting lines on each electrical component or between them ($E=V/d$) [42]. Figure 2.10 displays the pitch distance on a component and between two components under applying voltage and the creation of an electric field.

Literature review

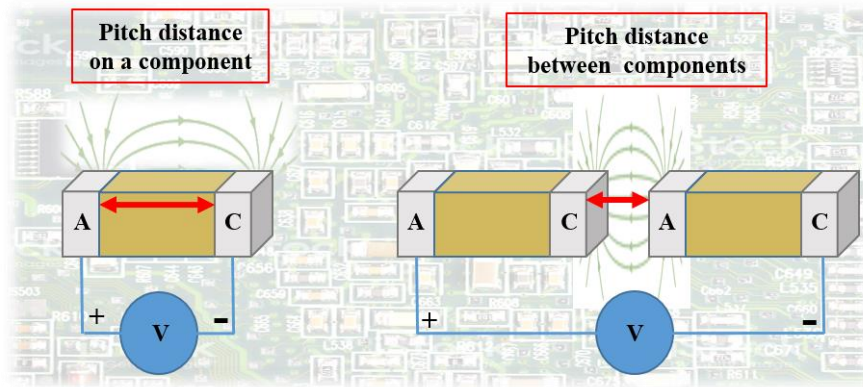


Figure 2.10 schematic of pitch distance, applying voltage, and creation of electric field on PCBAs.

The voltage is one of the critical factors for making failures on PCBAs [29]. Applied the voltage between two electrodes causes the dissolution of anodic metal ions in the conductive water form [29]. The conductive water film has been created due to climatic conditions and contamination. The dissolution of anodic metal ions of metal connections on the PCBA has migrated and then deposited at the cathode. Afterward, the metallic filaments of dendritic shape under the influence of the electric field due to the applied voltage will have made. It means the initial condition to create the permanent failure mode (short circuit) on PCBAs have made.

2.2.2.3 PCBA materials

PCBAs use a mixture of materials as substrates and components. Material selection and varying qualities depend on the requirements of the application, such as performance for special environment applications to warrant the survivability of mechanical/electrical/thermal stresses. Moreover, to follow governmental regulatory prerequisites such as the European Union's restriction of hazardous substances (RoHS), the use of materials containing any metals and restricted chemicals is forbidden [43]. The electrical components or PCB assemblies for diverse applications depend on electrical resistance and conductance, often using metals, polymers, and ceramics [44], [45], [46].

The PCBs commonly consists of three basic layers, from top to bottom, including solder mask, metal connector (copper layer), and substrate (FR-4) [47]. There are three most important types of materials that use for the PCB substrate fabrication, including; FR-4, Polytetrafluoroethylene (PTFE), and metal [48], [49]. The metal materials like aluminum provide suitable thermal performance, mechanical durability, and much longer product life for PCBs [50]. PTFE (Teflon) PCBs are a kind of flexible and lightweight plastic material

with very low resistance that is used for high-speed and high-frequency applications [51]. FR-4 is the most commonly used material in PCBs, having good strength-to-weight ratios and high tensile strength [52], [53]. Generally, FR-4, by having glass fiber woven in an epoxy resin, has good thermal and mechanical characteristics for use in most electronic applications [54], [55], [56]. FR is a common term for fire retardant, and 4 represents laminated epoxy composite, which can cover a large spectrum of materials [57], [58]. Table 2.2 shows the constituent, major functions, and instances of FR-4 materials [14], [59].

Table 2.2 Usual constituent, function, and example of FR-4 materials, adapted from [14], [59].

Constituent	Major functions	Example materials
REINFORCEMENT	Provides mechanical strength and electrical properties	Woven glass fiber
COUPLING AGENT	Bonds inorganic glass with organic resin	Organosilanes
RESIN	Acts as a binder and load transferring	Epoxy (DGEBA)
CURING AGENT	Enhances linear/cross-polymerization in the resin	Dicyandiamide (DICY), phenol novolac (phenolic)
FLAME RETARDANT	Reduces flammability of the laminate	Halogenated (TBBPA), halogen-free (P-compounds)
FILLER	Reduces thermal expansion and cost of the laminate	Silica, aluminium hydroxide
ACCELERATOR	Increases reaction rate, reduces curing temperature, controls cross-link density	Imidazole, organophosphone

Copper trace or PCB track refers to a copper conductor as the common metal connection on the PCBs, which conducts electric current through connected components with little resistance [60], [61]. Solder mask or solder resist is a robust and permanent coating that protects copper traces from corrosion and the conductive bridging between them on PCBs [62], [63]. Usually, to avoid copper trace oxidization and deterioration, the surface finish makes a crucial interface between the PCB and the component assembly. The surface finishes have two vital purposes, to preserve the exposed copper circuitry and to prepare a solderable surface before the electrical components to the PCB are assembled [64], [65], [66]. The chemical surface plating methods such as immersion tin (ISn), immersion silver (IAg), electroless nickel immersion gold (ENIG), besides electroless nickel electroless palladium immersion gold (ENEPIG) are commonly used by a low thickness layer on copper traces [66], [67], [68], [69]. Figure 2.11 illustrates the different layers with the electroless process and immersed materials, which are used for common PCB surface finishes [70], [71], [72].

Literature review

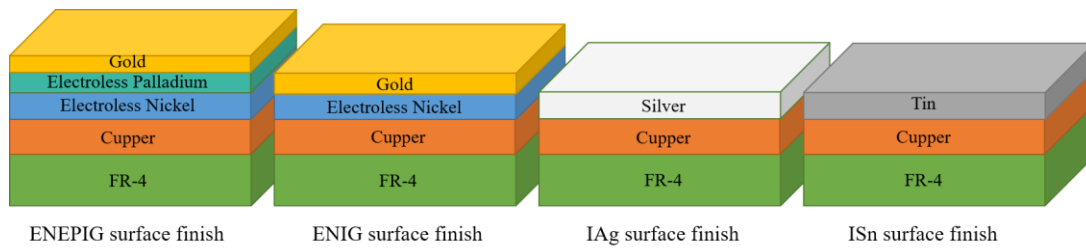


Figure 2.11 Comparisons of different widely used PCB surface finishes.

The hot air solder leveling (HASL) surface finish as the most popular cost-effective surface finish, also uses Tin (Sn); however, it is different from the ISn surface finish. HASL surface is produced by dipping the PCB with base copper tracks into a molten SAC (Sn-Ag-Cu) solder alloy bath, followed by removing excessive material using an air knife [73], [74]. **Figure 2.12** displays a schematic of a PCB HASL surface finished production in vertical process. HASL is usually used in the Tin alloy, and it does not need to be immersed and tinned, besides the PCB surface that is covered with Tin alloy, scraped by hot air for leveling the Tin alloy surface [75], [76], [77]. Table 2.3 displays the comparison of some influential features like solderability and popularity from the applications point of view, as well as cost and shelf life from a properties point of view for common PCB surface finishes [72], [78], [79].

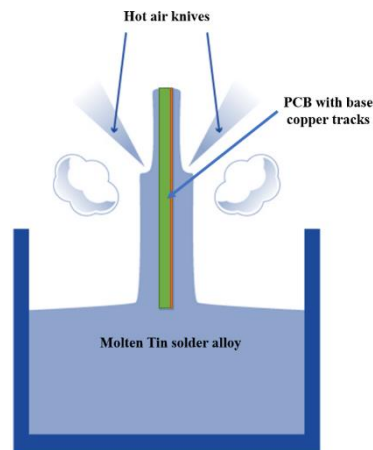


Figure 2.12 Schematic of in vertical HASL procedure.

Table 2.3 Comparison of common PCB surface finish in some influential features.

	HASL	ISn	IAg	ENIG	ENEPIG
Solderability	Very Good	Good	Excellent	Good	Good
Fabrication cost	Low	Medium	Medium	High	High
Shelf life	Long	Low	Medium	Long	Long
Popularity	High	Low	Medium	Medium	Medium

2.3 PCBA failures due to climatic conditions

PCBA failure under climatic conditions is an electrochemical corrosion mechanism occurring due to the PCBA characteristics and thin water layer formation on the PCB surface [80]. The combination of critical factors from all PCBA contamination, design, and materials aspects together with exposure to various climatic conditions generate electrochemical failures process on PCBAs. The thin water film formation is caused by flux residue on PCBAs, and climatic conditions due to deliquescence [81], [82]. Deliquescence is defined as a tendency of a transformation of the solid phase to a liquid solution phase under proper climatic conditions. It depends upon the solid properties (chemical potential for the interaction with surrounding humidity) and the atmospheric temperature [82], [83]. The deliquescence relative humidity of different contamination on PCBAs like WOAs that are commonly used in no-clean flux activators is diverse at various temperatures [82].

The existence of a high level of humidity and climatic conditions together with other PCBA characteristics and intrinsic factors of electronics creates in many failure modes related to corrosion [8]. The main failure modes on PCBA includes: reduction in SIR and LC, ECM, conductive anodic filament (CAF), galvanic corrosion, fretting corrosion, creep corrosion, gaseous corrosion, and polymer degradation due to moisture absorption [84], [8]. Since this thesis is focused on reduction in SIR and LC, and dendrite formation and ECM failure modes, more information have provided on these. Overall, these failure modes contained electrochemical mechanisms due to the corrosion of the involved different metallic materials and water layer as electrolyte. The electrochemical process is caused by the water film connecting between metallic points, while the soldering process related contamination will dissolve into the water film providing it good electrolyte properties. The two failure modes focused in thesis are independent, and the LC is the precursor for the ECM, although it is not a necessary condition that in each case LC leads to ECM. LC is produced due to the electrochemical process, which also involves metal dissolution. Dissolved metals, then migrate to the cathode and leave in the shape of the dendrite to create a short circuit [22]. Nevertheless, from the application point of view both steps in the failure mode is important as LC itself could influence the functionality of the electronics depending on its sensitivity, and ECM leads to irreversible failure mode.

Literature review

2.3.1 Surface insulation resistance reduction and LC

SIR refers to the electrical resistance and material properties between conductive electrodes, which are separated by dielectric materials [85], [86]. On a PCBA surface components are interconnected and while working with a potential bias. The glass epoxy laminate substrate provides required electrical resistance between the conduction lines as well dielectric properties. However, when the water film forms, current can also pass through the water film due to the electrochemical processes at the connected electrode. Therefore, SIR reduction occurs proportional to the increase of LC, which is usually an initial failure that results from the presence of ionic hygroscopic contamination and water film formation due to climatic conditions (temperature and humidity changes) [86]. Leak current through the water film act as stray current for the functioning of the PCBA influencing its overall functionality or functionality of a particular component. Decrease of SIR and increase of LC can grow due to increasing water film conductivity and applied high voltage between two small opposite electrodes (anode and cathode).

Leak current on a PCBA can be described as a current passage between conducting points. Figure 2.13 schematically displays three pathways for leak current between two conducting points, which are included; (I_1) current through the PCB laminate, (I_2) current on the PCB surface, and (I_3) current through the adsorbed water layer. The I_1 and I_2 are typically low (below nA, as well as below the SIR level of $G \Omega$) and almost constant based on PCBA design and material properties [8]. The I_3 (LC) is based on climatic conditions and contributing surface contamination (especially hygroscopic ionic residues from the wave solder process), which results in a water layer buildup, causing a significant increase and subsequently changing the functionality and failure of the electronics.

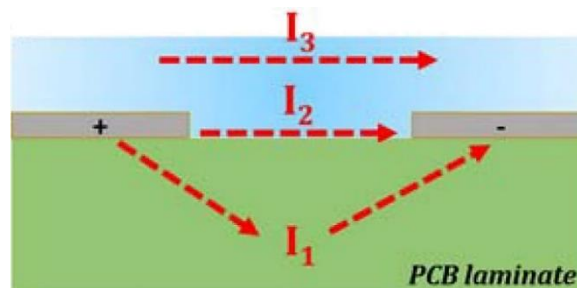


Figure 2.13 Different pathways for leak current on a PCBA, (I_1) current through the laminate, (I_2) current on the PCB surface, and (I_3) current through the electrolyte (water layer on the PCB surface), adapted from [8].

2.3.2 Electrochemical migration and short circuit

ECM is a continuation of the LC. In another word, LC is the forerunner for ECM, although it is not a necessary condition that LC leads to ECM in each case. ECM, as one of the most common failures in PCBAs under various climatic conditions, refers to migrate of metal ions through the conductive electrolyte (thin water layer formation on the PCB surface) under the effect of the electric field due to applying the potential bias (voltage) between two opposite point (anode and cathode) [87].

In the high electric field, the dissolution of metal ions like Sn from the anode passes through the created bridge of conductive water layer and makes the deposition of metal ions to the cathode side, causing dendrite growth from the cathode to the anode [88]. If the dendritic filament greaten enough to minimize the distance between cathode and anode in the surface conductive electrolyte, and finally making an enduring conductor bridging, the short circuit happens as the most significant failure mode in electronic devices [22], [29]. Figure 2.14 presents the dendrite formation mechanism under applying voltage and conductive water layer [89], [90].

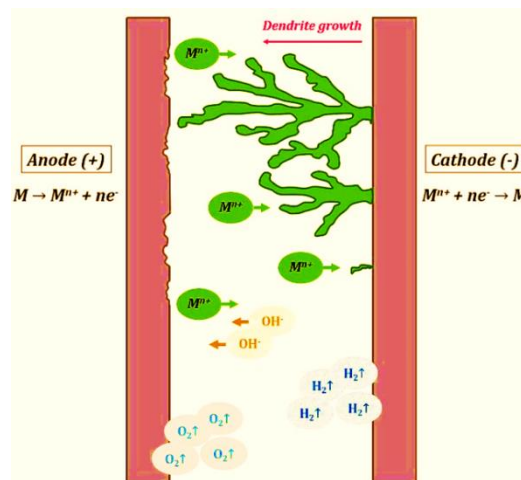


Figure 2.14 Dendrite formation mechanism, adapted from [14].

In general, based on three steps, the ECM grows from the cathode to the anode. In the first step, the water layer has electrolyzed at the anode electrode, and metal ions have dissolved with high level of contamination [91]. Secondly, the metal ions have diffuse (depending on the effective electrical field strength) to the cathode through conductive water film. Eventually, the hydroxide ions have diminished to metal at the cathode, which relating to the type and the level of contamination induced, LCs can emerge on the surface of PCB

Literature review

[92]. Subsequently, their deposition at the cathode then starts the creation of metallic filaments of dendritic shape under potential bias has applied. On the contrary, the ECM created will not form permanent metallic links between adjacent conductors, but if the dendritic filament grows adequate to minimize distance between cathode and anode in the surface conductive electrolyte, finally, a stable conductor bridging, in better words the short circuit will happen as the most important failure mode in electronic devices [22], [91]. This will lead to malfunctions performance of electronic components and systems owing to high level of LCs and electric short circuits [92], [93], [94], [95], [96], [97]. Figure 2.15 presents an example of ECM occurrence on a SIR PCB surface. The climatic conditions (humidity and temperature), as well as contamination types and levels, material surface finishes, the distance of the electrodes, and potential voltages from PCBA characteristics, are the main part of critical factors which influence the SIR reduction, consequence on ECM, and short circuit on PCBAs.

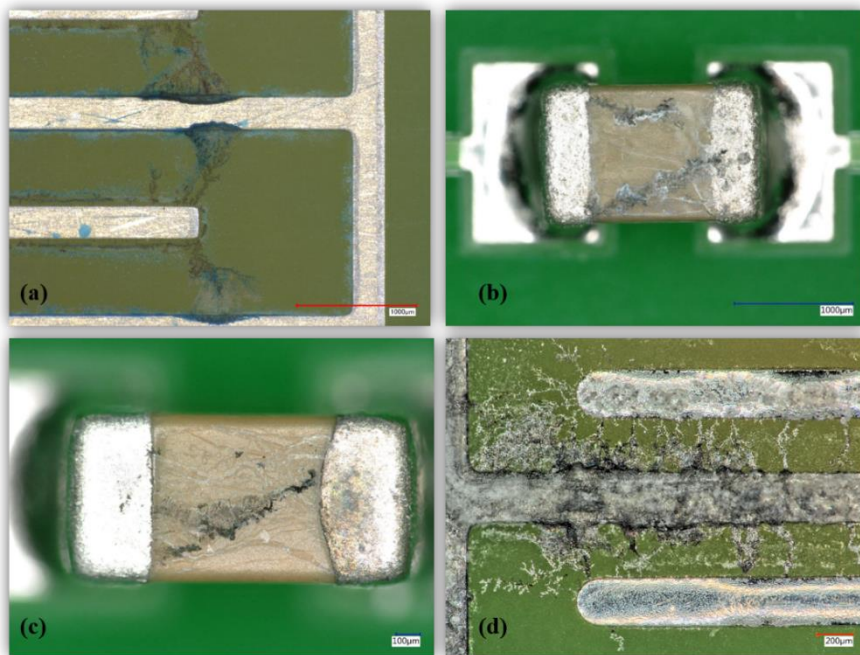


Figure 2.15 Example of ECM and dendrite formation on PCBA; (a) Optical microscope image of dendrite formation on SIR PCB with IAg surface finish under $100 \mu\text{g}/\text{cm}^2$ Glutaric acid, 10V, 95%RH, 40C, and at 300um pitch distance, (b) Optical microscope image of dendrite formation on 0805 SMT capacitor after droplet test under $2 \mu\text{g}/\text{cm}^2$ Glutaric acid, 10V, 25C, and 1000um pitch distance, (c) Optical microscope image of dendrite formation on 0603 SMT capacitor after droplet test under $1 \mu\text{g}/\text{cm}^2$ Glutaric acid, 10V, 25C, and 1000um pitch distance, (d) Optical microscope image of dendrite formation on SIR PCB with HASL surface finish under $100 \mu\text{g}/\text{cm}^2$ Adipic acid, 5V, 98%RH, 50C, and at 300um pitch distance.

2.4 Testing PCBA under humidity and current measurement

SIR testing is a practical test to reflect PCBA performance to assess lifetime, robustness, capability, and reliability based on IPC standards [98] for evaluating electronic assemblies quality; since attaining actual PCBA geometries is mostly tough to experiment, simulate, and predict [99], [14]. SIR DC testing is the most usual test designed for material quality, service life estimate, besides assessing various factors on the SIR values since it is a simplified manifestation of PCBAs without geometries [100], [101], [102]. As a test substrate, PCBs with interdigitated pattern (called SIR PCBs) having different pitch distances are used. Pitch distances used usually corresponds to distances found on PCBA surfaces. SIR PCBs are commonly made on the FR-4 laminate, similar to a comb pattern, having two conductors separated by a dielectric at different pitch distances. Testing is carried out under constant potential conditions, while the output can be measured either as resistance change (SIR change) or as LC [103], [104]. Figure 2.16 displays two commonly used IPC standard SIR test PCBs with different pitch distances.

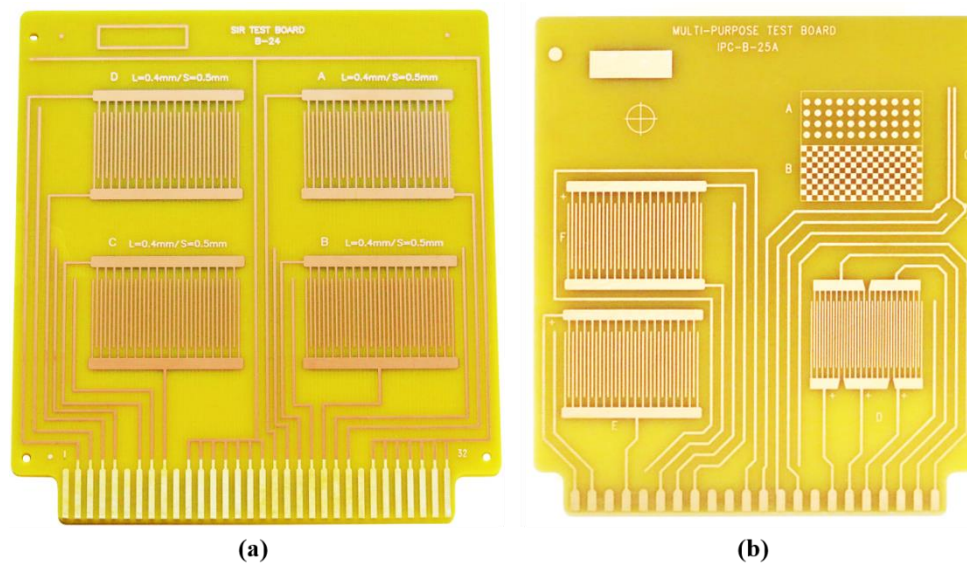


Figure 2.16 IPC standardized SIR test PCB; (a) IPC-B-24 [99] , (b) IPC-B-25A [81].

Current measurement as a main indicator to define different outputs like LC, Time to failure (TTF) due to ECM, and failure status under exposure to various climatic conditions is often employed in the testing of PCBA [105], [106], [107]. Chronoamperometry (CA) is a DC technique in the potentiostat that can measure the leak current to the pA level on the PCB surface under various climatic conditions with the low DC voltage in a range of 0 to

Literature review

10 V [108], [109]. Figure 2.17 presents a general current measurement and interdependency states of current behaviors to create the failure modes (LC and ECM) on the PCB surface that show three states corresponding to the corrosive environment, namely: stable part (getting LC value), transient part (getting TTF value due to ECM), and unstable part (getting failure status information) after the transient [22].

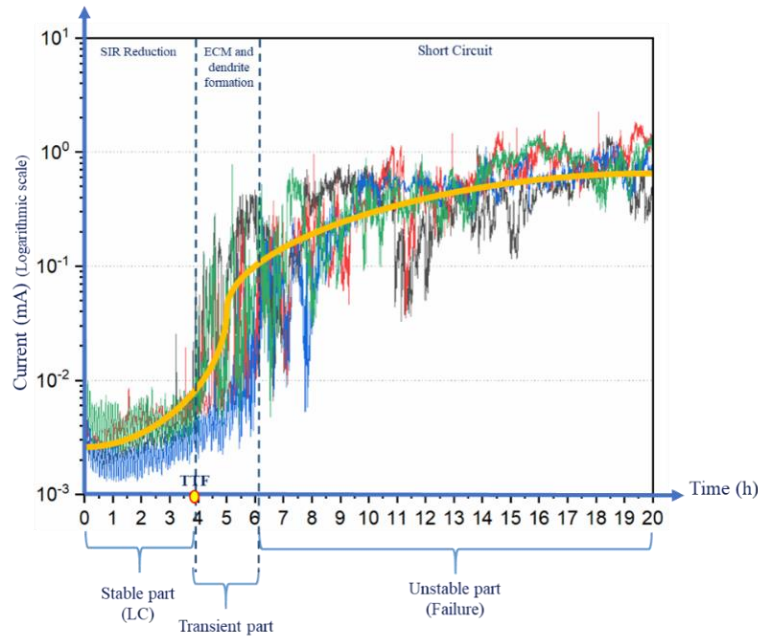


Figure 2.17 General current behavior from DC current measurement testing at three states on SIR PCBs, adapted from [22].

The early state of the measured current at each condition, below the current that abruptly raised, is considered as stable part. In this part, an average of current is taken into account as the LC value [22]. This part is created owing to the surface electrochemical process of forming the water layer and the potential biased connection between anode and cathode [22]. Following the continuation of electrochemical process, which is called transient part, the dissolved metal ions from the positively biased electrode (anode) gradually move to the negative one (cathode) and deposit in the shape of the dendrite, electrically bridging the two electrodes [29]. Corresponding to this, the behavior of current demonstrates an abrupt raise (jump) at the beginning of the second part, which the beginning of the second part taken into account as the start of the failure process due to ECM and is called TTF. The initial time and duration for this part can be determined by the conditions' aggressiveness combined with various factors and levels. With growing the dendrite filament and decreasing of the distance between two conductive electrodes on the PCB surface, the

stable conductor bridging has been made with a high current region [22]. Normally, the leakage current value bigger than the ECM threshold shows the short circuit created by an enduring dendrite in the unstable part [29]. This demonstrates a hierarchical failure mechanism, which causing a short circuit with interdependencies between the failures processes in current measurement testing [22].

2.4.1 Design of Experiment Methodology

Design of experiment (DOE) is a regular platform for doing studies using statistical procedures [110]. DOE approach, using a systematic design, attempted to address the one factor at a time (OFAT) method's drawbacks and investigate the significant factors and their interactions with fewer experiments [111], [112]. Moreover, the DOE approach was adopted to characterize the impact and interaction of the factors as well as help to formulate the relationship of independent variables with dependent variables (response), which aids in developing a predictive statistical model [113].

There are four key terminology and technical tools at DOE, which include interaction, randomization, blocking, and replication [114], [115], [116]. Interaction is defined as the behavior of two or more factors when they are together, and the interaction plot is most often used to visualize probable interactions between two or more factors during the DOE. Randomization is used to minimize potential uncontrollable inputs in the experiment by randomly assigning factors and levels [115], [116]. Blocking is used to maximize an experiment's precision and control by separating the experiment into similar parts for running all combinations in one condition. Moreover, replication is used to determine the common cause deviation and test error in the experimental results. For predicting the behavior and output of every process, doing a lot of experiments is essential. However, it takes time and money. DOE is a targeted tool for planning, investigate, and modifying a process [117], [118].

Figure 2.18 demonstrates the general overview of DOE phases, steps, and examples of each step related to the testing PCBA. The factorial design is a method of DOE methodology that perform the evaluation of main significant factors and their interaction effects between some independent variables (predictors) and dependent variables (responses) [119]. Among different methods in the early phase of DOE, such as Taguchi design, response surface

Literature review

design, etc., factorial design is the most popular method due to its simplicity, planning, arrangement, performance, and straightforwardness [112], [120], [121].

In addition, when multiple sets of measurements are made during one scientific investigation, repetition occurs. However, replication is when you redo the entire experiment. Repetition shows the results how close to each other, and replication displays the estimate's accuracy (assuming there is no bias or systematic error). In this thesis, due to variability of sources (like different specimens at various corrosive conditions) and resource constraints (like time and cost of lab experiments), both repeats and replicate have been used to examine multiple sources of variability.

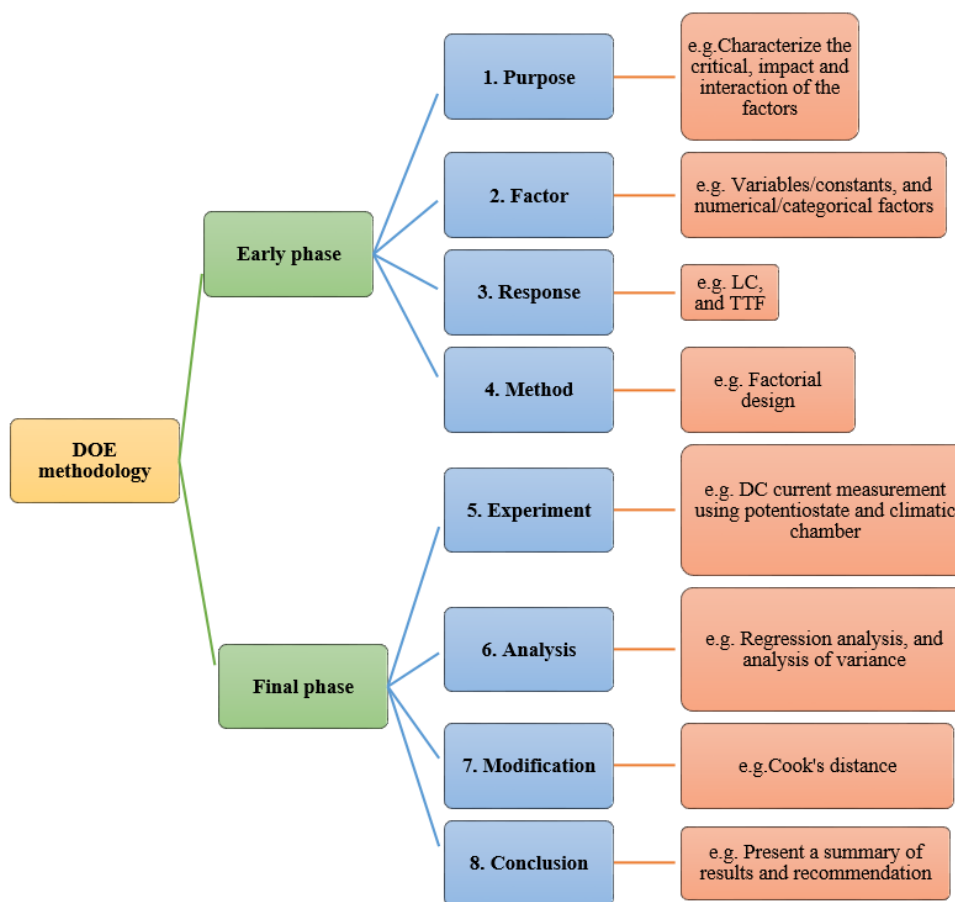


Figure 2.18 DOE phases and steps.

2.5 Data analytics framework

This part introduces the need for data analytics and analytical techniques with a focus on predictive analytics for PCBA failure prediction. It overviews the difference between experimental design and the organization of outcomes in descriptive analytics, exploration of datasets pattern and investigation of the prediction models in predictive analytics, and

expresses recommendations and decision making in prescriptive analytics [122], [123], [124]. In other words, in analytical data procedures, descriptive analytics try to answer 'what has already happened', and diagnose 'why did it happen' by proposing its root causalities [123], [124], [125]. Predictive analytics is the process of advanced analytics to realize the probability of future results founded on historical data and predict unknown prospective trends according to the descriptive analysis of data to answer the 'what is most likely to happen in future' questions [126], [127]. Usually, prescriptive analytics make optimizations, proactive decisions, and recommendations base on the predictive analytics outcomes, and it answers the 'what can be done for it' questions [128], [129]. Figure 2.19 presents the framework of data analytics in order from right to left, with a special question, explanation, and keyword from up to down [123], [124], [128], [130].

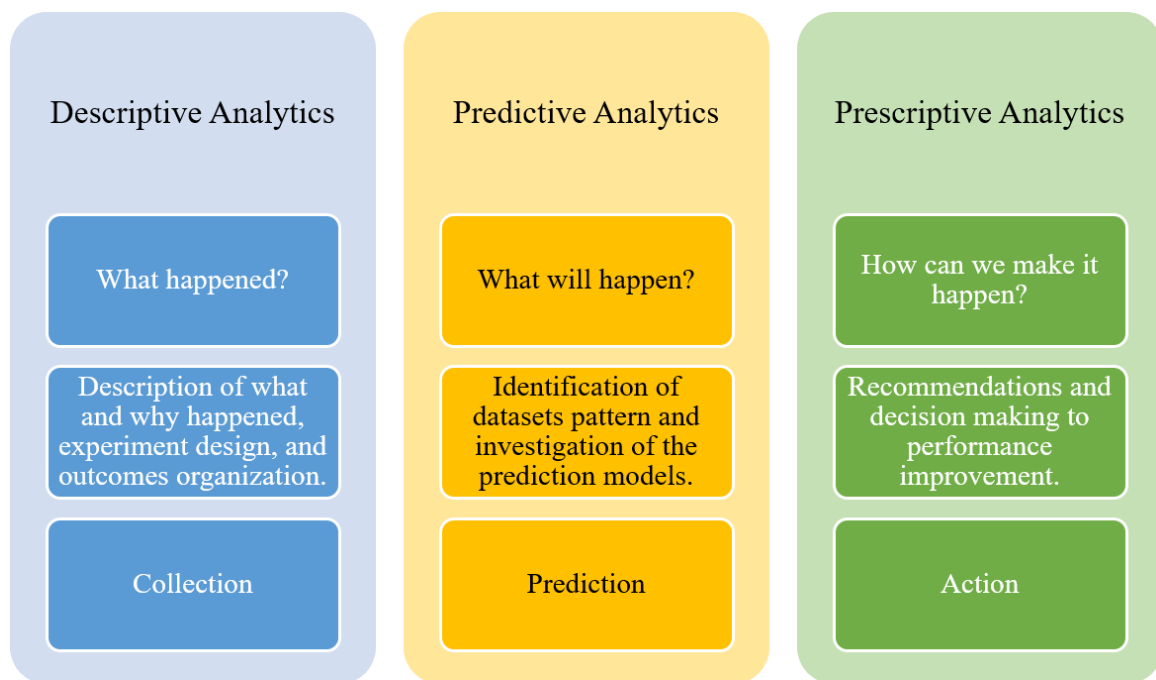


Figure 2.19 Data analytics framework showing different parts.

2.5.1 Predictive analytics for PCBA failure prediction

Predictive analytics has been extremely used today in various applications such as finance, healthcare, heavy industry, transportation, and consumer goods [131], [132]. Predictive analytics aims to forecast future conditions [133]. The conditions could be the probability of an event occurring in the future (such as ECM occurrence in electronics), estimating a point of the time at which an event might occur (for example time to failure), or forecasting

Literature review

a quantifiable amount of a dependent variable (leakage current when humidity form water film under different conditions) by applying the acquired predictive models [130], [134]. Predictive analytics use various statistical analyses, probabilistic approaches, and machine learning algorithms to assist in predicting and extrapolation data by incorporating the descriptive analytics output [128], [133], [135]. Figure 2.20 presents the framework of predictive analytics. In order to acquire information from a dataset, statistical analysis is used to predict a behavioural pattern like linear regression analysis [128]. Probabilistic approaches have been used to quantify the uncertainty by integrating information from a dataset in order to catch the appropriate distributions to calculate the likelihood, like the Weibull distribution and Monte Carlo simulation. Moreover, Machine Learning Algorithms have been used to predict the output according to training input datasets gained for analytical aims [136].

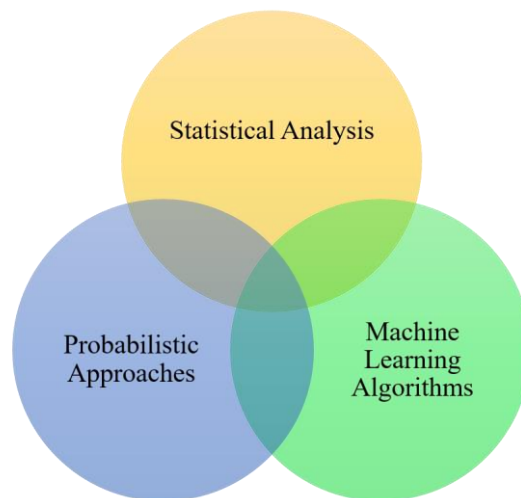


Figure 2.20 Various methods employed for Predictive analytics framework.

2.5.1.1 *Statistical analysis*

Statistical analysis is a branch of mathematical science that refers to gathering, organizing, investigating, interpreting, and presenting data [137]. The statistical analysis requires an appropriate design of the experiments upon the proper selection of samples to draw generalizations from the samples to the entire population [138]. Statistical analysis, in predictive analytics, deals with finding information from data to estimate variables' relationships and forecast behavior patterns [128].

Regression is a widespread and reliable statistical analysis technique that guesstimate the relationship between the dependent and independent variables [139], [140], [137]. A regression model is a mathematical function in which the assistance of the hypothesis test and analysis of variance (ANOVA) pursues a logical relationship between different variables [141], [142].

ANOVA is a statistical hypothesis test to compare the average of several populations based on the calculation of the ratio between variances using the F-Test statistical class [143], [144]. ANOVA aims to determine whether population averages are equal or not by considering the amount of variability in a population and noticing if the variability is greater between populations than within populations [143], [144], [145].

The regression model is necessary to establish a logical relationship between the factors in deciding to implement new variations and attain optimal conditions [146]. It also is used to predict one variable, given the values of the others [147]. Usually, there are two types of regression models that are used in predictive analytics; linear regression and logistic regression model [148]. The linear regression model is applied to model the linear relation of the independent (predictors) and dependent variables [148]. Besides, logistics regression is used to model the categories of discrete dependent variables based on independent variables [148]. Table 2.4 illustrates comparison of regression and ANOVA in statistical analysis [149], [150], [151].

Literature review

Table 2.4 Comparison of Regression and ANOVA in statistical analysis, adapted from [152].

	Regression	ANOVA
Definition	Regression is a very effective statistical method to establish the relationship between sets of variables.	ANOVA is the short form of analysis of variance. It is applied to unrelated groups to find out whether they have a common mean
Nature of Variable	Regression is applied to independent variables or fixed variables.	ANOVA is applied to variables which are random in nature
Types	Regression is mainly used in two forms. They are linear regression and multiple regression; the later is when the number of independent variables is more than one.	The three popular types of ANOVA are a random effect, fixed effect, and mixed effect.
Examples	A paint company uses solvent & monomers as its raw material, which is a derivative of crude; we can run a regression analysis between the price of that raw material and the price of Brent crude prices.	Suppose two separate research teams are researching different products not related to each other. ANOVA will help to find which one is providing better results.
Variables Used	Regression is applied to two sets of variables, one of them is the dependent variable, and the other one is the independent variable. The number of independent variables in regression can be one or more than one.	ANOVA is applied to variables from different, which not necessarily related to each other.
Use of the Test	Regression is mainly used by the practitioners or industry experts in order to make estimates or predictions for the dependent variable.	ANOVA is used to find a common mean between variables of different groups.
Errors	The predictions made by the regression analysis are not always desirable; that's because of the error term in a regression, this error term is also known as residual. In the case of regression, the number of the error term is one.	The number of errors in case ANOVA, unlike regression, is more than one.

Cook's distance as a modification tool is used to perform a regression analysis to estimate the influence of a data point by identifying outliers and views for predictor variables [153]. Cook's distance indicates the importance of each observation on the fitted response values, and data points having a large Cook's distance are considered as high force, which can garble the result and accuracy of regression [154]. In addition, backward elimination stepwise as another modification tool is performed through the regression analysis for making a reduced model based on significant factors [155]. The P-value or probability value in ANOVA is also a regression used to modify the analysis and determine the statistically significant (P-value < 0.05 has been selected as the cutoff) of factors and interactions [137], [156].

2.5.1.2 Probabilistic approaches

Probabilistic approaches refer to the incorporation of random variables and probability distributions to give a predictive model of an event by quantifying uncertainty [157], [158], [159]. The uncertainty arises because of limitations in the ability to observe the entire system, defective observations, limitations in the ability to model it, and feasibly even innate nondeterminism [160], [161]. The probabilistic approaches are a significant key to

reliability assessment and evaluating risk [162]. The probability concept builds the principal of reliability and risk engineering. Moreover, the probabilistic method provides the required techniques for risk characterization for complicated engineering systems [29], [163]. The probabilistic approach attempts to estimate the mean value and uncertainty bound related to a random variable, data trends, and quantitative information for comparison using mathematical parameters [164]. In predictive analytics, probabilistic approaches are utilized to estimate the likelihood of future occurrences of particular events. For example, TTF due to ECM is a specific event on PCBA as random variables to characterize failure data trend using correct distribution to present the data shape for quantification, and then predict and compare. Typically, three strategies are utilized to select a suitable and valid probabilistic distribution, which presents in Figure 2.21 [29], [163], [165], [166].

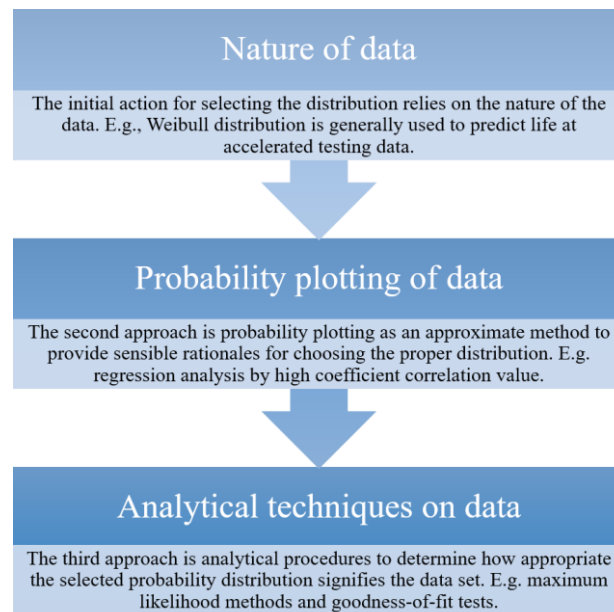


Figure 2.21 Diagram for determining the applicable probabilistic distribution.

Generally, Weibull, exponential, and lognormal distribution are used for a lifetime and TTF prediction in the different test plans, special in accelerated life testing of electronic components [167], [168], [169]. The lognormal distribution is used to model rather wide scatter data and predict various aspects of reliability engineering [168], [170], [171], [172]. The probability density function (PDF) in the lognormal distribution depends on location (mean) parameters (μ) and scale (variance) parameter (σ), is as follow [173], [174], [175]:

Literature review

$$f(t) = \frac{1}{\sigma t \sqrt{2\pi}} \cdot \text{Exp}\left(-\frac{1}{2} \left(\frac{\ln t - \mu}{\sigma}\right)^2\right)$$

The exponential distribution is broadly utilized in reliability engineering and describes electronic components' lifetime due to its simplicity and properties, like its constant failure rate [175], [176], [177]. The PDF of the single parameter (failure rate (λ)) exponential distribution is as follows [178]:

$$f(t) = \lambda \text{Exp}(-\lambda t)$$

One of the most appropriate and applicable distributions is Weibull distribution for the continuous events compared to other distributions owing to its flexibility and adaptability for modeling datasets with few failure data, as well as in the accelerated life tests is used explicitly for failure prediction [29], [179], [180], [181], [182]. The Weibull distribution provides more precise failure analysis and risk calculations with few number of samples without the necessity to catch a few more [183]. The PDF of the three-parameter (3P) Weibull distribution is showed as follows [29], [183], [184]:

$$f(t) = \frac{\beta}{\alpha - \theta} \left(\frac{t - \theta}{\alpha - \theta}\right)^{\beta-1} \cdot \text{Exp}\left[-\left(\frac{t - \theta}{\alpha - \theta}\right)^\beta\right]$$

Where θ (theta) is the location parameters, α (alfa) is a measure of the range and the characteristic value [29]. Further, β (beta) is the slope or shape parameter [185], [186]. Table 2.5 presents the effect of various beta values to determine failure rates. Figure 2.22 also shows the different PDFs of Weibull distribution at different beta values.

Table 2.5 Determination of failure rate by shape parameter changes [29].

When $\beta < 1 \Rightarrow$	Determines that the product has a decreasing failure rate.
When $\beta = 1 \Rightarrow$	Determines a constant failure rate. (exponential distribution)
When $\beta > 1 \Rightarrow$	Determines an increasing failure rate. (normal distribution when $\beta \sim 3.5$)

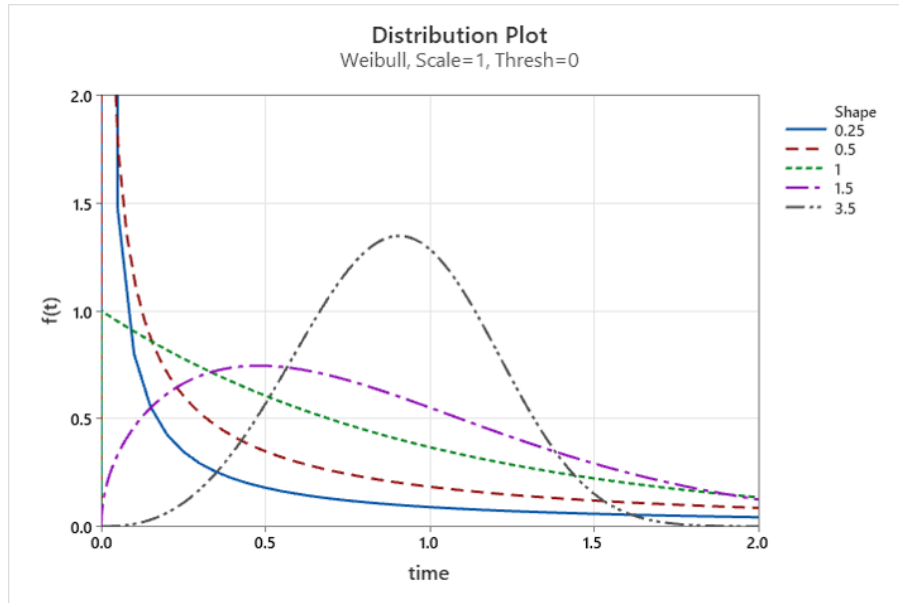


Figure 2.22 PDF of Weibull distribution at different beta values.

The CDF, which is the probability that a component will fail within time t , as well as the reliability function as the expectation of no failure operation for Weibull distribution, is calculated as follows [186], [187]:

$$F(t) = \int_0^t f(x) dx$$

After rearranging the equation,

$$F(t) = 1 - \exp\left[-\left(\frac{t}{\alpha}\right)^\beta\right]$$

$$R(t) = 1 - F(t) = \exp\left[-\left(\frac{t}{\alpha}\right)^\beta\right]$$

$$F(t) + R(t) = 1$$

The mean time to failure (MTTF) as the mean or average of TTF is the conventional parameter for characterizing the risk and reliability of the non-repairable component, and it obtains from the accumulated TTF of n components divided by the total number of failures. The inverse of the MTTF is commonly used to estimate the failure rate (λ) of components and vice versa. At Weibull distribution, λ can be described as [186], [187]:

$$\lambda = \frac{\beta}{\alpha} \cdot \left(\frac{t}{\alpha}\right)^{\beta-1}$$

Literature review

$$MTTF = 1/\lambda$$

2.5.1.3 Machine learning algorithms

Machine learning (ML) algorithms have been used for analytical purposes like predicting the outcome based on training input datasets without using explicit models [188]. Compared to other methods, ML algorithms provide more profound insights with; remarkable accuracy and ease of interpretation, managing the big data with good speed, mapping the nonlinear relationships, performing well with messy data (outliers and missing values), and visualizing multiple and complex interactions [189]. Supervised, unsupervised, and reinforcement learning are three main categories of ML algorithms, which are most widely used in different applications [190], [191], [192]. Figure 2.23 illustrates an overview of three main categorical ML algorithms, classes of supervised and unsupervised learning, with various applications for each one.

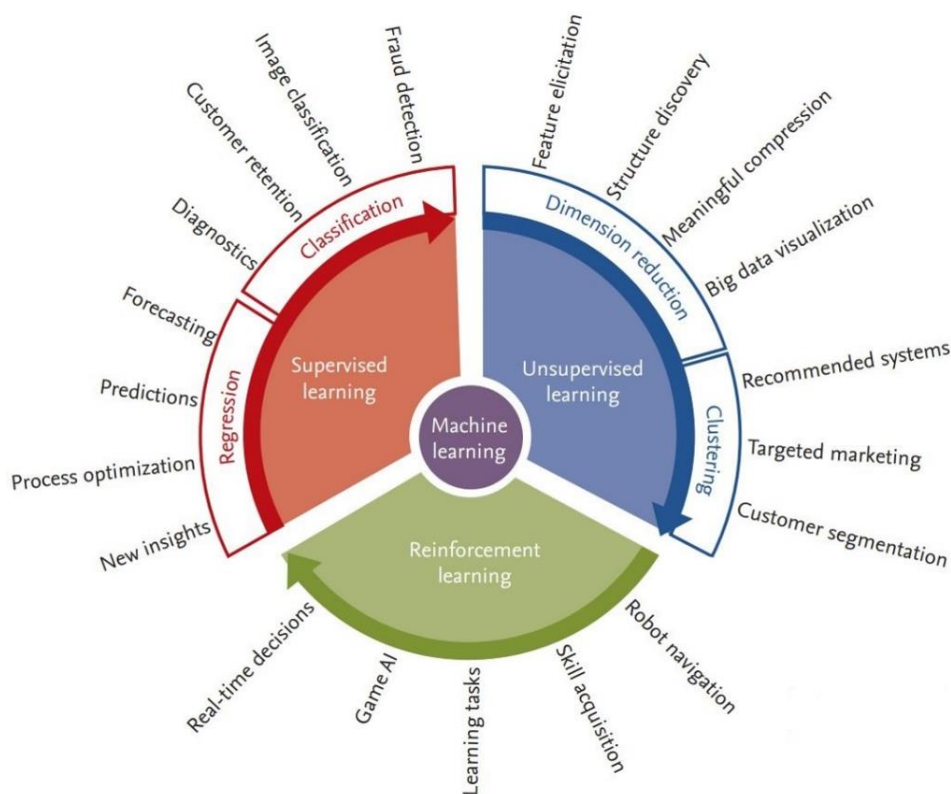


Figure 2.23 General overview of three main categorical ML algorithms, adapted from [190].

Supervised machine learning is the most common category of ML and provides the relationship between the input data that corresponds to the output data [193]. Meaning that, supervised learning has earlier information on the output for each input data and uses data that are well labeled [136], [194]. It makes a prediction model based on the training dataset

and assesses model performance using the test dataset [195]. There are two classes of supervised ML learning, including classification and regression [196]. The difference between them deals with output value, which for regression is a numerical and continuous value, whereas for classification is a categorical and discrete value [197]. In predictive analytics, ML algorithms are used to predict the future outcome from the input dataset based on its learned patterns. Figure 2.24 displays an overview of the most applicable supervised ML algorithms that are used in both classification and regression analysis. They included; k-nearest neighbors (k-NN), decision tree (DT), random forest (RF), support vector machines (SVM), and deep neural network (DNN), and in the following, they will express in detail [136], [198].

Unsupervised Learning is another category of ML algorithms and refers to identifying the structure and pattern of unlabeled data. Unsupervised learning is useful once just having accessibility to input data and training data which in some cases is hard to get or even unavailable [199], [200], [201]. Popular classes include dimension reduction and clustering for big data visualization and recommendations [201], [202].

Reinforcement learning is a reward-based category of ML in which the machine learns how to act in a specific environment (by using continuous observation gathered from the interaction with the environment) to get maximum rewards and minimize the risk [203], [204], [205]. Reinforcement learning is usually employed in robotics, autonomous vehicles, and artificial intelligent games [205], [206].

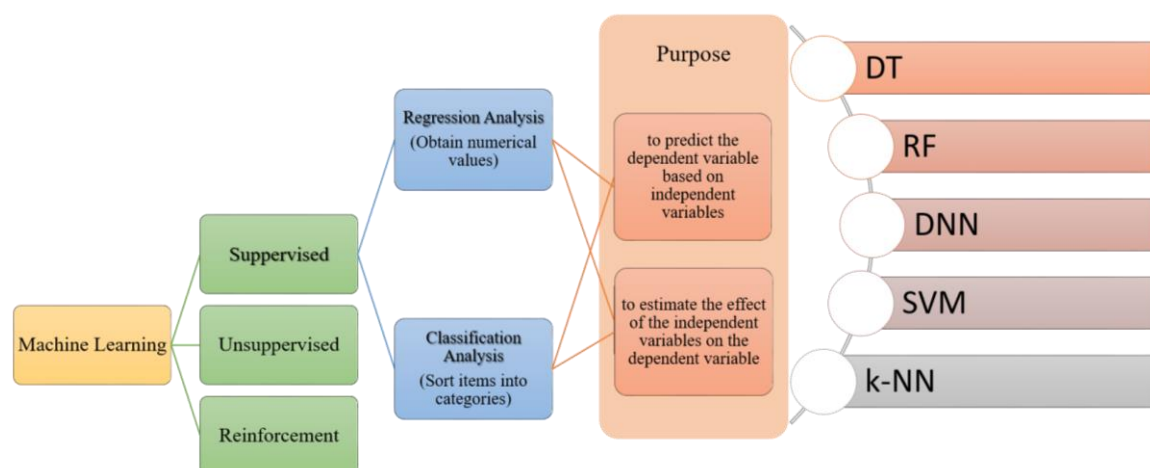


Figure 2.24 Overview of common ML algorithms utilized for both classification and regression analysis.

Literature review

2.5.1.3.1 *k-Nearest Neighbors*

The k-NN is a supervised ML algorithm used for both classification and regression analysis. k-NN recognizes the alike and nearest neighbors based on the preferences investigation [136], [207]. This algorithm consists of the K neighboring data in the feature space. The k denotes to the “number of nearest neighbors, whereas the nearest neighbor is a data point that is among the k closest data points to the data point under consideration” [136]. Two items are close if their distance is small [208]. When classifying a data point, k-NN votes overall labels of the neighboring data points, while k-NN regression predicts the value of the production variable by using a local average. K and weight are two primary hyperparameters of k-NN. K is the number of neighbors to evaluate, which is preferred have an odd value to avoid a tie between two or more class labels.

2.5.1.3.2 *Decision Tree*

The DT is a tree-based supervised ML algorithm, which can solve classification and regression issues [136]. DT algorithm by learning decision regulations deduced from the training dataset, forming decision nodes and leaf nodes branched from its root node [136]. The leaf nodes or terminal nodes are predefined as a category, and each branch from a decision node corresponds to a value of the corresponding attributes [209]. The main benefit of DT is that it is intuitive and simply understandable [136]. DT uses impurity measurement to find the optimal split on each node. Gini impurity is commonly used for classification-based DT, which gives the probability of misclassifying an observation [210]. DT has two significant hyperparameters; maximum depth of the tree and minimum samples to divide an internal node [136].

2.5.1.3.3 *Random Forest*

For splitting the root node for the DT method, having outlier variables and correlated independent variables might be ended up in an improper variable being chosen [208]. A random forest (RF) algorithm with the combination of multiple trees can overcome those challenges by making numerous DTs [211]. Actually, *random* denotes to the random sampling of data from the original experimental dataset, and *forest* relates to the construction of multiple DTs [211]. Where each DT focus on a sample set of the data. RF chooses samples accidentally and averages or votes over the predictions from all the DTs for classification or regression analysis [136]. The number of trees and the maximum

fraction of data features to be split for trees in the Gini criterion are two significant hyperparameters of RF [136].

2.5.1.3.4 Support Vector Machine

The SVM is a famous supervised ML algorithm used for classification as well as regression analysis [212]. It split up various target classes utilizing extreme or support vectors to make the hyperplane in multidimensional space [136]. By creating the best decision boundary, SVM can separate two or more classes with maximum margin to put new data points in the correct class [213]. Among the most key hyperparameters, gamma (γ), Kernel, and regularization (C) could be named, which directly influence the performance of SVM [136], [214]. Kernel functions are included in different kinds: linear, nonlinear, polynomial, sigmoid, and radial basis functions (RBFs). The penalty parameter is C [214], [215]. In order to control error, C is utilized [214], [215]. This study used RBF as the most preferred function because it makes appropriate separation once there is no former information of data [136], [216]. Besides, it is localized and has a limited response along the complete x-axis [217]. γ is defined as the effect of a probable line of separation or the speared of the RBF function [136]. The value of gamma varies from 0 to 1. The low γ means less curvature or far-off points taken into account [136]. C ranges from zero to infinity. The low C means low error and vis versa. A kernel hyperparameter is a mathematical function that manipulates the data by taking it as input and transforming it into the required form of processing data.

2.5.1.3.5 Artificial Neural Networks

The ANN includes the multilayer perceptron that supports understanding complex connections between inputs and outputs [136]. Mostly, an ANN contains three layers: the input layer, hidden layer, as well as output layer, each consisting of various nodes [136]. The input layer usually encloses the independent variables that are utilized to predict the output [136]. The hidden layer consisting of nodes like biological neuron connections is used to make sense of non-linearity and complicated relations to change the input variables into a higher-order function [211]. These layers are recognized as hidden since they are not observable as a network output. Deep learning originates from having multiple hidden layers [218]. In a regression, usually would be just one node in the output layer. In classification tasks, the output layer includes same number of nodes as classes that

Literature review

represent the dependent variables [219], while the output layer usually has one neuron (if the task is predicting one value). In the deep neural network (DNN) algorithm, the significant hyperparameters include the number of hidden layers and the number of neurons per each hidden layer [136].

2.6 Literature on the use of data analytics for corrosion data analysis and objective of present thesis

A usual data analytics process consists of three steps; the description of what and why happened and data collection, identification of data patterns and prediction, and making a prescription for the recommendation and reaction to evaluated and forecasted data to modify and decision-making. There are some data analysis of corrosion studies, related to metallic alloy corrosion rates [220], pitting corrosion [221], and corrosion resistance of steel [222]. However, some studies used data analytics process in predictive maintenance [223], and corrosion growth assessment [224]. Besides, only a limited studies has investigated, the data analytics process to detect, diagnose, and prevent impending failures in electronics [225], and used predictive analytics for detecting sensor corrosion failure [226]. Nonetheless, there is no clear discussion about data analytics, and especially predictive analytics, to forecast corrosion failures on PCBA surfaces. As the main objectives of the present PhD thesis, according to the different datasets of laboratory test results, the most important predictive analytics approaches from statistical, probabilistic, and machine learning models have been employed to predict numerical values of LCs and TTFs due to ECM failure, as well as categorical failure states of different conditions. In another word, related to the data analytics process, in this thesis, in the first step, plenty of PCB failure events in different corrosive conditions (composed of combined critical factors at different levels) occurred in the experimental tests using DOE and OFAT design are collected. Then the pattern of history data (experiments results), diagnosis, and various predictive models such as regression analysis, probabilistic distribution analysis, and different algorithms of machine learning technique in the second step are utilized to find the best prediction mode based on dataset, accuracy, limitations to prescribe a procedure of action to improve reliability and decrease failure risk in electronics.

References

- [1] R. Ambat, H. Conseil-Gudla, Improving intrinsic corrosion reliability of printed circuit board assembly, in: 2016 IEEE 18th Electron. Packag. Technol. Conf., IEEE, 2016: pp. 540–544. <https://doi.org/10.1109/EPTC.2016.7861538>.
- [2] S. Rastayesh, S. Bahrebar, F. Blaabjerg, D. Zhou, H. Wang, J.D. Sørensen, A system engineering approach using FMEA and bayesian network for risk analysis-a case study, *Sustain.* 12 (2020) 1–18. <https://doi.org/10.3390/SU12010077>.
- [3] M. Tencer, J.S. Moss, Humidity management of outdoor electronic equipment: methods, pitfalls, and recommendations, *IEEE Trans. Components Packag. Technol.* 25 (2002) 66–72. <https://doi.org/10.1109/6144.991177>.
- [4] U. Rathinavelu, M.S. Jellesen, R. Ambat, Effect of solder flux residue on the performance of silicone conformal coatings on printed circuit board assemblies, *Corros. Eng. Sci. Technol.* 48 (2013) 436–444. <https://doi.org/10.1179/1743278213Y.0000000096>.
- [5] H. Conseil-Gudla, Parametric study of interior climate in electronic device enclosures and corrosion reliability, Technical University of Denmark, 2017.
- [6] H. Conseil, M. Stendahl Jellesen, R. Ambat, Contamination profile on typical printed circuit board assemblies vs soldering process, *Solder. Surf. Mt. Technol.* 26 (2014) 194–202. <https://doi.org/10.1108/SSMT-03-2014-0007>.
- [7] K. Piotrowska, M.S. Jellesen, R. Ambat, Thermal decomposition of solder flux activators under simulated wave soldering conditions, *Solder. Surf. Mt. Technol.* 29 (2017) 133–143. <https://doi.org/10.1108/SSMT-01-2017-0003>.
- [8] R. Ambat, K. Piotrowska, *Humidity and Electronics: Corrosion Reliability Issues and Preventive Measures*, Elsevier, 2021. <https://doi.org/10.1016/B978-0-323-90853-5.00010-4>.
- [9] V. Cicek, *Corrosion Engineering*, John Wiley & Sons, Inc., Hoboken, NJ, USA, 2014. <https://doi.org/10.1002/9781118720837>.
- [10] Z. Huda, *Corrosion and Protection*, in: *Metall. Phys. Eng.*, CRC Press, 2020: pp. 231–259. <https://doi.org/10.1201/9780429265587-14>.
- [11] V. Verdingovas, L. Müller, M.S. Jellesen, F.B. Grumsen, R. Ambat, Effect of iodine on the corrosion of Au–Al wire bonds, *Corros. Sci.* 97 (2015) 161–171. <https://doi.org/10.1016/j.corsci.2015.05.003>.
- [12] K.R. DeVoe, S.J. Hoff, B.C. Ramirez, L.H. Baumgard, Climate Dependent Heat Stress Mitigation Modeling for Dairy Cattle Housing, in: 2017 Spokane, Washingt. July 16 - July 19, 2017, American Society of Agricultural and Biological Engineers, St. Joseph, MI, 2017. <https://doi.org/10.13031/aim.201700981>.
- [13] R. Ambat, K. Piotrowska, Factors determining water film buildup on surfaces and relevance to corrosion in electronics, in: *Humidity Electron.*, Elsevier, 2022: pp. 93–140. <https://doi.org/10.1016/B978-0-323-90853-5.00003-7>.
- [14] K. Piotrowska, Water film formation on PCBA surface - Investigation of aspects

Literature review

- contributing to premature corrosion failures and safety measures for electronics reliability improvement, Technical University of Denmark, 2018.
- [15] Y. Ko, C. Lee, Y. Kim, Y. Kim, Y.J. Yun, Y. Jun, Dew point temperature as an invariant replacement for relative humidity for advanced perovskite solar cell fabrication systems, *J. Mater. Chem. A*. 6 (2018) 20695–20701. <https://doi.org/10.1039/C8TA06689B>.
- [16] H.-J. Li, M.-H. Lo, J.-Y. Juang, J. Wang, C. Huang, Assessment of spatiotemporal dynamics of diurnal fog occurrence in subtropical montane cloud forests, *Agric. For. Meteorol.* 317 (2022) 108899. <https://doi.org/10.1016/j.agrformet.2022.108899>.
- [17] I. Humar, U. Hudomalj, A. Marinšek, M. Umberger, Optimizing the Power Usage of Anti-Sweat Heaters in Glass-Door Refrigerators According to the Dew Point, *Energies*. 15 (2022) 4601. <https://doi.org/10.3390/en15134601>.
- [18] M. Sieth, *Argus: A 16-Pixel Millimeter-Wave Spectrometer*, Stanford University, 2016.
- [19] M.H.B.M. Darus, M.H.B.A. Aziz, N.R. Ong, J.B. Alcaín, V. Retnasamy, PCBA depaneling stress minimization study, in: *AIP Conf. Proc.*, American Institute of Physics Inc., 2017: p. 020296. <https://doi.org/10.1063/1.5002490>.
- [20] R. Ambat, K. Piotrowska, Importance of PCBA cleanliness in humidity interaction with electronics, in: *Humidity Electron.*, Elsevier, 2022: pp. 141–196. <https://doi.org/10.1016/b978-0-323-90853-5.00005-0>.
- [21] M.S. Jellesen, P. Westermann, V. Verdingovas, P. Holm, R. Ambat, Relation Between PCBA Cleanliness and Climatic Reliability, in: *Core.Ac.Uk*, 2011.
- [22] S. Bahrebar, R. Ambat, Investigation of critical factors effect to predict leakage current and time to failure due to ECM on PCB under humidity, *Microelectron. Reliab.* 127 (2021) 114418. <https://doi.org/10.1016/j.microrel.2021.114418>.
- [23] S. Zhan, M.H. Azarian, M. Pecht, Reliability of Printed Circuit Boards Processed Using No-Clean Flux Technology in Temperature–Humidity–Bias Conditions, *IEEE Trans. Device Mater. Reliab.* 8 (2008) 426–434. <https://doi.org/10.1109/TDMR.2008.922908>.
- [24] K.S. Hansen, M.S. Jellesen, P. Moller, P.J.S. Westermann, R. Ambat, Effect of solder flux residues on corrosion of electronics, in: *2009 Annu. Reliab. Maintainab. Symp.*, IEEE, 2009: pp. 502–508. <https://doi.org/10.1109/RAMS.2009.4914727>.
- [25] V. Verdingovas, S. Joshy, M.S. Jellesen, R. Ambat, Analysis of surface insulation resistance related failures in electronics by circuit simulation, *Circuit World*. 43 (2017) 45–55. <https://doi.org/10.1108/CW-09-2016-0040>.
- [26] S. Zhan, M.H. Azarian, M. Pecht, Reliability of Printed Circuit Boards Processed Using No-Clean Flux Technology in Temperature–Humidity–Bias Conditions, *IEEE Trans. Device Mater. Reliab.* 8 (2008) 426–434. <https://doi.org/10.1109/TDMR.2008.922908>.
- [27] S. Zhan, M.H. Azarian, M.G. Pecht, Surface Insulation Resistance of Conformally Coated Printed Circuit Boards Processed With No-Clean Flux, *IEEE Trans. Electron. Packag. Manuf.* 29 (2006) 217–223. <https://doi.org/10.1109/TEPM.2006.882496>.
- [28] D. Minzari, *Investigation of Electronic Corrosion Mechanisms*, Technical University of Denmark, 2010.

- [29] S. Bahrebar, R. Ambat, Time to Failure Prediction on a Printed Circuit Board Surface Under Humidity Using Probabilistic Analysis, *J. Electron. Mater.* (2022) 1–19. <https://doi.org/10.1007/s11664-022-09668-7>.
- [30] M. Judd, K. Brindley, *Soldering in Electronics Assembly*, Elsevier, 1992. <https://doi.org/10.1016/C2013-0-01187-5>.
- [31] E. Guene, Solderability and reliability evolution of no clean solder fluxes for selective soldering, in: 2017 21st Eur. Microelectron. Packag. Conf. Exhib., IEEE, 2017: pp. 1–10. <https://doi.org/10.23919/EMPC.2017.8346874>.
- [32] V. Verdingovas, M.S. Jellesen, R. Rizzo, H. Conseil, R. Ambat, Impact of hygroscopicity and composition of solder flux residue on the reliability of PCBA under corrosive conditions, in: *EUROCORR*, 2013.
- [33] K. Piotrowska, F. Li, R. Ambat, Thermal decomposition of binary mixtures of organic activators used in no-clean fluxes and impact on PCBA corrosion reliability, *Solder. Surf. Mt. Technol.* 32 (2019) 93–103. <https://doi.org/10.1108/SSMT-05-2019-0020>.
- [34] V. Verdingovas, M.S. Jellesen, R. Ambat, Influence of sodium chloride and weak organic acids (flux residues) on electrochemical migration of tin on surface mount chip components, *Corros. Eng. Sci. Technol.* 48 (2013) 426–435. <https://doi.org/10.1179/1743278213Y.0000000078>.
- [35] M. Nasta, H.C. Peebles, A Model of the Solder Flux Reaction; Reactions at the Metal/ Metal Oxide/Electrolyte Solution Interface, *Circuit World.* 21 (1995) 10–13. <https://doi.org/10.1108/eb044043>.
- [36] B.A. Smith, L.J. Turbini, Characterizing the weak organic acids used in low solids fluxes, *J. Electron. Mater.* 28 (1999) 1299–1306. <https://doi.org/10.1007/s11664-999-0171-2>.
- [37] W.M. Haynes, D.R. Lide, T.J. Bruno, CRC Press, *CRC handbook of chemistry and physics: a ready-reference book of chemical and physical data*, *Choice Rev. Online.* 47 (2010) 47-3553-47–3553. <https://doi.org/10.5860/CHOICE.47-3553>.
- [38] T. Pannérec, Knowledge-Based Automatic Components Placement for Single-Layer PCB Layout, in: *Lect. Notes Artif. Intell. (Subseries Lect. Notes Comput. Sci., Springer, Berlin, Heidelberg, 2003: pp. 669–675.* https://doi.org/10.1007/978-3-540-45224-9_91.
- [39] V. Verdingovas, M.S. Jellesen, R. Ambat, Colorimetric visualization of tin corrosion: A method for early stage corrosion detection on printed circuit boards, *Microelectron. Reliab.* 73 (2017) 158–166. <https://doi.org/10.1016/j.microrel.2017.05.005>.
- [40] K. Piotrowska, M.S. Jellesen, R. Ambat, Water film formation on the PCBA surface and failure occurrence in electronics, in: 2018 IMAPS Nord. Conf. Microelectron. Packag., IEEE, 2018: pp. 72–76. <https://doi.org/10.23919/NORDPAC.2018.8423854>.
- [41] J. Niemann, S. Härter, C. Kästle, J. Franke, Challenges of the Miniaturization in the Electronics Production on the example of 01005 Components, in: *Tagungsband Des 2. Kongresses Montage Handhabung Ind., Springer Berlin Heidelberg, Berlin, Heidelberg, 2017: pp. 113–123.* https://doi.org/10.1007/978-3-662-54441-9_12.
- [42] V. Verdingovas, M.S. Jellesen, R. Ambat, Effect of pulsed voltage on electrochemical migration of tin in electronics, *J. Mater. Sci. Mater. Electron.* 26 (2015) 7997–8007.

Literature review

- <https://doi.org/10.1007/s10854-015-3454-9>.
- [43] H. Sriram, I. Jagadeeswaran, EU 2015/863: Restriction of Hazardous Substances (RoHS) - 3, in: *Med. Device Guidel. Regul. Handb.*, Springer International Publishing, Cham, 2022: pp. 297–307. https://doi.org/10.1007/978-3-030-91855-2_15.
- [44] C. Tong, *Process and Material Characterization in Printed Flexible Electronics*, in: *Springer Ser. Mater. Sci.*, Springer Science and Business Media Deutschland GmbH, 2022: pp. 53–117. https://doi.org/10.1007/978-3-030-79804-8_2.
- [45] Z.X. Guo, *Multiscale materials modelling*, Woodhead Publishing Limited, 2007. <https://doi.org/10.1533/9781845693374>.
- [46] W. Bolton, *The selection of materials*, in: *Eng. Mater.*, Elsevier, 1987: pp. 1–7. <https://doi.org/10.1016/B978-0-434-90169-2.50004-0>.
- [47] R.K. Ulrich, W.D. Brown, *Advanced Electronic Packaging*, IEEE, Hoboken, NJ ;[Chichester] :, 2006. <https://doi.org/10.1109/9780471754503>.
- [48] E. Cunaj, P.S. Petrou, G.D. Kaprou, S.E. Kakabakos, E. Gogolides, A. Tserepi, Stable hydrophilization of FR4 and polyimide-based substrates implemented in microfluidics-on-PCB, *Surf. Coatings Technol.* 334 (2018) 292–299. <https://doi.org/10.1016/j.surfcoat.2017.11.039>.
- [49] A. Eshkeiti, A.S.G. Reddy, S. Emamian, B.B. Narakathu, M. Joyce, M. Joyce, P.D. Fleming, B.J. Bazuin, M.Z. Atashbar, Screen Printing of Multilayered Hybrid Printed Circuit Boards on Different Substrates, *IEEE Trans. Components, Packag. Manuf. Technol.* 5 (2015) 415–421. <https://doi.org/10.1109/TCPMT.2015.2391012>.
- [50] E. Juntunen, A. Sitomaniemi, O. Tapaninen, R. Persons, M. Challingsworth, V. Heikkinen, Thermal Performance Comparison of Thick-Film Insulated Aluminum Substrates With Metal Core PCBs for High-Power LED Modules, *IEEE Trans. Components, Packag. Manuf. Technol.* 2 (2012) 1957–1964. <https://doi.org/10.1109/TCPMT.2012.2206390>.
- [51] D.N. Light, J.R. Wilcox, Process considerations in the fabrication of Teflon printed circuit boards, in: *1994 Proceedings. 44th Electron. Components Technol. Conf.*, IEEE, 1994: pp. 542–549. <https://doi.org/10.1109/ECTC.1994.367540>.
- [52] M. Adamek, P. Schnederle, I. Szendiuch, L. Lipavsky, The properties comparison of solder joints on ceramic and FR-4 substrates, in: *2012 4th Electron. Syst. Technol. Conf.*, IEEE, 2012: pp. 1–5. <https://doi.org/10.1109/ESTC.2012.6542191>.
- [53] I. Aggarwal, M.R. Tripathy, S. Pandey, A Novel Design of Fractal Antenna: Effect of Different Dielectric Substrate Materials, in: *Springer Proc. Phys.*, Springer Science and Business Media, LLC, 2017: pp. 521–526. https://doi.org/10.1007/978-3-319-29096-6_67.
- [54] E. Ozkan, N. Elginöz, F. Germirli Babuna, Life cycle assessment of a printed circuit board manufacturing plant in Turkey, *Environ. Sci. Pollut. Res.* 25 (2018) 26801–26808. <https://doi.org/10.1007/s11356-017-0280-z>.
- [55] P.L. Teh, M. Jaafar, H.M. Akil, K.N. Seetharamu, A.N.R. Wagiman, K.S. Beh, Thermal and mechanical properties of particulate fillers filled epoxy composites for electronic packaging application, *Polym. Adv. Technol.* 19 (2008) 308–315. <https://doi.org/10.1002/pat.1014>.

- [56] F. Fehrer, G. Haddick, Thermal-mechanical Processing and Repairability Observations for FR-4, Cyanate Ester and Cyanate Ester/Epoxy Blend PCB Substrates, *Circuit World*. 19 (1993) 39–44. <https://doi.org/10.1108/eb046201>.
- [57] L. Vigna, I. Babaei, R. Garg, G. Belingardi, D.S. Paolino, A. Calzolari, G. Galizia, An innovative fixture for testing the crashworthiness of composite materials, *Frat. Ed Integrità Strutt.* 15 (2020) 76–87. <https://doi.org/10.3221/IGF-ESIS.55.06>.
- [58] E.D. Weil, S. Levchik, A Review of Current Flame Retardant Systems for Epoxy Resins, *J. Fire Sci.* 22 (2004) 25–40. <https://doi.org/10.1177/0734904104038107>.
- [59] B. Song, M.H. Azarian, M.G. Pecht, Impact of dust on printed circuit assembly reliability, in: *IPC APEX EXPO 2012*, 2012: pp. 1643–1659.
- [60] E.M. Dede, P. Schmalenberg, T. Nomura, M. Ishigaki, Design of Anisotropic Thermal Conductivity in Multilayer Printed Circuit Boards, *IEEE Trans. Components, Packag. Manuf. Technol.* 5 (2015) 1763–1774. <https://doi.org/10.1109/TCPMT.2015.2473103>.
- [61] A. Konda, A. Rau, M.A. Stoller, J.M. Taylor, A. Salam, G.A. Pribil, C. Argyropoulos, S.A. Morin, Soft Microreactors for the Deposition of Conductive Metallic Traces on Planar, Embossed, and Curved Surfaces, *Adv. Funct. Mater.* 28 (2018) 1803020. <https://doi.org/10.1002/adfm.201803020>.
- [62] K. Piotrowska, R.U. Din, M.S. Jellesen, R. Ambat, Effect of Solder Mask Surface Chemistry and Morphology on the Water Layer Formation Under Humid Conditions, *IEEE Trans. Components, Packag. Manuf. Technol.* 8 (2018) 1756–1768. <https://doi.org/10.1109/TCPMT.2018.2792047>.
- [63] C. Hofmeister, S. Maaß, T. Fladung, K. Thiel, B. Mayer, Influence of copper layer on epoxy acrylate based solder mask surface chemistry and the effect on epoxy adhesion, *Appl. Adhes. Sci.* 3 (2015) 12. <https://doi.org/10.1186/s40563-015-0040-6>.
- [64] P.T. Vianco, An overview of surface finishes and their role in printed circuit board solderability and solder joint performance, *Circuit World*. 25 (1999) 6–24. <https://doi.org/10.1108/03056129910244518>.
- [65] A. Siewiorek, A. Kudyba, N. Sobczak, M. Homa, Z. Huber, Z. Adamek, J. Wojewoda-Budka, Effects of PCB Substrate Surface Finish and Flux on Solderability of Lead-Free SAC305 Alloy, *J. Mater. Eng. Perform.* 22 (2013) 2247–2252. <https://doi.org/10.1007/s11665-013-0492-4>.
- [66] M. Bacior, N. Sobczak, A. Siewiorek, A. Kudyba, M. Homa, R. Nowak, M. Dziula, S. Masłoń, Effects of PCB Substrate Surface Finish, Flux, and Phosphorus Content on Ionic Contamination, *J. Mater. Eng. Perform.* 24 (2015) 754–758. <https://doi.org/10.1007/s11665-014-1357-1>.
- [67] A. Ourdjini, M.A. Azmah Hanim, I.S.R. Aisha, Y.T. Chin, Effect of surface finish metallurgy on intermetallic compounds during soldering with tin-silver-copper solders, in: *2008 33rd IEEE/CPMT Int. Electron. Manuf. Technol. Conf.*, IEEE, 2008: pp. 1–4. <https://doi.org/10.1109/IEMT.2008.5507773>.
- [68] M.-S. Kim, H. Nishikawa, Thermal stability of electroless nickel/immersion gold surface finish for direct bond copper, in: *Proc. 5th Electron. Syst. Technol. Conf.*, IEEE, 2014: pp. 1–4. <https://doi.org/10.1109/ESTC.2014.6962845>.

Literature review

- [69] M. Arra, D. Shangguan, D. Xie, J. Sundelin, T. Lepistö, E. Ristolainen, Study of immersion silver and tin printed-circuit-board surface finishes in lead-free solder applications, *J. Electron. Mater.* 33 (2004) 977–990. <https://doi.org/10.1007/s11664-004-0025-x>.
- [70] M. Montazer, T. Harifi, Nanocoating and lamination, in: *Nanofinishing Text. Mater.*, Elsevier, 2018: pp. 95–107. <https://doi.org/10.1016/B978-0-08-101214-7.00007-8>.
- [71] San Francisco Circuits, PCB Surface Finishes, [Www.Sfcircuits.Com](http://www.sfcircuits.com). (2022).
- [72] J. Nable, PCB Surface Finishes: A General Review, [Www.Smtnet.Com](http://www.smtnet.com). (2014).
- [73] R. Berni, M. Catelani, C. Fiesoli, V.L. Scarano, A Comparison of Alloy-Surface Finish Combinations Considering Different Component Package Types and Their Impact on Soldering Reliability, *IEEE Trans. Reliab.* 65 (2016) 272–281. <https://doi.org/10.1109/TR.2015.2455973>.
- [74] C. Key Chung, F. Mustapha, F. Hua, R. Aspandiar, An assessment of lead free solder (Sn3.7Ag0.8Cu) wettability, in: *4th Electron. Packag. Technol. Conf. 2002.*, IEEE, 2002: pp. 1–5. <https://doi.org/10.1109/EPTC.2002.1185587>.
- [75] K.M. Ming, A. Lee, Evaluation of laminates in Pb-free HASL process and Pb-free assembly environment, in: *IPC APEX EXPO 2012*, 2012: pp. 780–803.
- [76] B. Medgyes, B. Illes, Investigating SIR of Cu, OSP, iSn and HASL surface finishes by THB test, in: *2011 IEEE 17th Int. Symp. Des. Technol. Electron. Packag.*, IEEE, 2011: pp. 345–348. <https://doi.org/10.1109/SIITME.2011.6102749>.
- [77] A. Wright, Printed circuit board surface finishes-advantages printed circuit board surface finishes-advantages and disadvantages and disadvantages, [Www.Epectec.Com](http://www.epectec.com). (2022).
- [78] Wei-Shan Chao, Wen-Hao Wang, Tzeng-Cherng Luo, Te-Chun Huang, Meng-Chieh Liao, Tzu-Hsia Wei, The comparison on the corrosion resistance of different kinds of PCB surface finishing: OSP, LF HASL and ENIG, in: *2012 7th Int. Microsystems, Packag. Assem. Circuits Technol. Conf.*, IEEE, 2012: pp. 159–162. <https://doi.org/10.1109/IMPACT.2012.6420301>.
- [79] F. Perdigones, J. Quero, Printed Circuit Boards: The Layers' Functions for Electronic and Biomedical Engineering, *Micromachines.* 13 (2022) 460. <https://doi.org/10.3390/mi13030460>.
- [80] J.J. Steppan, J.A. Roth, L.C. Hall, D.A. Jeannotte, S.P. Carbone, A Review of Corrosion Failure Mechanisms during Accelerated Tests: Electrolytic Metal Migration, *J. Electrochem. Soc.* 134 (1987) 175–190. <https://doi.org/10.1149/1.2100401>.
- [81] J.M. Shah, R. Anand, S. Saini, R. Cyriac, D. Agonafer, P. Singh, M. Kaler, Development of a Technique to Measure Deliquescent Relative Humidity of Particulate Contaminants and Determination of the Operating Relative Humidity of a Data Center, in: *ASME 2019 Int. Tech. Conf. Exhib. Packag. Integr. Electron. Photonic Microsystems*, American Society of Mechanical Engineers, 2019. <https://doi.org/10.1115/IPACK2019-6601>.
- [82] F. Li, Solder flux chemistry and climatic reliability of electronics : optimization of flux chemistry for robust performance, Technical University of Denmark, 2021.
- [83] L.J. Mauer, L.S. Taylor, Water-Solids Interactions: Deliquescence, *Annu. Rev. Food Sci.*

- Technol. 1 (2010) 41–63. <https://doi.org/10.1146/annurev.food.080708.100915>.
- [84] R. Ambat, H. Conseil-Gudla, V. Verdingovas, Corrosion in Electronics, in: *Encycl. Interfacial Chem.*, Elsevier, 2018: pp. 134–144. <https://doi.org/10.1016/B978-0-12-409547-2.13437-7>.
- [85] G. Sarkar, Y.F. Chong, P.A. Collier, A study of the factors affecting surface insulation resistance measurements, *J. Mater. Sci. Lett.* 17 (1998) 1963–1965. <https://doi.org/10.1023/A:1006635917381>.
- [86] P.-E. Tegehall, Impact of Humidity and Contamination on Surface Insulation Resistance and Electrochemical Migration, in: *ELFNET B. Fail. Mech. Test. Methods, Qual. Issues Lead-Free Solder Interconnects*, Springer London, London, 2011: pp. 227–253. https://doi.org/10.1007/978-0-85729-236-0_10.
- [87] V. Verdingovas, M.S. Jellesen, R. Ambat, Impact of NaCl contamination and climatic conditions on the reliability of printed circuit board assemblies, *IEEE Trans. Device Mater. Reliab.* 14 (2014) 42–51. <https://doi.org/10.1109/TDMR.2013.2293792>.
- [88] X. Zhong, L. Chen, B. Medgyes, Z. Zhang, S. Gao, L. Jakab, Electrochemical migration of Sn and Sn solder alloys: a review, *RSC Adv.* 7 (2017) 28186–28206. <https://doi.org/10.1039/C7RA04368F>.
- [89] W. Lawson, *The effects of design and environmental factors on the reliability of electronic products*, University of Salford, 2007.
- [90] S.J. Krumbein, Metallic electromigration phenomena, *IEEE Trans. Components, Hybrids, Manuf. Technol.* 11 (1988) 5–15. <https://doi.org/10.1109/33.2957>.
- [91] C. Matzner, K. Feldmann, Adapted strategies for dew condensation testing to evaluate the reliability of lead free surface finishes, in: *2009 IEEE Int. Reliab. Phys. Symp.*, IEEE, 2009: pp. 343–349. <https://doi.org/10.1109/IRPS.2009.5173276>.
- [92] C. Schimpf, K. Feldmann, C. Matzner, A. Steinke, Failure of electronic devices due to condensation, *Microsyst. Technol.* 15 (2009) 123–127. <https://doi.org/10.1007/s00542-008-0643-y>.
- [93] X. Zhong, G. Zhang, Y. Qiu, Z. Chen, W. Zou, X. Guo, In situ study the dependence of electrochemical migration of tin on chloride, *Electrochem. Commun.* 27 (2013) 63–68. <https://doi.org/10.1016/j.elecom.2012.11.010>.
- [94] M. Pecht, C. Hilman, E. Bumiller, Electrochemical migration on HASL plated FR-4 printed circuit boards, *J Surf Mt Technol.* (2004).
- [95] NIPC-TR-476A, Electrochemical migration: electrically induced failures in printed wiring assemblies, in: *Inst. Interconnecting Packag. Electron. Circuits*, 1997.
- [96] S.J. Krumbein, Electrolytic models for metallic electromigration failure mechanisms, *IEEE Trans. Reliab.* 44 (1995) 539–549. <https://doi.org/10.1109/24.475971>.
- [97] M. Zamanzadeh, S.L. Meilink, G.W. Warren, P. Wynblatt, B. Yan, Electrochemical Examination of Dendritic Growth on Electronic Devices in HCl Electrolytes, *CORROSION.* 46 (1990) 665–671. <https://doi.org/10.5006/1.3585165>.

Literature review

- [98] IPC, Surface Insulation Resistance Handbook, in: IPC-9201A, IPC, 2007.
- [99] M. Ferrill, M. Kelly, N. Ranadive, C. Ndiaye, J. Bielick, S. Bagheri, C. International, The ipc-b-52 sir test vehicle : a discussion of the current test vehicle design and possible modifications for the future, in: Orig. Publ. SMTA Int. Conf., 2012.
- [100] Association Connecting Electronics Industries, Design Guidelines for Reliable Surface Mount Technology Printed Board Assemblies (IPC-D-279), 1996.
- [101] S. Zhan, Surface insulation resistance of conformally coated printed circuit boards processed with no-clean flux, *Ieee Trans. Electron. Packag. Manuf.* 29 (2006) 217–223. <https://doi.org/10.1109/TEPM.2006.882496>.
- [102] P. Burton, P. Footner, D. Prichard, B. Richards, C. Hunt, Surface Insulation Resistance Measurements: A Review of the Various SIR Parameters NPL REPORT CMMT (A) 48, 1996.
- [103] G. Grossmann, C. Zardini, eds., The ELFNET Book on Failure Mechanisms, Testing Methods, and Quality Issues of Lead-Free Solder Interconnects, Springer London, London, 2011. <https://doi.org/10.1007/978-0-85729-236-0>.
- [104] P. Kamat, L. Spilar, J. Yeager, SIR system design ensures test accuracy, *Electron. Packag. Prod.* 35 (1995) 60–63.
- [105] Q.N. Xiao, F. Grunwald, K. Carlson, Surface Leakage Current (SLC) Methodology for Electrochemical Migration Evaluation, *Circuit World.* 23 (1997) 6–10. <https://doi.org/10.1108/03056129710370240>.
- [106] T. Kerekes, D. Sera, L. Mathe, Leakage current measurement in transformerless PV inverters, in: 2012 13th Int. Conf. Optim. Electr. Electron. Equip., IEEE, 2012: pp. 887–892. <https://doi.org/10.1109/OPTIM.2012.6231835>.
- [107] X. He, L. Zhou, J. Shen, A study for a typical leakage failure of PCBA with no-cleaning process, in: 2016 17th Int. Conf. Electron. Packag. Technol., IEEE, 2016: pp. 53–56. <https://doi.org/10.1109/ICEPT.2016.7583088>.
- [108] K. Piotrowska, M. Grzelak, R. Ambat, No-Clean Solder Flux Chemistry and Temperature Effects on Humidity-Related Reliability of Electronics, *J. Electron. Mater.* 48 (2019) 1207–1222. <https://doi.org/10.1007/s11664-018-06862-4>.
- [109] H. Conseil, V. Verdingovas, M.S. Jellesen, R. Ambat, Decomposition of no-clean solder flux systems and their effects on the corrosion reliability of electronics, *J. Mater. Sci. Mater. Electron.* 27 (2016) 23–32. <https://doi.org/10.1007/s10854-015-3712-x>.
- [110] D. Ferrero, A. Lanzini, P. Leone, M. Santarelli, DOE Methodologies for Analysis of Large SOFC Systems, in: CISM Int. Cent. Mech. Sci. Courses Lect., Springer International Publishing, 2017: pp. 265–289. https://doi.org/10.1007/978-3-319-46146-5_7.
- [111] A. Raychaudhuri, M. Behera, Review of the Process Optimization in Microbial Fuel Cell using Design of Experiment Methodology, *J. Hazardous, Toxic, Radioact. Waste.* 24 (2020) 04020013. [https://doi.org/10.1061/\(ASCE\)HZ.2153-5515.0000503](https://doi.org/10.1061/(ASCE)HZ.2153-5515.0000503).
- [112] T. Berling, P. Runeson, Efficient evaluation of multifactor dependent system performance using fractional factorial design, *IEEE Trans. Softw. Eng.* 29 (2003) 769–781.

- <https://doi.org/10.1109/TSE.2003.1232283>.
- [113] B.Y. Gajera, D.A. Shah, R.H. Dave, Development of an amorphous nanosuspension by sonoprecipitation-formulation and process optimization using design of experiment methodology, *Int. J. Pharm.* 559 (2019) 348–359. <https://doi.org/10.1016/j.ijpharm.2019.01.054>.
- [114] M.J. Anderson, P.J. Whitcomb, *DOE Simplified*, Productivity Press, 2017. <https://doi.org/10.1201/b18479>.
- [115] T.P. Ryan, *Design and Analysis of Experiments*, in: *Mod. Eng. Stat.*, John Wiley & Sons, Inc., Hoboken, NJ, USA, 2007: pp. 382–440. <https://doi.org/10.1002/9780470128442.ch12>.
- [116] K. Hinkelmann, *Design and Analysis of Experiments*, John Wiley & Sons, Inc., Hoboken, NJ, USA, 2012. <https://doi.org/10.1002/9781118147634>.
- [117] Martin Tanco; Elisabeth Viles; Laura Ilzarbe; Maria Jesus Alvarez, *Manufacturing Industries Need Design of Experiments (DoE)*, in: *World Congr. Eng.*, 2007: p. 33.
- [118] Y.M. Kolekar, Understanding of DoE and its advantages in Pharmaceutical development as per QbD Approach, *Asian J. Pharm. Technol.* 9 (2019) 271. <https://doi.org/10.5958/2231-5713.2019.00045.X>.
- [119] D. Nordstokke, S.M. Colp, *Factorial Design*, in: *Encycl. Qual. Life Well-Being Res.*, Springer Netherlands, Dordrecht, 2014: pp. 2144–2145. https://doi.org/10.1007/978-94-007-0753-5_982.
- [120] E. Brittain, J. Wittes, Factorial designs in clinical trials: The effects of non-compliance and subadditivity, *Stat. Med.* 8 (1989) 161–171. <https://doi.org/10.1002/sim.4780080204>.
- [121] C.R.T. Tarley, G. Silveira, W.N.L. dos Santos, G.D. Matos, E.G.P. da Silva, M.A. Bezerra, M. Miró, S.L.C. Ferreira, *Chemometric tools in electroanalytical chemistry: Methods for optimization based on factorial design and response surface methodology*, *Microchem. J.* 92 (2009) 58–67. <https://doi.org/10.1016/j.microc.2009.02.002>.
- [122] C.-H. Wang, H.-Y. Cheng, Y.-T. Deng, Using Bayesian belief network and time-series model to conduct prescriptive and predictive analytics for computer industries, *Comput. Ind. Eng.* 115 (2018) 486–494. <https://doi.org/10.1016/j.cie.2017.12.003>.
- [123] A.K. Sharma, D.M. Sharma, N. Purohit, S.K. Rout, S.A. Sharma, *Analytics Techniques: Descriptive Analytics, Predictive Analytics, and Prescriptive Analytics*, in: *EAI/Springer Innov. Commun. Comput.*, Springer Science and Business Media Deutschland GmbH, 2022: pp. 1–14. https://doi.org/10.1007/978-3-030-82763-2_1.
- [124] D. Roy, R. Srivastava, M. Jat, M.S. Karaca, *A Complete Overview of Analytics Techniques: Descriptive, Predictive, and Prescriptive*, in: *EAI/Springer Innov. Commun. Comput.*, Springer Science and Business Media Deutschland GmbH, 2022: pp. 15–30. https://doi.org/10.1007/978-3-030-82763-2_2.
- [125] M. Fleckenstein, L. Fellows, *Modern Data Strategy*, Springer International Publishing, Cham, 2018. <https://doi.org/10.1007/978-3-319-68993-7>.
- [126] W.E. Nagel, T. Ludwig, *Data Analytics*, *Inform. Spektrum.* 42 (2020) 385–386. <https://doi.org/10.1007/s00287-019-01231-9>.

Literature review

- [127] D. Delen, H. Demirkan, Data, information and analytics as services, *Decis. Support Syst.* 55 (2013) 359–363. <https://doi.org/10.1016/j.dss.2012.05.044>.
- [128] K. Lepenioti, A. Bousdekis, D. Apostolou, G. Mentzas, Prescriptive analytics: Literature review and research challenges, *Int. J. Inf. Manage.* 50 (2020) 57–70. <https://doi.org/10.1016/j.ijinfomgt.2019.04.003>.
- [129] R. Soltanpoor, T. Sellis, Prescriptive Analytics for Big Data, in: *Lect. Notes Comput. Sci. (Including Subser. Lect. Notes Artif. Intell. Lect. Notes Bioinformatics)*, Springer Verlag, 2016: pp. 245–256. https://doi.org/10.1007/978-3-319-46922-5_19.
- [130] H. Kaur, A. Phutela, Commentary upon descriptive data analytics, in: *2018 2nd Int. Conf. Inven. Syst. Control, IEEE, 2018: pp. 678–683*. <https://doi.org/10.1109/ICISC.2018.8398884>.
- [131] E. V. Burnaev, Algorithmic Foundations of Predictive Analytics in Industrial Engineering Design, *J. Commun. Technol. Electron.* 64 (2019) 1485–1492. <https://doi.org/10.1134/s1064226919120039>.
- [132] S. Stoyanov, M. Ahsan, C. Bailey, T. Wotherspoon, C. Hunt, Predictive analytics methodology for smart qualification testing of electronic components, *J. Intell. Manuf.* 30 (2019) 1497–1514. <https://doi.org/10.1007/s10845-018-01462-9>.
- [133] K.J. Harris, H. Franchino-Olsen, Predictive Analytics, in: *Paths to Prev. Detect. Hum. Traffick.*, IGI Global, 2022: pp. 85–105. <https://doi.org/10.4018/978-1-6684-3926-5.ch005>.
- [134] P. Grover, A.K. Kar, Big Data Analytics: A Review on Theoretical Contributions and Tools Used in Literature, *Glob. J. Flex. Syst. Manag.* 18 (2017) 203–229. <https://doi.org/10.1007/s40171-017-0159-3>.
- [135] S. Poornima, M. Pushpalatha, A survey of predictive analytics using big data with data mining, *Int. J. Bioinform. Res. Appl.* 14 (2018) 269. <https://doi.org/10.1504/IJBRA.2018.092697>.
- [136] S. Bahrebar, S. Homayoun, R. Ambat, Using Machine Learning Algorithms to Predict Failure on the PCB Surface under Corrosive Conditions, *Corros. Sci.* (2022) 110500. <https://doi.org/10.1016/J.CORSCI.2022.110500>.
- [137] R. Winters, A. Winters, R.A.-O. Journal, U. 2010, Statistics: a brief overview, *Ochsner J.* 10 (2010) 213–216.
- [138] Z. Ali, Sb. Bhaskar, Basic statistical tools in research and data analysis, *Indian J. Anaesth.* 60 (2016) 662. <https://doi.org/10.4103/0019-5049.190623>.
- [139] B. Quinto, *Next-Generation Machine Learning with Spark*, Apress, Berkeley, CA, 2020. <https://doi.org/10.1007/978-1-4842-5669-5>.
- [140] J.S. Armstrong, *Illusions in Regression Analysis*, SSRN Electron. J. (2011). <https://doi.org/10.2139/ssrn.1969740>.
- [141] K. Hinkelmann, *Design and Analysis of Experiments*, John Wiley & Sons, Inc., Hoboken, NJ, USA, 2012. <https://doi.org/10.1002/9781118147634>.
- [142] S. Weisberg, Linear Hypothesis: Regression (Basics), in: *Int. Encycl. Soc. Behav. Sci.*,

- Elsevier, 2001: pp. 8884–8888. <https://doi.org/10.1016/B0-08-043076-7/00454-X>.
- [143] D. Chanal, N. Yousfi Steiner, R. Petrone, D. Chamagne, M.-C. Péra, Online Diagnosis of PEM Fuel Cell by Fuzzy C-Means Clustering, in: *Encycl. Energy Storage*, Elsevier, 2022: pp. 359–393. <https://doi.org/10.1016/B978-0-12-819723-3.00099-8>.
- [144] F.A. Ardelean, Case study using analysis of variance to determine groups' variations, *MATEC Web Conf.* 126 (2017) 04008. <https://doi.org/10.1051/mateconf/201712604008>.
- [145] T. Karchiyappan, R.R. Karri, Process Optimization and Modeling of Hydraulic Fracturing Process Wastewater Treatment Using Aerobic Mixed Microbial Reactor via Response Surface Methodology, in: *Soft Comput. Tech. Solid Waste Wastewater Manag.*, Elsevier, 2021: pp. 351–363. <https://doi.org/10.1016/B978-0-12-824463-0.00023-9>.
- [146] A.M. McIntosh, M. Sharpe, S.M. Lawrie, Research methods, statistics and evidence-based practice, in: *Companion to Psychiatr. Stud.*, Elsevier, 2010: pp. 157–198. <https://doi.org/10.1016/B978-0-7020-3137-3.00009-7>.
- [147] C. Angelini, Regression Analysis, in: *Encycl. Bioinforma. Comput. Biol.*, Elsevier, 2019: pp. 722–730. <https://doi.org/10.1016/B978-0-12-809633-8.20360-9>.
- [148] V. Kumar, M.L. Garg, Predictive Analytics: A Review of Trends and Techniques, *Artic. Int. J. Comput. Appl.* 182 (2018) 975–8887. <https://doi.org/10.5120/ijca2018917434>.
- [149] K.L. Cottingham, J.T. Lennon, B.L. Brown, Regression versus ANOVA – response, *Front. Ecol. Environ.* 3 (2005) 358. <https://doi.org/10.2307/3868583>.
- [150] R.A. Fisher, *Statistical Methods for Research Workers*, in: *Springer Ser. Stat. Perspect. Stat.*, Springer, New York, NY, 1992: pp. 66–70. https://doi.org/10.1007/978-1-4612-4380-9_6.
- [151] G. Gaddis, Advanced biostatistics: Chi-square, ANOVA, regression, and multiple regression, in: *Doing Res. Emerg. Acute Care Mak. Order Out Chaos*, John Wiley & Sons, Ltd, Chichester, UK, 2015: pp. 213–222. <https://doi.org/10.1002/9781118643440.ch32>.
- [152] M. Thakur, Regression vs ANOVA | Top 7 Difference (with Infographics), *Wallstreetmojo.Com.* (n.d.). <https://www.wallstreetmojo.com/regression-vs-anova/>.
- [153] R.D. Cook, Influential Observations in Linear Regression, *J. Am. Stat. Assoc.* 74 (1979) 169. <https://doi.org/10.2307/2286747>.
- [154] M.G. Kim, A cautionary note on the use of Cook's distance, *Commun. Stat. Appl. Methods.* 24 (2017) 317–324. <https://doi.org/10.5351/CSAM.2017.24.3.317>.
- [155] D. Dunkler, M. Plischke, K. Leffondré, G. Heinze, Augmented Backward Elimination: A Pragmatic and Purposeful Way to Develop Statistical Models, *PLoS One.* 9 (2014) e113677. <https://doi.org/10.1371/journal.pone.0113677>.
- [156] T. Sellke, M.J. Bayarri, J.O. Berger, Calibration of ρ Values for Testing Precise Null Hypotheses, *Am. Stat.* 55 (2001) 62–71. <https://doi.org/10.1198/000313001300339950>.
- [157] F.S. Chaghaghi, P. Billingsley, Probability and Measure, *Stat.* 35 (1986) 561. <https://doi.org/10.2307/2987970>.
- [158] J. Spencer, The Probabilistic Method, in: *Graphs & Digraphs*, Chapman and Hall/CRC,

Literature review

- 2015: pp. 555–574. <https://doi.org/10.1201/b19731-23>.
- [159] E.C. Martínez, M.D. Cristaldi, R.J. Grau, Dynamic optimization of bioreactors using probabilistic tendency models and Bayesian active learning, *Comput. Chem. Eng.* 49 (2013) 37–49. <https://doi.org/10.1016/j.compchemeng.2012.09.010>.
- [160] M. Arabi, R.S. Govindaraju, M.M. Hantush, A probabilistic approach for analysis of uncertainty in the evaluation of watershed management practices, *J. Hydrol.* 333 (2007) 459–471. <https://doi.org/10.1016/j.jhydrol.2006.09.012>.
- [161] I. Farrance, R. Frenkel, Uncertainty of Measurement: A Review of the Rules for Calculating Uncertainty Components through Functional Relationships., *Clin. Biochem. Rev.* 33 (2012) 49–75.
- [162] M. Modarres, M. Amiri, C. Jackson, Probabilistic Physics of Failure Approach to Reliability, John Wiley & Sons, Inc., 2017. <https://doi.org/10.1002/9781119388692>.
- [163] P. V. Varde, M.G. Pecht, Probabilistic approach to reliability engineering, in: Springer Ser. Reliab. Eng., 2018. https://doi.org/10.1007/978-981-13-0090-5_3.
- [164] M. Modarres, M.P. Kaminskiy, V. Krivtsov, Reliability Engineering and Risk Analysis, CRC Press, 2009. <https://doi.org/10.1201/9781420008944>.
- [165] S. Rastayesh, S. Bahrebar, A.S. Bahman, J.D. Sørensen, F. Blaabjerg, Lifetime estimation and failure risk analysis in a power stage used in wind-fuel cell hybrid energy systems, *Electron.* 8 (2019). <https://doi.org/10.3390/electronics8121412>.
- [166] M.E.N.H. and B. Peacock, Statistical Distributions, Third Edition, *Meas. Sci. Technol.* 12 (2001). <https://doi.org/10.1088/0957-0233/12/1/702>.
- [167] P. Cygan, J.R. Laghari, Models for insulation aging under electrical and thermal multistress, *IEEE Trans. Electr. Insul.* 25 (1990) 923–934. <https://doi.org/10.1109/14.59867>.
- [168] R. Pan, A Bayes approach to reliability prediction utilizing data from accelerated life tests and field failure observations, *Qual. Reliab. Eng. Int.* 25 (2009) 229–240. <https://doi.org/10.1002/qre.964>.
- [169] I. Basak, Prediction of Times to Failure of Censored Items for a Simple Step-Stress Model with Regular and Progressive Type I Censoring from the Exponential Distribution, *Commun. Stat. - Theory Methods.* 43 (2014) 2322–2341. <https://doi.org/10.1080/03610926.2013.861489>.
- [170] P.G. Bishop, R.E. Bloomfield, Using a log-normal failure rate distribution for worst case bound reliability prediction, in: 14th Int. Symp. Softw. Reliab. Eng. 2003. ISSRE 2003., IEEE, 2003: pp. 237–245. <https://doi.org/10.1109/ISSRE.2003.1251046>.
- [171] J. Zhang, F. Liu, Y. Liu, H. Wu, W. Zhu, W. Wu, L. Wu, Life prediction for white OLED based on LSM under lognormal distribution, *Solid. State. Electron.* 75 (2012) 102–106. <https://doi.org/10.1016/j.sse.2011.12.004>.
- [172] W.J. Corlett, J. Aitchison, J.A.C. Brown, The Lognormal Distribution, With Special Reference to Its Uses in Economics., *Appl. Stat.* 6 (1957) 228. <https://doi.org/10.2307/2985613>.

- [173] A.S. Jordan, A comprehensive review of the lognormal failure distribution with application to LED reliability, *Microelectron. Reliab.* 18 (1978) 267–279. [https://doi.org/10.1016/0026-2714\(78\)90331-1](https://doi.org/10.1016/0026-2714(78)90331-1).
- [174] M.G. Mateu-Figueras, R.A. Olea, Lognormal Distribution, in: 2022: pp. 1–4. https://doi.org/10.1007/978-3-030-26050-7_441-1.
- [175] Reliability and Performance in Engineering Design, in: *Handb. Reliab. Availability, Maintainab. Saf. Eng. Des.*, Springer London, London, 2009: pp. 43–294. https://doi.org/10.1007/978-1-84800-175-6_3.
- [176] M. Catelani, L. Ciani, G. Guidi, G. Patrizi, Accelerated Testing and Reliability estimation of electronic boards for automotive applications, in: 2021 IEEE Int. Work. Metrol. Automot., IEEE, 2021: pp. 199–204. <https://doi.org/10.1109/MetroAutomotive50197.2021.9502884>.
- [177] M.G. Pecht, F.R. Nash, Predicting the reliability of electronic equipment, *Proc. IEEE.* 82 (1994) 992–1004. <https://doi.org/10.1109/5.293157>.
- [178] A.K. Gupta, W.-B. Zeng, Y. Wu, Exponential Distribution, in: *Probab. Stat. Model.*, Birkhäuser Boston, Boston, MA, 2010: pp. 23–43. https://doi.org/10.1007/978-0-8176-4987-6_2.
- [179] Y.-C. Zhang, H.-Q. Zhao, W. Jiang, S.-T. Tu, X.-C. Zhang, R.-Z. Wang, Time dependent failure probability estimation of the solid oxide fuel cell by a creep-damage related Weibull distribution model, *Int. J. Hydrogen Energy.* 43 (2018) 13532–13542. <https://doi.org/10.1016/j.ijhydene.2018.05.088>.
- [180] J. Wang, H. Yin, Failure Rate Prediction Model of Substation Equipment Based on Weibull Distribution and Time Series Analysis, *IEEE Access.* 7 (2019) 85298–85309. <https://doi.org/10.1109/ACCESS.2019.2926159>.
- [181] H. Rinne, History and meaning of the WEIBULL distribution, in: *Weibull Distrib.*, 2020. <https://doi.org/10.1201/9781420087444-8>.
- [182] S. Bahrebar, D. Zhou, S. Rastayesh, H. Wang, F. Blaabjerg, Reliability assessment of power conditioner considering maintenance in a PEM fuel cell system, *Microelectron. Reliab.* 88–90 (2018) 1177–1182. <https://doi.org/10.1016/j.microrel.2018.07.085>.
- [183] P. V. Varde, M.G. Pecht, *Risk-Based Engineering*, Springer Singapore, Singapore, 2018. <https://doi.org/10.1007/978-981-13-0090-5>.
- [184] M. Modarres, M.P. Kaminskiy, V. Krivtsov, *Reliability Engineering and Risk Analysis*, CRC Press, 2009. <https://doi.org/10.1201/9781420008944>.
- [185] N.T. Thomopoulos, *Statistical Distributions. Applications and Parameters Estimates*, 2017.
- [186] K.C. Kapur, M. Pecht, *Reliability Engineering*, John Wiley & Sons, Inc., Hoboken, NJ, USA, 2014. <https://doi.org/10.1002/9781118841716>.
- [187] J.I. McCool, *Using the Weibull Distribution: Reliability, Modeling and Inference*, Wiley Blackwell, 2012. <https://doi.org/10.1002/9781118351994>.
- [188] *Pattern Recognition and Machine Learning*, *J. Electron. Imaging.* 16 (2007) 049901.

Literature review

<https://doi.org/10.1117/1.2819119>.

- [189] S. Singh, A. Anand, S. Mukherjee, T. Choudhury, Machine Learning Applications in Decision Intelligence Analytics, in: EAI/Springer Innov. Commun. Comput., Springer Science and Business Media Deutschland GmbH, 2022: pp. 163–178. https://doi.org/10.1007/978-3-030-82763-2_15.
- [190] K.-J. Kim, I. Tagkopoulos, Application of machine learning in rheumatic disease research, *Korean J. Intern. Med.* 34 (2019) 708–722. <https://doi.org/10.3904/kjim.2018.349>.
- [191] R.K. Dhanaraj, K. Rajkumar, U. Hariharan, Enterprise IoT Modeling: Supervised, Unsupervised, and Reinforcement Learning, in: EAI/Springer Innov. Commun. Comput., Springer Science and Business Media Deutschland GmbH, 2020: pp. 55–79. https://doi.org/10.1007/978-3-030-44407-5_3.
- [192] P. Mishra, Supervised Learning Using PyTorch, in: PyTorch Recipes, Apress, Berkeley, CA, 2019: pp. 127–149. https://doi.org/10.1007/978-1-4842-4258-2_5.
- [193] B. Quinto, Supervised Learning, in: Next-Generation Mach. Learn. with Spark, Apress, Berkeley, CA, 2020: pp. 97–187. https://doi.org/10.1007/978-1-4842-5669-5_3.
- [194] A.F. Vermeulen, Supervised Learning: Using Labeled Data for Insights, in: Ind. Mach. Learn., Apress, Berkeley, CA, 2020: pp. 63–136. https://doi.org/10.1007/978-1-4842-5316-8_4.
- [195] A.M. Ibrahim, B. Bennett, The Assessment of Machine Learning Model Performance for Predicting Alluvial Deposits Distribution, *Procedia Comput. Sci.* 36 (2014) 637–642. <https://doi.org/10.1016/j.procs.2014.09.067>.
- [196] C. Crisci, B. Ghattas, G. Perera, A review of supervised machine learning algorithms and their applications to ecological data, *Ecol. Modell.* 240 (2012) 113–122. <https://doi.org/10.1016/j.ecolmodel.2012.03.001>.
- [197] P.C. Sen, M. Hajra, M. Ghosh, Supervised Classification Algorithms in Machine Learning: A Survey and Review, in: *Adv. Intell. Syst. Comput.*, Springer Verlag, 2020: pp. 99–111. https://doi.org/10.1007/978-981-13-7403-6_11.
- [198] M. Ayoub, A review on machine learning algorithms to predict daylighting inside buildings, *Sol. Energy.* 202 (2020) 249–275. <https://doi.org/10.1016/j.solener.2020.03.104>.
- [199] P. Singh, Unsupervised Machine Learning, in: *Learn PySpark*, Apress, Berkeley, CA, 2019: pp. 161–181. https://doi.org/10.1007/978-1-4842-4961-1_7.
- [200] C.C. Aggarwal, Unsupervised Learning, in: *Artif. Intell.*, Springer International Publishing, Cham, 2021: pp. 299–342. https://doi.org/10.1007/978-3-030-72357-6_9.
- [201] M. Kubat, Unsupervised Learning, in: *An Introd. to Mach. Learn.*, Springer International Publishing, Cham, 2017: pp. 273–295. https://doi.org/10.1007/978-3-319-63913-0_14.
- [202] R. Gentleman, V.J. Carey, Unsupervised Machine Learning, in: *Bioconductor Case Stud.*, Springer New York, New York, NY, 2008: pp. 137–157. https://doi.org/10.1007/978-0-387-77240-0_10.
- [203] F. Agostinelli, G. Hocquet, S. Singh, P. Baldi, From Reinforcement Learning to Deep

- Reinforcement Learning: An Overview, in: *Lect. Notes Comput. Sci. (Including Subser. Lect. Notes Artif. Intell. Lect. Notes Bioinformatics)*, Springer Verlag, 2018: pp. 298–328. https://doi.org/10.1007/978-3-319-99492-5_13.
- [204] F. AlMahamid, K. Grolinger, Reinforcement Learning Algorithms: An Overview and Classification, in: *2021 IEEE Can. Conf. Electr. Comput. Eng.*, IEEE, 2021: pp. 1–7. <https://doi.org/10.1109/CCECE53047.2021.9569056>.
- [205] A. Mellouk, ed., *Advances in Reinforcement Learning*, InTech, 2011. <https://doi.org/10.5772/557>.
- [206] S. Chen, Y. Li, An Overview of Robust Reinforcement Learning, in: *2020 IEEE Int. Conf. Networking, Sens. Control*, IEEE, 2020: pp. 1–6. <https://doi.org/10.1109/ICNSC48988.2020.9238129>.
- [207] A.J. Gallego, J.R. Rico-Juan, J.J. Valero-Mas, Efficient k-nearest neighbor search based on clustering and adaptive k values, *Pattern Recognit.* 122 (2022) 108356. <https://doi.org/10.1016/j.patcog.2021.108356>.
- [208] C. Vens, Random Forest, in: *Encycl. Syst. Biol.*, Springer New York, New York, NY, 2013: pp. 1812–1813. https://doi.org/10.1007/978-1-4419-9863-7_612.
- [209] T. Jo, Decision Tree, in: *Mach. Learn. Found.*, Springer International Publishing, Cham, 2021: pp. 141–165. https://doi.org/10.1007/978-3-030-65900-4_7.
- [210] S. Tangirala, Evaluating the impact of GINI index and information gain on classification using decision tree classifier algorithm, *Int. J. Adv. Comput. Sci. Appl.* 11 (2020) 612–619. <https://doi.org/10.14569/ijacsa.2020.0110277>.
- [211] V.K. Ayyadevara, *Pro Machine Learning Algorithms*, Apress, Berkeley, CA, 2018. <https://doi.org/10.1007/978-1-4842-3564-5>.
- [212] C. Cortes, V. Vapnik, L. Saitta, Support-vector networks, *Mach. Learn.* 1995 203. 20 (1995) 273–297. <https://doi.org/10.1007/BF00994018>.
- [213] J.J. Khanam, S.Y. Foo, A comparison of machine learning algorithms for diabetes prediction, *ICT Express.* (2021). <https://doi.org/10.1016/j.ict.2021.02.004>.
- [214] R. Laref, E. Losson, A. Sava, M. Siadat, On the optimization of the support vector machine regression hyperparameters setting for gas sensors array applications, *Chemom. Intell. Lab. Syst.* 184 (2019) 22–27. <https://doi.org/10.1016/j.chemolab.2018.11.011>.
- [215] H. Hu, Y. Wang, J. Song, Signal Classification Based on Spectral Correlation Analysis and SVM in Cognitive Radio, in: *22nd Int. Conf. Adv. Inf. Netw. Appl. (Aina 2008)*, IEEE, 2008: pp. 883–887. <https://doi.org/10.1109/AINA.2008.27>.
- [216] M. Aghaaminiha, R. Mehrani, M. Colahan, B. Brown, M. Singer, S. Nestic, S.M. Vargas, S. Sharma, Machine learning modeling of time-dependent corrosion rates of carbon steel in presence of corrosion inhibitors, *Corros. Sci.* 193 (2021) 109904. <https://doi.org/10.1016/j.corsci.2021.109904>.
- [217] P. Probst, A.L. Boulesteix, B. Bischl, Tunability: Importance of hyperparameters of machine learning algorithms, *J. Mach. Learn. Res.* 20 (2019). <http://arxiv.org/abs/1802.09596> (accessed January 9, 2022).

Literature review

- [218] V.R.S. Mani, A. Saravanaselvan, N. Arumugam, Performance comparison of CNN, QNN and BNN deep neural networks for real-time object detection using ZYNQ FPGA node, *Microelectronics J.* 119 (2022) 105319. <https://doi.org/10.1016/j.mejo.2021.105319>.
- [219] G. Asadollahfardi, Artificial Neural Network, in: *Pro Mach. Learn. Algorithms*, Apress, Berkeley, CA, Berkeley, CA, 2015: pp. 77–91. https://doi.org/10.1007/978-3-662-44725-3_5.
- [220] S.S. Raiman, S. Lee, Aggregation and data analysis of corrosion studies in molten chloride and fluoride salts, *J. Nucl. Mater.* 511 (2018) 523–535. <https://doi.org/10.1016/j.jnucmat.2018.07.036>.
- [221] R.E. Melchers, Statistical Characterization of Pitting Corrosion—Part 1: Data Analysis, *CORROSION*. 61 (2005) 655–664. <https://doi.org/10.5006/1.3278201>.
- [222] P.R. Roberge, E. Halliop, V.S. Sastri, Corrosion of Mild Steel Using Electrochemical Impedance Spectroscopy Data Analysis, *CORROSION*. 48 (1992) 447–454. <https://doi.org/10.5006/1.3315959>.
- [223] E. Rossouw, W. Doorsamy, Predictive Maintenance Framework for Cathodic Protection Systems Using Data Analytics, *Energies*. 14 (2021) 5805. <https://doi.org/10.3390/en14185805>.
- [224] M. Smith, S. Cronjaeger, N. Ershad, R. Nickle, M. Peussner, Pipeline Data Analytics: Enhanced Corrosion Growth Assessment Through Machine Learning, in: *Vol. 1 Pipeline Facil. Integr.*, American Society of Mechanical Engineers, 2018. <https://doi.org/10.1115/IPC2018-78364>.
- [225] S. Gupta, L. Saputelli, M. Nikolaou, Applying big data analytics to detect, diagnose, and prevent impending failures in electric submersible pumps, in: *Proc. - SPE Annu. Tech. Conf. Exhib.*, SPE, 2016: pp. 26–28. <https://doi.org/10.2118/181510-ms>.
- [226] K. Thiyagarajan, S. Kodagoda, L. Van Nguyen, Predictive analytics for detecting sensor failure using autoregressive integrated moving average model, *Proc. 2017 12th IEEE Conf. Ind. Electron. Appl. ICIEA 2017*. 2018-February (2018) 1926–1931. <https://doi.org/10.1109/ICIEA.2017.8283153>.

3 Materials and methods

This chapter provides an overview of the materials, specimens, experiments, and predictive methods employed in this project. Generally, the six critical factors, i.e., humidity (H), temperature (T), contamination type (CT), contamination level (C), pitch distance (P), and voltage (V), each of them at different levels, have been used at different experimental design for three individual studies. The combination of different factors and levels generated different conditions, and each condition presented different LC values, TTF, and distinct failure states based on DC current measurement. In order to monitor the general current behavior as the main indicator and define three different responses to it, the SIR DC measurement is applied to all of the experiments. The OFAT and DOE methodology has been used for data collection of experiences. The methods for predictive analytics on data, which were utilized, can be categorized into statistical, probabilistically, and machine learning analyses. Statistical analysis has been used to find information from data to estimate variables' relationships and forecast behavior patterns of the general current as a primary indicator. Probabilistic approaches have been used to estimate the likelihood of failure occurrence by quantifying the uncertainty and usage of appropriate distributions. Machine learning algorithms have been used to predict both numerical and categorical failure (LC and failure status) based on training input datasets obtained. A general introduction to each method used during this project is given in the following chapter. More detailed discussions of each experimental design and the applied predictive analytics methods can be found in the appended papers chapters (5-8).

3.1 SIR PCB specimens

The SIR PCBs including interdigitated electrodes separated by a dielectric. SIR PCBs based on the IPC standard testing is commonly used for electronics' climatic reliability. FR-4 laminate with a thickness of 1.6 mm was the base substrate for the SIR PCBs. The SIR PCBs had the HASL surface finished following the IPC-4101/21 standard. Four different SIR comb patterns were used for different experiments, and Figure 3.1 displays them with more details about pitch distances, dimensions, and areas on a PCB.

Materials and methods

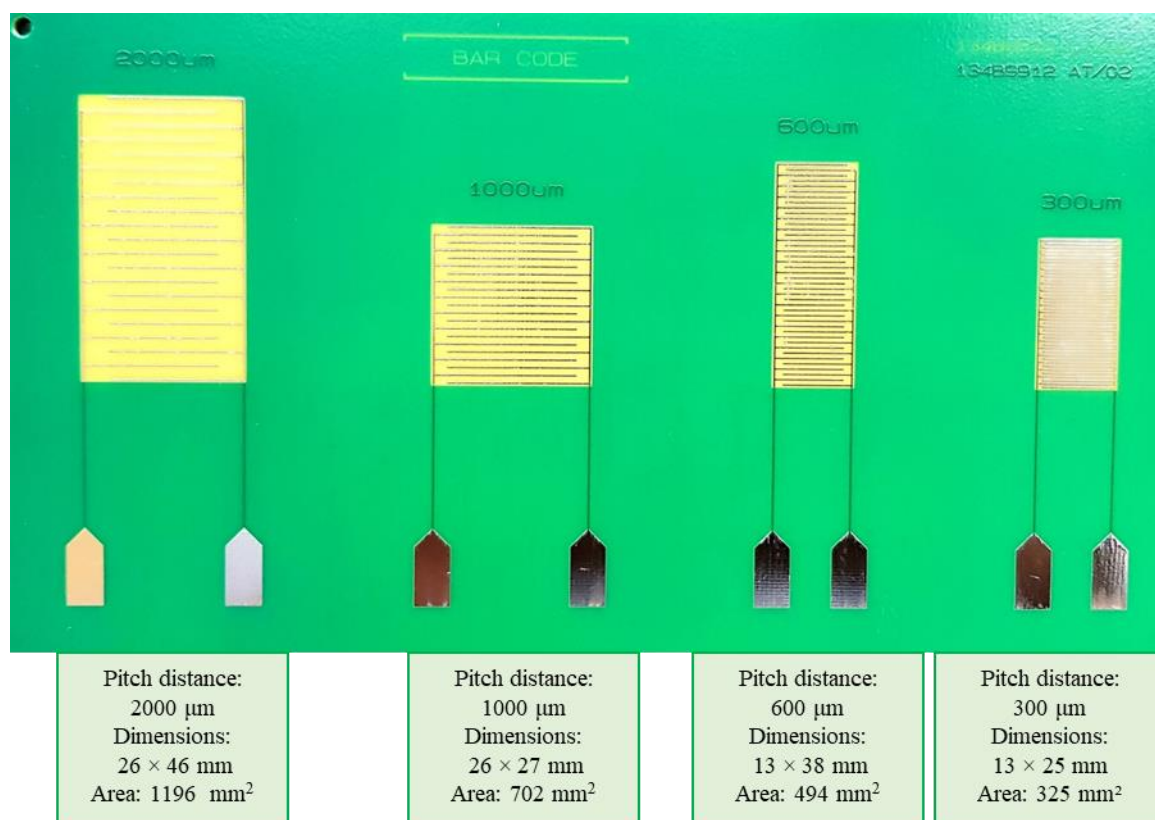


Figure 3.1 Picture of the test SIR PCB patterns.

3.2 Specimens preparation

X In preparation of SIR PCBs before starting the test, three steps have been accomplished, which are included soldering, cleaning, and pre-contaminate. Figure 3.2 illustrates three steps of sample preparations before starting the current measurement by a potentiostat and putting the samples inside a climatic chamber. In the first step, the PCB connections are made using hand soldering of small wires to the electrical contacts on the PCB. In the second step, the SIR PCBs were cleaned using a mixture of deionized water as well as isopropanol. In this step also, PCBs are dried by an air compressor without the hand touching the PCB surfaces. In the third step, the solutions of 2.5g of different WOAs (glutaric acid, adipic acid, and succinic acid) as contamination types were dissolved in 100 ml isopropanol at the 25g/l concentration. After calculation, the accurate amount of the solutions as contamination levels using a micropipette were distributed on the SIR patterns.



Figure 3.2 Three Steps before DC measurement and placing the specimens inside the climatic chamber.

3.3 SIR DC testing and equipment

SIR DC measurements have been used as a common test method for the climatic reliability and corrosion susceptibility testing of various factors in electronics. The BioLogic VSP potentiostat by multichannel workstation has been utilized to implement different DC voltages (from 0 to 10V) and measure leak current (from nA to A). An Espec climatic chamber by tolerances of $\pm 2.5\%$ RH and $\pm 0.3^\circ\text{C}$ has been used for creating various climatic conditions. The operational range of humidity and temperature is 10%RH to 98%RH and -70°C to 180°C, respectively.

All the experiments are performed to test the impact design specifications connected to the PCB, for example the pitch distance, voltage, and contamination type and levels under various climatic conditions using current DC measurement by the potentiostat and putting the specimens inside the climatic chamber. Moreover, a VHX digital microscope (Keyence, Japan) was utilized at ex-situ for the optical microscopy inspection of ECM and dendrite formation on the SIR surface boards and components. Figure 3.3 shows the real picture of the Espec climatic chamber, BioLogic VSP potentiostat with five channels, and VHX digital microscope that have been used in all experiments.

Materials and methods



Figure 3.3 Espec climatic chamber, BioLogic VSP potentiostat with five channels, and VHX digital microscope.

3.4 Statistical analysis

The statistical analysis has been used to plan data collection (design of experiments), study of experimental results (data analysis), and predict models (regression equation). The multivariate regression analysis and ANOVA are established to find the relationship between sets of variables, as well as to understand the effect on dependent variables (LC, TTF, and failure status) of the independent variables (P, T, H, CT, C, V) and their significant interactions.

3.5 Probabilistic analysis

The probabilistic approach using acquired methodologies and tools for risk and reliability analysis of electronics devices has been used to predict TTF owing to ECM on PCB surfaces and quantify the probability of failures (PoF) under various conditions. The suitable probability distribution for all condition (combined of various independent factors/levels) based on three methods; i. the nature of data, ii. probability plotting, and iii. analytical techniques have been studied. Applying goodness-of-fit tests (i.e., Anderson-Darling, Chi-square, and Kolmogorov-Smirnov tests) and maximum likelihood methods, the Weibull distributions as the most popular distributions for lifetime and failure prediction on the experimental conditions of the accelerated tests compared to other distributions have been chosen on entire TTFs dataset and utilized for making the prediction model.

3.6 Machine learning algorithms

To predict the outcome based on training input datasets, ML algorithms have been utilized. The most important and applicable supervised ML algorithms, including; DT, RF, k-NN, SVM, and DNN for both regression and classification, have used to predict LC values (regression analysis) and failure state (classification analysis) on the PCB surface under various corrosive conditions. The regression analysis has been used for the prediction of LC, which can give us an insight into the initial situation before creating a failure status and maybe can avoid that. Moreover, the classification analysis has been used to predict the failure states, which can give us a good understanding of the critical conditions to increase the climatic reliability and reduce the risk of electronics.

4 Summary of appended papers

4.1 Investigation of critical factors effect to predict leakage current and time to failure due to ECM on PCB under humidity

Highlights:

- The critical factors and their interactions on LC and TTF are characterized.
- The LC and TTF are predicted using significant factors by factorial regression analysis, and ANOVA.
- The general leak current behavior is analyzed under various critical conditions.
- The correlation between LC and TTF are studied.

Synopsis:

This study investigated the significant influence of various factors/levels/interactions on PCB surfaces once exposed to different conditions along with using DOE, simulating, and statistical modeling. Under considering conditions the V does not significantly affect the LC values, whereas T, C, as well as P have in the descending order of most important effects. Though, voltage has a major impact on TTF response owing to ECM. The main 2-way interactions for all responses have been C*T and P*T, and the 3-way interaction has been P*C*T. Generally, with ascending the LC values, the PoF has been increased, and roughly the lower TTF values have been related to the higher LC values. Figure 4.1 illustrates the three general parts of current behavior as the main indicator, which are measured to describe LC and TTF on the PCB surface, besides its simulations at entirely experimental conditions using the Logistic function.

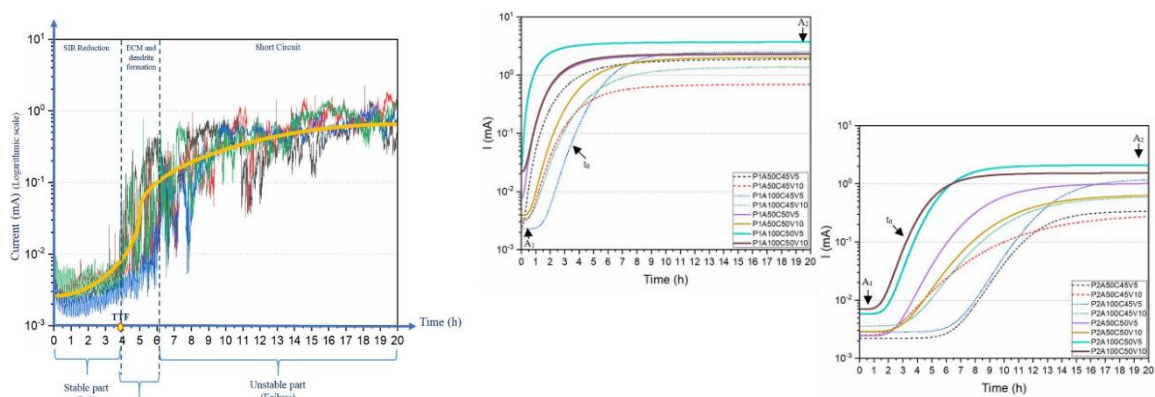


Figure 4.1 Three parts of the general current behavior, and its simulations for all conditions.

Summary of appended papers

4.2 Time to failure prediction on printed circuit board surface under humidity using probabilistic analysis

Highlights:

- The effect of four critical factors including P, T, C, and V are studied on the SIR PCBs under humidity using OFAT method.
- The trend of LC and TTF owing to ECM on PCB surface are studied on three levels for all critical factors.
- The Weibull distribution, multivariate regression analysis, and CART analysis are used to predict the probability of TTF.

Synopsis:

This study, with a sensitivity analysis of four critical factors, each of them at three levels, estimating the PoF, and predicting a model for TTF based on probabilistic distribution analysis, has given an broad understanding to the failure occurrence on PCB surfaces under humidity. The T and P had the most key impact on TTF values and the PoF of the very fast (under 1 Hour) and fast classes (between 1-4 Hours). The importance of pitch distance increases the electric field to easily form dendrite formation during ECM. The temperature importance corresponded to the humidity, influences altering the DP range, the size of dew droplet formation, and increasing the electrochemical kinetics on the PCB surface. Figure 4.2 as sample displays (a) the trend, and (b) PDF of pitch distance at three levels with details parameters.

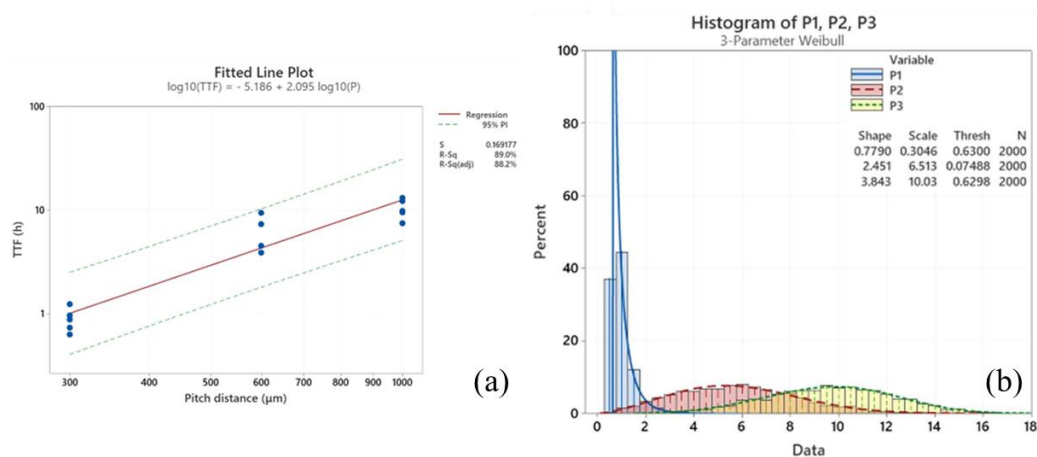


Figure 4.2 (a) Fitted line plot and (b) PDF histogram of pitch distance at three levels.

4.3 Using machine learning algorithms to predict failure on the PCB surface under corrosive conditions

Highlights:

- The PCB failure prediction has been investigated under various corrosive conditions created by the mixture of six critical factors, including contamination level, humidity, temperature, pitch distance, voltage, and contamination type, each of them at three levels.
- The typical supervised ML algorithms, including k-NN, DT, RF, SVM, and DNN, are utilized to train regressors and classifiers to forecast LC values and failed or Not-failed conditions, respectively.

Synopsis:

This study used the most common ML algorithms to predict both LCs (regression analysis) and failure state (classification analysis) on the PCB surface under various corrosive conditions. The regression analysis has been used to predict LC, which can give us an insight into the initial situation before creating a failure state and maybe can avoid that. Moreover, the classification analysis has been used to predict the failure states, which can give us a good understanding of the critical conditions to increase the climatic reliability and reduce the risk of electronics. The best-trained model by the RF model successfully delivered the best performance in predicting PCB failures and LC values on the test dataset. Figure 4.3 illustrates (a) the confusion matrices, and (b) KDE plot of RF for assessing the classification and regression accuracy, respectively.

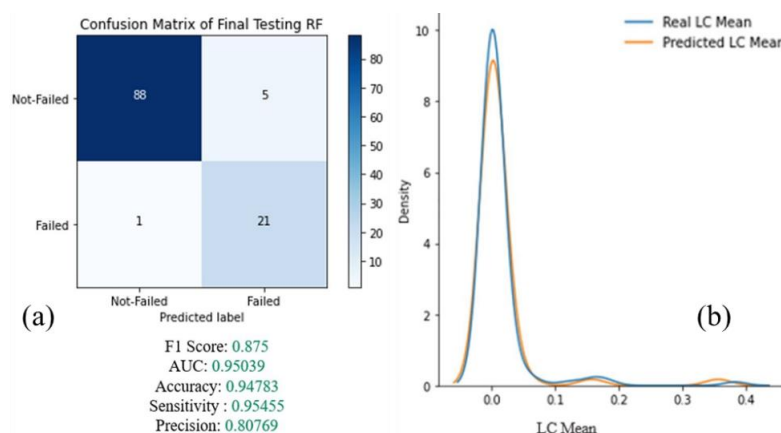


Figure 4.3 (a) Confusion matrices, and (b) KDE plot of RF on test dataset.

5 Manuscript I

Investigation of critical factors effect to predict leakage current and time to failure due to ECM on PCB under humidity

S. Bahrebar, R. Ambat, Investigation of critical factors effect to predict leakage current and time to failure due to ECM on PCB under humidity, Microelectron. Reliab. 127 (2021) 114418. <https://doi.org/10.1016/j.microrel.2021.114418>.

ABSTRACT- Experiments using the Design of Experiment (DoE) methodology were carried out to investigate the effects of pitch distance (P), temperature (T), voltage (V), and contamination (C) on the leak current measured on Surface Insulation Resistance (SIR) test boards. A 2⁴ full factorial design with eight replications was performed, and the response was measured continuously over a 20 hours period for each experiment. Current measured over time exhibited a clear pattern of an initial low and stable current, followed by a transition to a much higher current. Microscopic analysis of the boards indicates that the transition is due to dendrite formation due to electrochemical migration (ECM). The time at the start of this transition phase was identified as the Time to Failure (TTF) for each experiment. Leakage Current (LC) was also calculated as the mean current prior to failure. Analysis of Variance methods were used to model both TTF and LC. Both TTF and LC were found to be significantly affected by P, T, and C. However, the effect of V was found to be significant only for TTF. The general current behavior over the prolonged experimental period and the resulting statistical models give new insight into the failure process related to ECM.

Keywords: Design of Experiment, Full Factorial Design, Leakage Current, Time to Failure, PCB Surface.

5.1 Introduction

Climatic reliability of electronic devices is a significant issue today due to the widespread use of electronic devices in different climatic conditions depending on the place of use. An increase in the assembly design density and miniaturization of the Printed Circuit Board Assemblies (PCBAs) pose challenges for obtaining climatic reliability [1]. The PCBAs are the main part of electronic devices that are influenced by climatic changes such as humidity and temperature changes due to water film formation [2]. Water film formation can potentially occur at most climatic conditions due to unpredictable transient conditions as well as PCBA surface characteristics [3]. Under transient conditions, water film formation on the PCBA could be accelerated due to the presence of ionic and hygroscopic contaminants, which is mostly connected to the residues from the soldering process [4]. Formation of water film results in leak current between adjacent biased points on the PCBA surface and Electrochemical Migration (ECM) failure due to dendrite bridging. Subsequently, it can affect the product performance and lead to severe deterioration of the electronic devices [5], [6]. Generally, electrochemical interactions on electronic devices are defined as a process that leads to parasitic circuits resulting in leak current, impedance changes, and dendrite bridging [7].

To improve the robustness, most important aspect is to control the transient water layer build up [8]. Level of water film build up on the PCBA surface depends on the synergetic effects of various factors such as material characteristics, manufacturing and cleaning processes, potential bias, PCBA design, and climatic variations such as changes in humidity and temperature [8]. In other words, the assessment of the impact of these parameters is performed under the conditions relevant for the electronics operation and under accelerated tests for understanding the relationships between various parameters in determining the water film build-up and associated failures. The water film features are defined by the aspects of the PCBA design and electrochemical processes under various climatic conditions [9].

Although there are various failure mechanisms due to corrosion caused [10], [11], [12], [13] by humidity and ionic contaminations on the PCBA surface and electronic components, leak current and failures due to dendrite formation by ECM has special significance due to the possibility of intermittent failures when transient condensing

conditions exists during application. Therefore, vast majority of failures are due to the corrosion failure mechanisms caused by the water film formation on the PCBA surface as a result of the device exposure to the climatic conditions, which is induced by the electrochemical processes between the biased points on the PCBA surface.

The major failure mechanisms responsible for most failures of electronic components are the overstressed mechanisms [14], [15]. This means the conditions exceed the strength of materials and components, which frequently causes sudden and catastrophic failures, such as chemical failure mechanisms on the PBCA due to contamination and electrical failure mechanisms due to surface insulation resistance degradation [16], [17]. Both Surface Insulation Resistance (SIR) reduction and ECM can happen when the environmental conditions, e.g., water film formation, occur. Therefore both SIR and ECM can be considered as overstress mechanisms, which gives a short product lifetime. There are some literature on leak current or ECM investigation without considering the time and relation of them [18], [19], [20], [21] however, in most cases, individual parameters are investigated rather than multi-parameter interactions [22], [23], [24], [25]. Forasmuch as often there is no individual factor to create a failure, finding interactions of parameters and intensity impact of each interaction at least in two-way, and three-way interactions besides, the relation between leak current and time to ECM beginning are imperative for the right understanding of failure process and proper prediction.

There is some literature on models for TTF due to ECM based on physics of failure [26], [27], [28], [29] but, in this study, regression analysis as a probabilistic approach to reliability engineering was used to find regression model for both TTF and LC according to all critical factors/levels. The prediction range of the model was contained a single future response for the selected combination of variable settings. Besides, the general current behavior over the prolonged experimental period and the resulting statistical models were given into the failure process related to ECM.

Investigation in this paper focus on finding critical factors effect to predict leakage current and time to failure on PCB surface under humid conditions. Paper presents findings from 128 experiments at 16 different conditions in which leak current was measured continuously before, during, and after failures developed, subject to various parameters inside a climatic chamber. The SIR patterns used as test specimens were pre-contaminated,

Manuscript I

using adipic acid as contamination type, which is one of the Weak Organic Acids (WOAs) commonly used in the flux system used for the soldering process. For all the experiments, current measured over time displayed a similar pattern consisting of a stable current, followed by a transition period, and finally a significantly higher current. However, the magnitudes of the initial and final currents, and the time-points of the transition periods varied for different experiments. The time at the start of the transition state was identified as the TTF for each experiment. LC was also calculated as the mean currents before TTF. The LC and TTF as two main responses were considered to investigate the effect of the critical factors, their interactions as well as made a prediction model using full factorial design method and Analysis of Variance (ANOVA). Besides, this study recognized the high-risk conditions and the relationship between the responses including the leak current behavior model by applying statistical analysis and a logistic model. Examining all the outcomes created a more comprehensive understanding of the effects of different factors/interactions and risky conditions on the SIR boards when exposed to humidity in order to transfer the knowledge to the real PCBA of various electronic devices.

5.2 Materials and methods

The full factorial design, or fully crossed design, is a statistical method that has been used since the 1920s in many applied fields in order to determine the effect of multivariate factors upon a response [30]. In this method two or more factors are chosen for investigation, each with two or more values as levels [31]. Next, experiments are designed to take on all possible combinations of these levels across all such factors to investigate each factor's simultaneous effect on the response variable, besides the effects of interactions between factors on the response variable [32]. For this study, a full 2^4 factorial design was chosen with four factors: Pitch distance (P), temperature (T), voltage (V), and contamination (C). In addition, eight replications were carried out on each condition, therefore ensuring all possible interactions between the factors that can be tested for significance. In the following sections, materials and experimental methods are described. The experimental conditions, including the choice of factor levels that are used, are provided. Finally, the choice of response variables and their analysis by ANOVA are outlined.

5.2.1 Experimental setup

5.2.1.1 Interdigitated SIR test PCB used for experiments

The Test PCBs with two different Surface Insulation Resistance (SIR) patterns were used for the experimental work [33], [34]. Base substrate for the PCB was FR-4 laminate with thickness of 1.6 mm. The SIR pattern consisted of interdigitated electrodes separated by dielectric with two different pitch distances. The commonly used test method for the humidity related reliability testing of electronics is the SIR measurement, which include testing of the effect design characteristics related to the PCB such as the pitch distance, bias level, and hygroscopic contamination such as the one arising from the soldering process. The effect of humidity was assessed using the leakage current between the interdigitated pattern or measuring the Surface Insulation Resistance (SIR). Generally, the low SIR values (high LC) are related to the more aggressive conditions such as high humidity, high bias level, and high contamination conditions in addition to the low distance between the electrodes.

The test PCBs used in this include two different SIR patterns with two pitch distances namely 300 μm and 600 μm as shown in Figure 5.1. Surface finishing used for the electrode surface was Hot Air Solder Leveling (HASL) using a Sn solder alloy, in compliance with the IPC-4101/21 standard. The area of the small SIR pattern was 325 mm^2 (13 mm \times 25 mm) with a pitch distance of 300 μm (called P1), while the large SIR pattern had 494 mm^2 (13 mm \times 38 mm) area and a pitch distance of 600 μm (called P2).

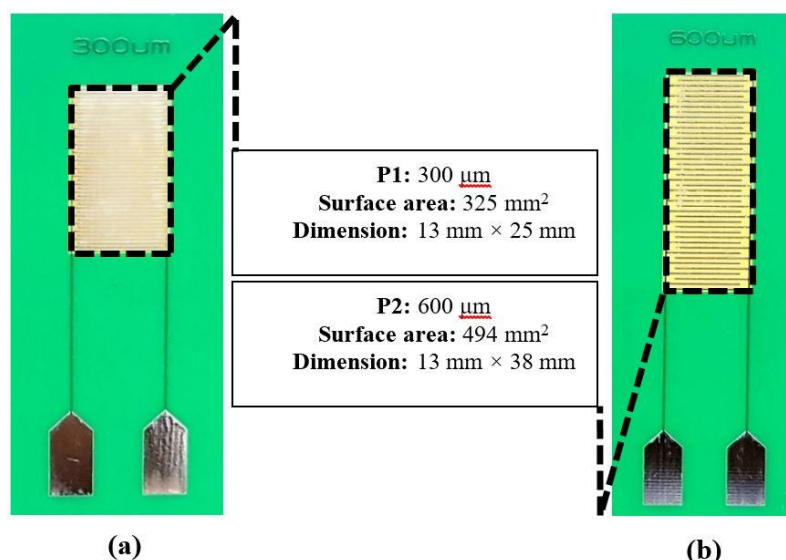


Figure 5.1 Picture of the SIR PCBs used in this investigation: (a) Small pitch distance (P1), (b) Big pitch distance (P2).

5.2.1.2 Preparation of the SIR Patterns

Before testing, PCBs were cleaned initially using an air compressor and a combination of deionized water and followed by isopropanol. Subsequently, the SIR patterns were contaminated with adipic acid mimicking an important Weak Organic Acid (WOA) activator commonly used in fluxes used for soldering process. Solution of this contamination was made up by dissolving 2.5 gram adipic acid in 100 ml of isopropanol (giving a concentration of 25g/L). Appropriate amount of this solution was applied on the SIR pattern and dried in order to obtain contamination levels of 50 and 100 $\mu\text{g}/\text{cm}^2$ matching with typical levels of flux residues usually seen after the wave soldering process [35].

5.2.1.3 Humidity testing

Humidity exposure was carried out in a climatic chamber (Espec PL 3kph) with $\pm 0.3^\circ\text{C}$ and $\pm 2.5\% \text{RH}$ tolerances. The RH, in accordance with the kind of contamination during the tests, was kept constant at 98%. RH level of 98% was chosen as the level is close to the Deliquescent Relative Humidity (DRH) for adipic acid, therefore prone to absorbing moisture under this condition. The stabilization time of 1.5 hours was used before each experiment in the climatic chamber. A BioLogic VSP, a multichannel electrochemical measurement system was used for applying potential to the SIR pattern and measuring the

current response (using chrono-amperometric method). A three electrode configuration was used by connecting one the electrode on SIR as working, while the other electrode was connected to both reference and counter. Two bias levels were used for investigation to mimic potential bias on the PCBA during application namely 5V and 10V. In addition, a digital microscope was used at ex-situ for the optical inspection of ECM and dendrite formation on the SIR surface board.

5.2.2 Experimental conditions

Sixteen different experimental conditions were considered, consisting of four critical controllable and changeable factors (pitch distance, contamination level, temperature, and voltage) each at two different levels (low and high), besides three constant factors (humidity, contamination type, and experiment time). All the experiments were conducted at high relative humidity. At each condition, the current was measured over a period of 72000 seconds (20 hours) in addition to a 1.5 hours period at the beginning of each experiment as a stabilization period of the condition inside the climatic chamber. Each experimental condition follows the naming process as follows; P1 or P2 (low and high level of pitch distance), a50 or a100 (low and high level of adipic acid as contamination), c45 or c50 (low and high level of temperature), v5 or v10 (low and high level of voltage) e.g. P1a100c50v10 condition, which illustrates P1 (small pitch distance), a100 (high-level adipic acid), c50 (high-level temperature), and v10 (high-level voltage), respectively. Table 5.1 provides an overview of all the experimental conditions. The following sections present further details related to the importance of each factor and choice of factor levels.

Table 5.1 The overall view of the various factors/ levels in this study.

Factors	Low Level	High Level	Unit	Symbol
Pitch distance	300	600	μm	P
Contamination	50	100	$\mu\text{g}/\text{cm}^2$	C
Temperature	45	50	$^{\circ}\text{C}$	T
Voltage	5	10	V	V
Humidity	(Constant) 98% RH			
Contamination Type	(Constant) Adipic acid			
Time of exposure	(Constant) 20 hours			

Manuscript I

5.2.2.1 *Pitch distance on SIR PCB*

The pitch distance is a significant parameter in connection with humidity effects on electronics due to the increased electric field between points with decreasing distance when water film forms. Today, one major factor increasing the climatic reliability of electronics is the miniaturization for high component density, therefore reducing the spacing on PCBA surface.

5.2.2.2 *Contamination*

Cleanliness is an essential issue for the failure of PCBAs. In other words, the formation of the water layer and the potential for corrosion occurrence are both determined by the PCBA cleanliness [36]. The detrimental effects of the contamination depend on different factors such as the type of contamination, the amount of contamination (contamination level), and the location of the contamination. Origin of contamination can be from the PCBA manufacturing process or from service conditions [37], [38], although the residues resulting from soldering process is most important.

The contamination effects on the PCBAs with the combination of climatic conditions cause different issues, such as the reduction of surface insulation resistance and increase in corrosion. Due to the hygroscopic properties as well as high solubility in water, they can accelerate the water film formation and failures on PCBA. The WOAs solubility is specified as the residue amount, which can dissolve at a specific temperature. Moreover, the WOAs strength defined by the dissociation of the acids [39]. The solubility and strength of WOAs determine the conductivity of the water film formed on the PCBA surface, while high conductivity leads to high leakage current value. The main source of contamination on a PCBA surface is from the component assembling process, which is related to the use of solder flux for the automated soldering process [40]. Adipic acid is a common activator compound used in such kind of flux system, hence used for this investigation at two levels namely $50 \mu\text{g}/\text{cm}^2$ and $100 \mu\text{g}/\text{cm}^2$.

5.2.2.3 *Climate conditions*

The climatic conditions to which the electronics exposed include many factors such as humidity, temperature, and other atmospheric contaminations. External atmospheric contamination influence on electronics is usually less due to the relatively tight packaging.

Daily humidity and temperature variation influence the humidity build up inside the device causing transient condensation effects, which is also depends on the hygroscopic nature of the PCBA surface such as the presence of ionic residues (for example the adipic acid used in this investigation). In this investigation only the temperature is varied, while keeping the humidity level above the deliquescent humidity level for the adipic acid. The deliquescent humidity level for adipic acid is reported to be 98-99 %RH at temperatures 25, 40, 60 °C [41]. Hence, two levels of temperature 45 °C and 50 °C are used.

5.2.2.4 Voltage

The voltage is another critical factor in relation to humidity related failure on a PCBA surface. Bias level on an actual PCBA surface can vary from low voltage to high voltage levels. For the present investigation, two levels of voltages are used namely 5 and 10 V.

5.2.3 Typical response from testing and failure modes

Each experiment provided a leak current profile over the 20 hours of duration as shown in Figure 5.2. The first step in the analysis of the data was to understand the behavior of the current over time and link this behavior to the physical events. Microscopic examination of the SIR patterns before and after the experiment was carried out for any dendrite build up and compared with the current profile. Dendrite formation leads to a substantial increase in leak current compared to the base level leak current. It was found that the functional form of the current over time could be approximated by a logistic growth curve, and this curve was fitted to the results at each condition for further insight.

In the second part of the statistical analysis, two key quantities of interest were defined, denoted by the Leakage Current (LC) average value and Time to Failure (TTF). The responses are extracted from the current profile of each experiment resulting in 128 values of LC and TTF for the eight replications corresponding to the 16 conditions. Significant effects for each response is determined through Analysis of Variance (ANOVA) using Minitab Statistical Software. First, a full model with all main and interaction effects was fitted. Next, a stepwise, backward elimination procedure was performed with a significance level of $\alpha=0.05$ until only significant terms remained in the model.

5.3 Results and discussion

5.3.1 Leak current profiles from testing and microscopic analysis

The experimental results showing leak current versus time from various experiments are shown in Figures 13 and 14 in the Appendix. As represented in Figure 5.2, general behavior of the leak current was S-shape current behavior under each exposure condition, which can be approximated as the yellow line in Figure 5.2. As shown in Figure 5.2, generally the current follows three state corresponds to the increasing effect of humidity on the SIR failure namely: initial stable current, transient, and higher and sometime unstable current after the transient.

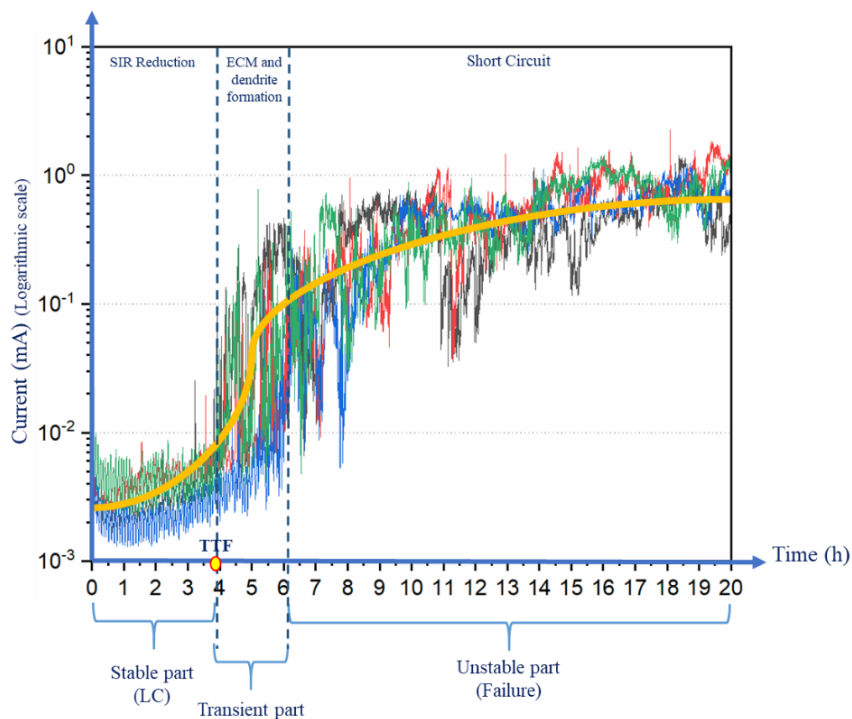


Figure 5.2 Typical result from humidity testing: Three interdependency states of current behaviors create a failure mode on the PCB surface.

The stable state included the initial part of the measured current at each condition below the current suddenly increases. This initial stable current part is due to the surface electrochemical process when the water film forms and the corresponding faradic current between the positively biased electrode (anode) and negative biased electrode (cathode). The tangible LC value in the SIR reduction state is around 1 μA in the present case. Depending on the sensitivity of the PCBA in question and the value of the base level leak

current, first level of failures can occur just due to the parasitic leak current interfering with the functionality of the PCBA. With continued electrochemical process, in the second stage, the dissolved metal ions from the anode slowly migrate to the cathode and deposit in the form of dendrite electrically bridging the anode and cathode. Corresponds to this, the leak current curves show a sudden jump in current (transient part), which can be considered as the beginning of the second level of failure due to ECM (TTF). The time corresponds to this transient state depends on the aggressiveness of the conditions. For instance, the transient state for low pitch distance at a high level of other factors such as temperature, contamination, and voltage is very short. The threshold of around 100 μA for this state is defined for the present analysis, which is detected for the ECM and dendrite formation.

The transient part of the curve where the dendrite filament grows reducing the distance between anode and cathode in the surface conductive electrolyte (therefore corresponding current increase) finally leads to a permanent conductor bridging (high current region after the transient). Generally, the LC value larger than the ECM threshold represents the short circuit caused by a permanent dendrite in the third state [42]. In other words, ECM will be continued until reaching the short circuit. This represents a hierarchical failure mechanism, which leads to a short circuit with interdependencies between the failures.

The Logistic function as a nonlinear growth function has the appropriate shape for describing the current behavior. A logistic function is a familiar S-shaped curve (sigmoid curve) and a popular model for predicting later changes with the below equation [43], [44]:

$$\text{Current value } (t) = A_2 + \frac{A_1 - A_2}{1 + \left(\frac{t}{t_0}\right)^p}$$

Where A_1 is the lower asymptote, A_2 is the upper asymptote, p is the power, and one important point on the logistic curve is the center point or the inflection point, t_0 , where the curvature of the graph changes from concave-upward to concave-downward.

Figure 5.3 displays the current profiles based on the logistic model for the various experimental conditions. Each curve has presented the current average of 8 replications for each condition, which included the average of LCs (stable part) as A_1 , the average of currents of the unstable parts as A_2 , and the center point's average of the transient parts as t_0 . The initial value for all large pitch distance (P2) experiments is less than 100 mA. The

slope of the transition part for P2 experiments is slower than the P1 experiments, which refers to the longer time dendrite formation for the P2 compare to P1 test PCB. Table 5.2 illustrates the logistic model parameters as well as four qualitative classifications of failure risk (<1h, very high risk – 1h< <3h, high risk – 3h< <6h, medium risk - >6h, low risk) according to the average of TTF for each condition. Approximately, the increasing power values and center point values have an inverse relationship with the probability of failure risk on PCB surface for each condition.

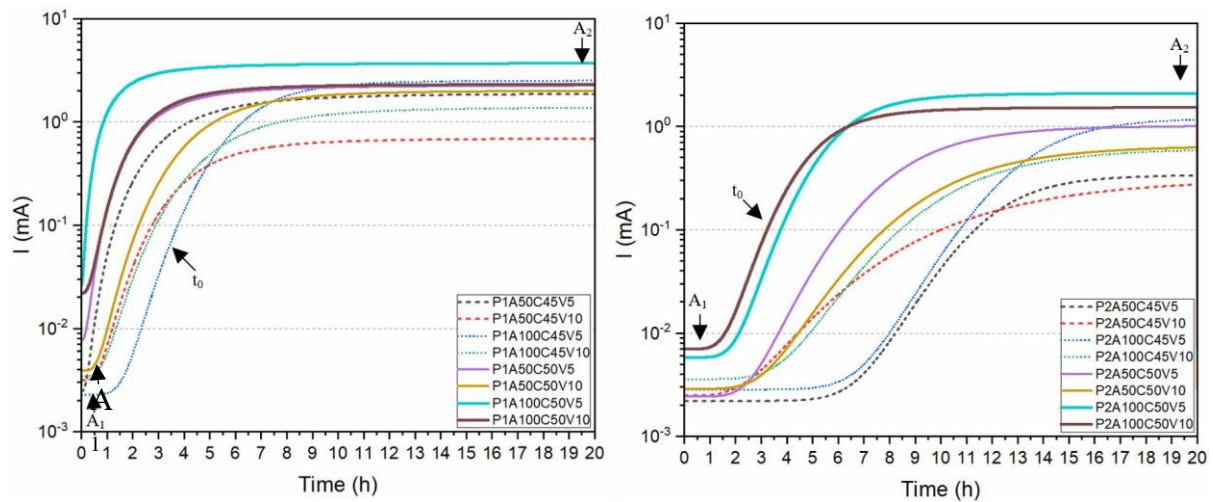


Figure 5.3 The logistic model of current behavior at wholly experimental conditions.

Table 5.2 The logistic model parameters along with failure risk at each condition.

Experiment condition	A_1 (mA)	A_2 (mA)	t_0 (s)	p	Failure risk
<i>P1a100c50v10</i>	0.02204	2.33	10509	2.69	less than 1 hour
<i>P1a100c50v5</i>	0.0266325	3.73	5311	1.89	less than 1 hour
<i>P1a50c50v10</i>	0.0038688	2.01	18680	3.54	between 1-3 hours
<i>P1a100c45v10</i>	0.0034275	1.39	21503	3.58	between 1-3 hours
<i>P1a50c50v5</i>	0.0077025	2.26	10750	2.52	between 1-3 hours
<i>P1a50c45v10</i>	0.003135	0.69	16838	3.39	between 1-3 hours
<i>P1a50c45v5</i>	0.0024775	1.89	14473	2.61	between 1-3 hours
<i>P2a100c50v10</i>	0.0070088	1.53	20231	4.92	between 1-3 hours
<i>P2a50c50v10</i>	0.0028675	0.66	40069	4.91	between 3-6 hours
<i>P1a100c45v5</i>	0.0022775	2.52	24429	5.41	between 3-6 hours
<i>P2a100c50v5</i>	0.0058138	2.1	23372	5.57	between 3-6 hours
<i>P2a100c45v10</i>	0.003575	0.62	41681	5.28	between 3-6 hours
<i>P2a50c45v10</i>	0.0024788	0.33	45877	3.55	between 3-6 hours
<i>P2a50c50v5</i>	0.0024113	1.02	33630	5.24	between 3-6 hours
<i>P2a100c45v5</i>	0.0028438	1.21	50424	9.13	more than 6 hours
<i>P2a50c45v5</i>	0.0022038	0.34	45103	8.91	more than 6 hours

Figure 5.4 and Figure 5.5 present the formation of dendrite filament and permanent electrical connection between anode and cathode on the SIR board surface corresponds to different parameters for testing for which the leak current with transient increase was obtained. The SIR reduction occurs by increasing the surface electrochemical activities (conductivity) between the two electrodes (Anode-Cathode) due to dissolved ionic flux residues in the adsorbed water molecules, which are created by the combination of PCB material, contamination of flux residues, and climatic conditions factors on the SIR pattern surface (stable part-A₁). The ECM is formed by generating conductive electrolyte between two electrodes, and the dissolution of anodic metal ions, and migration and deposition at the cathode. Formation of dendrite from the cathode and growth towards anode is represented by the transient part (t_0). Eventually, the dendritic filament grows adequately large to reduce the minimum distance between the anode and the cathode. With having continuity of the conditions, the metal ionic filaments produce a permanent conductor bridging, and then the short circuit occurs as the most major failure mode on the PCBAs (unstable part-A₂).

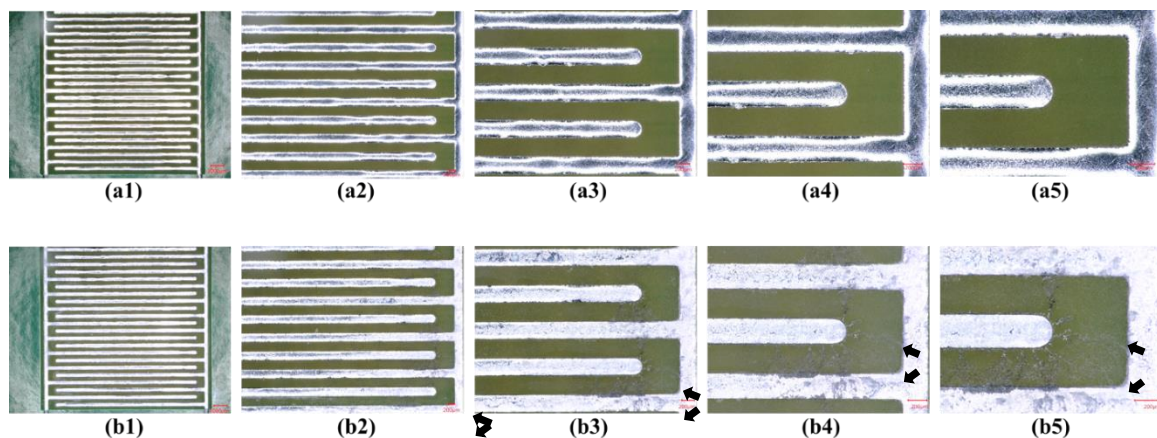


Figure 5.4 The optical appearance of ECM and short circuit on the P1 SIR board before and after exposure to 100 mg/cm², 45°C and 10V. (a before and b after experiment). (1): 20x magnification, (2): 50x magnification, (3): 100x magnification, (4): 150x magnification, (5): 200x magnification.

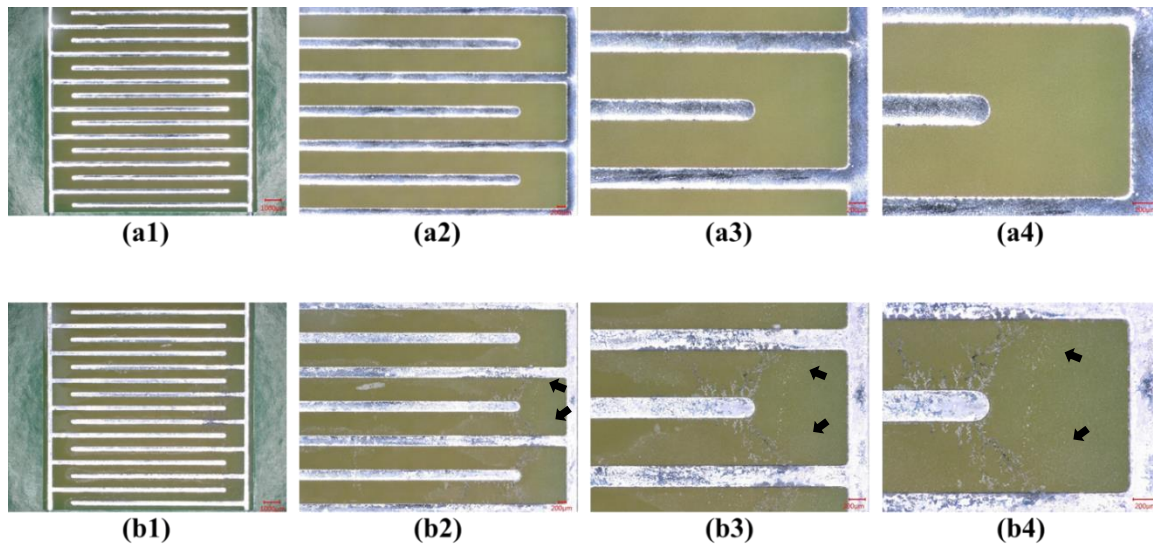


Figure 5.5 The optical appearance of ECM and short circuit on the P2 SIR board before and after exposure to 100 mg/cm², 45°C and 10V. (a before and b after experiment). (1): 20x magnification, (2): 50x magnification, (3): 100x magnification, (4): 150x magnification.

5.3.2 Distribution of LC and TTF

From each experiment, the LC and TTF values were extracted by visual examination of the graphs. Box plots of the eight replications for all sixteen conditions intended for LCs and TTFs are shown in Figure 5.6 and Figure 5.7, respectively. For the LC box plot, there are two extreme values; one of them belongs to the fifth experimental condition at the low level of pitch distance and the high level of other factors (P1a100c50v10) (P1 (small pitch distance)- a100 (high level adipic acid as contamination- c50 (high level temperature)- v10 (high level voltage)), and another one belongs to the experimental condition at the high level of temperature and low levels of other factors (P1a50c50v5).

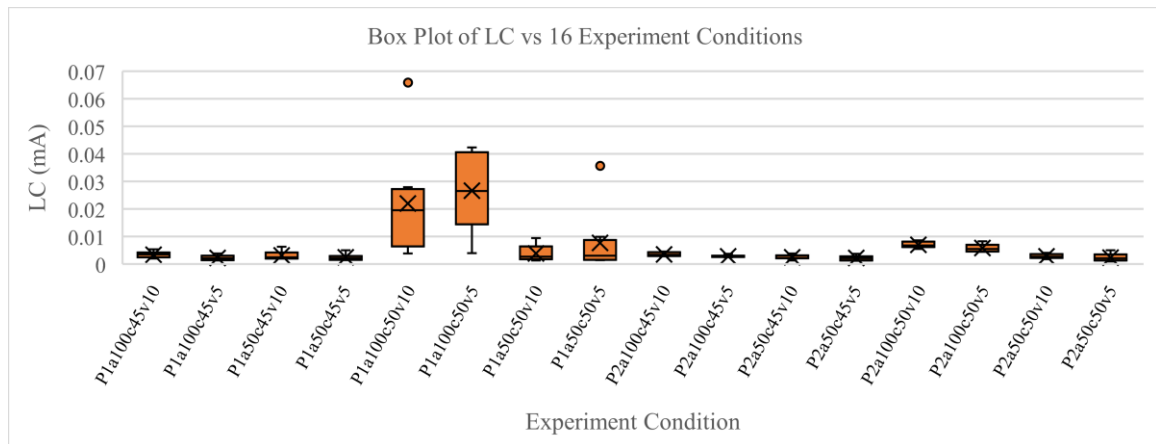


Figure 5.6 Box plot for base leak current values from various experiments.

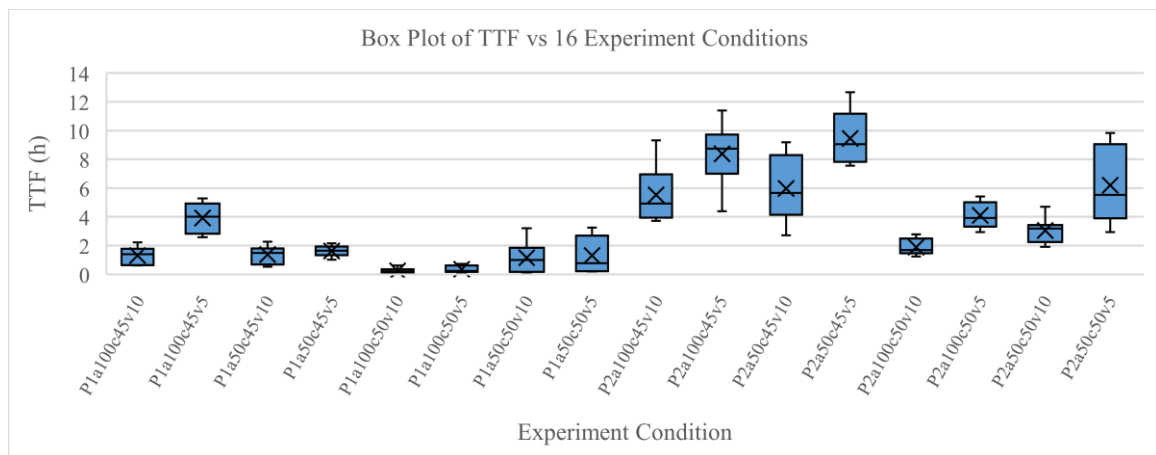


Figure 5.7 Box plot for TTF by ECM from various experiments.

The LC average of just two experimental conditions (P1a100c50v10 and P1a100c50v5) exceeds 0.01 mA. They had similar pitch distance (P1-low level), contamination ($100 \mu\text{g}/\text{cm}^2$ – high level), temperature (50°C - high level), and only dissimilar voltage levels. The mean TTF of these two experimental conditions is also much lower than the other experimental conditions.

Figure 5.8 clearly shows the relation between the average TTFs and the average LCs for all experimental conditions. Approximately, it can be expressed that TTF happened under one hour for all high LC levels (more than 0.01 mA or $10 \mu\text{A}$). In other words, if LC is greater than 0.01 mA, then TTF is always less than 1 hour. Besides, the failure happened after 6 hours for the only high level of the pitch distance at low temperature and voltage levels.

Manuscript I

There is an explicit effect of the pitch distance factor on the average of TTF (Figure 5.8 - left). The lowest TTFs belong to the conditions with small pitch distances, and the highest one belongs to the big pitch distances, regardless of other factors. The experimental conditions versus the average of LCs (Figure 5.8 - right) show the importance of the interaction between factors, especially in the highest LC value, which is independent of an individual factor effect. In the next section using ANOVA, all individual and interaction effects have been explained.

Figure 5.9 describes the relationship and interactions between TTF and LC values using a logistic curve. Considering each x as a LC value, it can predict the proportional TTF according to the estimated parameters from the model inside Figure 5.9.

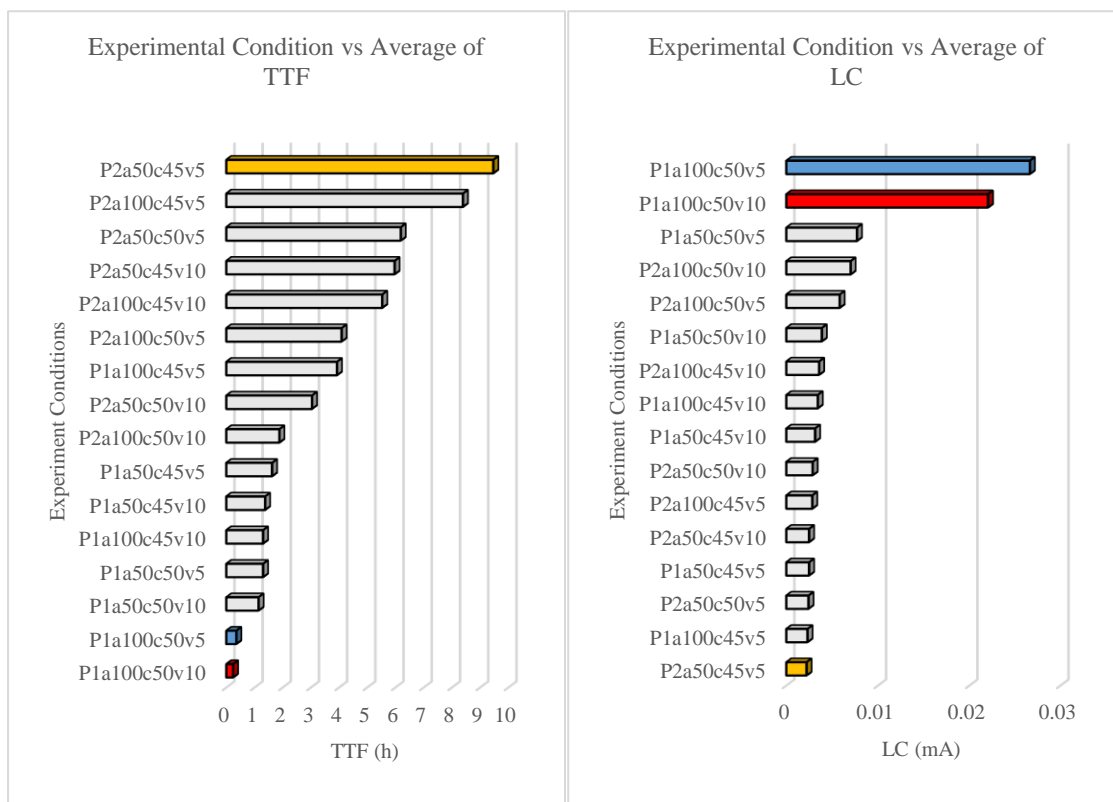


Figure 5.8 The 16 experimental conditions vs. the average of TTF and LC.

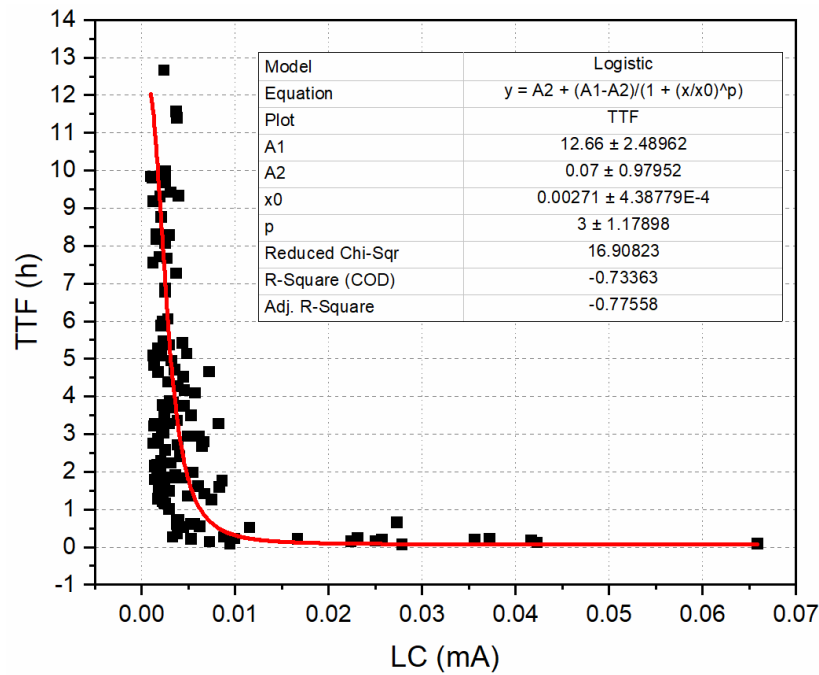


Figure 5.9 TTF versus LC with fitted logistic curve.

5.3.3 ANOVA models for LC and TTF

Due to the skewed distributions of both LC and TTF, a log transform was applied before performing the ANOVA analysis. The stepwise backward elimination procedure was applied to remove non-significant terms in the model, starting with a full model containing all main effects and interactions [45]. After running the procedure and examining the residuals, it appeared that the LC observation had an outlier with a high value for Cook's Distance. This observation was removed before repeating the model selection procedure for the LC model. It was not necessary to remove any outliers for the TTF model. The estimated effects (where factor levels are coded as -1 and 1 for the low and high levels, respectively), as well as the ANOVA table for the final models, are shown in Table 5.3 and Table 5.4. The first column of these two tables, have presented the effect of each significant factor and their interactions along with the negative or positive effect of them on LC and TTF, respectively.

Table 5.3 The ANOVA table with the coded coefficients for LC.

Source	Effect	DF	SS	Contribution	MSS	F-Value	P-Value
Model		6	57.228	65.68%	9.538	38.28	0
Linear		3	39.773	45.65%	13.2333	53.11	0
P	-0.3158	1	3.267	3.75%	3.165	12.7	0.001

Manuscript I

C	0.7884	1	19.794	22.72%	19.7256	79.16	0
T	0.721	1	16.712	19.18%	16.4998	66.22	0
2-Way Interactions		2	14.661	16.83%	7.3507	29.5	0
P*T	-0.3275	1	3.556	4.08%	3.4033	13.66	0
C*T	0.5939	1	11.105	12.75%	11.1959	44.93	0
3-Way Interactions		1	2.794	3.21%	2.7942	11.21	0.001
P*C*T	-0.2967	1	2.794	3.21%	2.7942	11.21	0.001
Error		120	29.901	34.32%	0.2492		
Lack-of-Fit		9	2.705	3.10%	0.3005	1.23	0.286
Pure Error		111	27.196	31.21%	0.245		
Total		126	87.129	100.00%			

Table 5.4 The ANOVA table with the coded coefficients for TTF.

Source	Effect	DF	SS	Contribution	MSS	F-Value	P-Value
Model		7	161.696	78.63%	23.0994	63.07	0
Linear		4	148.569	72.25%	37.1424	101.42	0
P	1.7531	1	98.348	47.82%	98.3483	268.54	0
C	-0.2886	1	2.665	1.30%	2.6648	7.28	0.008
T	-1.0887	1	37.928	18.44%	37.9284	103.56	0
V	-0.5485	1	9.628	4.68%	9.628	26.29	0
2-Way Interactions		2	10.512	5.11%	5.2562	14.35	0
P*T	0.3621	1	4.195	2.04%	4.1946	11.45	0.001
C*T	-0.4443	1	6.318	3.07%	6.3178	17.25	0
3-Way Interactions		1	2.614	1.27%	2.6142	7.14	0.009
P*C*T	0.2858	1	2.614	1.27%	2.6142	7.14	0.009
Error		120	43.947	21.37%	0.3662		
Lack-of-Fit		8	3.094	1.50%	0.3867	1.06	0.396
Pure Error		112	40.854	19.87%	0.3648		
Total		127	205.643	100.00%			

Table 5.5 presents the full factorial regression summaries, including the significant factors and interactions. The significant factors and both interactions (2-ways and 3-ways) are presented at each column in order of highest to lowest significance. In other words, the contamination, temperature, pitch distance on the LC response, as well as the pitch distance, temperature, voltage, and contamination factors on the TTF, have been ranked from the most significant to the least significant effect, respectively. Moreover, the interaction of contamination*temperature (C*T) has more effect than pitch distance*temperature (P*T)

as significant two-way interactions. In addition, the regression equations in un-coded variable units with the determination coefficient (R-sq) and the standard deviation of the error between the model and experiment (S) on responses is accessible. The factors having the biggest effect on TTF were P followed by T. According to this model, the LC value and TTF can be predicted based on the critical factors changes. Approximately, the prediction models for both LC and TTF can predict conditions with 20% upper than the high level and 20% lower than the low level of each factor.

Table 5.5 The full factorial regression model summary.

Response	Significant Factors	Significant 2-Way Interactions	Significant 3-Way Interactions	Factorial Regression Equation	R-sq	S
LC	C	C*T	P*C*T	$\ln(\text{LC}(\text{mA})) = -5.5861$ $- 0.1579 \times P + 0.3942 \times C + 0.3605 \times T$	65.68%	0.499172
	T	P*T		$- 0.1637 \times P \times T + 0.297 \times C \times T$		
	P			$- 0.1484 \times P \times C \times T$		
TTF	P	C*T	P*C*T	$\ln(\text{TTF}(\text{h})) = 0.6858 + 0.8766 \times P$	78.63%	0.605169
	T	P*T		$- 0.1443 \times C - 0.5443 \times T$		
	V			$- 0.2743 \times V + 0.181 \times P \times T$		
	C			$- 0.2222 \times C \times T$ $+ 0.1429 \times P \times C \times T$		

5.3.4 Model validation

The validity of the ANOVA results depends on the assumptions of normality, independence and constant variance of the errors [46]. Diagnostic plots to check these assumptions are shown in Figure 5.10. The normal probability plots and histograms suggest that the residuals for both models follow a normal distribution. There is no indication that the independence assumption of the errors is violated from the plots of residuals over time. The assumption of constant variance could be debated, as for LC, residual variance appears to increase with increasing fitted values, whilst for TTF, the residual variance appears to decrease with increasing fitted values. However, there is no extreme departure from constant variance, and overall the results are deemed acceptable.

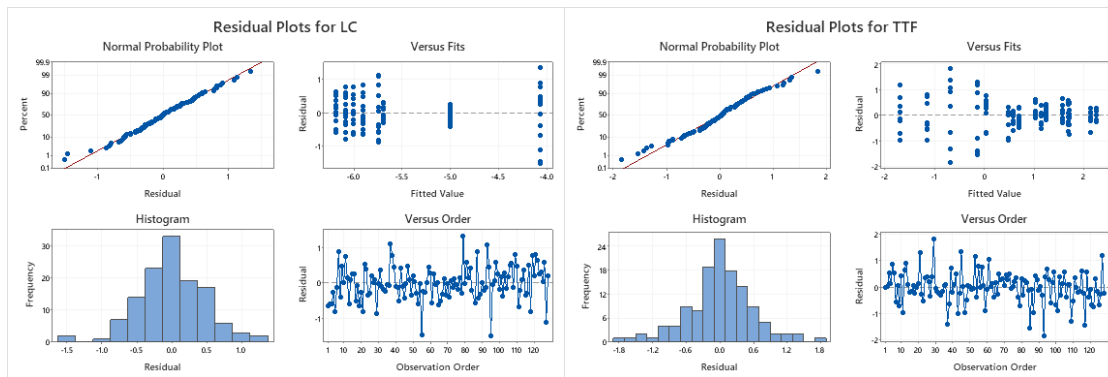


Figure 5.10 Residual plots for LC (left) and TTF (right).

5.3.5 Model interpretation

The ANOVA models show that P has a large positive effect on TTF, whilst C, T, and V all negatively affect TTF. In the LC model, P has a small negative effect on LC, whilst C and T have a larger positive effect on LC. It is noteworthy that effect of V on LC is not significant, however V is more important for ECM failure. Lower influence of V on LC might be due to the fact there is a limit of current that can be passed through the limiting thickness of water film. Hence, increase in V will not significantly influence the leak current unless other parameters such as P or C changes. On the other hand, voltage is an important parameters determining the electric field for dendrite growth, therefore shows bigger influence on TTF due to dendrite growth. Moreover, the LC as mentioned in the first part of this section, belongs to SIR reduction part and occurs by increasing the conductivity between the anode and cathode due to dissolved ionic flux residues in the adsorbed water molecules, which has created by the combination of PCB surface material, contamination of flux residues, and climatic conditions factors before ECM.

The contamination and temperature interaction has more significant effect on LC and TTF compared to other interactions on LC prediction. Following this, the interaction of pitch distance with temperature and contamination significantly affects LC values. These factors and interaction effects on LC refer to initial stage part of the leak current curves, which represents the initial current due to the faradic process before culminating into the dendrite formation.

Figure 5.12 in the Appendix also shows all the LC and TTF interactions by the contour plots. Generally, there is an interaction effect between two different factors if they show

the different behavior (decreasing or increasing) of diverse levels on the response. For instance, the contamination and temperature interaction (C*T), as one common two-way interaction in both responses, visually are displayed the interaction. For TTF response, in the low level of temperature, increasing level of contamination, causes a little incremental effect on TTF value, but in the high level of the temperature, increasing contamination level causes a high decrement effect on TTF.

As the models contain many interactions, direct interpretation of the coefficients is challenging. However, predictions from the models can be calculated for a range of inputs in order to reveal the implications of the model. For examining the model's accuracy, as an instance, five levels of contamination at the low level of temperature and the high levels of the pitch distance and voltage, with five replications on each level, have been measured. The predicted values of both responses (average of LC and TTF) together with the Prediction Interval (PI) are shown in Figure 5.11. These figures present the accuracy of the prediction model compared with experimental results for LC and TTF. The model predictions are close to the observed experimental responses, suggesting that the models extrapolate reasonably well to contamination levels outside the original experimental range.

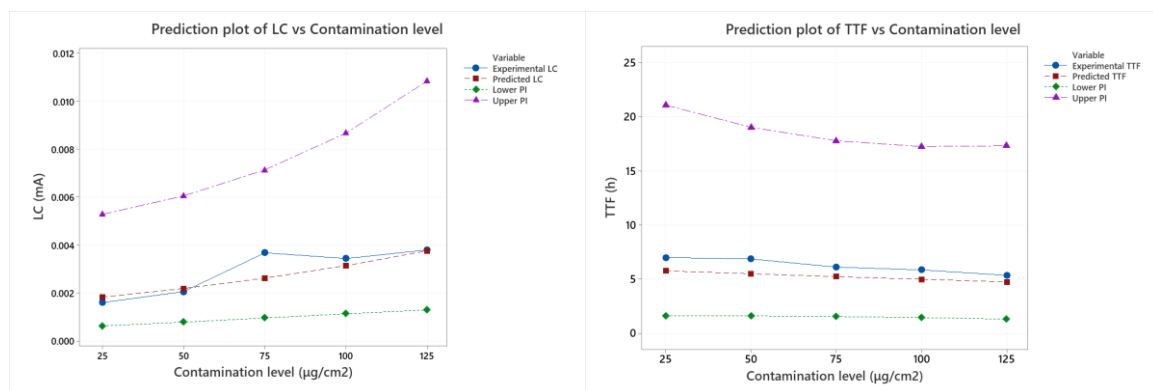


Figure 5.11 Prediction plot for LC (left) and TTF (right). Each blue point is the mean of 5 experiments. The red squares show the model predictions. The purple triangles and green diamonds show the model 95 % prediction interval.

5.3.6 Overall discussion

This section provides a summary of main outcomes and new insight from this investigations:

Manuscript I

- In this study, the full factorial regression analysis has been used to investigate the significance of four changeable factors (P, C, T and V) and their interactions effects under the constant relative humidity, one contamination type, and longtime of experiments on two main failure modes (leakage current (LC) and time to failure (TTF) due to ECM that cause the short circuit on the PCBAs), simultaneously. In tables 3, 4, and 5, investigation of main significant factors effects, their interactions, as well as how they will affect responses (i.e., LC and TTF), with more details have been presented. One novelty of this study is to consider the combination of critical factors together and assessing their interactions on PCB surface at the same time, which shows a new insight for doing DoE, simulate, and model close to realistic conditions. In addition, from the scientific contribution point of view, it creates a more comprehensive understanding of the effects of different factors/levels/interactions on PCB surface when exposed to various conditions.
- Another important aspect is that the LC and TTF have been measured together at 8 replications for each condition (Figure 5.13 and Figure 5.14). The correlation between responses (i.e., LC and TTF) is calculated and presented in Figure 5.9. Moreover, the correlation between inputs (i.e., 4 critical factors) and responses (i.e., LC and TTF) by using factorial regression equation have been estimated and presented in table 5. Without waiting until failure happen for some conditions which can take a long time, to reach and observe TTF; having LC and its relation with TTF (which is presented in Figure 5.9) at various conditions, TTF can be predicted. Here the new insight is to study and investigate the LC and TTF interactions on the PCB surface at various conditions and finding appropriate equation to predict TTF based on LC changes. Moreover, the adequacy and the accuracy of the regression model, which is the correlation between factors and responses, have been investigated and displayed in Figures 10 and 11.
- Partitioning the current (C) behavior in Figure 5.2 at three general parts (stable, transient, and unstable parts) gives us another insight into the overall current (C) behavior, which is like a sigmoid curve. The mathematical simulation of the entire current (C) behavior and their parameters is presented in Figure 5.3 and Table 5.2 by the Logistic function (as a nonlinear growth function for predicting later changes). This provides the possibility for making the prediction model of whole

current (C) behavior at various conditions. The combination of logistic function and regression equation can be used for creating a logistic prediction model to predict the current behavior at different conditions as another novelty of this study. In addition, the classification of risky conditions is another new insight of this research according to the average of TTF for each condition, which presented in Table 5.2.

5.4 Conclusion

- i. The pitch distance has a major effect in both responses but in different directions; in other words, for LC, pitch distance has a negative effect, while for TTF, it has a positive effect.
- ii. The voltage does not affect the LC values significantly, while temperature, contamination, and pitch distance have in the decreasing order of most significant effects. However, voltage has significant effect of TTF due to ECM.
- iii. The common significant 2-way interactions for both responses are contamination*temperature (C*T) and pitch distance*temperature (P*T), and 3-way interaction is pitch distance*contamination*temperature (P*C*T).
- iv. The best setting of factors have been identified in order to reach to the minimum LC and maximum TTF for more sustainable PCBAs in the high level of pitch distance and the low level of other factors. Having this condition, means the low level of each factor except pitch distance, the lowest LC value can presented between 0.0015-0.0026 mA and the TTF range between 8-11 hours.
- v. Approximately the higher LC has related to the lower TTF. It means that with increasing the LC, the probability of failure increases.
- vi. The prediction models with a reasonable extrapolation for both LC and TTF can approximately predict conditions with 20% upper than the high level and 20% lower than the low level of each factor.

Acknowledgements

The present research work was carried out as a part of work in CELCORR/CreCon consortium (<https://celcorr.dtu.dk>). The authors would like to acknowledge the

CELCORR/CreCon consortium, and Innovation Fund Denmark for the funding support. Moreover, the authors would like to acknowledge Murat Kulahci and Max Peter Spooner from DTU compute for their support.

References

- [1] J.B. Jacobsen, J.P. Krog, L. Rimestad, A. Riis, A.H. Holm, Climate-Protective Packaging: Using Basic Physics to Solve Climatic Challenges for Electronics in Demanding Applications, *IEEE Ind. Electron. Mag.* 8 (2014) 51–59. <https://doi.org/10.1109/MIE.2014.2330912>.
- [2] V. Verdingovas, M.S. Jellesen, R. Ambat, Relative effect of solder flux chemistry on the humidity related failures in electronics, *Solder. Surf. Mt. Technol.* 27 (2015) 146–156. <https://doi.org/10.1108/SSMT-11-2014-0022>.
- [3] H. Conseil, V.C. Gudla, M.S. Jellesen, R. Ambat, Humidity build-up in a typical electronic enclosure exposed to cycling conditions and effect on corrosion reliability, *IEEE Trans. Compon. Packag. Manuf. Technol.* 6 (2016) 1379–1388. <https://doi.org/10.1109/TCPMT.2016.2590779>.
- [4] K. Piotrowska, V. Verdingovas, R. Ambat, Humidity-related failures in electronics: effect of binary mixtures of weak organic acid activators, *J. Mater. Sci. Mater. Electron.* 29 (2018) 17834–17852. <https://doi.org/10.1007/s10854-018-9896-0>.
- [5] V. Verdingovas, M.S. Jellesen, R. Ambat, Impact of NaCl contamination and climatic conditions on the reliability of printed circuit board assemblies, *IEEE Trans. Device Mater. Reliab.* 14 (2014) 42–51. <https://doi.org/10.1109/TDMR.2013.2293792>.
- [6] M.A.M. Piah, A. Darus, Modeling Leakage Current and Electric Field Behavior of Wet Contaminated Insulators, *IEEE Trans. Power Deliv.* 19 (2004) 432–433. <https://doi.org/10.1109/TPWRD.2003.820409>.
- [7] V. Verdingovas, S. Joshy, M.S. Jellesen, R. Ambat, Analysis of surface insulation resistance related failures in electronics by circuit simulation, *Circuit World.* 43 (2017) 45–55. <https://doi.org/10.1108/CW-09-2016-0040>.
- [8] K. Piotrowska, M.S. Jellesen, R. Ambat, Water film formation on the PCBA surface and failure occurrence in electronics, in: 2018 IMAPS Nord. Conf. Microelectron. Packag., IEEE, 2018: pp. 72–76. <https://doi.org/10.23919/NORDPAC.2018.8423854>.
- [9] K. Piotrowska, F. Li, R. Ambat, Thermal decomposition of binary mixtures of organic activators used in no-clean fluxes and impact on PCBA corrosion reliability, *Solder. Surf. Mt. Technol.* 32 (2019) 93–103. <https://doi.org/10.1108/SSMT-05-2019-0020>.
- [10] D. Minzari, M.S. Jellesen, P. Møller, R. Ambat, Morphological study of silver corrosion in highly aggressive sulfur environments, *Eng. Fail. Anal.* 18 (2011) 2126–2136. <https://doi.org/10.1016/j.engfailanal.2011.07.003>.
- [11] L. Hua, H.N. Hou, Electrochemical corrosion and electrochemical migration of 64Sn-35Bi-1Ag solder doping with xGe on printed circuit boards, *Microelectron. Reliab.* 75 (2017) 27–36. <https://doi.org/10.1016/j.microrel.2017.06.005>.
- [12] H.F. Church, B.C. Roberts, Failure mechanisms of electronic components, in: 4th Annu.

- Symp. Phys. Fail. Electron. IRPS 1965, IEEE, 1965: pp. 156–178. <https://doi.org/10.1109/IRPS.1965.362319>.
- [13] R. Ambat, H. Conseil-Gudla, V. Verdingovas, Corrosion in Electronics, in: *Encycl. Interfacial Chem.*, Elsevier, 2018: pp. 134–144. <https://doi.org/10.1016/B978-0-12-409547-2.13437-7>.
- [14] S. Bahrebar, D. Zhou, S. Rastayesh, H. Wang, F. Blaabjerg, Reliability assessment of power conditioner considering maintenance in a PEM fuel cell system, *Microelectron. Reliab.* 88–90 (2018) 1177–1182. <https://doi.org/10.1016/j.microrel.2018.07.085>.
- [15] S. Rastayesh, S. Bahrebar, A.S. Bahman, J.D. Sørensen, F. Blaabjerg, Lifetime estimation and failure risk analysis in a power stage used in wind-fuel cell hybrid energy systems, *Electron.* 8 (2019). <https://doi.org/10.3390/electronics8121412>.
- [16] A. Dasgupta, M. Pecht, Material Failure Mechanisms and Damage Models, *IEEE Trans. Reliab.* 40 (1991) 531–536. <https://doi.org/10.1109/24.106769>.
- [17] J. Swingler, *Reliability Characterisation of Electrical and Electronic Systems*, Elsevier, 2015. <https://doi.org/10.1016/C2013-0-16487-2>.
- [18] V. Verdingovas, M.S. Jellesen, R. Ambat, Influence of sodium chloride and weak organic acids (flux residues) on electrochemical migration of tin on surface mount chip components, *Corros. Eng. Sci. Technol.* 48 (2013) 426–435. <https://doi.org/10.1179/1743278213Y.0000000078>.
- [19] V. Verdingovas, M.S. Jellesen, R. Ambat, Colorimetric visualization of tin corrosion: A method for early stage corrosion detection on printed circuit boards, *Microelectron. Reliab.* 73 (2017) 158–166. <https://doi.org/10.1016/j.microrel.2017.05.005>.
- [20] B.I. Noh, S.B. Jung, Behaviour of electrochemical migration with solder alloys on printed circuit boards (PCBs), *Circuit World.* 34 (2008) 8–13. <https://doi.org/10.1108/03056120810918060>.
- [21] H. Conseil-Gudla, M.S. Jellesen, R. Ambat, Printed Circuit Board Surface Finish and Effects of Chloride Contamination, Electric Field, and Humidity on Corrosion Reliability, *J. Electron. Mater.* 46 (2017) 817–825. <https://doi.org/10.1007/s11664-016-4974-7>.
- [22] X. He, L. Zhou, J. Shen, A study for a typical leakage failure of PCBA with no-cleaning process, in: *2016 17th Int. Conf. Electron. Packag. Technol.*, IEEE, 2016: pp. 53–56. <https://doi.org/10.1109/ICEPT.2016.7583088>.
- [23] J. Dempere, N. Papakonstantinou, B. O’Halloran, D.L. Van Bossuyt, Risk modeling of variable probability external initiating events, *Proc. - Annu. Reliab. Maintainab. Symp.* (2017). <https://doi.org/10.1109/RAM.2017.7889704>.
- [24] F. Cirolia, The effects of environmental contaminants on electronic power supplies, in: *Twenty-Third Int. Telecommun. Energy Conf. INTELEC 2001, IEE*, 2001: pp. 30–34. <https://doi.org/10.1049/cp:20010575>.
- [25] V. Verdingovas, M.S. Jellesen, R. Ambat, Effect of pulsed voltage on electrochemical migration of tin in electronics, *J. Mater. Sci. Mater. Electron.* 26 (2015) 7997–8007. <https://doi.org/10.1007/s10854-015-3454-9>.
- [26] B. Rudra, M. Pecht, D. Jennings, Assessing time-to-failure due to conductive filament formation in multi-layer organic laminates, *IEEE Trans. Components, Packag. Manuf.*

- Technol. Part B. 17 (1994) 269–276. <https://doi.org/10.1109/96.311773>.
- [27] Y. Zhou, Y. Chen, Q. Xie, Y. Li, Modeling Research of Electrochemical Migration Failure on Printed Circuit Board, in: Proc. - 2018 Progn. Syst. Heal. Manag. Conf. PHM-Chongqing 2018, IEEE, 2019: pp. 209–214. <https://doi.org/10.1109/PHM-Chongqing.2018.00042>.
- [28] B. Rudra, M.J. Li, M. Pecht, D. Jennings, Electrochemical Migration in Multichip Modules, Circuit World. 22 (1996) 67–70. <https://doi.org/10.1108/03056129610799868>.
- [29] Y. Zhou, Y. Li, Y. Chen, M. Zhu, Life Model of the Electrochemical Migration Failure of Printed Circuit Boards under NaCl Solution, IEEE Trans. Device Mater. Reliab. 19 (2019) 622–629. <https://doi.org/10.1109/TDMR.2019.2938010>.
- [30] K. Hinkelmann, Design and Analysis of Experiments, John Wiley & Sons, Inc., Hoboken, NJ, USA, 2012. <https://doi.org/10.1002/9781118147634>.
- [31] S. Dahbi, H. El Moussami, L. Ezzine, Multiple regression model for surface roughness using full factorial design, in: Proc. 2015 Int. Conf. Ind. Eng. Syst. Manag. IEEE IESM 2015, IEEE, 2016: pp. 439–444. <https://doi.org/10.1109/IESM.2015.7380194>.
- [32] R. Mead, S.G. Gilmour, A. Mead, Statistical principles for the design of experiments, Cambridge University Press, Cambridge, 2009. <https://doi.org/10.1017/CBO9781139020879>.
- [33] G. Sarkar, Y.F. Chong, P.A. Collier, A study of the factors affecting surface insulation resistance measurements, J. Mater. Sci. Lett. 17 (1998) 1963–1965. <https://doi.org/10.1023/A:1006635917381>.
- [34] A.S.L. Chan, T.A. Shankoff, Interrelating surface insulation resistance test patterns, Circuit World. 15 (1989) 34–38. <https://doi.org/10.1108/EB044007>.
- [35] H. Conseil, M. Stendahl Jellesen, R. Ambat, Contamination profile on typical printed circuit board assemblies vs soldering process, Solder. Surf. Mt. Technol. 26 (2014) 194–202. <https://doi.org/10.1108/SSMT-03-2014-0007>.
- [36] K. Piotrowska, R. Ambat, Residue-Assisted Water Layer Build-Up Under Transient Climatic Conditions and Failure Occurrences in Electronics, IEEE Trans. Components, Packag. Manuf. Technol. 10 (2020) 1617–1635. <https://doi.org/10.1109/TCPMT.2020.3005933>.
- [37] B. Song, M.H. Azarian, M.G. Pecht, Impact of dust on printed circuit assembly reliability, in: IPC APEX EXPO 2012, 2012: pp. 1643–1659.
- [38] F. Cirolia, C. Finan, The effects of environmental contaminants on electronic power supplies, in: IEE Conf. Publ., 2001: pp. 30–34. <https://doi.org/10.1049/cp:20010575>.
- [39] K. Piotrowska, R. Ud Din, F.B. Grumsen, M.S. Jellesen, R. Ambat, Parametric Study of Solder Flux Hygroscopicity: Impact of Weak Organic Acids on Water Layer Formation and Corrosion of Electronics, J. Electron. Mater. 47 (2018) 4190–4207. <https://doi.org/10.1007/s11664-018-6311-9>.
- [40] K. Piotrowska, R.U. Din, M.S. Jellesen, R. Ambat, Effect of solder mask surface chemistry and morphology on the water layer formation under humid conditions, IEEE Trans. Components, Packag. Manuf. Technol. 8 (2018) 1756–1768. <https://doi.org/10.1109/TCPMT.2018.2792047>.
- [41] K. Piotrowska, M. Grzelak, R. Ambat, No-Clean Solder Flux Chemistry and Temperature

- Effects on Humidity-Related Reliability of Electronics, *J. Electron. Mater.* 48 (2019) 1207–1222. <https://doi.org/10.1007/s11664-018-06862-4>.
- [42] G. Rza¸dkowski, L. Sobczak, A Generalized Logistic Function and its Applications, *Found. Manag.* 12 (2020). <https://doi.org/10.2478/fman-2020-0007>.
- [43] N.A. Kudryashov, Logistic function as solution of many nonlinear differential equations, *Appl. Math. Model.* 39 (2015). <https://doi.org/10.1016/j.apm.2015.01.048>.
- [44] J. Antoy, *Design of Experiments for Engineers and Scientists*, Elsevier, 2014. <https://doi.org/10.1016/C2012-0-03558-2>.
- [45] R.M. Heiberger, Computation for the analysis of designed experiments, *Comput. Anal. Des. Exp.* (2015) 1–683. <https://doi.org/10.1002/9781119102809>.

Appendix

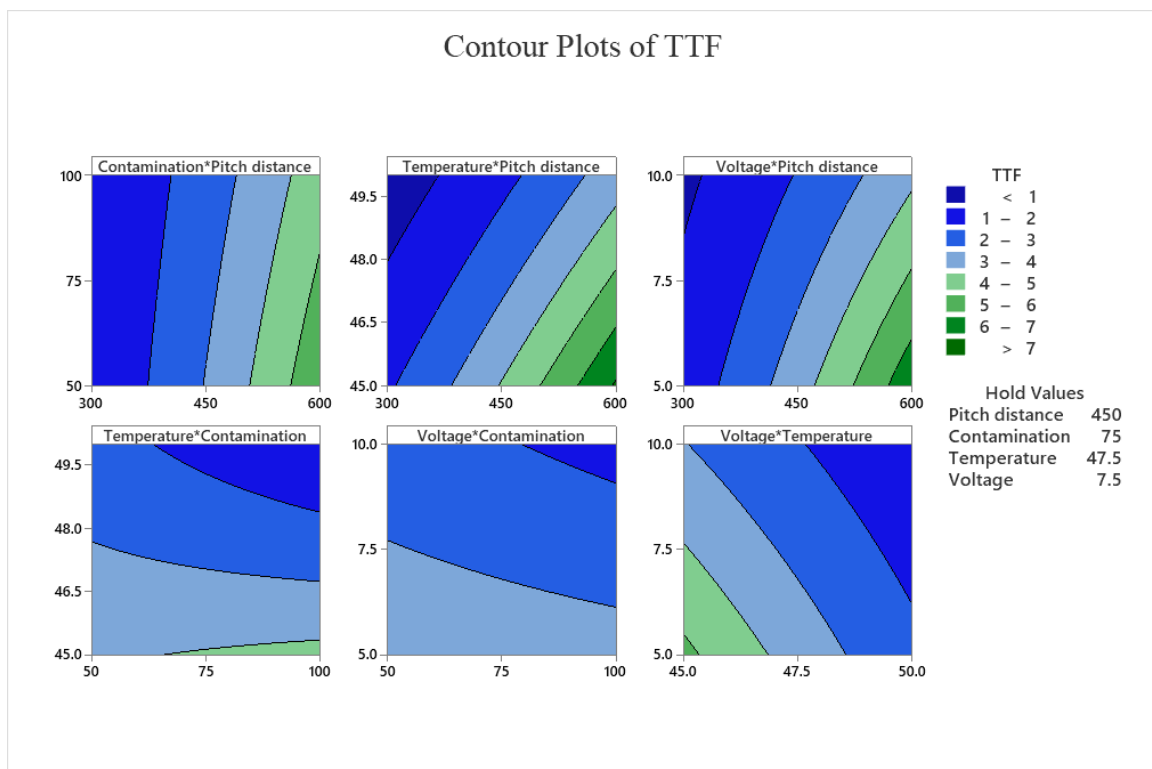
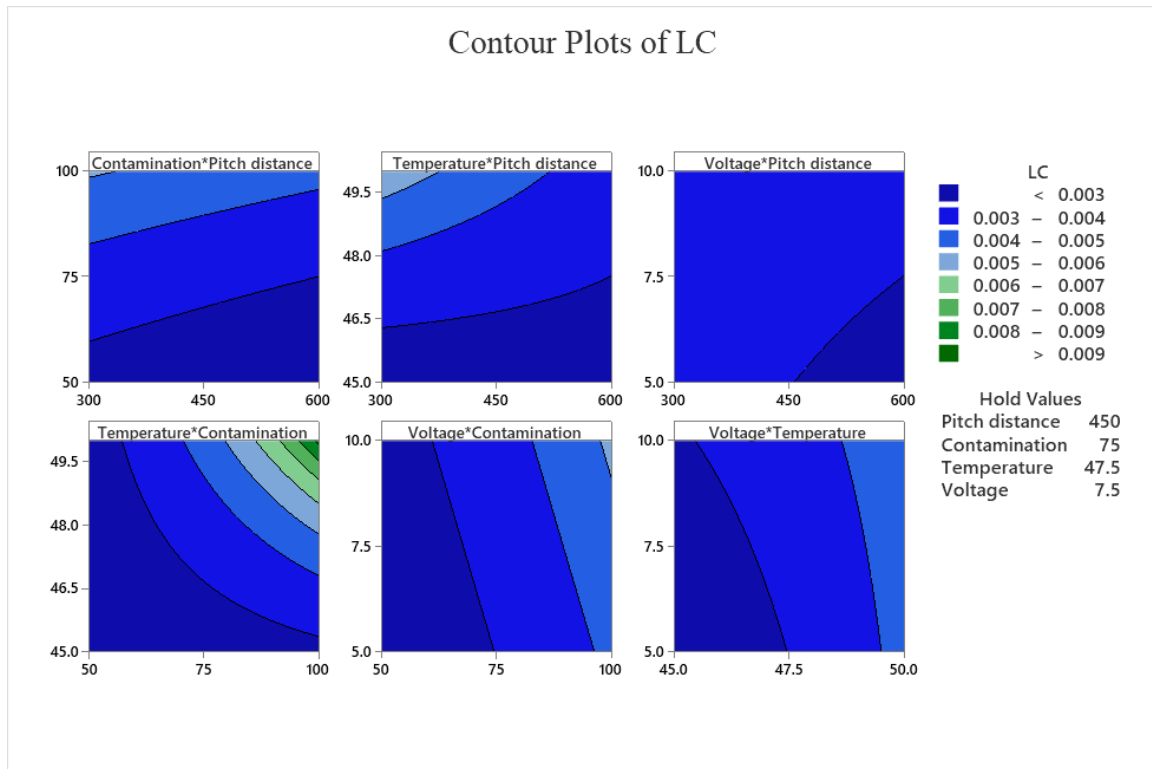


Figure 5.12 The contour plot for LC (up) and TTF (down).

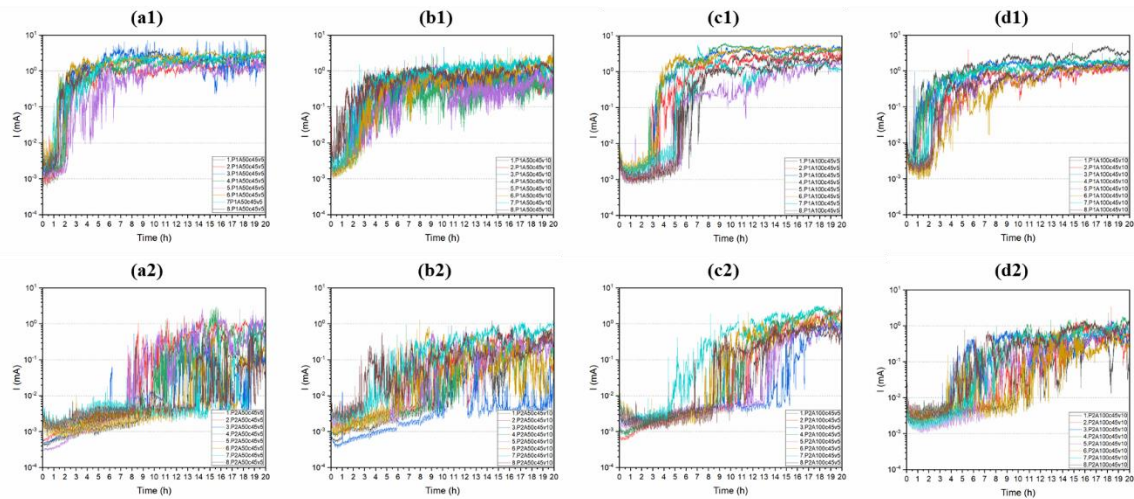


Figure 5.13 Overall leakage current results with exposure to all factors and levels on the SIR patterns at the low level of temperature (45°C): (a1) the low pitch distance, contamination, and voltage level. (b1) The low pitch distance, contamination, and high voltage level. (c1) The low pitch distance, voltage, and high contamination level. (d1) The low pitch distance, high contamination, and voltage level. (a2) The high pitch distance, low contamination, and voltage level. (b2) The high pitch distance, voltage, and contamination level. (c2) The high pitch distance, contamination, and low voltage level. (d2) The high pitch distance, contamination, and voltage level.

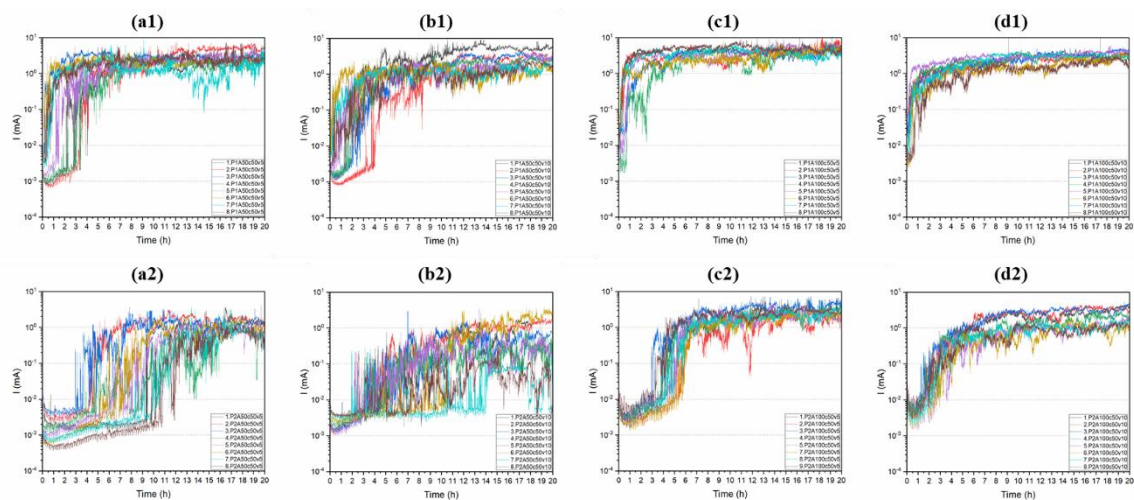


Figure 5.14 Overall leakage current results with exposure to all factors and levels on the SIR patterns at the high level of temperature level (50°C): (a1) the low pitch distance, contamination and voltage level, (b1) The low pitch distance, contamination, and high voltage level, (c1) The low pitch distance, voltage, and high contamination level, (d1) The low pitch distance, high contamination, and voltage level, (a2) The high pitch distance, low contamination, and voltage level, (b2) The high pitch distance, voltage, and high contamination level, (c2) The high pitch distance, contamination, and low voltage level, (d2) The high pitch distance, contamination and voltage level.

6 Manuscript II

Time to Failure Prediction on Printed Circuit Board Surface under Humidity using Probabilistic Analysis

*S. Bahrebar, R. Ambat, Time to Failure Prediction on a Printed Circuit Board Surface Under Humidity Using Probabilistic Analysis, J. Electron. Mater. (2022) 1–19.
<https://doi.org/10.1007/s11664-022-09668-7>.*

ABSTRACT- This paper presented the probabilistic study of time to failure (TTF), which is caused by combinations of various important controllable factors on printed circuit board (PCB) surface under humidity. The study investigated the impact of four changeable factors including pitch distance, temperature, contamination, and voltage, each of them at three levels upon the surface insulation resistance (SIR) test boards. Constant 98% relative humidity (RH) with adipic acid as contamination related to flux residue was used for a 20 hours parametric experiments. Two main states were considered on the whole output current measurements: the stable part before and the unstable part after the short transition phase due to electrochemical migration (ECM) on the PCB surface. Leakage current (LC) in the first state and TTF at the beginning of the second stage was measured with five replications for each condition as the predictive indicator in all models. The trend of LC and TTF was also investigated on three levels of each factor. In addition, probabilistic distribution analysis using fitted Weibull distribution, multivariate regression analysis, and the classification and regression tree (CART) analysis were used to predict the probability of TTF and failure risk prediction on the PCB surface. All the prediction models had an acceptable prediction of TTF at diverse accuracy levels, according to changing factors/levels. Nevertheless, the multivariate regression analysis had the best prediction, highest R-sq, and lowest error compared to the other models.

Keywords: probabilistic analysis, prediction model, probability of failure, PCB surface, time to failure.

6.1 Introduction

Development in electronics usage, causes an increase in the user demand for robust performance in various environments, while miniaturization is occurring at system, printed circuit board assembly (PCBA), and component level [1]. The use of a smaller size of components is growing due to PCBA miniaturization, which causes a higher electric field at the same conditions compared to a larger size when exposed to humid conditions resulting in water film formation [2]. The increase in component density and their influence on each other under the space reduction on the PCBAs is a challenging issue today especially for use under harsh conditions [3]. Many of the small-sized electric components consequently have smaller pitch distances that play an important role in their failure mechanisms [4], [5]. Hence, pitch distance (P) has been considered as one of the critical factors having a direct effect on increasing or decreasing the time to failure (TTF) on PCBAs when exposed to various climatic conditions. It refers to the spacing between two oppositely charged conduction lines or between electrodes of a component on PCBAs.

The soldering process, especially wave soldering introduce contamination during manufacturing process, which together with other factors influence the humidity related corrosion failures on PCB surface [6], [7]. Moreover, the hygroscopic nature of the flux residue changes the humidity boundary for water film formation when exposed to a climatic profile during operational environment [8]. Adipic acid as active components in flux residue could have different deliquescence relative humidity (DRH) and efflorescence relative humidity (ERH) level depending on the chemistry [9]. Hence, the contamination (C) is one of the other critical factors beside pitch distance for failure creation on PCB surface under humid exposure. Generally, contamination on a PCB surface originates from three cases namely: (i) manufacturing process such as flux residue as described before, (ii) service related contamination for example atmospheric particles settling on the PCB surface, and (iii) handling of PCB such as finger prints resulting from without use of gloves [10]. Among these, the manufacturing process is most important as the other two sources of contamination are mostly removed by careful handling and proper packaging. Manufacturing process related contamination could again be divided into that originating from base PCB manufacturing process and PCB assembling process. Among this PCB assembling process is the last process and the use of no-clean flux resulting in a dominating factor for contamination.

The climatic conditions have a fundamental role in the initial failure process on PCB surface. Climatic conditions means level of humidity, temperature, and their variations. These two factors can determine the water vapor range that starts to condense on the PCB surface. Additionally, this water condensation is also dependent on the hygroscopic nature of ionic residues from soldering process under transient conditions of varying humidity and temperature [11]. Therefore, the temperature (T), is another important factor beside pitch distance and the contamination for failure creation on PCB surface. Furthermore, temperature plays a crucial role in accelerating the corrosion of metallic materials on PCB surface [12]. It should be noted that, in this study only the temperature is considered in different levels, while keeping the humidity level above the deliquescent humidity level proportional to the adipic acid as the only contamination type [13].

The water layer formation due to pitch distance, ionic contamination remained from the soldering process, climatic conditions change, and surface material properties, leading to the surface insulation resistance (SIR) reduction on PCB surface if closely spaced biased points are connected. The thin water layer formation easily acts as a conductor by making electrochemical cells for corrosion failure mechanisms [14]. By applying the voltage, the electric field is made through the thin water layer, subsequently leading to corrosion failure in the form of dendrite formation due to ECM on the PCB surface. This event will cause a sudden increase in the leakage current (LC), resulting in the operational capacity of the PCBs. Thus, the voltage (V) is considered as another critical factor that creates a distinct potential bias between the anode and cathode, and makes the migration of anodic metal ions in the conductive water layer and subsequent deposition at the cathode [15].

In this study, the pitch distance levels of 300, 600, and 1000 μm as P1, P2, and P3 have been considered proportional to actual surface mount devices (SMD) components. As one of the important WOAs, adipic acid is studied for all experiments in three contamination levels of 50, 75, and 100 $\mu\text{g}/\text{cm}^2$ as C1, C2, and C3 matching with typical levels of flux residues usually seen after the wave soldering process [16]. The temperature is varied at three levels; 40, 45, 50 $^{\circ}\text{C}$, while keeping the humidity level above the deliquescent relative humidity level (98%) for the adipic acid. Beside, three levels of the voltage have been considered for this study, which contained 5, 7.5, and 10 V matching with input voltage range of low power components and devices [17]. Figure 6.1 presents the overview of short

circuit failure mechanisms between biased points on PCB surface, and critical factors of its failure causes.

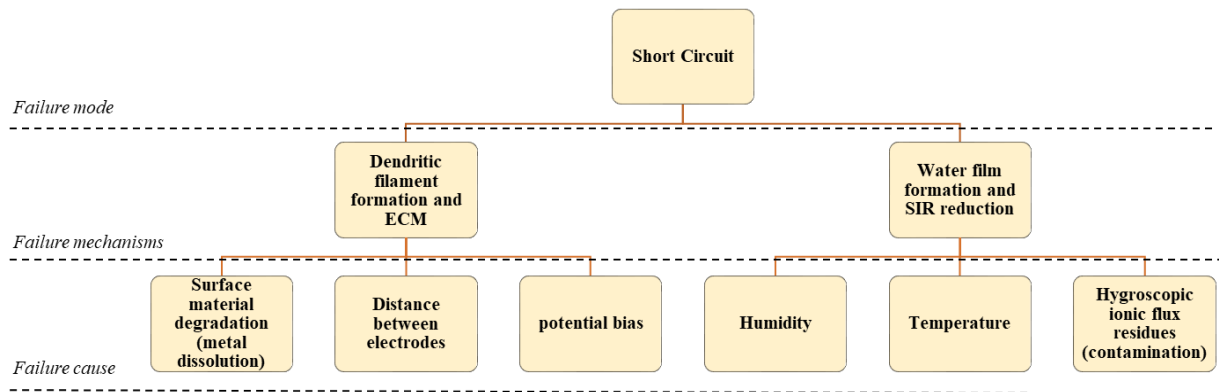


Figure 6.1 Failure mechanisms and failure causes of short circuit as the main failure mode on PCB surface.

Different studies have focused on the effect of climate conditions at various potential biases [18], [19], as well as the effect of PCB surface failure and contamination types [20], [21]. Nonetheless, only a limited body of research has experimentally investigated failure prediction on PCBs [22], [23] while there is no discussion about all of critical factors effects and TTF prediction using probabilistic approaches at critical conditions, along with combination factors. While the probabilistic approach provides the required methods and tools for reliability and risk assessment [24]; it works well in lifetime prediction and the estimation of the probability of failure of electronic components as well [25]. For the humidity robustness of electronic devices, it is also important to predict and determine TTFs. Usually, the probabilistic approaches are applied for the reliability assessment of electronics devices, predicting TTFs and quantifying the probability of failures at various conditions.

Accordingly, this study addresses the probabilistic approach of various controllable factors influencing the TTF due to ECM on PCB surface, as well as the resulting probability of failure (PoF) and risk prediction at various conditions. The outcomes are monitored as an evaluation criterion for four appraised and changeable factors of pitch distance, contamination, temperature, and voltage, each at low, medium, and high levels. Additionally, 98% (RH) and one kind of important contamination (adipic acid) for a 20 hour experimental period as constant factors are considered on the SIR test boards. The effects of factors/levels with five replications in each condition on TTFs and LCs and their

relationship are statistically studied in the primary step. Focusing more on pitch distance and temperature as the two most significant factors, the best understanding of these two factor effects has been obtained on the PCB surface failure. In the next step, using probabilistic distribution analysis, the appropriate probability distribution for each condition according to three approaches; based on the nature of data, based on probability plotting, and analytical techniques have been investigated. Using goodness-of-fit tests (i.e., Chi-square, Anderson-Darling, and Kolmogorov-Smirnov tests) and maximum likelihood methods, the Weibull distributions as the main distribution for life prediction on the accelerated tests compared to other distributions (e.g., exponential and lognormal distributions) have been selected on all TTFs. Furthermore, four periods of time, namely, highly fast (under 1 hour), fast (between 1 and 4 hours), medium (between 4 and 7 hours), and slow (upper 7 hours) to reach the TTF are considered for estimating the PoF for each condition. Next, the classification and regression tree (CART) analysis, as a supervised machine learning method, is used to classify and predict TTF data based on changeable factors. In addition, a multivariate regression analysis is applied to identify a formula that can explain how factors influence TTF with deterministic and probabilistic data of every 21 different experimental conditions. Finally, a combination of statistical, probabilistic distribution, multivariate regression, and CART analyses have provided a complete understanding of critical factors, levels, and conditions for having the best TTF probability prediction knowledge on PCB surfaces.

6.2 Material and methods

6.2.1 Method and experiment design

The One-factor-at-a-time (OFAT) method is a traditional design in which all factors are considered as constant variables, and the only effect of one factor is measured on the response [26]. Hence, the conclusion of OFAT experimental results represents the one-factor behavior effect without any interaction effect [27]. Table 6.1 presents the three different levels of each important and changeable factor (pitch distance, contamination, temperature, and voltage) with their units and symbols. The constant level of each factor in every vertical column (P2, C3, T2, V3) follows up the red color. Further, the horizontal rows are displaying the low, medium, and high levels of each factor, and horizontal column shows three new conditions at each level. If there are four factors, each of them at three

Manuscript II

levels, then the number of experiments in the OFAT method will be equal to nine different experimental conditions [28]. In other words, 45 experiments in vertical conditions (nine different conditions), and 15 different experiments in horizontal conditions (three different conditions), besides 10 more experiments for two specific conditions on pitch distance and temperature factors due to the existing high effect on responses, have specified (fourteen different experimental conditions) in this study. Six out of these fourteen experimental conditions (P1a100c45v10, P1a100c50v10, P2a100c45v5, P2a100c45v10, P2a100c50v10, and P2a50c45v10, partly retrieved in this study from our previous work [29]. For example, P1a100c50v10 represented the low level of pitch distance and the high level of other factors (P1 (small pitch distance)- a100 (high level adipic acid as contamination- c50 (high level temperature)- v10 (high level voltage)). In two specific experiments only for pitch distance and temperature as two most significant factors (instead of the constant condition (C3, T2, V3)), another experimental condition with a different level of temperature (C3, T3, V3) is investigated for the pitch distance column. Similarly, in addition to the constant condition (P2, C3, V3), another condition with P1 (P1, C3, V3) is measured for the temperature column.

Table 6.1 Three levels of four critical factors for performing the OFAT experiments.

Level	Pitch Distance	Contamination	Temperature	Voltage	Horizontal Condition
Low	P1 (300 μm)	C1 (50 $\mu\text{g}/\text{cm}^2$)	T1 (40 $^{\circ}\text{C}$)	V1 (5 V)	P1, C1, T1, V1
Medium	P2 (600 μm)	C2 (75 $\mu\text{g}/\text{cm}^2$)	T2 (45 $^{\circ}\text{C}$)	V2 (7.5 V)	P2, C2, T2, V2
High	P3 (1000 μm)	C3 (100 $\mu\text{g}/\text{cm}^2$)	T3 (50 $^{\circ}\text{C}$)	V3 (10 V)	P3, C3, T3, V3
Vertical conditions	C3, T2, V3	P2, T2, V3	P2, C3, V3	P2, C3, T2	
	C3, T3, V3		P1, C3, V3		

The current behavior as an important indicator is measured to define LC and TTF on the PCB surface. Figure 6.2 depicts the general current behavior of the entire experimental results, assuming two main parts and specifying two responses. First, there are LCs in the SIR reduction part, and second, TTF points in the initial failure part. The SIR reduction part (the stable part) is assigned to LC, and the failure part (the unstable region), is referred to start the failure process on PCB surfaces with a large jump in LC. The effects of

factors/levels on TTFs and LCs and their relationship are statistically evaluated in the initial part of the paper, while the modeling part focused only on TTFs predictions.

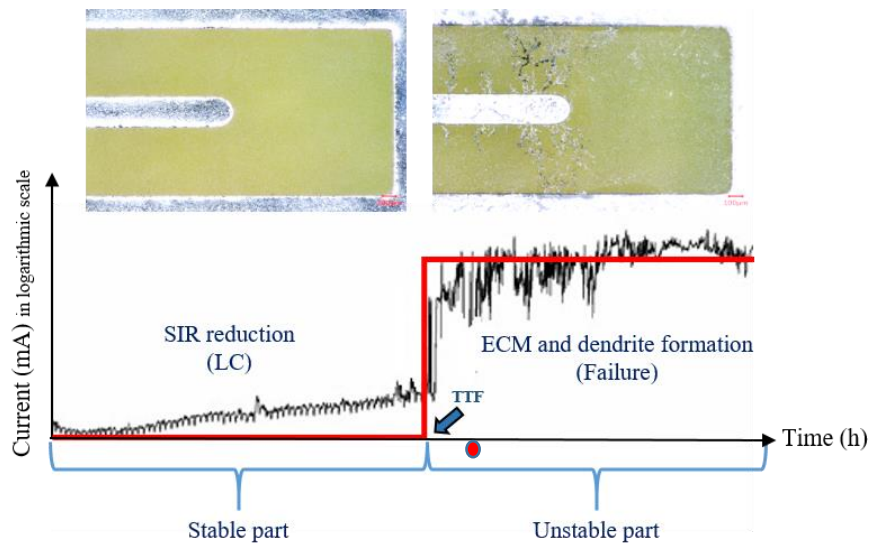


Figure 6.2 The overall current behavior on exposure to various conditions with the actual pictures of the PCB electrodes of two main regions.

6.2.2 Specimens, preparations, and test equipment

SIR comb patterns are commonly used and their measurements is one of the most usual test methods for the process of reliability and quality control [30], [31]. Figure 6.3 displays the individual SIR patterns that included three different surface areas and three pitch distances made on FR-4 laminate with a thickness of 1.6 mm complying with the IPC-4101/21 standard. The SIR patterns have three pitch distances namely of 0.3, 0.6, and 1 mm. They are proportional to actual distances on a typical PCBA. The dimensions, areas, and pitch distances of each SIR pattern are displayed in Figure 6.3.

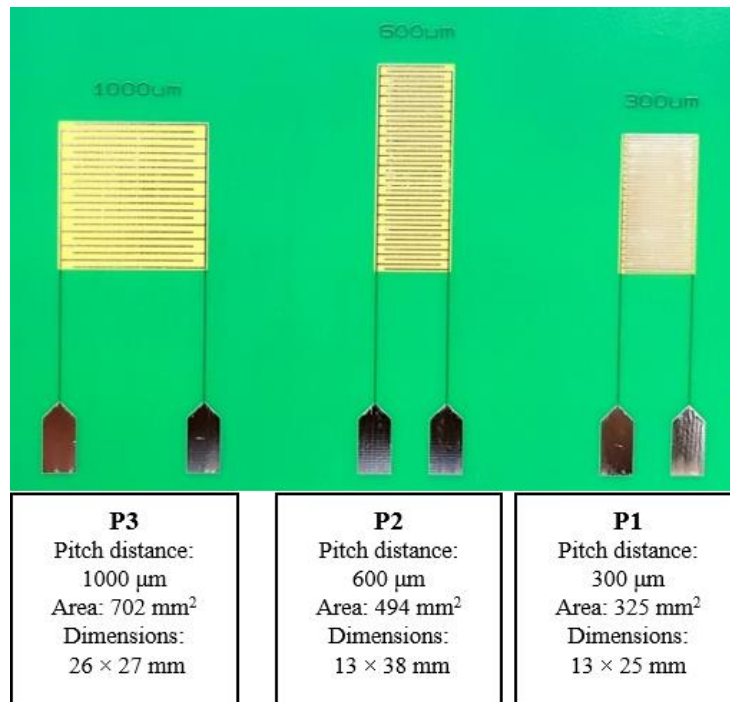


Figure 6.3 The overall view of SIR pattern PCB test boards with three different pitch distances.

In preparation before starting the test, the PCBs are cleaned and then dried by an air compressor using a combination of deionized water and isopropanol. Then, each SIR pattern is contaminated with the solution of 2.5g adipic acids dissolved in 100 ml isopropanol at the concentration of 25g/L. Right amount of this solution was dispensed on the surface of SIR patterns using a micropipette and dried in order to obtain contamination levels 50, 75, and 100 µg/cm² matching with typical levels of flux residues usually seen after the wave soldering process. Electrical connection to the PCB board is made by hand soldering of wires to the electrical contacts on the board.

All experiments are performed inside the Espec climatic chamber with the tolerances of ±0.3 °C and ±2.5% RH. In accordance with the adipic acid as contamination during the tests, the RH (proportionated with the deliquescence data) kept constant at 98% for the experiments. For each experiment, 1.5 hour period is used in the climatic chamber before each test as the stabilization period. A multichannel BioLogic VSP system is used for the application of potential (5V, 7.5V, and 10V) and accurate measurement of leak current.

6.2.3 Multivariate regression model

The multivariate regression model is a mathematical function, which pursues a logical relationship between different significant variables by the statistical estimation and the analysis of variance (ANOVA) [34], [35]. The multivariate regression model has been used for analyzing the statistical significance of four critical factor effects and for determining a significant correlation in terms of multiple factors [32]. The backward elimination stepwise investigation has been performed through multivariate regression analysis for making a reduced model on TTFs based on significant factors [33].

6.2.4 Probabilistic distribution analysis

The probability concept constructs the core of risk and reliability engineering, and the probabilistic approach is the key to assess risk and reliability by providing the needed techniques and methods [34]. The probabilistic distribution analysis has been used to achieve a mathematical function that gives the probabilities of TTFs and estimates the risk presented by the various conditions. It initiates with assumptions about selecting an appropriate distribution. Usually, three approaches are used to select an appropriate and applicable probabilistic distribution. The initial action for selecting the distribution relies on the nature of the data. For example, Weibull distribution is generally used to predict lifetime at accelerated tests [35]. The second approach is probability plotting as an approximate method to provide sensible rationales for choosing the proper distribution. The third approach is analytical procedures to determine how appropriate the selected probability distribution signifies the data set [36]. Generally, finding a specific distribution for various experimental conditions on diverse TTFs is impossible. However, Weibull distribution, compared with other distributions (i.g., exponential distribution), is selected for TTF data sets at each condition separately. It implies that the exponential distribution that is a useful distribution for life prediction in accelerated tests with a single parameter (failure rate λ) is unsuitable for these TTF data sets. Moreover, maximum likelihood methods and goodness-of-fit tests comprising Chi-square, Kolmogorov-Smirnov, and Anderson-Darling tests as an analytical technique have determined the proper fitted Weibull distribution on TTF data [36], [37].

Weibull distribution is one of the most desirable distributions for the continuous event due to its flexibility and adaptability for modeling data with a negligible amount of failures. It

Manuscript II

is specifically used for failure prediction in the accelerated life tests [38], [39]. The Weibull distribution offers accurate failure analysis and risk calculations with enormously tiny samples without the necessity to crash a few more [40]. The probability density function (PDF) of the three-parameter (3P) Weibull distribution is presented as follows [40]:

$$f(t) = \frac{\beta}{\alpha - \theta} \left(\frac{t - \theta}{\alpha - \theta}\right)^{\beta-1} \cdot \text{Exp}\left[-\left(\frac{t - \theta}{\alpha - \theta}\right)^\beta\right]$$

Where θ (theta) is the location parameters, α (alfa) is a measure of the range and the characteristic value. Further, β (beta) is the slope or shape parameter, which designates whether the failure rate is increasing, constant, or decreasing and follows the following roles [41], [42]:

- When $\beta < 1 \Rightarrow$ Determines that the product has a decreasing failure rate.
- When $\beta = 1 \Rightarrow$ Determines a constant failure rate. (exponential distribution)
- When $\beta > 1 \Rightarrow$ Determines an increasing failure rate. (This is typical of products that are wearing out, and the property of normal distribution is exhibited when $\beta \sim 3.5$)

6.2.5 CART analysis

CART analysis as one of the supervised machine learning algorithms provides insight into a wide range of applications such as manufacturing quality control, and the result is applied to identify important variables and predict response values [43], [44]. This method as a decision tree illustrates important relationships between a response and important predictors, in which each fork is split among a predictor, and each end node contains a prediction for the response [45]. CART method has been used for creating a predictive model of the dependent variable (TTF) based on the independent variables (P,C,T,V). In addition, it has been performed through classification as a qualitative prediction at four hypothetical periods of time, followed by discussing the regression tree for TTF responses as a quantitative prediction in terms of changeable factors in this study.

6.3 Results and discussion

6.3.1 LC and TTF study for each factor

The behavior of two responses (i.e., LC and TTF from Figure 6.2) in three levels of each factor (vertical columns of **Error! Reference source not found.**), along with the fitted line plot, prediction interval (PI), and regression equation on their trends is exhibited in Figure

6.4. The figure clearly shows the effect of increasing pitch distance and decreasing other factors for TTF response and inverse behavior for LC response. All the experiments were conducted in a constant condition with a combination of the medium level of pitch distance and temperature factors and the high level of contamination and voltage factors (P2, C3, T2, V3) according to Table 6.1.

Approximately, by doubling the pitch distance (from P1 to P2), TTF increases about 7 times (or reducing pitch distance from P2 to P1, TTF shows 7 times decrease). However, by doubling the values of voltage (from V1 to V3) the average of TTF decreases about 1.5 times. Interestingly increase of contamination level (from C1 to C3) showed only little change in failure time compared to other parameters. Temperature on the other hand showed 8.5 times decrease in TTF for a change of temperature from T1 – T3. The regression equations (shown above the graphs) on TTF trends for each factor at the same experimental condition can be used for forecasting the approximate failure time.

Figure 6.5 shows the comparison of the average of two responses in three levels of each factor, as an overview. Generally, the TTF decreases by increasing the LC with respect of various parameters because increasing LC represents more dissolution of metallic ions (in this case Sn ions), which will assist earlier ECM formation. As shown by Figure 6.5, temperature clearly demonstrates greater effect compared to other factors, which shows maximum change in LC and TTF. Following this, pitch distance showed significant effect on TTF, while LC was not significantly affected. Voltage and contamination showed lower effect on LC values, while voltage showed more effect on TTF.

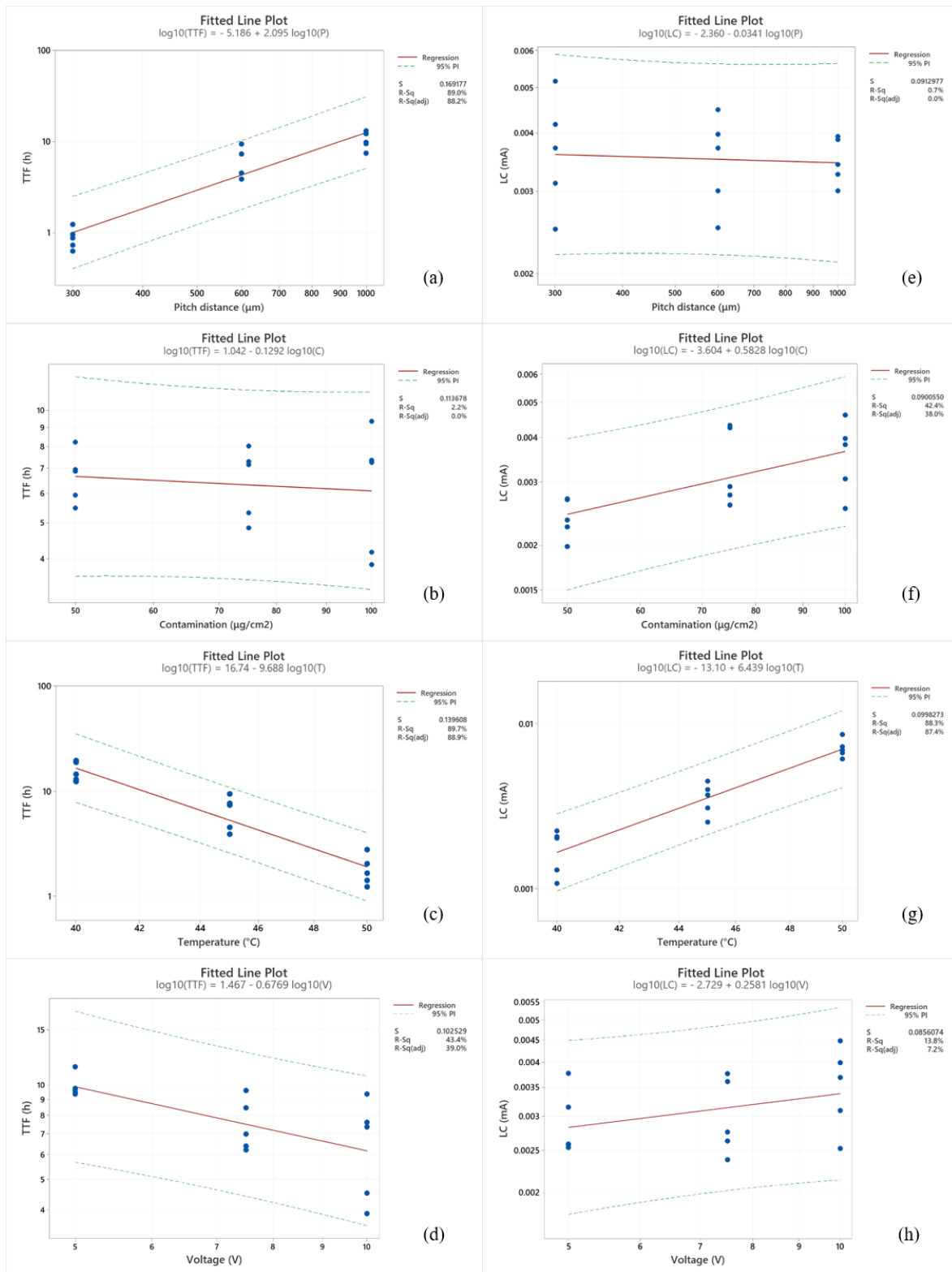


Figure 6.4 The TTF values versus three levels of each factor, along with the fitted line plot, prediction interval (PI), and regression equation on their trends at the same experimental condition for four critical factors included; (a) Pitch distance, (b) Contamination, (c) Temperature, (d) Voltage. In addition, The LC values versus three levels of each factor, along with the fitted line plot, prediction interval (PI), and regression equation on their trends at the same experimental condition for four critical factors included; (e) Pitch distance, (f) Contamination, (g) Temperature, (h) Voltage.

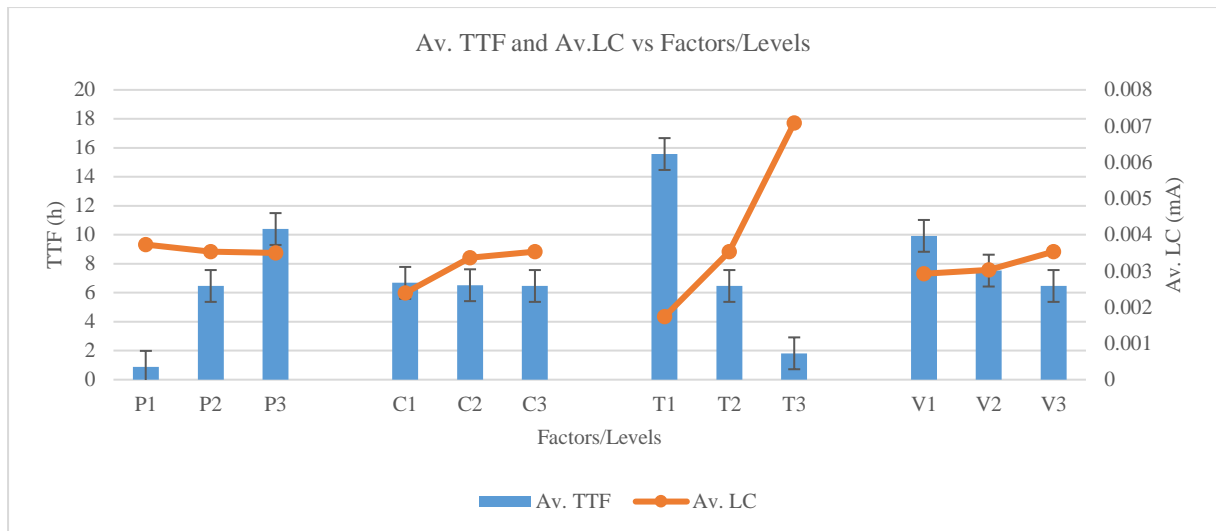


Figure 6.5 The comparison of the average of two responses in three levels of each factor.

Figure 6.6 illustrates the Weibull distribution parameters estimated in the Minitab statistical software using goodness of fitness tests and maximum likelihood method. Further, it shows the probability density function (PDF) of four changeable factors that belong to four vertical columns of Table 6.1 with 2000 random number simulations. The TTF distribution of pitch distance and temperature effects represent high PoF in the initial time of experiments. However, TTF distribution of contamination and voltage show that high PoF is in around 7 and 8 hours, respectively. Table 6.2 presents the appropriate distribution using goodness-of-fit tests for the pitch distance factor. Similarly goodness-of-fit tests have been checked for all other conditions to fit the proper distribution with their parameters at different risk values (α).

Table 6.2 The goodness-of-fit test summary for pitch distance factor.

Weibull Distribution					
Kolmogorov-Smirnov					
Sample Size	2000				
Statistic	0.01667				
P-Value	0.62853				
α	0.2	0.1	0.05	0.02	0.01
Critical Value	0.0239	0.0273	0.0303	0.0339	0.0364
Reject?	No	No	No	No	No
Anderson-Darling					
Sample Size	2000				
Statistic	0.38585				
α	0.2	0.1	0.05	0.02	0.01
Critical Value	1.3749	1.9286	2.5018	3.2892	3.9074
Reject?	No	No	No	No	No
Chi-Squared					
Deg. of freedom	10				
Statistic	5.8576				
P-Value	0.82708				
α	0.2	0.1	0.05	0.02	0.01
Critical Value	13.442	15.987	18.307	21.161	23.209
Reject?	No	No	No	No	No

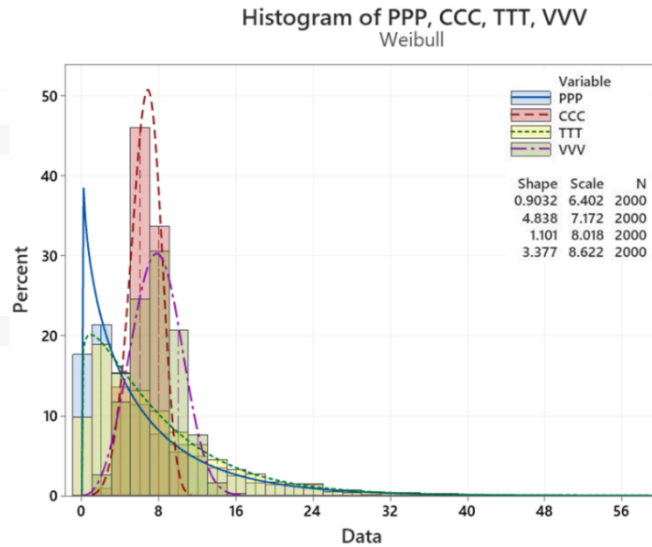


Figure 6.6 PDF of TTF for four critical factors.

The average of TTFs and LCs for each factor, as well as the PoF at four time periods (extremely fast under 1 hour, fast between 1 and 4 hours, medium between 4 and 7 hours, and slow over 7 hours) based on appropriate Weibull distribution, is provided in Error! Reference source not found.. The table presents the overall insight of the PoF of each factor in similar experimental conditions on PCB surfaces. Generally, pitch distance, temperature, contamination, and voltage with three levels of measurement in this study have the highest risk of creating failure on the PCB surface, respectively. Among the individual parameters, pitch distance and temperature showed more significant effect compared to contamination and voltage. Although, contamination effect is temperature dependant, greater effect of pitch distance and temperature shows the increasing reliability issues connected to the miniaturization and use of electronics in varying climatic conditions exposing them to different temperatures [46], [13].

Table 6.3 The PoF summary of critical factors at four hypothetical periods of time.

Factors	Symbol	Av.TTF (h)	Av.LC (mA)	PoF under hour	1	PoF under 4 hours	PoF under 7 hours
Pitch distance	P	5.92	0.003588	17%		48%	66%
Contamination	C	6.53	0.003117	0%		5%	58%
Temperature	T	7.98	0.004127	10%		37%	59%
Voltage	V	8.00	0.003170	0%		7%	39%

6.3.2 Investigation of vertical experimental conditions

In order to make the experimental conditions more simplified for analysis, two categories of conditions (vertical and horizontal parts) have been defined. The SIR measurement of three levels of each factor in conditions (P2, C3, T2, V3, and adipic acid as the only contamination at 98% RH for the chosen duration of 20 hours) have been conducted at nine different experimental conditions in the vertical part of Table 1. For example, in the vertical part in the second column of Table 1, the three different conditions are explained, considering just pitch distance being variable at a fixed condition (C3T2V3). Table 6.4 lists the Weibull distribution parameters for the TTF data of the entire factors/levels, along with the PoF on four time periods (highly fast, fast, medium, and slow) in vertical experimental conditions. This table presents the numerical average values of TTF and LC based on five replication experiments, besides Weibull parameters and PoF in the four-time periods of each experimental condition. The P1A100C45V10 and P2a100c50v10 conditions have displayed the highest PoF in all time periods. Small pitch distance (P1) in the first condition and highest temperature (T3) in the second conditions have a key role in making the risky condition on PCB surface. Compared to Error! Reference source not found., Table 6.4 presents the details of all factors levels instead of each factor. Figure 6.7 shows the PDF of the Weibull distribution for three levels of each factor. It visually displays the probability behavior of TTF data for each condition over time.

Table 6.4 The probability distribution parameters and the probability of failure for each level of each factor at 12 vertical conditions.

<i>Experiment Conditions</i>	<i>Sy mb ol</i>	<i>Av. TT F (h)</i>	<i>Av. LC (mA)</i>	<i>Fitted Distribution by Simulation</i>	β	α	θ	<i>PoF Under 1 Hour</i>	<i>PoF Under 4 Hours</i>	<i>PoF Under 7 Hours</i>
<i>P1A100C4 5V10</i>	P1	0.89	0.00373	Weibull (3P)	0.77440	0.30216	0.63001	69%	99%	100%
<i>P2A100C4 5V10</i>	P2	6.47	0.00354	Weibull (3P)	2.45100	6.51270	0.07488	1%	25%	69%
<i>P3A100C4 5V10</i>	P3	10.40	0.00350	Weibull (3P)	3.84270	10.02800	0.62985	0%	1%	16%
<i>P2a50c45v 10</i>	C1	6.68	0.00239	Weibull (3P)	8.18240	7.53340	-0.78882	0%	2%	73%
<i>P2a75c45v 10</i>	C2	6.52	0.00336	Weibull (3P)	3.59300	6.33070	0.43679	0%	12%	68%
<i>P2a100c45 v10</i>	C3	6.47	0.00354	Weibull (3P)	2.45100	6.51270	0.07488	1%	25%	69%
<i>P2a100c40 v10</i>	T1	15.57	0.00174	Weibull (3P)	4.31580	17.04700	-0.94876	0%	0%	4%
<i>P2a100c45 v10</i>	T2	6.47	0.00354	Weibull (3P)	2.45100	6.51270	0.07488	1%	25%	69%
<i>P2a100c50 v10</i>	T3	1.82	0.00709	Weibull	3.70360	1.72750	0	12%	100%	100%
<i>P2a100c45 v5</i>	V1	9.92	0.00293	Weibull	42.2590	9.65760	0	0%	0%	0%
<i>P2a100c45 v7.5</i>	V2	7.53	0.00303	Weibull (3P)	6.40520	8.79980	-1.23850	0%	3%	48%
<i>P2a100c45 v10</i>	V3	6.47	0.00354	Weibull (3P)	2.45100	6.51270	0.07488	1%	25%	69%

Approximately the average of TTF at similar conditions has increased from P1 to P3. However, the LC values represent a uniform behavior with an extremely low and negative movement from P1 to P3. The Weibull distribution for TTF estimates the P1 is highly risky, especially in a highly fast failure class with a probability rate of about 70%.

The effect of three contamination levels (C1, C2, C3) of one WOA type on TTF and LC has provided the decreasing and an ascending trend from the low to the high level, respectively. The high level of contamination has the greatest, but not severe effect on TTF

and LC. It is because of more water adsorption by the high level of the contamination (C3), which increases surface electrochemical activities (conductivity) by the dissolution of the metal ions on the PCB surface. The PoF in C3 also has presented the high value especially in the initial hours of experiments compare to other levels (C1, and C2).

The three levels of the temperature factor at T1, T2, and T3 are shown a completely different range of TTFs and LCs. Temperature is the only factor that significantly effects the behavior of LC at all levels; since LC has increased about 2 times from T1 to T2 and has increased 4 times from T1 to T3. The effect of T3 for creating the failure is about 2 times and 15 times higher than T2 and T1, respectively. The PoFs in T3 also has presented the high value compared to the other levels of temperature.

The V1, V2, and V3 are considered low, medium, and high levels of the voltage factor. The effect of V3 is higher than other levels. In other words, with increasing the voltage level (from V1 to V3) at the same conditions, about 3 hours on TTF and about 0.6 micro Ampere on LC, changes are obvious. Generally, voltage similar to contamination follows the significant shallow effect on responses. The PoF results specifically show the effect of high level compared to low level of voltage in the last assumed time period (under 7 hour).

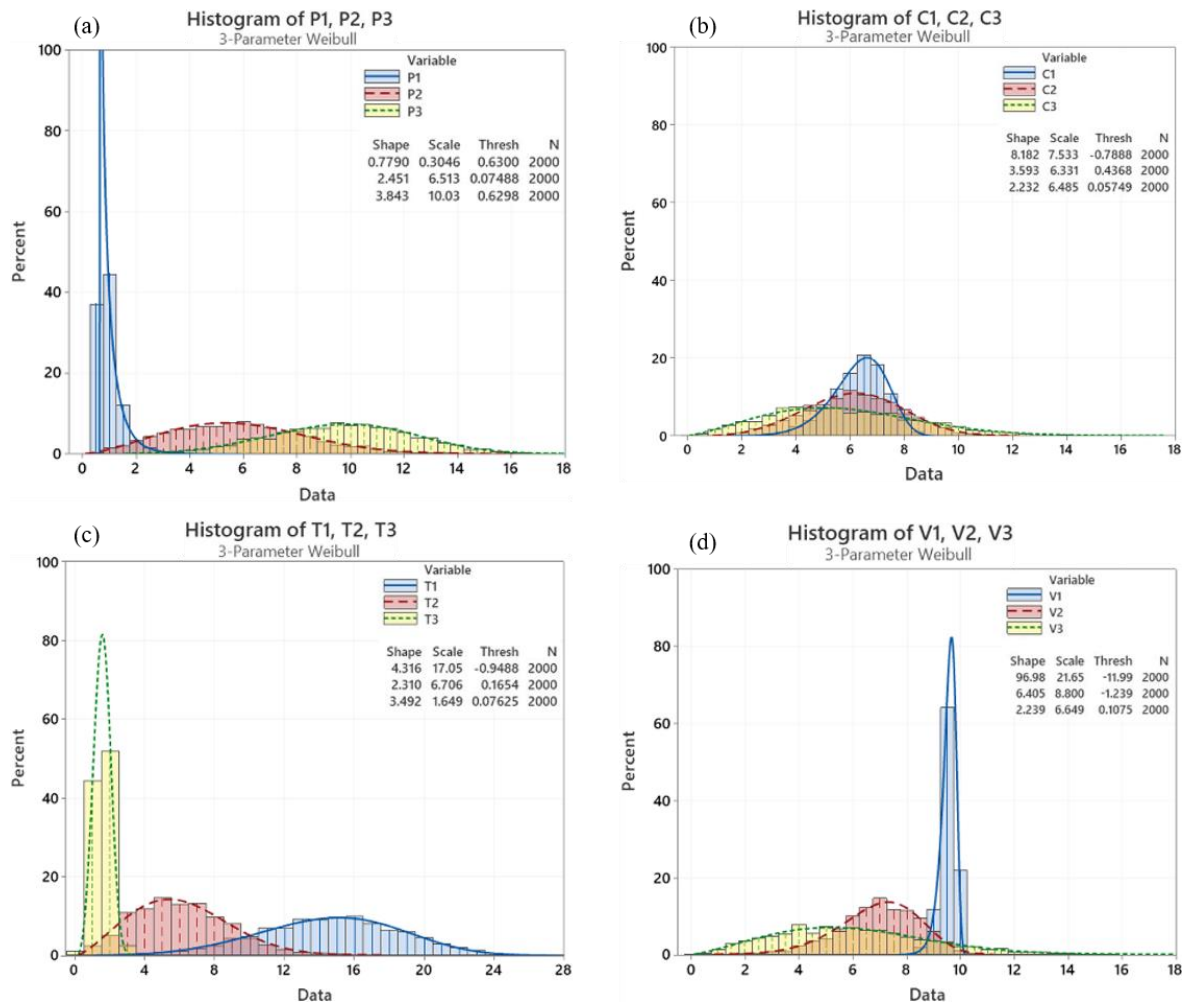


Figure 6.7 The probability failure distribution plot for three levels of four critical factors included; (a) Pitch distance, (b) Contamination, (c) Temperature, (d) Voltage.

6.3.3 Investigation of horizontal experimental conditions

In the horizontal part, three other conditions with low, medium, and high levels of each factor together, have been investigated. Table 6.5 provides the average of TTFs and LCs of three different conditions at low, medium, and high levels of the horizontal part of Table 1, as well as their probability distribution parameters and probability of failure for each time period that is assumed. It can be concluded from the percentages that the combination of the low levels of each factor has the highest risk rather than other conditions. It can be comprehended that pitch distance has a significant effect in the probability of failure as mentioned before. As seen from the vertical conditions, by increasing the V, T, and C and decreasing P, the PoF is increased. The conclusion from the horizontal condition approves the latter conclusion from the vertical condition. However, the horizontal conditions display the important effect of the pitch distance factor, which by increasing the other parameters

except for P, the PoF decreases, and the P3a100c50v10 condition has the lowest PoF, and the P1a50c40v5 condition has the highest risk.

Table 6.5. The probability distribution parameters and the probability of failure for each condition at the horizontal part.

<i>Experiment Conditions</i>		<i>Av.T TF (h)</i>	<i>Av.LC (mA)</i>	<i>Fitted Distribution by 2000 Random Numbers</i>	β	α	θ	<i>PoF Under 1 Hour</i>	<i>PoF under 4 Hours</i>	<i>PoF Under 7 Hours</i>
P1a50c40v5	Ro w1	7.01	0.0009	Weibull (3P)	2.97 39	7.04 91	0.05 538	0%	16%	62%
P2a75c45v7.5	Ro w2	8.06	0.0023	Weibull (3P)	3.07 08	8.47 68	- 717	0%	12%	47%
P3a100c50v10	Ro w3	8.26	0.0046	Weibull (3P)	7.61 77	7.13 07	0.83 666	0%	0%	28%

Figure 6.8 (a) and Figure 6.8 (b) depicts the comparison of the LC average and average of TTF versus three different levels of all factors together, as well as the Weibull probability density distribution of TTF versus time data for all low, medium, and high levels of four changeable factors, respectively. Both TTF and LC demonstrate an increasing trend from a low level to a high level. However, the average range of LC change from low to high is higher compared to TTF. Row 3 (high level combination of each factor) from the distribution plot, exhibits denser TTF data in comparison with other levels, representing the TTF dataset with more density and lower scattering in this condition.

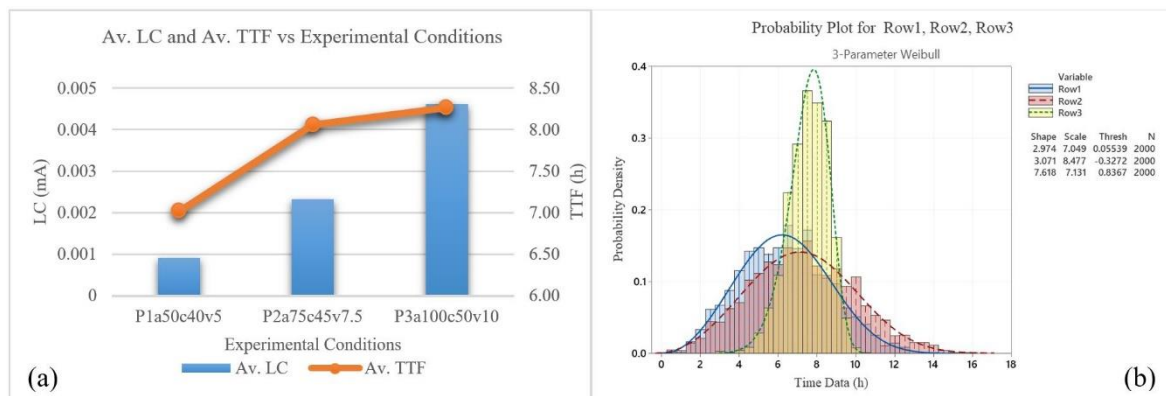


Figure 6.8 (a) The average comparison of the LC and TTF versus three different levels of all factors together. (b) The probability distribution of failure for three levels of four changeable factors in horizontal part.

6.3.4 Comparison of pitch distance and temperature as two significant factor

According to the results of vertical and horizontal experimental conditions, the pitch distance and temperature factors are more significant than other parameters. Therefore, one more experimental condition has been considered for each of them to obtain the best understanding of these two factor effects. For pitch distance at the similar contamination and voltage levels (C3, V3), and only changes the temperature levels to T3 (50 °C), the LC and TTF of three different levels of pitch distance have been measured. Furthermore, the average of LC and TTF of three temperature levels on smaller pitch distance (P1) and similar contamination and voltage levels (C3, V3) at 98% RH with adipic acid for 20 hours have been examined.

The average of TTF and LC values of three levels of pitch distance at two different temperatures (i.e., P1C3T2V3, P2C3T2V3, P3C3T2V3 and P1C3T3V3, P2C3T3V3, P3C3T3V3 conditions) display in Figure 6.9. However, the TTF trend at both temperatures from P1 to P3 follows an increasing tendency while at the high level of temperature (50 °C), the average of TTF at each pitch distance is lower than the low level of temperature (45 °C). This difference is more than 40, 280, and 160 minutes for P1, P2, and P3, respectively.

The small pitch distance demonstrates the very fast class (under 1 hour) of failure time at both temperatures. Besides, the large pitch distance in both temperatures shows the low class (upper 7 hour) of TTF. The LC trends for both temperatures also show the same decreasing behavior from P1 to P3. For P3, there is a more scatter in the result of TTF contrary to P1 experiment owing to a high distance between the two electrodes, therefore dynamic formation of water film and connection between both electrodes are more random.

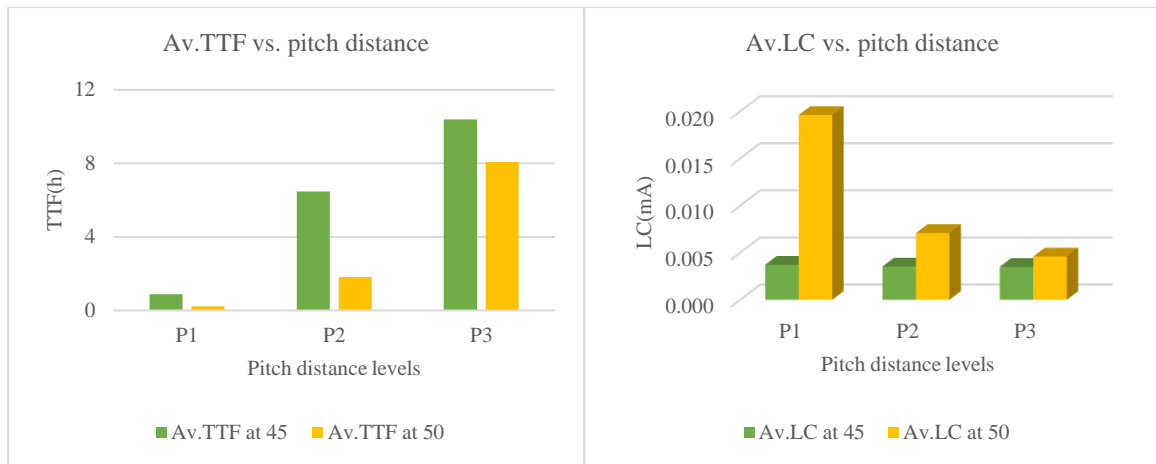


Figure 6.9 The average TTF and LC values of three levels of pitch distance at two different temperatures.

Figure 6.10 illustrates the average comparison of TTF and LC for the temperature at three levels by two different pitch distances. The TTFs of both pitches simultaneously follow a similar reducing trend while LCs follow an ascending trend. The difference of TTFs for T1, T2, and T3 at P2 is about one and a half hours more than P1. TTF reduction intensity from T1 to T3 for P2 is more in comparison with P1. However, LC increasing intensity from T1 to T3 for P1 is higher compared to P2, especially at the high temperature level (T3).

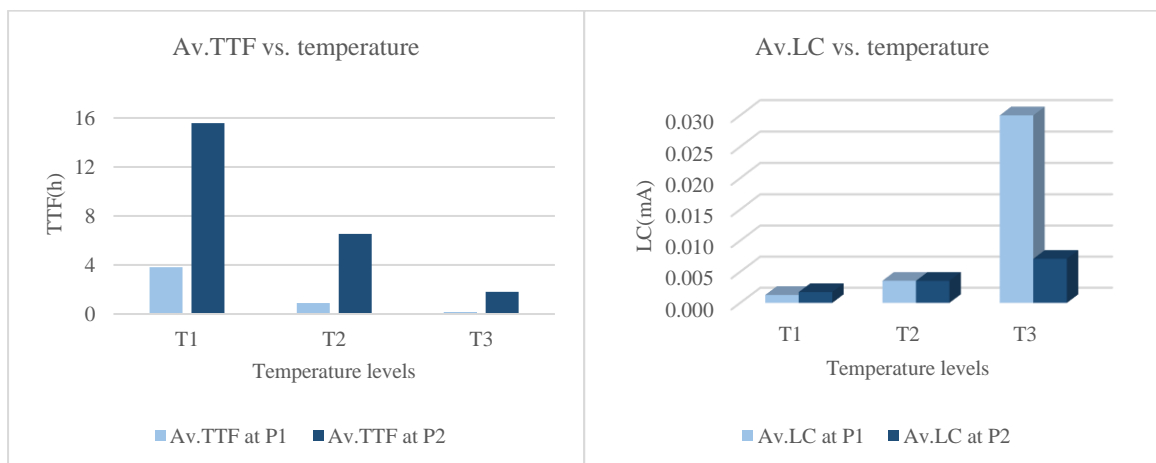


Figure 6.10 The comparison of two different temperature conditions.

6.3.5 CART and Multivariate regression analysis

The classification tree using the Gini method in Minitab statistical software as a splitting method is applied to gain the best group splits into 70 TTFs data of all experiments. This tree considers all multinomial predictors (i.e., pitch distance, contamination, temperature, and voltage) at each node, and the calculation for the split improvement amount, results in predicted probabilities for terminal nodes at four classes (i.e., highly fast, fast, medium, and low). The validation of the classification model has been performed by the k-fold cross validation method. It is one of the most popular methods widely used for model validation [47], [48]. The 10-fold cross-validation is used to estimate the model performance in prediction. The area under receiver operating characteristics (ROC) curve, which is called AUC, is one of the important metrics to distinguish the model's performance [49]. ROC is a probability curve, which graphically shows the tradeoff between true positive rate (sensitivity) and false positive rate (specificity) [50]. The AUC of the average of all classes presents 0.93 value, which indicates good classification performance for prediction. Table 6.6 exhibits the details of the 10-fold cross validation method by minimum misclassification tree criteria in training and testing the dataset. The optimal nine nodes by minimum misclassification criteria are estimated for all TTF data and has presented in Figure 6.11. The node split view of the classification tree (below and left side of Figure 6.11) presents the condensed view of factors effects to create separate classes. For an instant, the most probability of failure (90%) in the highly fast (under 1 hour, the green color) situation belongs to the terminal node 3, which follows only two factors of pitch distance with less than 450 μm and temperature with higher than 42.5 $^{\circ}\text{C}$.

Table 6.6 Model validation by minimum misclassification tree criteria.

Classification Tree (10-fold cross validation, and minimum misclassification criteria)	
Node	9
AUC	0.93
Misclassification rate (Training)	0.23
Misclassification rate (Test)	0.39

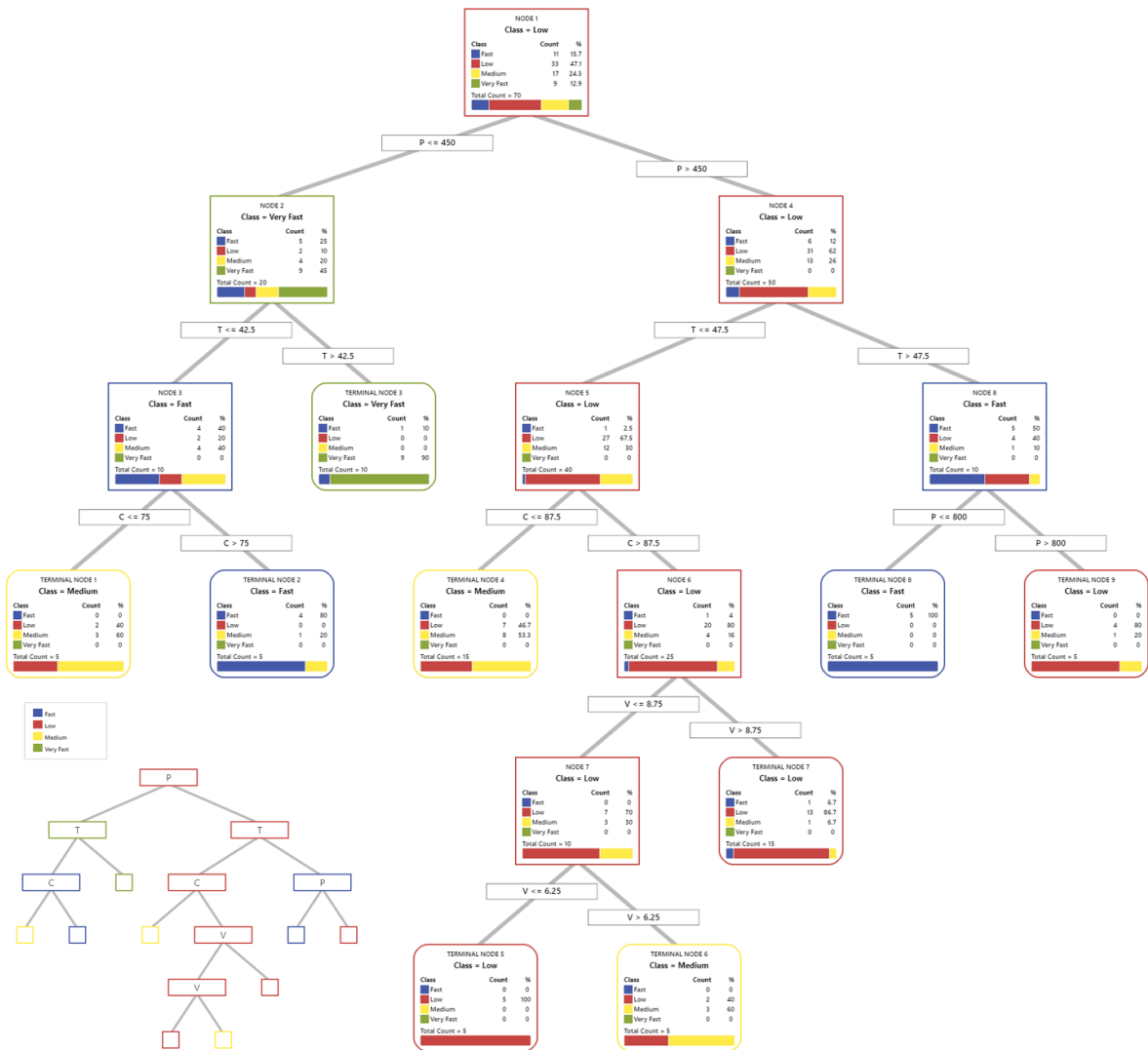


Figure 6.11 Classification tree diagram for TTF data with four predictors and classes provided.

The regression tree is employed to visualize and identify the most important predictors and discover combinations of predictor settings that are most likely to lead to a lower or higher TTF. Figure 6.12 shows a regression tree diagram with seven optimal nodes selected by maximum R-sq criteria. Similar to the classification tree, the regression tree works by splitting the TTF data into divisions based on the predictor settings that best separate the data into identical TTF values.

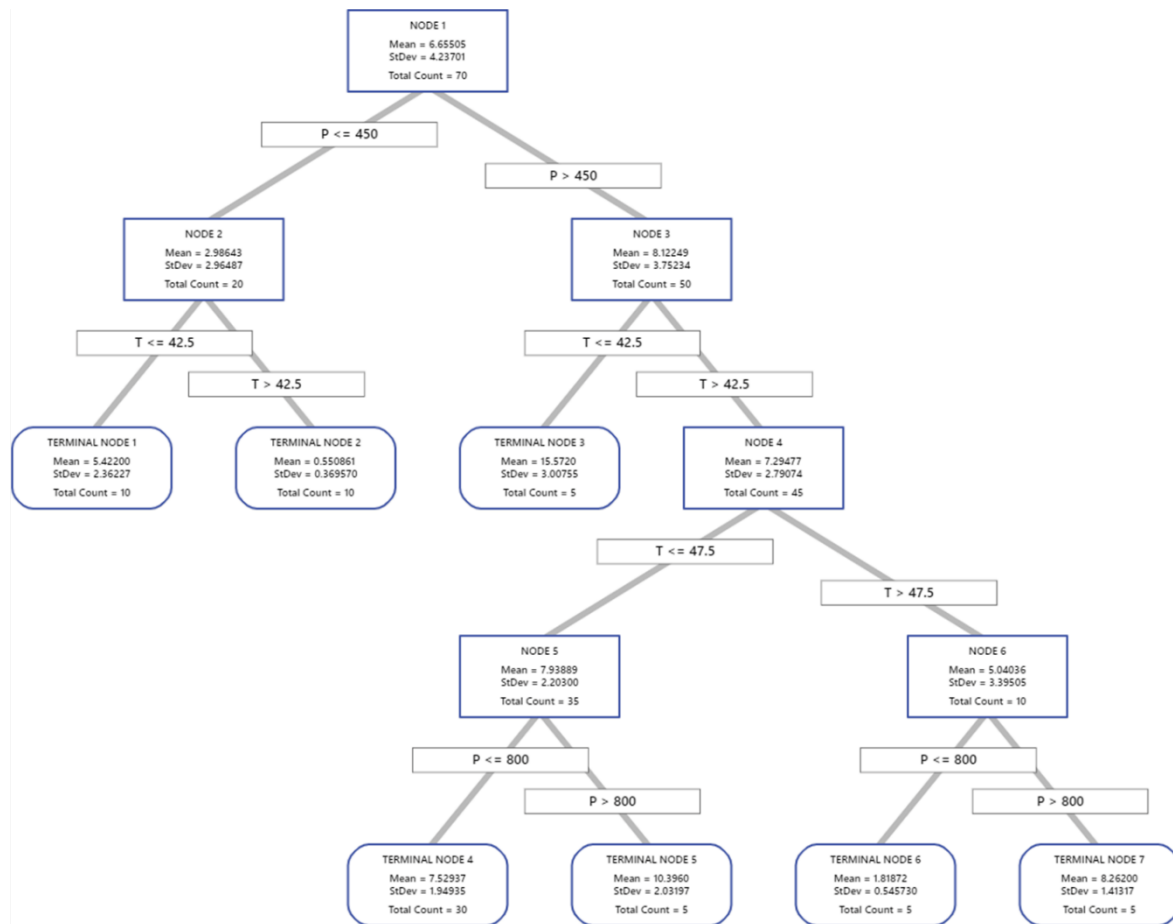


Figure 6.12 The optimal regression tree diagram for TTF response.

Figure 6.13 displays the ANOVA table of the reduced model on TTF response using the stepwise backward elimination method and the residual plot for TTF dataset that presents the normality of residual data and constant variance without following a specific trend to emphasize the adequacy of the model. Additionally, the regression equation presented below, that can predict the TTF value based on four critical factors. According to the table, pitch distance, temperature, voltage, and contamination are the most significant effect. Similar to the multivariate regression model on TTF response, another regression analysis has been performed on the Weibull distribution parameters estimated for each condition as a specific novelty in this study. It means a regression analysis is used to estimate the critical factor effects on probabilistic distribution parameters. There are no significant terms for γ , and the regression equation of the probabilistic distribution parameters is made only from α and β .

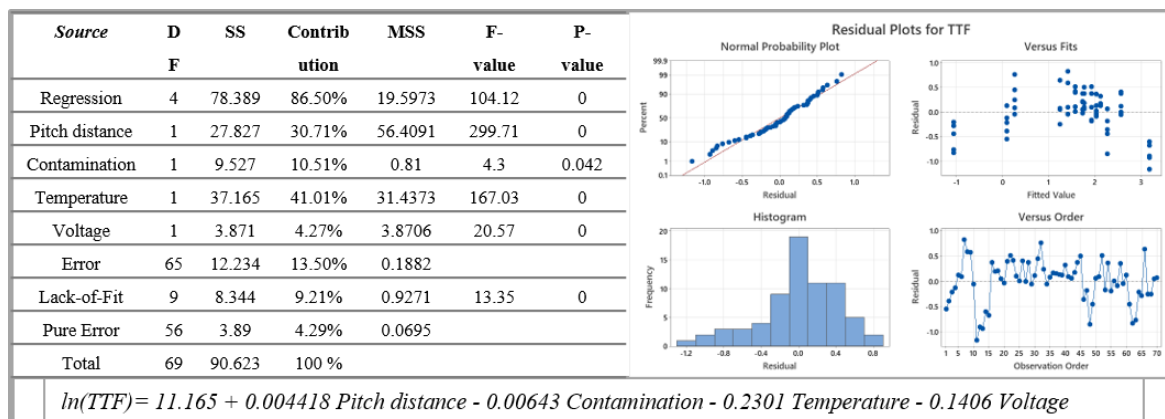


Figure 6.13 The ANOVA table, residual plots, and regression model summary for TTF data set.

6.3.6 Models validation and interpretation

The validation of three regression models has been performed by the k-fold cross validation method. The k-fold cross validation is commonly used for model validation and model selection [51]. Table 6.7 displays the summarizes of the regression models with the determination coefficient (R-sq) and the standard deviation of the error between the model and experiment on the TTF dataset with 10-fold cross validation. The R-sq is the percentage of variation in the response that the model explains, and close to 1 demonstrates how fine the data are fitted in the regression model [52], [53]. The table also includes R-sq for the training and testing of the TTF dataset. The test R-sq usually gives a better scale of how the model works for the prediction [54].

Table 6.7 The comparison of three regression models.

	Multivariate regression model	Probabilistic distribution regression model	Regression Tree Model
R-sq (training)	87%	64%	80%
R-sq (test)	84%	59%	65%
error (training)	0.43	0.56	0.37
error (test)	0.45	0.58	0.51

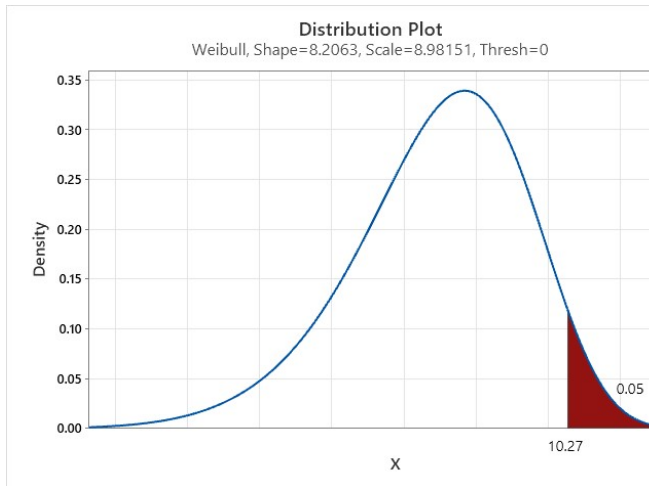
For examining the models accuracy, as an instance a specific condition (600 μm pitch distance, 60 $\mu\text{g}/\text{cm}^2$ contamination, 46 $^{\circ}\text{C}$ temperature, and 6 voltage) has been investigated. The TTF predicted values of (b) the classification tree, (c) the regression tree, (d) the multivarious regression analysis, and (e) the probabilistic distribution regression models, have been calculated to compare with (a) experimental data of 5 replications. Table 6.8 compares the accurate prediction of each model, as well as their comparison with five experimental results of TTFs at the instance condition. The prediction interval (PI) is a

Manuscript II

range that is likely to contain a single future response, and it is used to assess the precision of the predictions.

Table 6.8 The comparison of TTF predictor models together is based on five experimental results of one specific condition.

Prediction Models	Note	Fitted Value	Lower PI	Upper PI
a. Experimental data of 5 replications	5.84 7.09 8.12 5.58 9.96	7.32	5.58	9.96
b. Classification tree	Terminal node ID=3 (Medium class)	53% probability of medium class and 47% probability of low class	0%	100%
c. Regression tree	Terminal node ID=4	7.53	5.58	9.48
d. Multivariate regression		7.40	2.99	18.28
e. Probabilistic distribution regression	Weibull distribution with these parameters: $\alpha=8.9815$ $\beta=8.2063$ 0	With 95% probability, all of the TTFs in this condition happen under a 10.27 hour period		



All the prediction models can correctly forecast the TTF of all conditions between the lower and upper PIs. The probabilistic distribution regression model was employed for the

probability of TTF estimation. It had straightforward interpretation; however, it was challenging to fit applicable distribution on some datasets and had the lowest R-sq compared to the other regression models. The regression tree model with 65% test R-sq was utilized for visual and fast decisions. It had acceptable accuracy with standard deviation variation, which needs more data for its training part for more precision. Generally, these models can be selected for each case study according to the dataset, accuracy, and prediction limit at various conditions. Nevertheless, the multivariate regression model had the best prediction with the highest test R-sq (84%) and lowest test error value (0.45) for the TTF dataset.

6.3.7 Perspectives on modelling result in relation to humidity effects on electronics

Given that there are various conditions (combination of different factors and levels) that affect TTF due to ECM, different approaches such as probabilistic distribution analysis, multivariate regression analysis, and CART analysis have been studied to predict the probability of TTF and failure risk prediction on the PCB surface. Comparing with literature information on the effect of various parameters on humidity robustness of electronics [55], [56], [57], [58] the models described in this paper are based on the combinations of three levels of four critical factors showing the prediction of time to failure due to ECM on PCB surface. Moreover, these models that are statistical, probabilistic, and machine learning methods have been selected based on the probabilistic predictive analytics framework [59]. Therefore, finding the best approach and prediction model can give a better perception of PCB reliability, which can be used for preventive measures.

This study has also evaluated the predictive modelling of TTF and demonstrates that the TTF distribution using Weibull provides a better understanding of critical conditions for having the best TTF probability prediction based on the results in this paper. The Weibull distribution has been utilized in probabilistic analysis since it is most widely used to predict life and failure data sets under the influence of multiparameter. Table 6.9 displays the effect of each factor in creating different TTF prediction models. The percentage influence of pitch distance and temperature in all predictive models is more remarkable than the effect of contamination and voltage factors.

Table 6.9 The percentage of factors effects on each TTF prediction model.

	<i>Multivariate regression model</i>	<i>Probabilistic distribution regression model</i>	<i>Regression Tree Model</i>	<i>Classification Tree Model</i>
<i>Pitch distance</i>	46%	47%	39%	31%
<i>Temperature</i>	35%	26%	44%	28%
<i>Contamination</i>	13%	21%	9%	23%
<i>Voltage</i>	6%	6%	8%	18%

6.3.7.1 *Effect of pitch distance and temperature*

The effect of the factors concerning the humidity effects are clearly visible in the classification and regression tree (Figures 11, and 12), as well as ANOVA table (Figure 13). The classification and regression tree illustrates pitch distance and temperature as significant factors. Since, they have presented the pitch distance and temperature as the initial splitters in the top of the trees, which define how the nodes can be partitioned. Moreover, the contribution percentage of pitch distance and temperature on the multivariate regression model in the ANOVA table have shown the high effect of these factors compared to the contamination and voltage. The pitch distance is a significant factor in relation to the humidity effect on electronic failures, which is reduced considerably due to constant electronic miniaturization for reducing the space of PCB and high component density. The importance of pitch distance is due to increasing the electric field, therefore making it easy for dendrite formation during electrochemical migration [60], [61]. The smaller pitch distance (P1) on the PCB surface can make an electrochemical cell easier due to water layer formation between two electrical points. According to the TTF dataset, with increasing every 100µm pitch distance, approximately one hour will be increased to the TTF. Temperature is found to be a significant factor in causing the failure. Temperature can influence the humidity effects in different ways, namely: (i) increasing the absolute humidity in the environment to interact with PCB surface, (ii) reducing the deliquescent humidity level for contamination and increasing its solubility, and (iii) increasing the kinetics of electrochemical process including the deposition process for ECM. For condensation, the dew point range and the size of dew droplet formation on the PCB surface are affected by temperature [62], [63].

6.3.7.2 *Effect of contamination and voltage*

As shown in Figure 6.3, Table 6.4, and modelling results, the contamination effect on TTF is not as significant as pitch distance and temperature. However, the effect of contamination should be considered together with temperature. It is because when the deliquescence occurs, a near saturated solution of contamination to the absorbed water forms, which will always remain saturated irrespective of the level of contamination unless temperature is different. Therefore, although the contamination on the surface of the PCB has changed, concentration in the water layer will not change significantly; hence it should not influence the TTF significantly at constant temperature. The voltage in relation to humidity also has been shown a low effect on TTF. It might be due to the fact that the extent of current, can be passed through the limited thickness of the water layer. Therefore, an increase in voltage will not significantly influence the leak current and SIR reduction for starting metal ions dissolution and dendrite formation on PCB surface, unless other parameters such as P, T, or C change. However, after pitch distance and temperature, voltage has also significant effect on TTF, forasmuch as with increasing two times, TTF decreases more than 3 hours.

6.3.7.3 *Combined effect of pitch distance, contamination, and temperature*

Comparing the interaction between all three factors together with voltage effect is indirectly linked to the pitch distance, temperature play a big role in enhancing the effect of pitch distance and temperature due to the factors mentioned above. Kamila et al [64], [65], [66] have reported that the hygroscopic nature of residues is determined by the chemistry of activating part of flux formation and temperature. An increase of temperature strengthens the interaction between the acids and water vapor, leading to high uptake the moisture by flux residues. And increase of temperature shifts the critical relative humidity level for deliquescence of flux activators towards lower RH range, and the solubility of the residues increases. At higher ambient temperatures, the formation of a conductive electrolyte is accelerated, and an increase in LC and subsequent electrochemical metal ion migration occur at lower RH levels.

6.4 Conclusion

- The consensus of characterizing the critical factors/ levels, probability of failure, and failure time prediction modeling have given an extensive insight into the failure occurrence on PCB surfaces under humidity.
- Statistically, the temperature, and pitch distance had the most significant effect on TTFs, respectively. They were especially significant in the risky failure period of the very fast and fast classes.
- The importance of pitch distance in significantly decreasing TTF is due to increasing the electric field to make easier dendrite formation during electrochemical migration. Besides, the temperature importance TTF is because of the influence on humidity to alter the dew point range and the size of dew droplet formation on the PCB surface, as well as increasing the electrochemical kinetics.
- Results indicated that by increasing every 100 μm pitch distance, TTF approximately eighty minutes increased. Moreover, it also increased around eighty minutes by decreasing every one-degree centigrade. Nevertheless, the increase of TTF by raising every voltage was almost about forty minutes. And for every 10 $\mu\text{g}/\text{cm}^2$ enlargement of contamination level, it only showed around 2.5 minutes increase.
- The temperature and pitch distance factors with the large amount and distance rather than voltage and contamination factors also had the strongest effect on the LCs. Additionally, the combination of small pitch distance (P1) and the high temperature level (T3) displayed a critical condition with the highest LC value and failure probability percentage compared to other conditions.
- The classification tree was used for the qualitative estimation of TTFs for a different period. It shows a satisfactory probability prediction of the periods and gives an excellent and quick insight into the dataset. For instance, the very fast class, which shows the critical conditions with happening failure under 1 hour (TTF < 1 hour), belongs to only having conditions of low pitch distances and high temperatures (P < 450 μm and T > 42.5 $^{\circ}\text{C}$).
- From all regression models, the multivariate regression analysis with analyzing the statistical significance of factors effects and determining their correlation had the

best validation, and prediction with the close value to real data, highest R-sq, and lowest error.

Acknowledgements

The present research work was carried out as a part of work in CELCORR/CreCon consortium (<https://celcorr.dtu.dk>). The authors would like to acknowledge the CELCORR/CreCon consortium, and Innovation Fund Denmark for the funding support.

Conflict of interest

The authors declare that they have no conflict of interest.

Reference

- [1] R. Ambat, H. Conseil-Gudla, V. Verdingovas, Corrosion in Electronics, in: *Encycl. Interfacial Chem.*, Elsevier, 2018: pp. 134–144. <https://doi.org/10.1016/B978-0-12-409547-2.13437-7>.
- [2] J. Sjoberg, D.A. Geiger, D. Shanguan, Process development and reliability evaluation for inline Package-on-Package (pop) assembly, in: *2008 58th Electron. Components Technol. Conf.*, IEEE, 2008: pp. 2005–2010. <https://doi.org/10.1109/ECTC.2008.4550259>.
- [3] K. Vijay, Miniaturization - Solder paste attributes for maximizing the print & reflow manufacturing process window, in: *2012 4th Electron. Syst. Technol. Conf. ESTC 2012*, IEEE, 2012: pp. 1–13. <https://doi.org/10.1109/ESTC.2012.6542145>.
- [4] K. Piotrowska, M.S. Jellesen, R. Ambat, Water film formation on the PCBA surface and failure occurrence in electronics, in: *2018 IMAPS Nord. Conf. Microelectron. Packag.*, IEEE, 2018: pp. 72–76. <https://doi.org/10.23919/NORDPAC.2018.8423854>.
- [5] J. Niemann, S. Härter, C. Kästle, J. Franke, Challenges of the Miniaturization in the Electronics Production on the example of 01005 Components, in: *Tagungsband Des 2. Kongresses Montage Handhabung Ind.*, Springer Berlin Heidelberg, Berlin, Heidelberg, 2017: pp. 113–123. https://doi.org/10.1007/978-3-662-54441-9_12.
- [6] E. Guene, Solderability and reliability evolution of no clean solder fluxes for selective soldering, in: *2017 21st Eur. Microelectron. Packag. Conf. Exhib.*, IEEE, 2017: pp. 1–10. <https://doi.org/10.23919/EMPC.2017.8346874>.
- [7] M. Judd, K. Brindley, *Soldering in Electronics Assembly*, Elsevier, 1992. <https://doi.org/10.1016/C2013-0-01187-5>.
- [8] K.S. Hansen, M.S. Jellesen, P. Moller, P.J.S. Westermann, R. Ambat, Effect of solder flux residues on corrosion of electronics, in: *2009 Annu. Reliab. Maintainab. Symp.*, IEEE, 2009: pp. 502–508. <https://doi.org/10.1109/RAMS.2009.4914727>.
- [9] Y. Gao, S.B. Chen, L.E. Yu, Efflorescence relative humidity for ammonium sulfate particles, *J. Phys. Chem. A*. 110 (2006) 7602–7608. <https://doi.org/10.1021/jp057574g>.

- [10] M.S. Jellesen, D. Minzari, U. Rathinavelu, P. Møller, R. Ambat, Corrosion in Electronics at Device Level, *ECS Trans.* 25 (2019) 1–14. <https://doi.org/10.1149/1.3321952>.
- [11] J. Romero, M.H. Azarian, C. Morillo, M. Pecht, Effects of Moisture and Temperature on Membrane Switches in Laptop Keyboards, *IEEE Trans. Device Mater. Reliab.* 18 (2018) 535–545. <https://doi.org/10.1109/TDMR.2018.2866776>.
- [12] H. Conseil-Gudla, Z. Staliulionis, S. Mohanty, M.S. Jellesen, J.H. Hattel, R. Ambat, Humidity build-up in electronic enclosures exposed to different geographical locations by RC modelling and reliability prediction, *Microelectron. Reliab.* 82 (2018) 136–146. <https://doi.org/10.1016/j.microrel.2018.01.013>.
- [13] K. Piotrowska, M. Grzelak, R. Ambat, No-Clean Solder Flux Chemistry and Temperature Effects on Humidity-Related Reliability of Electronics, *J. Electron. Mater.* 48 (2019) 1207–1222. <https://doi.org/10.1007/s11664-018-06862-4>.
- [14] V. Verdingovas, S. Joshy, M.S. Jellesen, R. Ambat, Analysis of surface insulation resistance related failures in electronics by circuit simulation, *Circuit World.* 43 (2017) 45–55. <https://doi.org/10.1108/CW-09-2016-0040>.
- [15] V. Verdingovas, M.S. Jellesen, R. Ambat, Effect of pulsed voltage on electrochemical migration of tin in electronics, *J. Mater. Sci. Mater. Electron.* 26 (2015) 7997–8007. <https://doi.org/10.1007/s10854-015-3454-9>.
- [16] H. Conseil, M. Stendahl Jellesen, R. Ambat, Contamination profile on typical printed circuit board assemblies vs soldering process, *Solder. Surf. Mt. Technol.* 26 (2014) 194–202. <https://doi.org/10.1108/SSMT-03-2014-0007>.
- [17] C.H. Liao, S.H. Yang, M.Y. Liao, K.C. Chung, N. Kumari, K.H. Chen, Y.H. Lin, S.R. Lin, T.Y. Tsai, Y.Z. Juang, A 23.6ppm/°C Monolithically Integrated GaN Reference Voltage Design with Temperature Range from -50°C to 200°C and Supply Voltage Range from 3.9 to 24V, *Dig. Tech. Pap. - IEEE Int. Solid-State Circuits Conf. 2020-February (2020)* 72–74. <https://doi.org/10.1109/ISSCC19947.2020.9062940>.
- [18] J.Y. Li, C.X. Sun, S.A. Sebo, Humidity and contamination severity impact on the leakage currents of porcelain insulators, *IET Gener. Transm. Distrib.* 5 (2011) 19–28. <https://doi.org/10.1049/iet-gtd.2009.0559>.
- [19] K. Piotrowska, F. Li, R. Ambat, Thermal decomposition of binary mixtures of organic activators used in no-clean fluxes and impact on PCBA corrosion reliability, *Solder. Surf. Mt. Technol.* 32 (2019) 93–103. <https://doi.org/10.1108/SSMT-05-2019-0020>.
- [20] V. Verdingovas, M.S. Jellesen, R. Ambat, Solder Flux Residues and Humidity-Related Failures in Electronics: Relative Effects of Weak Organic Acids Used in No-Clean Flux Systems, *J. Electron. Mater.* 44 (2015) 1116–1127. <https://doi.org/10.1007/s11664-014-3609-0>.
- [21] V. Verdingovas, M.S. Jellesen, R. Ambat, Relative effect of solder flux chemistry on the humidity related failures in electronics, *Solder. Surf. Mt. Technol.* 27 (2015) 146–156. <https://doi.org/10.1108/SSMT-11-2014-0022>.
- [22] T. Zheng, Z. Wang, C. Tan, R. Wang, Research on fault prediction and diagnosis method of PCB circuit, in: *2020 Int. Conf. Artif. Intell. Comput. Eng., IEEE, 2020*: pp. 387–390. <https://doi.org/10.1109/ICAICE51518.2020.00081>.

- [23] Z. Zhang, F. Gong, Prediction and Analyze of PCB Common-Mode Radiation Based on Current-Driven Mode, in: 2008 Work. Power Electron. Intell. Transp. Syst., IEEE, 2008: pp. 320–323. <https://doi.org/10.1109/PEITS.2008.63>.
- [24] M. Modarres, M.P. Kaminskiy, V. Krivtsov, Reliability Engineering and Risk Analysis, CRC Press, 2009. <https://doi.org/10.1201/9781420008944>.
- [25] T. Sreenuch, A. Alghassi, S. Perinpanayagam, Y. Xie, Probabilistic Monte-Carlo Method for Modelling and Prediction of Electronics Component Life, Int. J. Adv. Comput. Sci. Appl. 5 (2014). <https://doi.org/10.14569/ijacsa.2014.050113>.
- [26] K. Poorghasemi, R.K. Saray, E. Ansari, S.M. Mousavi, A. Zehni, Statistical analysis on the effect of premixed ratio, EGR, and diesel fuel injection parameters on the performance and emissions of a NG/ Diesel RCCI engine using a DOE method, (n.d.). <https://doi.org/10.1177/09544070211015478>.
- [27] D. El Sherbiny, M.E.K. Wahba, OFAT versus DOE as two optimization protocols for the chromatographic analysis of some OTC pharmaceuticals carrying negative cardiovascular effects and administered by pregnant and breast-feeding females: Application to dose dependent effect, Acta Chromatogr. 33 (2020) 11–24. <https://doi.org/10.1556/1326.2020.00708>.
- [28] Ž.R. Lazić, Design of Experiments in Chemical Engineering, Wiley, 2004. <https://doi.org/10.1002/3527604162>.
- [29] S. Bahrebar, R. Ambat, Investigation of critical factors effect to predict leakage current and time to failure due to ECM on PCB under humidity, Microelectron. Reliab. 127 (2021) 114418. <https://doi.org/10.1016/j.microrel.2021.114418>.
- [30] S. Zhan, Surface insulation resistance of conformally coated printed circuit boards processed with no-clean flux, Ieee Trans. Electron. Packag. Manuf. 29 (2006) 217–223. <https://doi.org/10.1109/TEPM.2006.882496>.
- [31] G. Grossmann, C. Zardini, eds., The ELFNET Book on Failure Mechanisms, Testing Methods, and Quality Issues of Lead-Free Solder Interconnects, Springer London, London, 2011. <https://doi.org/10.1007/978-0-85729-236-0>.
- [32] O. El Aissaoui, Y. El Alami El Madani, L. Oughdir, A. Dakkak, Y. El Alloui, A Multiple Linear Regression-Based Approach to Predict Student Performance, in: Adv. Intell. Syst. Comput., 2020. https://doi.org/10.1007/978-3-030-36653-7_2.
- [33] M. Iwasaki, Multiple Regression Analysis from Data Science Perspective, in: 2020. https://doi.org/10.1007/978-981-15-2700-5_8.
- [34] M. Modarres, M. Amiri, C. Jackson, Probabilistic Physics of Failure Approach to Reliability, John Wiley & Sons, Inc., 2017. <https://doi.org/10.1002/9781119388692>.
- [35] S. Rastayesh, S. Bahrebar, A.S. Bahman, J.D. Sørensen, F. Blaabjerg, Lifetime estimation and failure risk analysis in a power stage used in wind-fuel cell hybrid energy systems, Electron. 8 (2019). <https://doi.org/10.3390/electronics8121412>.
- [36] P. V. Varde, M.G. Pecht, Probabilistic approach to reliability engineering, in: Springer Ser. Reliab. Eng., 2018. https://doi.org/10.1007/978-981-13-0090-5_3.

Manuscript II

- [37] M.E.N.H. and B. Peacock, Statistical Distributions, Third Edition, Meas. Sci. Technol. 12 (2001). <https://doi.org/10.1088/0957-0233/12/1/702>.
- [38] H. Rinne, History and meaning of the WEIBULL distribution, in: Weibull Distrib., 2020. <https://doi.org/10.1201/9781420087444-8>.
- [39] S. Bahrebar, D. Zhou, S. Rastayesh, H. Wang, F. Blaabjerg, Reliability assessment of power conditioner considering maintenance in a PEM fuel cell system, Microelectron. Reliab. 88–90 (2018) 1177–1182. <https://doi.org/10.1016/j.microrel.2018.07.085>.
- [40] P. V. Varde, M.G. Pecht, Risk-Based Engineering, Springer Singapore, Singapore, 2018. <https://doi.org/10.1007/978-981-13-0090-5>.
- [41] N.T. Thomopoulos, Weibull, in: Stat. Distrib., Springer International Publishing, Cham, 2017: pp. 59–68. https://doi.org/10.1007/978-3-319-65112-5_7.
- [42] K.C. Kapur, M. Pecht, Reliability Engineering, John Wiley & Sons, Inc., Hoboken, NJ, USA, 2014. <https://doi.org/10.1002/9781118841716>.
- [43] J. Kruppa, STATISTICAL REGRESSION AND CLASSIFICATION Norman Matloff (2017). Boca Raton, FL: Chapman & Hall/ CRC Press. 528 pages, ISBN: 978-1498710916, Biometrical J. 60 (2018) 658–659. <https://doi.org/10.1002/bimj.201800029>.
- [44] G. Giordano, M. Aria, Regression trees with moderating effects, in: Stud. Classif. Data Anal. Knowl. Organ., 2011. https://doi.org/10.1007/978-3-642-11363-5_45.
- [45] R.A. Berk, Classification and Regression Trees (CART), in: 2016. https://doi.org/10.1007/978-3-319-44048-4_3.
- [46] H. Huang, X. Guo, G. Zhang, Z. Dong, The effects of temperature and electric field on atmospheric corrosion behaviour of PCB-Cu under absorbed thin electrolyte layer, Corros. Sci. 53 (2011) 1700–1707. <https://doi.org/10.1016/J.CORSCI.2011.01.031>.
- [47] D. Berrar, Cross-Validation, Encycl. Bioinforma. Comput. Biol. ABC Bioinforma. 1–3 (2019) 542–545. <https://doi.org/10.1016/B978-0-12-809633-8.20349-X>.
- [48] G. Jiang, W. Wang, Error estimation based on variance analysis of k-fold cross-validation, Pattern Recognit. 69 (2017) 94–106. <https://doi.org/10.1016/j.patcog.2017.03.025>.
- [49] E.K. Ampomah, Z. Qin, G. Nyame, Evaluation of tree-based ensemble machine learning models in predicting stock price direction of movement, Inf. 11 (2020). <https://doi.org/10.3390/INFO11060332>.
- [50] A. Debón, A. Carrión, E. Cabrera, H. Solano, Comparing risk of failure models in water supply networks using ROC curves, Reliab. Eng. Syst. Saf. 95 (2010) 43–48. <https://doi.org/10.1016/J.RESS.2009.07.004>.
- [51] Y. Jung, Multiple predicting K-fold cross-validation for model selection, J. Nonparametr. Stat. 30 (2018) 197–215. <https://doi.org/10.1080/10485252.2017.1404598>.
- [52] S. Dahbi, H. El Moussami, L. Ezzine, Multiple regression model for surface roughness using full factorial design, in: Proc. 2015 Int. Conf. Ind. Eng. Syst. Manag. IEEE IESM 2015, IEEE, 2016: pp. 439–444. <https://doi.org/10.1109/IESM.2015.7380194>.

- [53] F.E. Harrell , Regression Modeling Strategies, (2015). <https://doi.org/10.1007/978-3-319-19425-7>.
- [54] W.D. Dupont, Statistical modeling for biomedical researchers: A simple introduction to the analysis of complex data, second edition, Cambridge University Press, Cambridge, 2009. <https://doi.org/10.1017/CBO9780511575884>.
- [55] B. Song, M.H. Azarian, M.G. Pecht, Effect of Temperature and Relative Humidity on the Impedance Degradation of Dust-Contaminated Electronics, *J. Electrochem. Soc.* 160 (2013) C97–C105. <https://doi.org/10.1149/2.024303jes>.
- [56] A. Khangholi, F. Li, K. Piotrowska, S. Loulidi, R. Ambat, G. Van Assche, A. Hubin, I. De Graeve, Humidity Robustness of Plasma-Coated PCBs, *J. Electron. Mater.* 49 (2020) 848–860. <https://doi.org/10.1007/S11664-019-07714-5>.
- [57] W.S. Hong, C. Oh, Lifetime Prediction of Electrochemical Ion Migration with Various Surface Finishes of Printed Circuit Boards, *J. Electron. Mater.* 49 (2020) 48–58. <https://doi.org/10.1007/s11664-019-07595-8>.
- [58] S. Joshy, V. Verdingovas, M.S. Jellesen, R. Ambat, Circuit analysis to predict humidity related failures in electronics - Methodology and recommendations, *Microelectron. Reliab.* 93 (2019) 81–88. <https://doi.org/10.1016/J.MICROREL.2018.12.010>.
- [59] K. Lepenioti, A. Bousdekis, D. Apostolou, G. Mentzas, Prescriptive analytics: Literature review and research challenges, *Int. J. Inf. Manage.* 50 (2020) 57–70. <https://doi.org/10.1016/j.ijinfomgt.2019.04.003>.
- [60] M. Sun, H.G. Liao, K. Niu, H. Zheng, Structural and morphological evolution of lead dendrites during electrochemical migration, *Sci. Rep.* 3 (2013) 3227. <https://doi.org/10.1038/srep03227>.
- [61] D. Minzari, F.B. Grumsen, M.S. Jellesen, P. Møller, R. Ambat, Electrochemical migration of tin in electronics and microstructure of the dendrites, *Corros. Sci.* 53 (2011) 1659–1669. <https://doi.org/10.1016/J.CORSCI.2011.01.009>.
- [62] H.W. Zhang, Y. Liu, J. Wang, F.L. Sun, Effect of elevated temperature on PCB responses and solder interconnect reliability under vibration loading, in: *Microelectron. Reliab.*, Elsevier Ltd, 2015: pp. 2391–2395. <https://doi.org/10.1016/j.microrel.2015.07.033>.
- [63] K. Piotrowska, R. Ud Din, F.B. Grumsen, M.S. Jellesen, R. Ambat, Parametric Study of Solder Flux Hygroscopicity: Impact of Weak Organic Acids on Water Layer Formation and Corrosion of Electronics, *J. Electron. Mater.* 47 (2018) 4190–4207. <https://doi.org/10.1007/s11664-018-6311-9>.
- [64] K. Piotrowska, V. Verdingovas, R. Ambat, Humidity-related failures in electronics: effect of binary mixtures of weak organic acid activators, *J. Mater. Sci. Mater. Electron.* 29 (2018) 17834–17852. <https://doi.org/10.1007/s10854-018-9896-0>.
- [65] K. Piotrowska, R. Ambat, Residue-Assisted Water Layer Build-Up Under Transient Climatic Conditions and Failure Occurrences in Electronics, *IEEE Trans. Components, Packag. Manuf. Technol.* 10 (2020) 1617–1635. <https://doi.org/10.1109/TCPMT.2020.3005933>.

7 Manuscript III

Using Machine Learning Algorithms to Predict Failure on the PCB Surface under Corrosive Conditions

*Sajjad Bahrebar, Sajad Homayoun and Rajan Ambat, Using Machine Learning Algorithms to Predict Failure on the PCB Surface under Corrosive Conditions, Corrosion Science, (2022)
doi:<https://doi.org/10.1016/j.corsci.2022.110500>*

ABSTRACT- A printed circuit board (PCB) surface can fail by corrosion due to various environmental factors. This paper focuses on machine learning (ML) techniques to build predictive models to forecast PCB surface failure due to electrochemical migration (ECM) and leakage current (LC) levels under corrosive conditions containing the combination of six critical factors. The modeling methodology in this paper used common supervised ML algorithms by accomplishing significant evaluation metrics to show the performance of each algorithm. The conclusion of this study presents those ML algorithms can create predictive models to forecast PCB failures and estimate LC values effectively and quickly.

Keywords: machine learning algorithm, classification, regression, predictive analytics, PCB failure, leakage current.

7.1 Introduction

Bulk Today electronic systems worldwide experience several corrosion failure issues due to their extensive use under various environmental exposure conditions [1], [2]. Enhanced use of power electronics as part of renewable energy systems and electrification of the vehicles enhances corrosion problems due to increased exposure to harsh environmental conditions as well as the required enhanced performance boundaries, therefore requiring to use higher power and bias level on the parts such as PCBs. Main reason for the corrosion failure is due to the formation of water film on PCB surface under exposure to humid conditions, which acts as connecting electrolyte layer between biased components triggering electrochemical failure modes. Multiple factors are involved in such corrosion failures, which involve different failure modes caused by electrochemical process resulting from water film formation on the PCB surface due to atmospheric humidity and condensation [3], [4]. Electrochemical failure modes leads to malfunction of the electronic devices as the stray currents caused by the electrochemical process interfere with PCB functionality [5], [6]. Two types corrosion failures are important in this respect, namely surface leakage current (LC) produced in the connecting electrolyte due to electrochemical reactions and subsequent dendrite formation due to electrochemical migration (ECM) between positively and negatively biased points causing electrical short circuits [7], [8]. Among the several factors involved in causing these failure modes, although effect of individual factors can be determined, dependency of the combination of factors are more complex, however more realistic to understand in connection with failures in actual practice. The combination of critical factors are humidity (H) and temperature (T) related to the climatic conditions category (assuming that the electronic device is well protected from ingress of aerosols), process related contamination (residues) types existing on the PCB surface (CT) and levels (C), pitch distance (P) meaning the distance between positively and negatively biased points on the PCB surface, and bias level (V) at the concerned area of the PCB. Corrosion failure modes on PCBs under various conditions of combination of critical factors like H, T, CT, C, P, and V include failures described above such as LC influencing the functionality of a particular component or whole PCB and electrical short circuit due to ECM [9], [10].

The remedial and preventive action of PCBs failure at an initial stage based on optimization of the design, process optimization to reduce contamination, and such protection strategies

require predictive analytics approaches to understand the multi-parameter influences [11], [12], [13]. Machine learning (ML), as an important technique of predictive analytics, plays an important role with the high performance in failure predictive analytics [14], [15]. Failure prediction using ML techniques has acquired considerable attention due to its high ability to discover patterns and create accurate models to predict future actions [16]. ML deal with the issues of how to build and design computer programs that improve their efficiency and accuracy for some specific task based on past events or observations [17], [18]. There are two main purposes of ML, which include: (i) to predict the dependent variable based on independent variables and (ii) to estimate the effect of the independent variables on the dependent variable [18], [19]. Generally, ML has three different categories, namely supervised, unsupervised, and reinforcement learning [20], [21]. Supervised learning is commonly used to build the prediction model that links input data with output ones based on many input-output pairs datasets [22]. In other words, supervised learning has prior knowledge of the output values for each input variable and tries to learn a pattern of the relationship between predictors (input) and response (output) [23], [24]. Learning of each algorithm is the process of building itself a model from the training dataset [25]. Classification and regression are two categories of supervised ML [26]. The difference of the regression from the classification is that its output value is continuous. Therefore the regression may be mapped into the classification by discretizing the output value [27]. There is much literature on applying supervised classification ML algorithms in different applications like wastewater plant, software, aircraft engine reliability, and COVID-19 effective prediction [28], [29], [30], [31]; as well as there are much literature on using supervised regression ML algorithms in diverse requests like healthcare [32], finance [33], robotics [34], travel [35], the automotive industry [36], and atmospheric corrosion [37].

Furthermore, there are some studies on PCB using ML algorithms have performed like fault recognition regarding the PCB glue [38], detection of various types of defects in PCB inspection [39], reliability prediction of solder joints failures [40], prediction of solder joint health [41], and evaluation of the life prediction effect of ECM on PCB using three regression methods [42], which these only used some of the ML algorithms, or they used one of the classifications or regression analysis for some limited critical factors and in low diverse corrosive conditions. However, none of these works considered LC predictions and connected ECM failures in detail. Generally, The ML-based approach for predicting PCB

Manuscript III

failures has not been considered enough in the past, as ML generally needs enough data samples to build efficient prediction models. Data collection is time consuming in relation to humidity effects on electronics in order to gather enough data samples suitable for machine learning tasks. Therefore, this study has made ML possible by doing many experiments to study how ML help in predicting PCB failure status as well as leakage current.

In this work, both classification and regression analysis using most applicable supervised ML algorithms included [43]; k-nearest neighbors (k-NN), decision tree (DT), random forest (RF), support vector machines (SVM), and deep neural network (DNN) was utilized in prediction of short circuit failure mode due to ECM and LC on PCB surface due to corrosion process. The 729 different conditions constructed of a 3^6 complete crossed design of three levels of six critical factors; H, T, CT, C, P, and V at 4374 hours experiments runs inside a climatic chamber. Surface insulation resistance (SIR) PCBs with interdigitated electrodes are used as test boards, pre-contaminated with three weak organic acids (WOAs), namely adipic, glutaric, and succinic acids, which are common activators in the solder flux used for the PCB manufacturing process. Hence, the presence of these residues lead to water film formation under humid conditions and corrosion process assisting final failure development, namely LC and ECM. The LC measurement due to electrochemical process for all 729 conditions over time showed a pattern of initial stable level followed by a sudden jump depending on whether the corrosion process leading to ECM dendrite formation and short circuit. The failure conditions in classification and the LC in regression categories of the supervised ML algorithms were investigated to determine the best model for prediction using F1 score and mean squared error (MSE), respectively, which are influential evaluation metrics for classification and regression analysis, respectively [44], [45]. The k-fold cross-validation was used to select the best-tuned hyperparameters values of each ML algorithm along with grid search approach. The grid search approach has been used to set a grid of discrete hyperparameter values based on the metrics for scoring the best algorithm performance [46]. Eventually, the applicable predictive model was chosen by performance estimation using the 115 new and unseen data conditions in the test dataset. The results presented the SVM and RF models for classification with the highest F1 score, accuracy, sensitivity, precision, and area under the receiver operating characteristic (ROC) curve (AUC) metrics values, as well as DT and RF models in regression with the lowest

values of the variety of errors, had the top score as the best models of the test dataset. The conclusion of this study presented that the RF model in the training validation, predicting both PCB failure conditions and LC values, offered the best results.

7.2 Materials and methods

7.2.1 Experimental data conditions

The experimental data conditions were obtained from systematic experiments using interdigitated SIR PCB surfaces mimicking PCB layout and exposed to various conditions. Each condition was made of combinations of one categorical and five numerical factors. Each contamination type as a categorical factor has collected 243 different data conditions. Each condition is a unique compound of P, C, T, H, V, and CT at 21600 seconds measurements. The experimental conditions were designed to cover all conditions with three levels of the six critical factors with performing a 3^6 complete crossed design. In general, 729 different conditions of all combinations factors/levels at 4374 hours experimental time have been employed to train and validate all supervised ML algorithms. Table 7.1 displays the five numerical factors included H, T, C, P, V besides CT as a categorical factor, each of them at three levels, along with symbols, values, and units. Actually, the aggressiveness increases from level 1 to 3 for all factors except pitch distance (inverse) and contamination type (aggressiveness of G(glutaric acid) is more than S (succinic acid) and A(adipic acid), and S is more than A). The following segment presents a brief overview of selecting the critical factors and levels in this study.

Table 7.1 Chosen critical factors and levels along with symbols, values, and units.

Level	Pitch Distance	Voltage	Temperature	Humidity	Contamination Level	Contamination Type
1	P1 (300 μ m)	V1 (2V)	T1 (25°C)	H1 (78%RH)	C1 (25 μ g/cm ²)	A (Adipic acid)
2	P2 (600 μ m)	V2 (6V)	T2 (40°C)	H2 (88%RH)	C2 (50 μ g/cm ²)	G (Glutaric acid)
3	P3 (1000 μ m)	V3 (10V)	T3 (55°C)	H3 (98%RH)	C3 (75 μ g/cm ²)	S (Succinic acid)

7.2.1.1 Pitch Distance

The various demand and the remarkable tendency to miniaturize electronic devices cause reducing the space of PCB and high component density [4]. Hence, the pitch distance is a significant factor in PCB failure due to the special effect on increasing the electric field

Manuscript III

power and making it easy for dendrite formation during ECM [47]. Three pitch distances of the SIR PCB used are similar to actual component size with electronic industries association (EIA) codes; 0201, 0402, and 0603.

7.2.1.2 Voltage

The voltage is another critical factor for the electrochemical and corrosion process on PCB, which creates the electric field between water film connection biased points, which not only cause electrochemical reactions at the biased points but also migration of ions through the water film resulting in ECM [48], [49]. The three voltage levels are considered in this work following the real range of bias on low power electronic devices and stress direct current (DC) voltage standard [48].

7.2.1.3 Climatic Conditions

The climatic conditions have a major role in the PCB failure as it leads to the water film formation. It refers to the level of humidity, temperature, and their variations. These two factors can determine the condensation range of water vapor on the PCB surface [50]. For condensation, the dew point range and the size of dew droplet formation on the PCB surface are affected by climatic conditions [51]. Climatic conditions can also influence in increasing the absolute humidity (AH) to interact with PCB surface, reducing the deliquescent relative humidity (RH) level and increasing solubility for contamination, and extending the deposition process for ECM through the increasing electrochemical process [52], [53]. The levels of both temperature and RH have proportional with the actual environment and deliquescence of solder flux activators [54].

7.2.1.4 Contamination

Cleanliness is an essential issue from the PCB failure point of view. In other words, the potential for corrosion occurrence is determined by the PCB cleanliness [55]. The detrimental effects of the contamination depend on different factors such as the type of contamination (CT), the quantity of contamination or contamination level (C), and the location of the contamination [56], [57]. The importance of contamination effects with the combination of climatic conditions is to induce water film formation due to deliquescence, contributing to the conductivity of the water layer, and depending on the type of contamination acting as an aggressive species for corrosion to occur [54]. The main type

of contaminations originated from the component assembling process of the PCB manufacturing, such as wave and reflow soldering process is related to the use of solder flux chemistry containing WOAs [58]. Between wave and reflow soldering process, wave soldering contributes higher contamination due to the use of liquid flux and application by spraying process. The adipic acid, glutaric acid, and succinic acid as important activator WOA compounds are considered in this work, each of them in three levels, which match with typical levels of flux residues usually seen after the wave soldering process [59], [60].

7.2.2 Experimental setup

7.2.2.1 SIR PCB Specimen

According to the IPC standard testing, SIR PCBs with interdigitated electrodes are frequently used for finding climatic effects on reliability, material qualification, service life estimation, and evaluating different factors on the PCB surface [61], [62]. Individual SIR patterns included three different surface areas, and three pitch distances of 0.3, 0.6, and 1 mm are shown in Table 7.1. They were made on FR-4 laminate with a thickness of 1.6 mm, complying with the IPC-4101/21 standard.

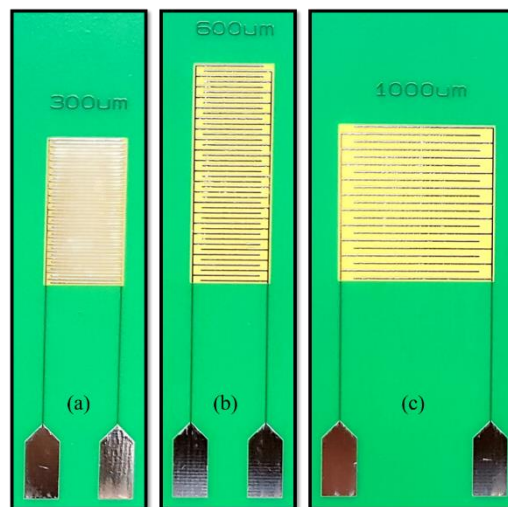


Figure 7.1 SIR PCBs with three different pitch distances and surface area, (a) 300 μm pitch distance, with 325 mm^2 surface area, (b) 600 μm pitch distance, with 494 mm^2 surface area, (c) 1000 μm pitch distance, with 702 mm^2 surface area.

Manuscript III

7.2.2.2 *SIR PCB preparation for testing*

Before starting the experiment, the two electrodes for each SIR pattern are hand soldered to two small external wires to connect with the SIR measurement system instrument. The PCBs are cleaned and then dried by an air compressor using isopropanol for three times. Then, each SIR pattern is contaminated with the solution of one critical WOAs, which is made up of 2.5g WOAs dissolved in 100 ml isopropanol at the concentration of 25g/L. Three levels of the solution are dispensed on the surface of SIR patterns using a micropipette to obtain three levels of contamination.

7.2.2.3 *Climatic chamber for testing and electrochemical system for LC measurement*

All experiments are performed using the Espec climatic chamber with the tolerances of ± 0.3 °C and $\pm 2.5\%$ RH. The 1.5 hours stabilization time is considered to be in the climatic chamber before each test. The BioLogic VSP with the multichannel workstation (5 channels) is used to apply bias to the board and measure leak current. For electrodes connections set up, two wires were used. One of them from the test board was connected to the working electrode, while another electrode was used both for reference and counter.

7.2.2.4 *ML algorithms and designation of their hyperparameters*

Recently, ML techniques are being adopted for a variety of applications of predictive analytics [63], [64]. Predictive analytics can include ML algorithms to analyze data quickly and efficiently [65]. ML algorithm predicts the outcome based on training input data obtained for analytical purposes [66]. The five commonly used supervised ML algorithms (k-NN, DT, RF, SVM, and DNN) have been used for both regressions (obtain numerical values, e.g., LC values) and classifications (sort items into appropriate categories, e.g., for failed or not-failed prediction in various conditions) [43].

In order to improve the precision and commission of each ML algorithm, there need several hyperparameters to tune [67]. Hyperparameters are important individual parameters for each algorithm to improve the model's performance, such as its complexity or its learning rate, and are commonly chosen based on some insights and trials for the training datasets [68]. This study has considered two main hyperparameters of each algorithm that are understood to have the most considerable influence on the algorithms' performance [69].

In contrast, for other hyperparameters, the default value is given by *scikit-learn* ML library of Python version 3 [70].

k-NN is a common supervised ML algorithm that identifies the similar and nearest neighbors of an data sample based on the preferences investigation [71]. The k refers to the number of nearest neighbors, while the nearest neighbor is a data point that is among the k closest data points to the data point under consideration [72]. The weight (W) in k-NN can be *uniform* that points to equal worth/weight given to each neighbor, or *distance*, which alludes to nearer neighbors having more weight than the others.

Decision tree (DT) algorithm belongs to the tree-based family of supervised ML algorithms, which builds decision rules from training data in form of decision nodes and leaf nodes branched from its root node [73]. The primary advantage of DT is that it is intuitive and easily explainable to the users. DT has two important hyperparameters, *maximum depth* of the tree (mD) and *minimum samples* (mSS), which is the minimum number of samples required to split an internal node. Random Forests (RF) is a common ensemble learning method for classification and regression tasks that operates by constructing a multitude of decision trees at training time, where each decision tree works on a sample set of the data. RF selects samples randomly and votes or averages over the predictions from all the decision trees for classification or regression tasks [72]. The *number of trees* (nE) in the forest and the *maximum fraction of data features to be split for trees* (mF) are the two important hyperparameters affecting the performance of the trained models in RF algorithm.

Support vector machine (SVM) is a supervised ML algorithm that separates different target classes using extreme or support vectors to create the hyperplane in multidimensional space [74]. Kernel, gamma (γ), and regularization (C) are among the most important hyperparameters which directly affect the performance of SVM [75]. Radial basis function (RBF) kernel is the most preferred function to make proper separation when there is no prior knowledge of data [69]. C is greater than zero and tells the SVM optimization how much you want to avoid misclassification [75], where a smaller value of C allows the optimizer to ignore points close to the boundary and increases the margin. γ can be between 0 and 1 and is the influence of a plausible line of separation or the spread of the RBF function. Lower γ means less curvature or far away points considered.

The artificial neural network (ANN) is a supervised learning algorithm consisting of the multilayer perceptron that helps learn complex relations between inputs and outputs. Generally, an ANN comprises three layers: the input, hidden, and output layer, each containing different neurons (nodes). The term of deep learning comes from having multiple hidden layers [76]. The input layer typically contains the independent variables that are used to predict the output. The output layer may have a different number of neurons based on the target labels/values [77]. The hyperparameters in the deep neural network (DNN) algorithm include the *number of hidden layers* (hL) and the *number of nodes or neurons in each hidden layer* (nN).

7.2.2.5 Evaluation metrics for ML algorithms

The evaluation metrics are used to assess how well ML algorithms have performed the training and testing of the dataset. Moreover, the evaluation metrics by comparing the difference between the model prediction and actual experimental data can measure the accuracy of each model [43]. Four commonly used evaluation metrics for classification include F1 score, precision, sensitivity, accuracy, and area under the receiver operating characteristic (ROC) curve (AUC). i.e., accuracy as an instinctive performance is measured using the confusion matrix. It is defined as the ratio of correct predictions to all observations. Similarly, four applicable metrics while predicting continuous variables have been utilized for regression analysis. These include mean squared error (MSE), root mean squared error (RMSE), mean absolute error (MAE), and mean absolute percentage error (MAPE). However, for unsophisticated selection of the best ML algorithm, F1 score and MSE as important evaluation metrics using the grid search approach have been employed for classification and regression, respectively. F1 score can be interpreted as a harmonic mean of precision and sensitivity. The best F1 score reaches 1, and the worst score at 0. In the regression, the best values, as well as best ML algorithms, have been obtained from comparing the MSE from 0 to 1, which the lower value indicates lower errors between predicted and real values and thus a better algorithm [78], [79]. The supported criterion hyperparameter for regression is also by default considered mean squared error (MSE), which is equal to variance reduction. Table 7.2 illustrates different metrics for both classification and regression, which can be acquired from the formulas [80], [81].

Table 7.2 Overview of different evaluation metrics and formulas for classification and regression supervised ML algorithms. (TP: true positive, FP: false positive, FN: false negative, TN: true negative, n: total number of the samples in the dataset, y_i : *experimental value*, y_i^{\wedge} : *predicted value*)

Classification		Regression	
Metrics	Formula	Metrics	Formula
F1 score	$\frac{2TP}{(2TP + FP + FN)}$	MSE	$\frac{1}{n} \sum_{i=1}^n (y_i - y_i^{\wedge})^2$
Accuracy	$\frac{(TP + TN)}{(TP + FN + FP + TN)}$	RMSE	$\sqrt{\frac{1}{n} \sum_{i=1}^n (y_i - y_i^{\wedge})^2}$
Precision	$\frac{TP}{(TP + FP)}$	MAE	$\frac{1}{n} \sum_{i=1}^n (y_i - y_i^{\wedge}) $
Sensitivity	$\frac{TP}{(TP + FN)}$	MAPE	$\frac{100\%}{n} \sum_{i=1}^n \left \frac{(y_i - y_i^{\wedge})}{y_i^{\wedge}} \right $

7.3 Results and Discussion

7.3.1 Results of humidity testing: leak current data and electrochemical migration failure

Using interdigitated PCB test structure, two responses resulting from exposure to various corrosive conditions are investigated for failure, namely the LC resulting from the corrosion action as well as the failure due to ECM. The LC consequent from SIR reduction due to electrochemical process occurring between two water film connected electrodes due to the influencing factors such as electric field (based on bias level and pitch distance), flux residues (from the soldering process), and climatic conditions factors such as temperature. The failure status due to ECM is formed by begetting conductive electrolytes between two electrodes, besides the dissolution of anodic metal ions and migration then deposition at the cathode due to the bias condition, finally leading to short circuit. Figure 7.2 illustrates the typical electrochemical current behavior as an important indicator to define LC levels due to initial current leaking through the water layer and dendrite formation current due to ECM. Curves represent failure conditions of the three contamination types in the same corrosive conditions, including P2, C3, V1, T3, and H3, with three different magnitudes, specifying two responses. First, there are LC before dendrite formation (show with yellow upward arrows) used for regression supervised ML modeling, and second, failure state due

Manuscript III

to dendrite formation (show with green downward arrows after the sudden jump) used for classification supervised ML modeling. The LC is assigned to the stable part, and the failure part is referred to initiate the process of failure on SIR PCB surfaces with a considerable jump in LC due to dendrite formation bridging between conductors (examples in Figure 7.3). The threshold of around 100 μA for this state is defined for the present analysis, which is detected for the ECM and dendrite formation. This value of current is commonly accepted as the threshold for failure due to ECM. This figure also clearly shows, in overall glutaric acid, succinic acid, and adipic acid due to being the relative difference in aggressivity of contamination, respectively, having varying LCs and failure times due to ECM [82], [83]. Among these contaminations, Glutaric acid is more aggressive due to its deliquescent relative humidity (DRH) value and high solubility in water film due to higher dissociation constant followed by succinic acid, and adipic acid [84], [85]. Glutaric acid has DRH in the range of 80-87%RH for a temperature range of 25-60°C, while values for adipic and succinic acid for the same range of temperature are around 83-99%RH and 81-95%RH, respectively [54], [82], [83], [86]. Table 7.3 displays the snippet of the experimental data results with the average of LC and failure state in each condition gathered by such kinds of the graphs from Figure 7.2 and used for the ML modeling part in the next section. Figure 7.13 and Figure 7.14 in the appendix present all experimental data results for the LC values and failure state at each condition, respectively.

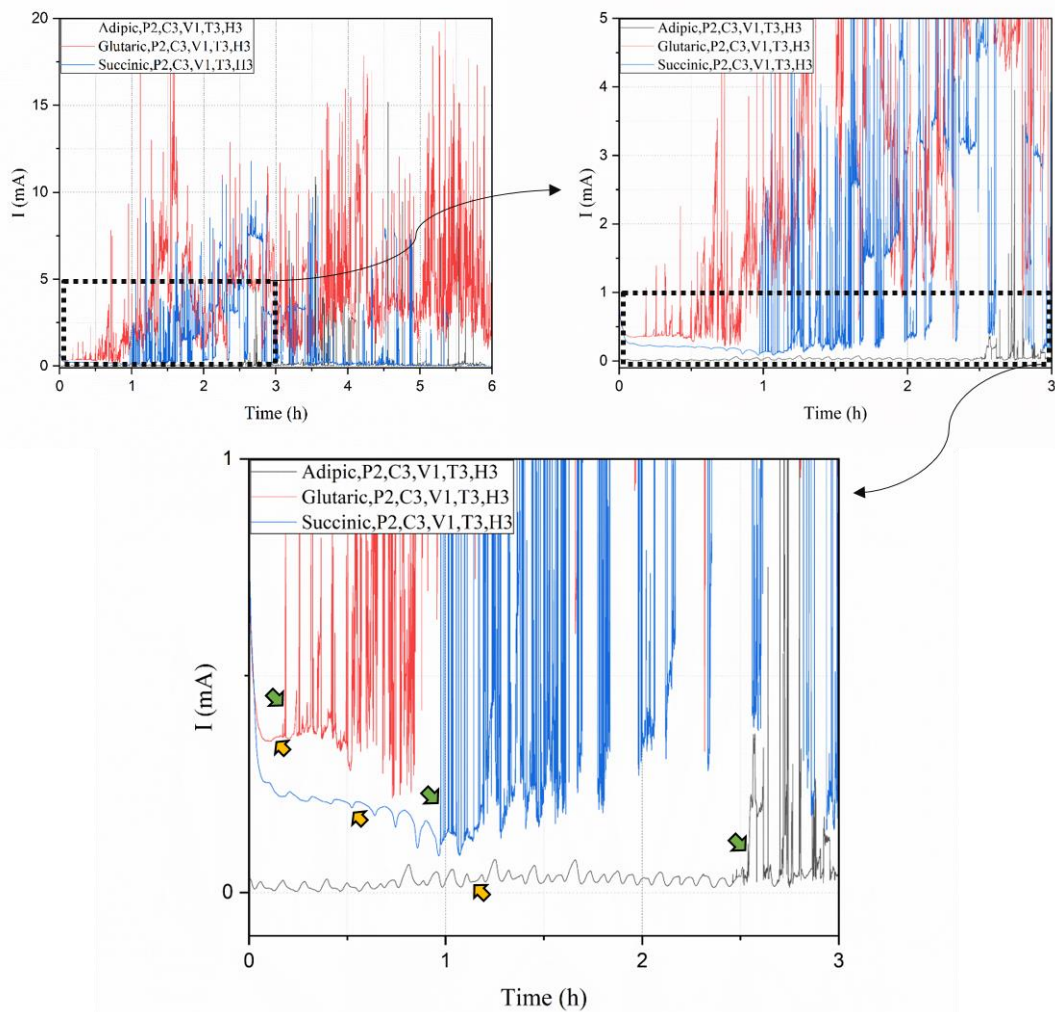


Figure 7.2 Typical leak current behavior in the same corrosive condition to define two responses (LCs and failure state) for supervised ML algorithms of three contamination types; adipic acid (black), glutaric acid (red), and succinic acid (blue).

Table 7.3 Snipped of the experimental data results with the failure state and average of LC in each condition constructed of a combination of CT, P, C, V, T, and H factors at different levels.

<i>Condition</i>	<i>CT</i>	<i>P</i>	<i>C</i>	<i>V</i>	<i>T</i>	<i>H</i>	<i>State of condition due to ECM</i>	<i>Mean of LC value</i>
1	Adipic	300	75	10	25	78	Not-Failed	6.04E-07
2	Adipic	600	75	10	25	78	Not-Failed	4.72E-06
3	Adipic	1000	75	10	25	78	Not-Failed	5.05E-07
4	Glutaric	300	50	2	55	88	Failed	3.06E-01
5	Glutaric	600	50	2	55	88	Failed	4.34E-02
6	Glutaric	1000	50	2	55	88	Not-Failed	1.40E-02
7	Succinic	300	25	6	40	98	Failed	2.88E-01
8	Succinic	600	25	6	40	98	Failed	7.81E-02
9	Succinic	1000	25	6	40	98	Not-Failed	1.96E-02

Manuscript III

Figure 7.3 shows the typical surface view of test PCB showing permanent dendrite filament between two electrodes on SIR PCB surface when applied corrosive conditions (P2, C3, V1, T3, and H3) for three different contamination types (the current measurement curves of them are shown in Figure 7.2) using a digital microscope at ex-situ for the optical inspection of dendrite formation (failure state) as an example. Pictures in Figure 7.3 shows ECM dendrite formation for all contamination types due to the higher humidity, temperature and contamination level, while succinic and adipic acid shows less susceptibility for the formation of dendrite at lower humidity, temperature and contamination levels. In general, tendency for formation of ECM increases with increasing aggressivity of conditions (shown in Table 7.1) namely increase in bias, contamination level, temperature, humidity and decrease in pitch distance. This is also clear in snipped data shown in Table 7.3, which shows lower LC values and no-failed conditions for less aggressive contaminations (succinic and adipic) and in general for low bias, temperature, humidity and high pitch distances.

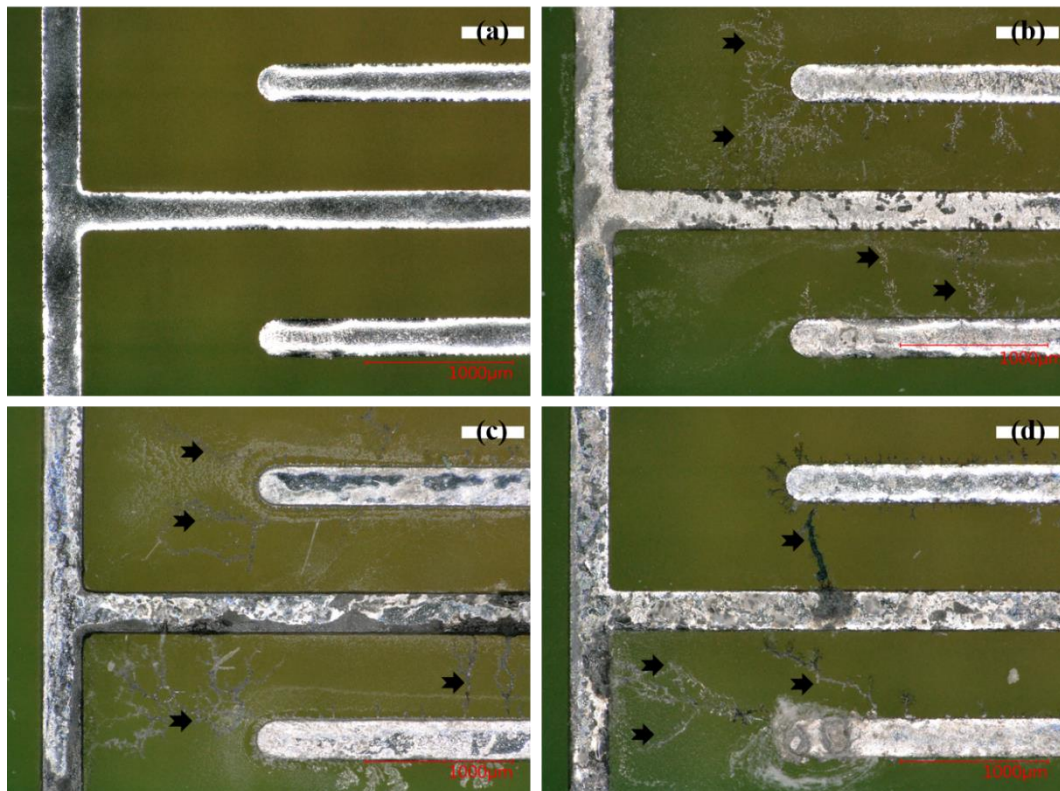


Figure 7.3 Optical appearance of dendrite formation and ECM on P2 (600µm) SIR PCB surface before and after exposure to C3 (75µg/cm²), V1 (2V), T3 (55°C), and H3 (98%RH) for (a) before exposure and clean PCB, (b) contaminated by adipic acid, (c) contaminated by glutaric acid, (d) contaminated by succinic acid.

7.3.2 Validation and hyperparameters tuning of ML algorithms

The training set is automatically divided into two parts; training and validation dataset. Selecting the validation method usually depends on the dataset size and is categorized into three methods; leave one-out cross-validation (small sample size), K-fold cross-validation (moderate sample size), and validation with test set (large sample size) [87]. This study has used K-fold cross-validation with having K equal to 5 for all algorithms. In 5-fold cross-validation, the training dataset is separated into five subsets, of which four subsets are for training an ML model, and the fifth subset evaluates the quality of the trained ML model. This means that this method uses 20% of the data for testing, and this is usually very accurate. This procedure has been repeated five times, choosing different subsets for validation [88].

The grid search approach is a common technique for hyperparameters tuning [89]. It searches exhaustively through the grid for each set of hyperparameters and evaluates each algorithm score based on an evaluation metric (F1 score, MSE, etc.). This approach methodically selects the best combination of hyperparameters ranges values in a specific mixture grid [46].

7.3.3 ML algorithms setup

All of the experimental results obtained from 729 different conditions have been used for the training set of five different ML algorithms in classification analysis to predict failed or not-failed conditions. We use all not-failed data samples for regression analysis to predict LC values which is around 71.5 % of all data means 521 conditions. We only use not-failed data in our regression task, as LC values were obtained from the initial part of the current measurement in the stable part before the failure [90].

Table 7.4 shows two hyperparameters of each algorithm that have been assigned at different levels. Combining different values for each hyperparameter of Table 7.4 gives 100 separate combinations for SVM, DT, and RF algorithms, 20 combinations in the k-NN, and 84 combinations in the DNN algorithm. We used grid search to select the best value of each hyperparameter, giving the best models trained by each algorithm.

Table 7.4 Hyperparameters and their ranges of the studied ML algorithms.

Algorithms	k-NN		DT		RF		SVM		DNN	
Hyperparameters	K	W	mD	mSS	nE	mF	γ	C	hL	nN
Ranges	2	uniform distance	3	2	50	0.1	1	1	1	5
	3		4	3	100	0.2	0.5	5	2	10
	4		5	4	150	0.3	0.1	10	3	15
	5		6	5	200	0.4	0.05	25		20
	6		7	6	250	0.5	0.01	50		
	7		8	7	300	0.6	0.005	100		
	8		9	8	350	0.7	0.001	200		
	9		10	9	400	0.8	0.005	300		
	10		11	10	450	0.9	0.0001	400		
	11		12	11	500	1	0.0005	500		

Once the best set of hyperparameters for each ML algorithm is selected by the grid search and the 5-fold cross validation, the best trained model of each algorithm was chosen for predicting the test dataset. Our test dataset consists of 115 unseen data samples with new conditions of combinations of six critical factors, which have not been in the training dataset used by grid search. Figure 7.4 generally shows our overall pipeline for finding the best machine learning models of both classification and regression tasks. The next section displays the visual comparison of different range values of all ML algorithm hyperparameters to select the best values.

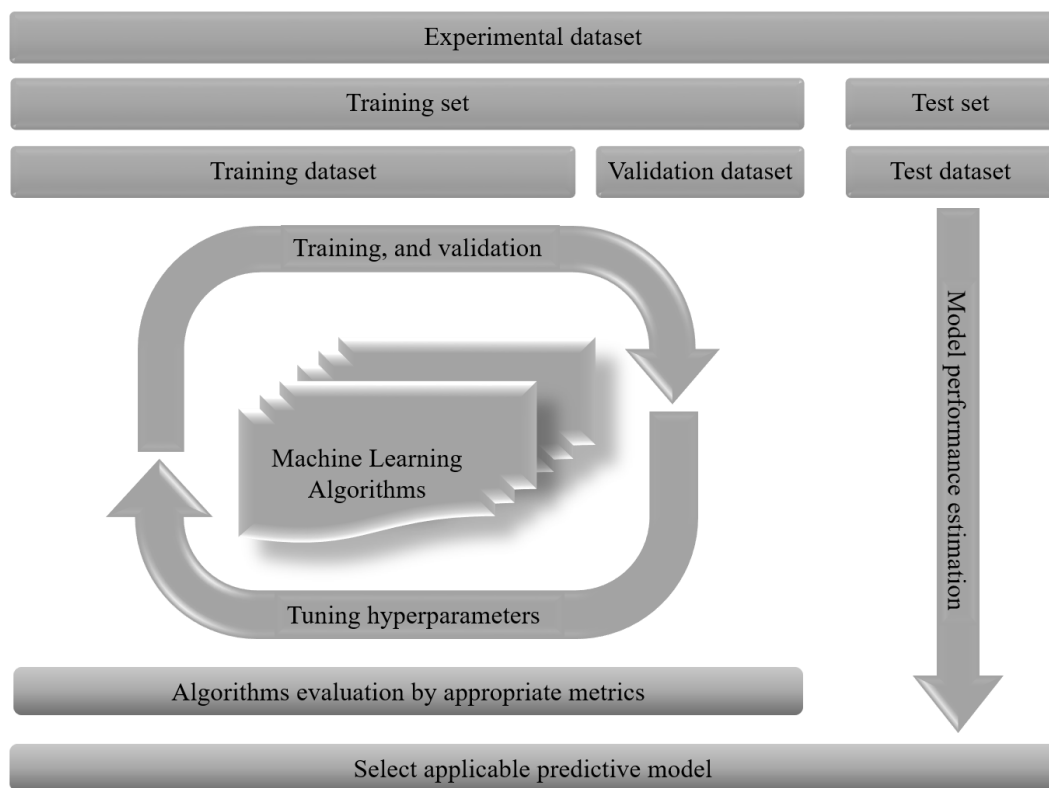


Figure 7.4 General pipeline for building the applicable predictive model and performance estimation in ML.

7.3.4 Evaluation of trained ML algorithms for classifying PCB failures

Figure 7.5 describe the results of the 5-fold cross-validation of each ML algorithm with different hyperparameters for classification task. The 5-fold cross-validation randomly divides the dataset into 5 sets of approximately equal size, then the first fold is kept for testing and the model is trained on 4 folds to reduce the data bias and the variance of the result estimation. We used F1 score as comparison metrics in grid search for classification. Figure 7.5 (a) compares F1 score attained by k-NN classification algorithm with different values of K and W where each diagram represents a W value. The figure illustrates a shape similar to the parabola downwards curve that F1 score first increase and then decrease by increasing the K values. K equals 5 represents the climax of F1 score.

Figure 7.5 (b) compares F1 score acquired by DT classification algorithm with diverse values of mD and mSS where each diagram characterizes an mSS value. The figure displays that F1 score increase entirely by increasing the Md values. The F1 score for the $mD \leq 5$ are the same, and after that mSS equal 7 shows the highest F1 score for all mD values.

Figure 7.5 (c) also compares F1 score obtained by RF classification algorithm with different ranges of nE and mF where each diagram describes an mF value. The figure at a glance indicates similar effect of the mF and nE ranges upon the F1 score. Since, F1 score for all the 100 set of different values of mF and nE presents the very close value between 0.92 to 0.96.

Figure 7.5 (d) compares F1 score achieved by SVM classification algorithm with different values of γ and C where each diagram represents a γ value. The figure shows that F1 score increase by incrementing C for all γ values especially for $\gamma > 0.05$ and converges with $C > 300$.

In order to simplify the presentation of 84 different combinations of neurons in four hidden layers in Figure 7.5 (e), for comparison F1 score, we have dedicated 84 numbers for each combination. Table 7.7 in the appendix shows the arrangement of the neurons and hidden layers with dedicated numbers. Comparison of the number of hidden layers combined with how to arrange the neurons for each layer allocates the different values of F1 score. For instance, N equals 83 presents a DNN structure of 3 hidden layers (hL) in order of 20 neurons for the first hL, 20 neurons for the second hL, and 15 neurons for the third hL. The

Manuscript III

N is used to enumerate the available DNN architectures, and it is not a hyperparameter. The figure demonstrates that generally F1 score achieved by DNN classification algorithm increase with increasing the complexity of the neural network (number of neurons and hidden layers (L)) although the F1 score converges between 0.91 to 0.93 even in more complex networks.

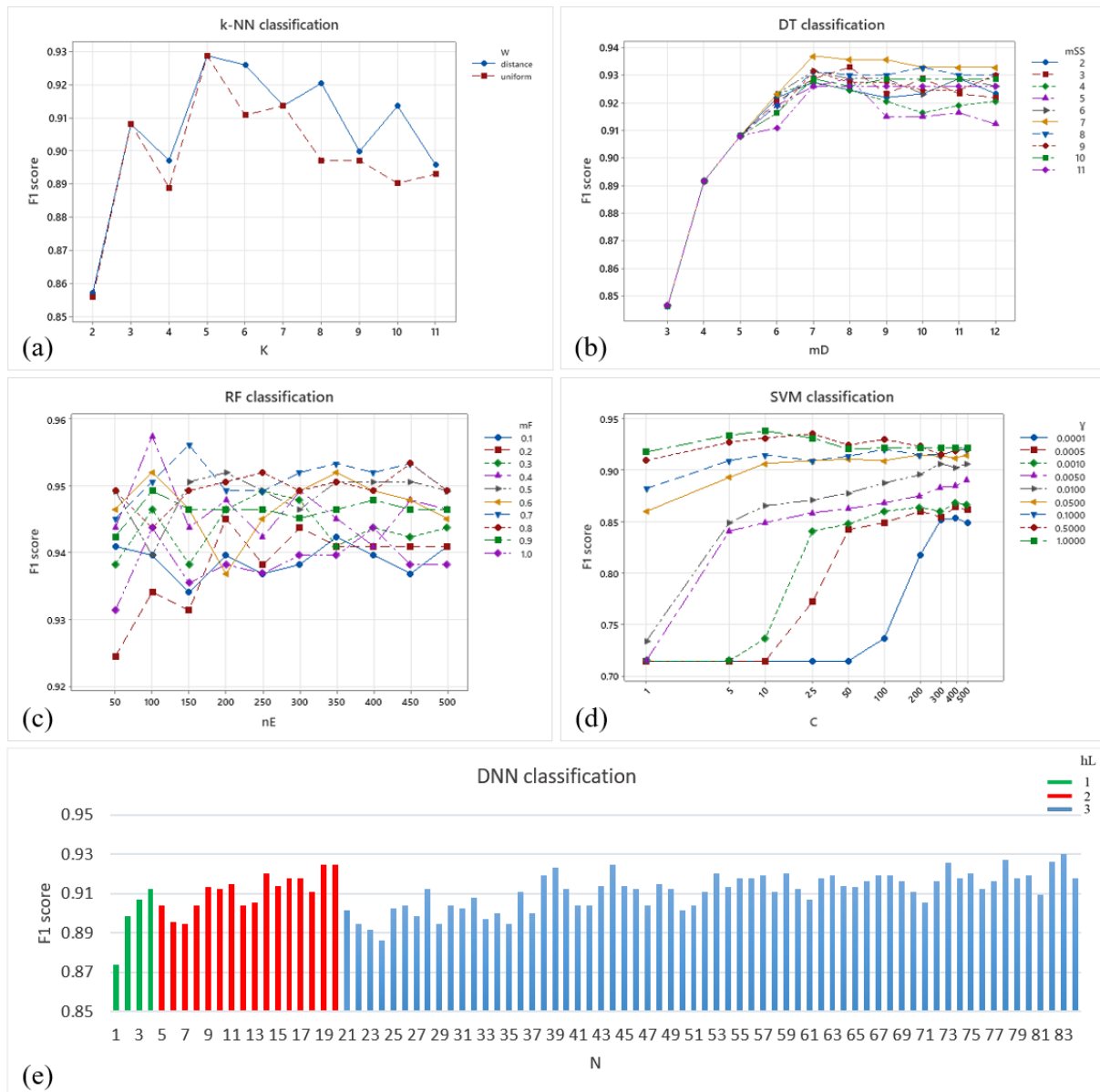


Figure 7.5 Performance diagrams of classification (a) k-NN algorithm, (b) DT algorithm, (c) RF algorithm, (d). SVM algorithm, and (e) DNN algorithm on the training dataset of PCB failure classification for different values of the hyperparameters. (K: the number of neighbors, W: the weight of each neighbor, mD: the maximum depth of the tree, mSS: the minimum samples needed to split an internal node, nE: the number of trees, mF: the maximum fraction of data features to be split for trees, C: the misclassification or error term, γ : the influences of plausible separation, N: the

number of each combination of neurons and layers based on Table 7.7 (N is not a hyperparameter), hL: the number of hidden layers).

7.3.5 Evaluation of trained ML algorithms for estimating LC values

Figure 7.6 expresses the results of the 5-fold cross validation of each ML algorithm with different hyperparameters for regression analysis. We used MSE as comparison metrics in grid search for regression analysis. Figure 7.6 (a) compares MSE achieved by k-NN regression with different values of K and W where in contrast to Figure 7.5 (a) presents MSE decrease and increase from K equal 5. The *distance* hyperparameter compared to the *uniform* displays a slightly better function in both classification and regression.

Figure 7.6 (b) compares MSE earned by DT regression algorithm with various values of mD and mSS, where each diagram characterizes an mSS value. The figure displays MSE decrease by increasing the mD until 5 value, then the uniform behavior for each mSS range. The figure shows the lowest mSS values offer the lowest MSE amount.

Figure 7.6 (c) also compares MSE obtained by RF regression algorithm with different ranges of nE and mF where each diagram describes an mF value. Similar to Figure 7.5 (c), this figure only displays the mF and nE ranges effect upon the MSE.

Figure 7.6 (d) compares MSE achieved by SVM regression algorithm with different values of γ and C where each diagram represents a γ value. The figure shows that MSE decreases by incrementing C for $\gamma < 0.01$, and for others is approximately uniform.

Figure 7.6 (e) also used Table 7.7 for simply present to compares MSE obtained by DNN regression algorithm with different combinations (84 different assortments) of neural and hidden layers. This figure shows MSE in 2, and 3 hidden layers approximately give the same value; however, increasing the number of neurons/nodes decreases MSE values. For instance, according to Figure 7.6 (e) and Table 7.7, the best MSE value (lowest one) belongs to number 20, which represents the combination of two layers wherein each layer exists highest neurons/nodes ([20; 20]).

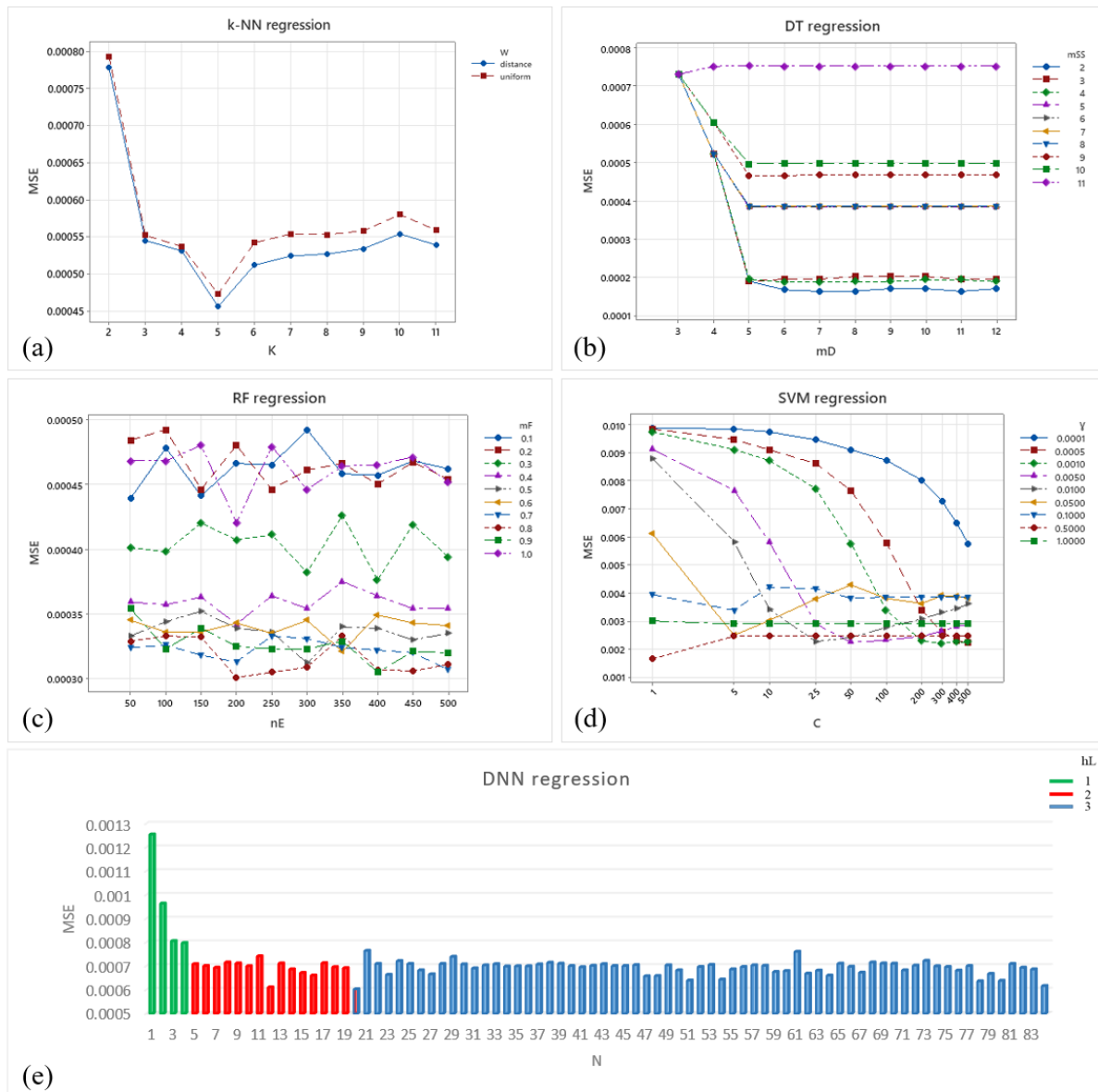


Figure 7.6 Performance diagrams of regression (a) k-NN algorithm, (b) DT algorithm, (c) RF algorithm, (d) SVM algorithm, and (e) DNN algorithm on the training dataset of LC regression for different values of the hyperparameters (Refer to Figure 7.5 captions).

7.3.6 Selection of the best trained ML models

Generally, the best k-NN model obtained from the set of K equals 5 with *uniform* as a weight hyperparameter for classification and with *distance* as another weight hyperparameter for regression. DT and RF models demonstrated the very close values of F1 score and MSE for each set of their hyperparameters at various ranges, which average of the metrics values compared to other models for both classification and regression give us the bests on them. The high ranges of the γ and low ranges of the C gave the highest F1

score and lowest MSE for SVM model. The best DNN model also illustrated the significant effect of neurons numbers in all hidden layers. Table 7.5 includes the optimum set of all hyperparameters for each studied ML algorithm, where a list of values of hyperparameters as well as the performance achieved is reported. We considered maximum of F1 scores for classification and minimum of MSE values for regression to select the best models.

Table 7.5 Best values for each ML algorithm were obtained from 5-fold cross-validation of training data.

ML Algorithm	k-NN		DT		RF		SVM		DNN	
	K	W	mD	mSS	nE	mF	γ	C	hL	nN
Best range for classification	5	uniform	7	7	100	0.4	1	10	3	(20,20,15)
F1 score	0.9286 \pm 0.0166		0.9368 \pm 0.0203		0.9575 \pm 0.0153		0.9382 \pm 0.0116		0.93 \pm 0.0224	
Best range for regression	5	distance	7	2	200	0.8	0.5	1	2	(20,20)
MSE	0.0005 \pm 0.0004		0.0002 \pm 0.0002		0.0003 \pm 0.0002		0.0016 \pm 0.0006		0.0006 \pm 0.0006	

Figure 7.12 in the appendix, visually shows the recap of Table 7.5, which contains the best models of each studied algorithm for both classification and regression tasks. The RF was found as the best ML algorithm among this study with F1 score of around 0.96 ± 0.01 for prediction of PCB failure (Table 7.5 and Figure 7.12). Moreover, in LC values prediction, DT with about 0.0001 MSE difference of RF was seen as the best ML algorithm for regression analysis with 0.0002 ± 0.0002 (Table 7.5 and Figure 7.7). Nevertheless, there is no significant difference between all ML algorithms on the training dataset for both classification and regression analysis. In other words, the results show that ML algorithms are able to learn the distribution of our data and effectively predict failures of PCB boards as well as estimating the LC values. Therefore, the best of each algorithm has been used to predict of test dataset for finding the accuracy and performance of all applicable predictive models in the next section.

7.3.7 Evaluating the best-trained models

We use the test dataset to evaluate the performance of the best-selected trained model by each ML algorithm. The test data set comprised 115 new conditions of the mixture of different levels of the six critical factors.

Table 7.8 in the appendix displays the different levels of the test dataset, which have been used for making other different conditions for test data, and those have not been used for the training in the ML algorithms. It is because of having the actual estimation of the accuracy and proficiency of the applicable predictive ML algorithms. Figure 7.7 presents a confusion matrix achieved by each algorithm showing a summary of the classification results. All our classification performance metrics (i.e. F1 score, AUC, accuracy, sensitivity, and precision) can be calculated from the confusion matrix.

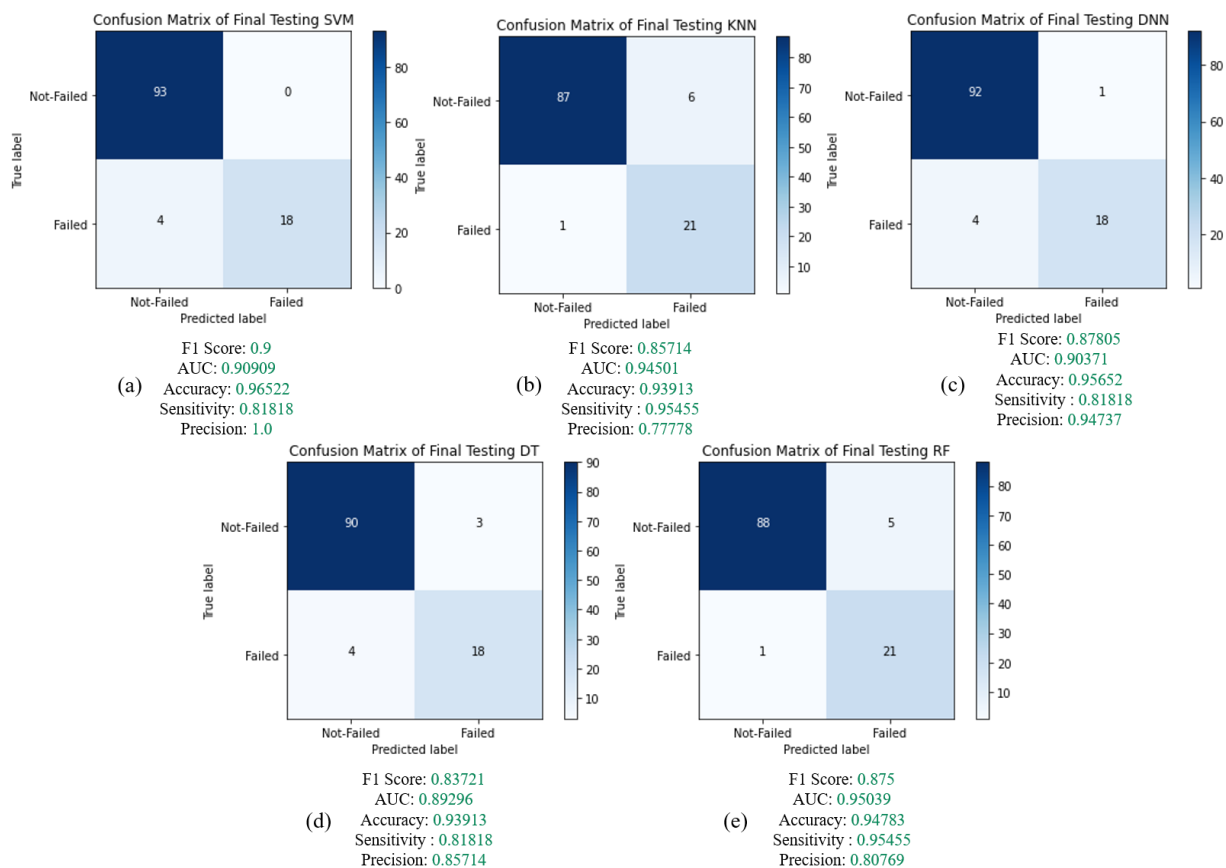


Figure 7.7 Overview of the confusion matrices for assessing the classification accuracy of a) SVM algorithm, b) k-NN algorithm, c) DT algorithm, d) RF algorithm, and e) DNN algorithm on test dataset to predict failure on PCB surface.

According to Figure 7.7, SVM model in the F1 score, accuracy, and precision metrics have provided the highest values, and the RF model in AUC and sensitivity has given the best amounts. We prefer the F1 score over other metrics because it is effective for imbalanced datasets [91], and our test data consists of 76% failed and 24% Not-failed conditions, which is an imbalanced dataset. After F1 score, AUC with the highest value represented the best

predictive model [92]. Figure 7.8 compares ROC curves and AUC of the best-trained model by each algorithm.

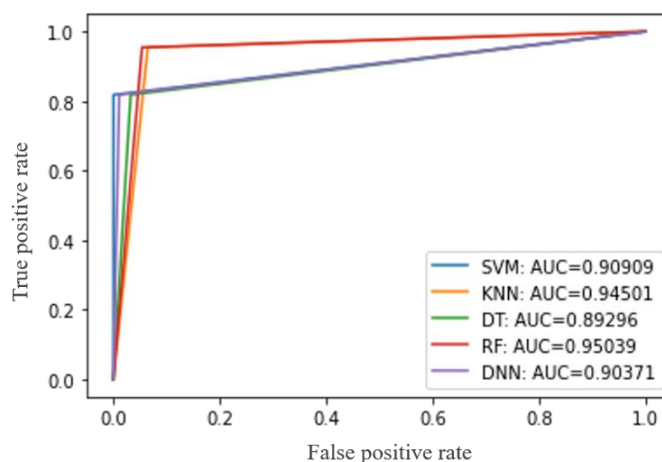


Figure 7.8 ROC curves for different ML algorithms.

Table 7.6 compares MSE, RMSE, MAD, and MAPE of our studied regression algorithms to find the best ML model for LC predictions. The k-NN and the DNN models have the lowest MSE and RMSE and high MAD and MAPE values compared to others except for SVM. However, RF and DT have the lowest MAD and MAPE values. There is no significant difference to the MSE and RMSE values for whole models and they are following the same magnitude. Kernel density estimate (KDE) plot in Figure 7.9 clearly shows that the predictions of LC values are obtained through different ML algorithm' compared to real LC's averaging in experimental measurement. The KDE plot is used for visualizing the density distribution of the real mean of LC and the predicted values [93]. Based on comparisons of Table 7.6 and Figure 7.9, it can be concluded that the RF and DT models have demonstrated better prediction according to the test dataset in this study. In other words, density of predicted LC Mean closely follows the density of real LC values for RF (Figure 7.9 (e)) and DT (Figure 7.9 (d)) in comparison with other studied regression algorithms. Figure 7.10 presents the overview of the best ML algorithm of the testing dataset according to the F1 score and AUC metrics for classification, as well as MSE and MAD metrics for regression.

Table 7.6 Comparison of the regression metrics on the test dataset.

	<i>k-NN</i>	<i>DT</i>	<i>RF</i>	<i>SVM</i>	<i>DNN</i>
<i>MSE</i>	0.0019	0.0028	0.0021	0.0022	0.0019
<i>RMSE</i>	0.0436	0.0532	0.0462	0.0465	0.0432
<i>MAD</i>	0.0004	0.0001	0.0002	0.0137	0.0038
<i>MAPE</i>	37.46	2.51	3.78	1236.21	611.06

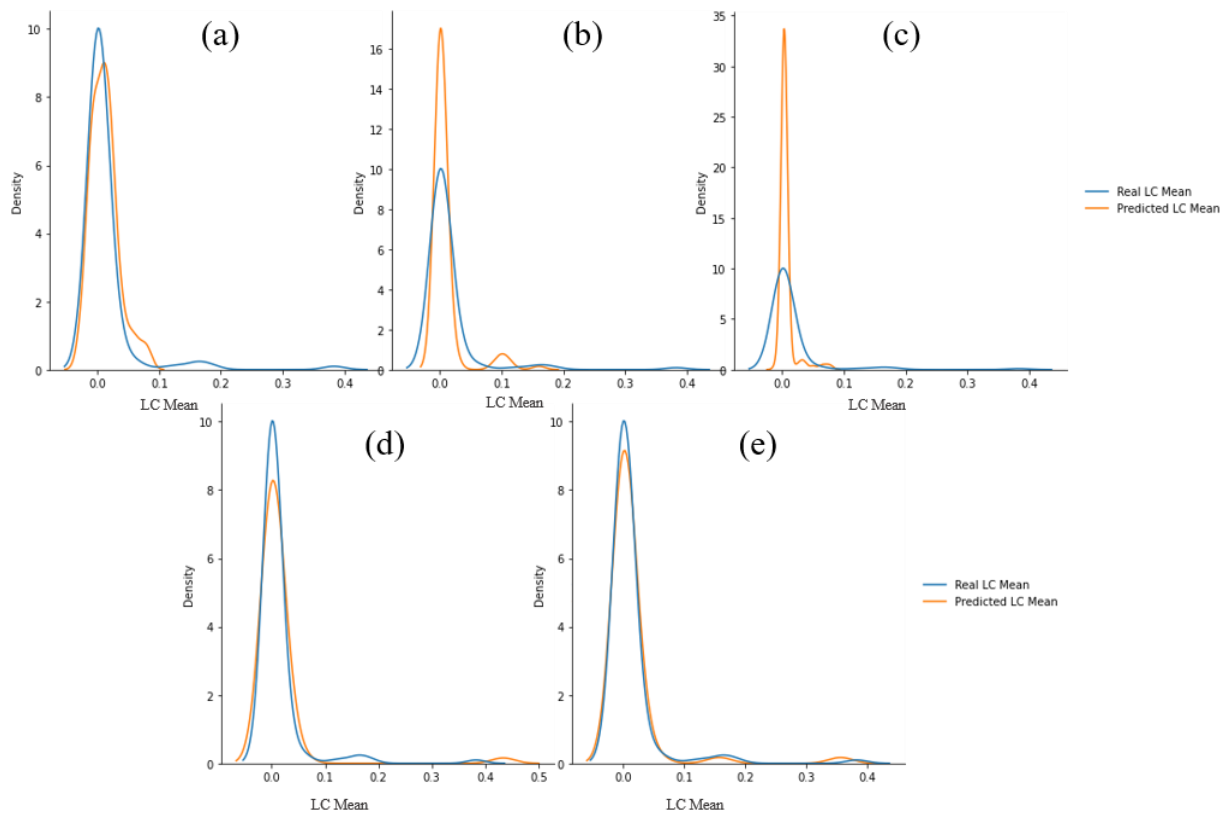


Figure 7.9 KDE plots for each algorithm comparing the density of real and predicted LC values; (a) SVM algorithm, (b) k-NN algorithm, (c) DNN algorithm, (d) DT algorithm, and (e) RF algorithm.

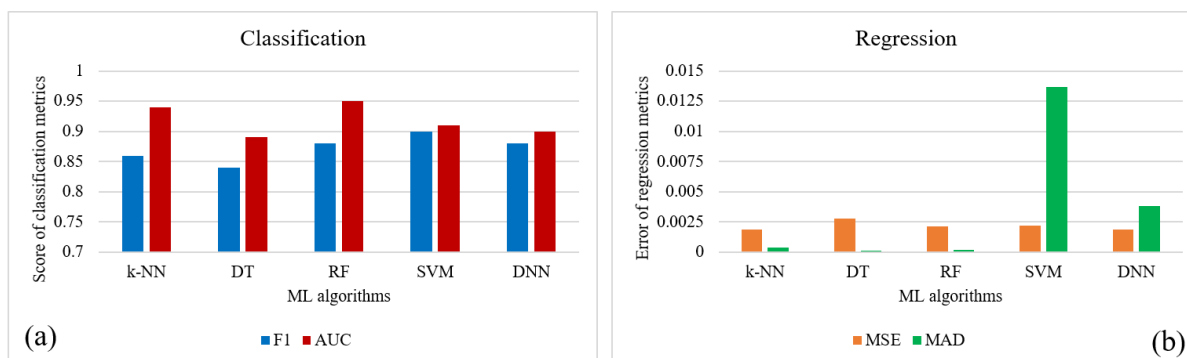


Figure 7.10 Overview of the best ML algorithm of the testing dataset according to; (a) the F1 score and AUC metrics for classification, as well as (b) MSE and MAD metrics for regression, as the most significant metrics.

7.3.8 Overall discussion

ML has gained a lot of attention because of its ability to effectively solve complex problems across various industries. This study aims to create a generalized ML model for predicting PCB failure and LC values based on the input conditions combining six critical factors (i.e. pitch distance, contamination level, temperature, humidity, voltage, and contamination type). The results of our study on common ML algorithms prove that well-trained ML model can efficiently forecast failures of a specific PCB provided that the PCB is exposed to a condition where relevant descriptors are known. Predicting failures under known conditions is very much useful for pro-active design strategy for PCBs to increase robustness to prevent failure in exposure to critical conditions. As another anchor of this paper, LC prediction can be used to estimate the possibility of failure or even time to failure if we could find the correlation between LC and failure in different applications.

Comparing with the number of failures conditions on the SIR PCB surface at the same condition except for different CTs, the models based on machine learning had a satisfactory prediction performance even with the limited training dataset. For instance, the experiments indicated that glutaric acid compare to other CTs has a high number of corrosion failure conditions in the same corrosive condition on PCB surfaces, that ML models also emphasized it and could precisely predict different new conditions.

We followed two main steps for training and testing our predictive models: 1. Training and validation where we build predictive models using common ML algorithms (k-NN, DT, RF, SVM, DNN), and use validation data to find best trained models, and 2. Testing is our

Manuscript III

final evaluation of the best trained models using new input data (conditions) which have never been seen by the algorithm during the training procedure. Both regression and classification tasks were used as a trade-off between the model's inference and the model's complexity to avoid underfitting and overfitting. Underfitting occurs when a trained model is too simple to capture the relationship between the input and output. Overfitting occurs when the model has been overtrained and is good at predicting training data while at the same time showing high errors in predicting new test data.

The RF model in evaluating trained ML algorithms for classifying PCB failures with around 0.96 F1 score and estimating LC values about 0.0003 MSE illustrated the best-trained ML algorithm. Furthermore, in validating the best-trained models based on the test dataset, RF for failure prediction with 0.87 F1 score and highest AUC and for LC prediction with 0.0021 MSE presented one of the best models, which can be used for both classification and regression analysis.

Figure 7.11 illustrates relative factor importance in classification and regression analysis according to the best ML model selected. The humidity factor has a major effect in both analyses (classification for ECM and regression for LC). Humidity is the key factor causing water film formation on the board, which is required as a medium for causing electrochemical failure [94]. Humidity factor is also important in connection with contamination effects as the hygroscopic nature of the ionic residue (e.g. adipic, succinic or glutaric acids) represented by the DRH value reduces the humidity level required for water film formation on a PCB surface under transient climatic conditions. This observation is in agreement with the combined effect of humidity, and contamination types resulting from flux residue are reported in the literature [94], [95], [96], [97], [98]. However, it is interesting to note that the contamination level for LC (Figure 7.11 (b)) shows significant effect, while less for classification (ECM) in Figure 7.11 (a). This is attributed to the fact that contamination level provides conductivity for the water film to produce LC, therefore triggering electrochemical process, while the ECM depends on the amount of metal ion and migration to cathode, which is independent of contamination level. Contamination type has significant effect on ECM failure meaning that more aggressive contamination (e.g. glutaric acid) caused more ECM failures [54], [82], [84]. This is due to the increased acidity and aggressiveness of solution due to the high solubility of glutaric acid, therefore resulting in increased tin ion dissolution for migration. It has been reported that among the acid testing,

glutaric acid cause high levels of ECM above ~85% humidity level [54], [82], [99]. Similarly, although voltage shows less effect on both ECM failure and LC, while pitch distance showed more significant effect due to increased electric field with bias levels. This is significant especially in connection with miniaturization for which reduction in component sizes and distances cause higher electric field [100], [101]. Temperature is effect is also significant for LC (regression), which is due to two factors namely: (i) reduction in DRH level for contaminations and (ii) increased solubility of acids giving higher conductivity. Kamila et al. have extensively investigated the combined effect of flux residue contaminations, temperature, and humidity conditions, which showed significant reduction in DRH values, increase in water absorption capability of contaminations, LC, and ECM susceptibility with increase in temperature [83], [85], [102], [103]. Overall relative factor importance from the ML analysis fit with experimental observations not only from the theoretical point of view in connection with humidity caused electrochemical failures in electronics, but also the reported experimental results in the literature.

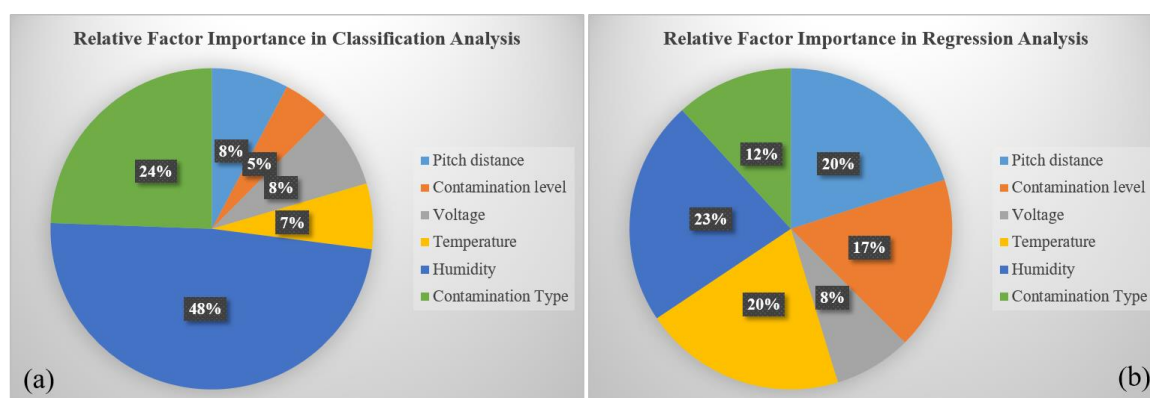


Figure 7.11 Relative factor importance in both; (a) classification (failure state), and (b) regression (LC) analysis.

7.4 Conclusion

The study presents how machine learning is able to forecast corrosion failure on PCBs based on experimental data set. Using classification for predicting failure status in the form of Failed and Not-Failed labels, the PCB failures are adapted into a binary classification problem and then solved by the classification task. Relative factor importance of both classification and regression shows the importance of various influencing factors in agreement with experimental observations. Further, given that many corrosive conditions are combined with various factors/ levels that affect the PCB failure, use of well-trained

Manuscript III

ML algorithms in both classification and regression can be used as a tool to predict failure status and LC values reducing the number of experiments needed at different new conditions.

All ML algorithms in the training dataset showed suitable learning in both classification and regression. According to the results, the F1 score for all ML algorithms were between 0.71 to 0.96. Moreover, AUC, as another significant metric, could present a value of more than 0.9 in all of them. In addition, for classification, the range value of MSE was between 0.01 to the best value of 0.0002, which showed the acceptable error for all ML algorithms. High performance in both classification and regression shows that ML is interesting for predicting failures of PCBs as well as estimating the LC values. We believe that there is room for more accurate ML models with higher number of experiments (conditions). Based on our evaluation, SVM and RF algorithms could achieve the highest scores (F1 score, AUC, accuracy, sensitivity, and precision) for predicting PCB failures under different conditions of critical factor combinations.

Our study shows that DT and RF regression algorithms could achieve the lowest values of errors on the test dataset. The RF algorithm could train the most effective model with high performance in predicting PCB failure as well as LC values as the best classifier and regressor, respectively.

Acknowledgements

The present research work was carried out as a part of work in CELCORR/CreCon consortium (<https://celcorr.dtu.dk>). The authors would like to acknowledge the CELCORR/CreCon consortium, and Innovation Fund Denmark for the funding support.

Conflict of interest

The authors declare that they have no known competing financial interests or personal relationships that could have appeared to influence the work reported in this paper.

References

- [1] J.B. Jacobsen, J.P. Krog, L. Rimestad, A. Riis, A.H. Holm, Climate-Protective Packaging: Using Basic Physics to Solve Climatic Challenges for Electronics in Demanding Applications, *IEEE Ind. Electron. Mag.* 8 (2014) 51–59. <https://doi.org/10.1109/MIE.2014.2330912>.
- [2] S. Rastayesh, S. Bahrebar, F. Blaabjerg, D. Zhou, H. Wang, J.D. Sørensen, A system engineering approach using FMEA and bayesian network for risk analysis-a case study, *Sustain.* 12 (2020) 1–18. <https://doi.org/10.3390/SU12010077>.
- [3] K. Piotrowska, M.S. Jellesen, R. Ambat, Water film formation on the PCBA surface and failure occurrence in electronics, in: 2018 IMAPS Nord. Conf. Microelectron. Packag., IEEE, 2018: pp. 72–76. <https://doi.org/10.23919/NORDPAC.2018.8423854>.
- [4] S. Bahrebar, R. Ambat, Investigation of critical factors effect to predict leakage current and time to failure due to ECM on PCB under humidity, *Microelectron. Reliab.* 127 (2021) 114418. <https://doi.org/10.1016/j.microrel.2021.114418>.
- [5] M. Bâzu, T. Băjenescu, Failure Analysis: A Practical Guide for Manufacturers of Electronic Components and Systems, John Wiley and Sons, 2011. <https://doi.org/10.1002/9781119990093>.
- [6] S. Bahrebar, D. Zhou, S. Rastayesh, H. Wang, F. Blaabjerg, Reliability assessment of power conditioner considering maintenance in a PEM fuel cell system, *Microelectron. Reliab.* 88–90 (2018) 1177–1182. <https://doi.org/10.1016/j.microrel.2018.07.085>.
- [7] V. Verdingovas, M.S. Jellesen, R. Ambat, Relative effect of solder flux chemistry on the humidity related failures in electronics, *Solder. Surf. Mt. Technol.* 27 (2015) 146–156. <https://doi.org/10.1108/SSMT-11-2014-0022>.
- [8] M.S. Jellesen, D. Minzari, U. Rathinavelu, P. Møller, R. Ambat, Corrosion in Electronics at Device Level, *ECS Trans.* 25 (2019) 1–14. <https://doi.org/10.1149/1.3321952>.
- [9] J.F.J.M. Caers, X.J. Zhao, Failure modes and failure analysis, in: *Solid State Light. Reliab. Components to Syst.*, Springer New York, New York, NY, 2013: pp. 111–184. https://doi.org/10.1007/978-1-4614-3067-4_4.
- [10] R. Ambat, S.G. Jensen, P. Møller, Corrosion Reliability of Electronic Systems, *ECS Trans.* 6 (2019). <https://doi.org/10.1149/1.2900650>.
- [11] S. Zhao, F. Blaabjerg, H. Wang, An Overview of Artificial Intelligence Applications for Power Electronics, *IEEE Trans. Power Electron.* 36 (2021) 4633–4658. <https://doi.org/10.1109/TPEL.2020.3024914>.
- [12] J. Lee, H.A. Kao, H.D. Ardakani, D. Siegel, Intelligent Factory Agents with Predictive Analytics for Asset Management, in: *Ind. Agents Emerg. Appl. Softw. Agents Ind.*, Elsevier, 2015: pp. 341–360. <https://doi.org/10.1016/B978-0-12-800341-1.00019-X>.
- [13] A.C. Lure, X. Du, E.W. Black, R. Irons, D.J. Lemas, J.A. Taylor, O. Lavilla, D. de la Cruz, J. Neu, Using machine learning analysis to assist in differentiating between necrotizing

- enterocolitis and spontaneous intestinal perforation: A novel predictive analytic tool, *J. Pediatr. Surg.* 56 (2021) 1703–1710. <https://doi.org/10.1016/j.jpedsurg.2020.11.008>.
- [14] B. Mohammed, I. Awan, H. Ugail, M. Younas, Failure prediction using machine learning in a virtualised HPC system and application, *Cluster Comput.* 22 (2019) 471–485. <https://doi.org/10.1007/s10586-019-02917-1>.
- [15] H. Agrawal, J. Chandiwala, S. Agrawal, Y. Goyal, Heart Failure Prediction using Machine Learning with Exploratory Data Analysis, in: *2021 Int. Conf. Intell. Technol. CONIT 2021, IEEE, 2021*: pp. 1–6. <https://doi.org/10.1109/CONIT51480.2021.9498561>.
- [16] P. Wang, Y. Li, C.K. Reddy, Machine learning for survival analysis: A survey, *ACM Comput. Surv.* 51 (2019) 1–36. <https://doi.org/10.1145/3214306>.
- [17] M. Paluszek, S. Thomas, An Overview of Machine Learning, in: *MATLAB Mach. Learn.*, Apress, Berkeley, CA, 2017: pp. 3–15. https://doi.org/10.1007/978-1-4842-2250-8_1.
- [18] M. Mohammed, M.B. Khan, E.B.M. Bashie, *Machine learning: Algorithms and applications*, CRC Press, 2016. <https://doi.org/10.1201/9781315371658>.
- [19] I. Hammad, K. El-Sankary, J. Gu, A comparative study on machine learning algorithms for the control of a wall following robot, in: *IEEE Int. Conf. Robot. Biomimetics, ROBIO 2019, IEEE, 2019*: pp. 2995–3000. <https://doi.org/10.1109/ROBIO49542.2019.8961836>.
- [20] T. Oladipupo, Types of Machine Learning Algorithms, in: *New Adv. Mach. Learn.*, InTech, 2010. <https://doi.org/10.5772/9385>.
- [21] I.H. Sarker, *Machine Learning: Algorithms, Real-World Applications and Research Directions*, *SN Comput. Sci.* 2 (2021) 160. <https://doi.org/10.1007/s42979-021-00592-x>.
- [22] T. Jiang, J.L. Gradus, A.J. Rosellini, Supervised Machine Learning: A Brief Primer, *Behav. Ther.* 51 (2020) 675–687. <https://doi.org/10.1016/j.beth.2020.05.002>.
- [23] H.K. Gianey, R. Choudhary, Comprehensive Review On Supervised Machine Learning Algorithms, in: *Proc. - 2017 Int. Conf. Mach. Learn. Data Sci. MLDS 2017, IEEE, 2018*: pp. 38–43. <https://doi.org/10.1109/MLDS.2017.11>.
- [24] A. Singh, N. Thakur, A. Sharma, A review of supervised machine learning algorithms, in: *Proc. 10th INDIACom; 2016 3rd Int. Conf. Comput. Sustain. Glob. Dev. INDIACom 2016, 2016*: pp. 1310–1315. <https://ieeexplore.ieee.org/abstract/document/7724478> (accessed January 6, 2022).
- [25] O. F.Y, A. J.E.T, A. O, H. J. O, O. O, A. J, Supervised Machine Learning Algorithms: Classification and Comparison, *Int. J. Comput. Trends Technol.* 48 (2017) 128–138. <https://doi.org/10.14445/22312803/ijctt-v48p126>.
- [26] C. Crisci, B. Ghattas, G. Perera, A review of supervised machine learning algorithms and their applications to ecological data, *Ecol. Modell.* 240 (2012) 113–122. <https://doi.org/10.1016/j.ecolmodel.2012.03.001>.
- [27] P.C. Sen, M. Hajra, M. Ghosh, Supervised Classification Algorithms in Machine Learning: A Survey and Review, in: *Adv. Intell. Syst. Comput.*, Springer Verlag, 2020: pp. 99–111.

- https://doi.org/10.1007/978-981-13-7403-6_11.
- [28] L.Z. Velimirović, R. Janković, J.D. Velimirović, A. Janjić, Wastewater plant reliability prediction using the machine learning classification algorithms, *Symmetry (Basel)*. 13 (2021) 1518. <https://doi.org/10.3390/sym13081518>.
- [29] A. Jaiswal, R. Malhotra, Software reliability prediction using machine learning techniques, in: *Adv. Intell. Syst. Comput.*, Springer Verlag, 2016: pp. 141–163. https://doi.org/10.1007/978-981-10-0448-3_12.
- [30] D. Singh, M. Kumar, K. V. Arya, S. Kumar, Aircraft Engine Reliability Analysis using Machine Learning Algorithms, in: *2020 IEEE 15th Int. Conf. Ind. Inf. Syst. ICIIIS 2020 - Proc.*, IEEE, 2020: pp. 443–448. <https://doi.org/10.1109/ICIIIS51140.2020.9342675>.
- [31] A. Kumari, A.K. Mehta, Effective Prediction of COVID-19 Using Supervised Machine Learning with Ensemble Modeling, in: *2022*: pp. 537–547. https://doi.org/10.1007/978-981-16-5747-4_45.
- [32] E. Gambhir, R. Jain, A. Gupta, U. Tomer, Regression Analysis of COVID-19 using Machine Learning Algorithms, in: *Proc. - Int. Conf. Smart Electron. Commun. ICOSEC 2020*, IEEE, 2020: pp. 65–71. <https://doi.org/10.1109/ICOSEC49089.2020.9215356>.
- [33] J. Rani P, A. Kulkarni, A.V. Kamath, A. Menon, P. Dhatwalia, R. Jain, Prediction of Player Price in IPL Auction Using Machine Learning Regression Algorithms, in: *Proc. CONECCT 2020 - 6th IEEE Int. Conf. Electron. Comput. Commun. Technol.*, IEEE, 2020: pp. 1–6. <https://doi.org/10.1109/CONECCT50063.2020.9198668>.
- [34] D. Di Domenico, A. Marinelli, N. Boccardo, M. Semprini, L. Lombardi, M. Canepa, S. Stedman, A.D. Bellingegni, M. Chiappalone, E. Gruppioni, M. Laffranchi, L. De Michieli, Hannes Prosthesis Control Based on Regression Machine Learning Algorithms, in: *2021 IEEE/RSJ Int. Conf. Intell. Robot. Syst.*, IEEE, 2021: pp. 5997–6002. <https://doi.org/10.1109/iros51168.2021.9636391>.
- [35] I. Hapsari, I. Surjandari, Komarudin, Visiting time prediction using machine learning regression algorithm, in: *2018 6th Int. Conf. Inf. Commun. Technol. ICoICT 2018*, IEEE, 2018: pp. 495–500. <https://doi.org/10.1109/ICoICT.2018.8528810>.
- [36] C. EL Mazgualdi, T. Masrou, I. El Hassani, A. Khoudi, Machine learning for KPIs prediction: a case study of the overall equipment effectiveness within the automotive industry, *Soft Comput.* 25 (2021) 2891–2909. <https://doi.org/10.1007/s00500-020-05348-y>.
- [37] Z. Pei, D. Zhang, Y. Zhi, T. Yang, L. Jin, D. Fu, X. Cheng, H.A. Terry, J.M.C. Mol, X. Li, Towards understanding and prediction of atmospheric corrosion of an Fe/Cu corrosion sensor via machine learning, *Corros. Sci.* 170 (2020) 108697. <https://doi.org/10.1016/j.corsci.2020.108697>.
- [38] T. Vafeiadis, N. Dimitriou, D. Ioannidis, T. Wotherspoon, G. Tinker, D. Tzovaras, A framework for inspection of dies attachment on PCB utilizing machine learning techniques, *J. Manag. Anal.* 5 (2018) 81–94. <https://doi.org/10.1080/23270012.2018.1434425>.
- [39] E.H. Yuk, S.H. Park, C.S. Park, J.G. Baek, Feature-learning-based printed circuit board inspection via speeded-up robust features and random forest, *Appl. Sci.* 8 (2018) 932.

- <https://doi.org/10.3390/app8060932>.
- [40] S. Yi, R. Jones, Machine learning framework for predicting reliability of solder joints, *Solder. Surf. Mt. Technol.* 32 (2020) 82–92. <https://doi.org/10.1108/SSMT-04-2019-0013>.
- [41] Y.M. Chang, C.C. Wei, J. Chen, P. Hsieh, An Implementation of Health Prediction in SMT Solder Joint via Machine Learning, in: 2019 IEEE Int. Conf. Big Data Smart Comput. BigComp 2019 - Proc., IEEE, 2019: pp. 1–4. <https://doi.org/10.1109/BIGCOMP.2019.8679428>.
- [42] Y. Zhou, L. Yang, Y. Li, W. Lu, Exploring the Data-Driven Modeling Methods for Electrochemical Migration Failure of Printed Circuit Board, in: Proc. - 2019 Progn. Syst. Heal. Manag. Conf. PHM-Paris 2019, IEEE, 2019: pp. 100–105. <https://doi.org/10.1109/PHM-Paris.2019.00025>.
- [43] M. Ayoub, A review on machine learning algorithms to predict daylighting inside buildings, *Sol. Energy.* 202 (2020) 249–275. <https://doi.org/10.1016/j.solener.2020.03.104>.
- [44] M. Sokolova, N. Japkowicz, S. Szpakowicz, Beyond accuracy, F-score and ROC: A family of discriminant measures for performance evaluation, in: *AAAI Work. - Tech. Rep.*, Springer, Berlin, Heidelberg, 2006: pp. 24–29. https://doi.org/10.1007/11941439_114.
- [45] A. Rácz, D. Bajusz, K. Héberger, Multi-Level Comparison of Machine Learning Classifiers and Their Performance Metrics, *Molecules.* 24 (2019) 2811. <https://doi.org/10.3390/molecules24152811>.
- [46] B.H. Shekar, G. Dagnev, Grid search-based hyperparameter tuning and classification of microarray cancer data, in: 2019 2nd Int. Conf. Adv. Comput. Commun. Paradig. ICACCP 2019, IEEE, 2019: pp. 1–8. <https://doi.org/10.1109/ICACCP.2019.8882943>.
- [47] D. Minzari, F.B. Grumsen, M.S. Jellesen, P. Møller, R. Ambat, Electrochemical migration of tin in electronics and microstructure of the dendrites, *Corros. Sci.* 53 (2011) 1659–1669. <https://doi.org/10.1016/J.CORSCI.2011.01.009>.
- [48] V. Verdingovas, M.S. Jellesen, R. Ambat, Effect of pulsed voltage on electrochemical migration of tin in electronics, *J. Mater. Sci. Mater. Electron.* 26 (2015) 7997–8007. <https://doi.org/10.1007/s10854-015-3454-9>.
- [49] D. Minzari, M.S. Jellesen, P. Møller, R. Ambat, On the electrochemical migration mechanism of tin in electronics, *Corros. Sci.* 53 (2011) 3366–3379. <https://doi.org/10.1016/J.CORSCI.2011.06.015>.
- [50] J. Romero, M.H. Azarian, C. Morillo, M. Pecht, Effects of Moisture and Temperature on Membrane Switches in Laptop Keyboards, *IEEE Trans. Device Mater. Reliab.* 18 (2018) 535–545. <https://doi.org/10.1109/TDMR.2018.2866776>.
- [51] H. Conseil-Gudla, V.C. Gudla, S. Borgaonkar, M.S. Jellesen, R. Ambat, Investigation of moisture uptake into printed circuit board laminate and solder mask materials, *J. Mater. Sci. Mater. Electron.* 28 (2017) 6138–6151. <https://doi.org/10.1007/s10854-016-6292-5>.
- [52] R. Ambat, H. Conseil-Gudla, V. Verdingovas, Corrosion in Electronics, in: *Encycl. Interfacial Chem.*, Elsevier, 2018: pp. 134–144. <https://doi.org/10.1016/B978-0-12-409547->

- 2.13437-7.
- [53] H.W. Zhang, Y. Liu, J. Wang, F.L. Sun, Effect of elevated temperature on PCB responses and solder interconnect reliability under vibration loading, in: *Microelectron. Reliab.*, Elsevier Ltd, 2015: pp. 2391–2395. <https://doi.org/10.1016/j.microrel.2015.07.033>.
- [54] K. Piotrowska, R. Ud Din, F.B. Grumsen, M.S. Jellesen, R. Ambat, Parametric Study of Solder Flux Hygroscopicity: Impact of Weak Organic Acids on Water Layer Formation and Corrosion of Electronics, *J. Electron. Mater.* 47 (2018) 4190–4207. <https://doi.org/10.1007/s11664-018-6311-9>.
- [55] K. Piotrowska, R. Ambat, Residue-Assisted Water Layer Build-Up Under Transient Climatic Conditions and Failure Occurrences in Electronics, *IEEE Trans. Components, Packag. Manuf. Technol.* 10 (2020) 1617–1635. <https://doi.org/10.1109/TCPMT.2020.3005933>.
- [56] B. Song, M.H. Azarian, M.G. Pecht, Impact of dust on printed circuit assembly reliability, in: *IPC APEX EXPO 2012*, 2012: pp. 1643–1659.
- [57] F. Cirolia, C. Finan, The effects of environmental contaminants on electronic power supplies, in: *IEE Conf. Publ.*, 2001: pp. 30–34. <https://doi.org/10.1049/cp:20010575>.
- [58] K. Piotrowska, R.U. Din, M.S. Jellesen, R. Ambat, Effect of solder mask surface chemistry and morphology on the water layer formation under humid conditions, *IEEE Trans. Components, Packag. Manuf. Technol.* 8 (2018) 1756–1768. <https://doi.org/10.1109/TCPMT.2018.2792047>.
- [59] J. Hörber, J. Franke, Wave Soldering, in: *CIRP Encycl. Prod. Eng.*, Springer Berlin Heidelberg, Berlin, Heidelberg, 2019: pp. 1807–1811. https://doi.org/10.1007/978-3-662-53120-4_16837.
- [60] K. Piotrowska, F. Li, R. Ambat, Transformation of reflow solder flux residue under humid conditions, *Microelectron. Reliab.* 123 (2021) 114195. <https://doi.org/10.1016/j.microrel.2021.114195>.
- [61] V. Verdingovas, S. Joshy, M.S. Jellesen, R. Ambat, Analysis of surface insulation resistance related failures in electronics by circuit simulation, *Circuit World.* 43 (2017) 45–55. <https://doi.org/10.1108/CW-09-2016-0040>.
- [62] S. Zhan, M.H. Azarian, M. Pecht, Reliability of Printed Circuit Boards Processed Using No-Clean Flux Technology in Temperature–Humidity–Bias Conditions, *IEEE Trans. Device Mater. Reliab.* 8 (2008) 426–434. <https://doi.org/10.1109/TDMR.2008.922908>.
- [63] A. Vinoth, S. Datta, Fundamentals of Machine Learning, in: *Mach. Learn. Ind.*, 2022: pp. 1–27. https://doi.org/10.1007/978-3-030-75847-9_1.
- [64] K.J. Kim, I. Tagkopoulos, Application of machine learning in rheumatic disease research, *Korean J. Intern. Med.* 34 (2019) 708–722. <https://doi.org/10.3904/kjim.2018.349>.
- [65] K. Lepenioti, A. Bousdekis, D. Apostolou, G. Mentzas, Prescriptive analytics: Literature review and research challenges, *Int. J. Inf. Manage.* 50 (2020) 57–70. <https://doi.org/10.1016/j.ijinfomgt.2019.04.003>.

- [66] M.K. Tran, S. Panchal, V. Chauhan, N. Brahmabhatt, A. Mevawalla, R. Fraser, M. Fowler, Python-based scikit-learn machine learning models for thermal and electrical performance prediction of high-capacity lithium-ion battery, *Int. J. Energy Res.* (2021). <https://doi.org/10.1002/er.7202>.
- [67] L. Yang, A. Shami, On hyperparameter optimization of machine learning algorithms: Theory and practice, *Neurocomputing.* 415 (2020) 295–316. <https://doi.org/10.1016/j.neucom.2020.07.061>.
- [68] H.J.P. Weerts, A.C. Mueller, J. Vanschoren, Importance of Tuning Hyperparameters of Machine Learning Algorithms, *Arxiv.Org.* (2020). <https://arxiv.org/abs/2007.07588> (accessed January 9, 2022).
- [69] M. Aghaaminiha, R. Mehrani, M. Colahan, B. Brown, M. Singer, S. Nestic, S.M. Vargas, S. Sharma, Machine learning modeling of time-dependent corrosion rates of carbon steel in presence of corrosion inhibitors, *Corros. Sci.* 193 (2021) 109904. <https://doi.org/10.1016/j.corsci.2021.109904>.
- [70] F. Pedregosa, G. Varoquaux, A. Gramfort, V. Michel, B. Thirion, O. Grisel, M. Blondel, P. Prettenhofer, R. Weiss, V. Dubourg, J. Vanderplas, A. Passos, D. Cournapeau, M. Brucher, M. Perrot, É. Duchesnay, Scikit-learn: Machine learning in Python, *J. Mach. Learn. Res.* 12 (2011) 2825–2830. <http://jmlr.org/papers/v12/pedregosa11a.html> (accessed December 30, 2021).
- [71] A.J. Gallego, J.R. Rico-Juan, J.J. Valero-Mas, Efficient k-nearest neighbor search based on clustering and adaptive k values, *Pattern Recognit.* 122 (2022) 108356. <https://doi.org/10.1016/j.patcog.2021.108356>.
- [72] V.K. Ayyadevara, Random Forest, *Pro Mach. Learn. Algorithms.* (2018) 105–116. https://doi.org/10.1007/978-1-4842-3564-5_5.
- [73] T. Jo, Decision Tree, in: *Mach. Learn. Found.*, Springer International Publishing, Cham, 2021: pp. 141–165. https://doi.org/10.1007/978-3-030-65900-4_7.
- [74] C. Cortes, V. Vapnik, L. Saitta, Support-vector networks, *Mach. Learn.* 1995 203. 20 (1995) 273–297. <https://doi.org/10.1007/BF00994018>.
- [75] R. Laref, E. Losson, A. Sava, M. Siadat, On the optimization of the support vector machine regression hyperparameters setting for gas sensors array applications, *Chemom. Intell. Lab. Syst.* 184 (2019) 22–27. <https://doi.org/10.1016/j.chemolab.2018.11.011>.
- [76] V.R.S. Mani, A. Saravanaselvan, N. Arumugam, Performance comparison of CNN, QNN and BNN deep neural networks for real-time object detection using ZYNQ FPGA node, *Microelectronics J.* 119 (2022) 105319. <https://doi.org/10.1016/j.mejo.2021.105319>.
- [77] G. Asadollahfardi, Artificial Neural Network, in: *Pro Mach. Learn. Algorithms*, Apress, Berkeley, CA, Berkeley, CA, 2015: pp. 77–91. https://doi.org/10.1007/978-3-662-44725-3_5.
- [78] F. Balali, J. Nouri, A. Nasiri, T. Zhao, Machine Learning Principles, in: *Data Intensive Ind. Asset Manag.*, Springer International Publishing, Cham, 2020: pp. 115–157. https://doi.org/10.1007/978-3-030-35930-0_8.

- [79] P. Kumar, Y. Singh, An empirical study of software reliability prediction using machine learning techniques, *Int. J. Syst. Assur. Eng. Manag.* 3 (2012) 194–208. <https://doi.org/10.1007/s13198-012-0123-8>.
- [80] D.C. Feng, Z.T. Liu, X.D. Wang, Z.M. Jiang, S.X. Liang, Failure mode classification and bearing capacity prediction for reinforced concrete columns based on ensemble machine learning algorithm, *Adv. Eng. Informatics.* 45 (2020) 101126. <https://doi.org/10.1016/j.aei.2020.101126>.
- [81] U. Dagdeviren, B. Kaymak, A regression-based approach for estimating preliminary dimensioning of reinforced concrete cantilever retaining walls, *Struct. Multidiscip. Optim.* 61 (2020) 1657–1675. <https://doi.org/10.1007/s00158-019-02470-w>.
- [82] V. Verdingovas, M.S. Jellesen, R. Ambat, Solder Flux Residues and Humidity-Related Failures in Electronics: Relative Effects of Weak Organic Acids Used in No-Clean Flux Systems, *J. Electron. Mater.* 44 (2015) 1116–1127. <https://doi.org/10.1007/s11664-014-3609-0>.
- [83] K. Piotrowska, M. Grzelak, R. Ambat, No-Clean Solder Flux Chemistry and Temperature Effects on Humidity-Related Reliability of Electronics, *J. Electron. Mater.* 48 (2019) 1207–1222. <https://doi.org/10.1007/s11664-018-06862-4>.
- [84] H. Conseil, V. Verdingovas, M.S. Jellesen, R. Ambat, Decomposition of no-clean solder flux systems and their effects on the corrosion reliability of electronics, *J. Mater. Sci. Mater. Electron.* 27 (2016) 23–32. <https://doi.org/10.1007/s10854-015-3712-x>.
- [85] K. Piotrowska, F. Li, R. Ambat, Thermal decomposition of binary mixtures of organic activators used in no-clean fluxes and impact on PCBA corrosion reliability, *Solder. Surf. Mt. Technol.* 32 (2019) 93–103. <https://doi.org/10.1108/SSMT-05-2019-0020>.
- [86] F. Li, I. Mantis, M.S. Jellesen, R. Ambat, Amino Acids as Activators for Wave Solder Flux Systems: Investigation of Solderability and Humidity Effects, *IEEE Trans. Components, Packag. Manuf. Technol.* 12 (2022) 857–868. <https://doi.org/10.1109/TCPMT.2022.3167389>.
- [87] D. Berrar, Cross-Validation, *Encycl. Bioinforma. Comput. Biol. ABC Bioinforma.* 1–3 (2019) 542–545. <https://doi.org/10.1016/B978-0-12-809633-8.20349-X>.
- [88] G. Jiang, W. Wang, Error estimation based on variance analysis of k-fold cross-validation, *Pattern Recognit.* 69 (2017) 94–106. <https://doi.org/10.1016/j.patcog.2017.03.025>.
- [89] D.M. Belete, M.D. Huchaiyah, Grid search in hyperparameter optimization of machine learning models for prediction of HIV/AIDS test results, *Int. J. Comput. Appl.* (2021) 1–12. <https://doi.org/10.1080/1206212X.2021.1974663>.
- [90] S. Bahrebar, R. Ambat, Time to Failure Prediction on a Printed Circuit Board Surface Under Humidity Using Probabilistic Analysis, *J. Electron. Mater.* (2022) 1–19. <https://doi.org/10.1007/s11664-022-09668-7>.
- [91] F.A. Naim, U.H. Hannan, M. Humayun Kabir, Effective Rate of Minority Class Over-Sampling for Maximizing the Imbalanced Dataset Model Performance, in: *Lect. Notes Data Eng. Commun. Technol.*, Springer, Singapore, 2022; pp. 9–20. <https://doi.org/10.1007/978->

981-16-6285-0_2.

- [92] K. Hajian-Tilaki, Receiver operating characteristic (ROC) curve analysis for medical diagnostic test evaluation, *Casp. J. Intern. Med.* 4 (2013) 627–635. [/pmc/articles/PMC3755824/](#) (accessed January 12, 2022).
- [93] C.J. Spencer, C. Yakymchuk, M. Ghaznavi, Visualising data distributions with kernel density estimation and reduced chi-squared statistic, *Geosci. Front.* 8 (2017) 1247–1252. <https://doi.org/10.1016/j.gsf.2017.05.002>.
- [94] K. Piotrowska, V. Verdingovas, R. Ambat, Humidity-related failures in electronics: effect of binary mixtures of weak organic acid activators, *J. Mater. Sci. Mater. Electron.* 29 (2018) 17834–17852. <https://doi.org/10.1007/s10854-018-9896-0>.
- [95] V. Verdingovas, Climatic Reliability of Electronics: Early Prediction and Control of Contamination and humidity effects, Technical University of Denmark (DTU), 2015.
- [96] K. Piotrowska, S. Lagana, M.S. Jellesen, R. Ambat, Impact of Process-Related Flux Contamination on the Electronics Reliability Issues Under Detrimental Climatic Conditions, in: 2019 Pan Pacific Microelectron. Symp. (Pan Pacific), IEEE, 2019: pp. 1–8. <https://doi.org/10.23919/PanPacific.2019.8696890>.
- [97] M. Bixenman, M. McMeen, Electrochemical Reliability as a Function of Component Standoff, in: 2020 Pan Pacific Microelectron. Symp. (Pan Pacific), IEEE, 2020: pp. 1–9. <https://doi.org/10.23919/PanPacific48324.2020.9059382>.
- [98] B.A. Smith, L.J. Turbini, Characterizing the weak organic acids used in low solids fluxes, *J. Electron. Mater.* 28 (1999) 1299–1306. <https://doi.org/10.1007/s11664-999-0171-2>.
- [99] V. Verdingovas, M.S. Jellesen, R. Rizzo, H. Conseil, R. Ambat, Impact of hygroscopicity and composition of solder flux residue on the reliability of PCBA under corrosive conditions, in: 2013. <https://findit.dtu.dk/en/catalog/537f109374bed2fd2100e8ee> (accessed May 24, 2022).
- [100] G. Reiss, B. Kosednar-Legenstein, J. Riedler, W. Eßl, Impact of electric field at rough copper lines on failure time due to electrochemical migration in PCBs, *Microelectron. Reliab.* 117 (2021) 114035. <https://doi.org/10.1016/j.microrel.2021.114035>.
- [101] K.L. Rogers, M.G. Pecht, A variant of conductive filament formation failures in PWBs with 3 and 4 mil spacings, *Circuit World.* 32 (2006) 11–18. <https://doi.org/10.1108/03056120610663362>.
- [102] K. Piotrowska, M.S. Jellesen, R. Ambat, Thermal decomposition of solder flux activators under simulated wave soldering conditions, *Solder. Surf. Mt. Technol.* 29 (2017) 133–143. <https://doi.org/10.1108/SSMT-01-2017-0003>.
- [103] K. Piotrowska, R.U. Din, M.S. Jellesen, R. Ambat, Effect of Solder Mask Surface Chemistry and Morphology on the Water Layer Formation Under Humid Conditions, *IEEE Trans. Compon., Packag. Manuf. Technol.* 8 (2018) 1756–1768. <https://doi.org/10.1109/TCPMT.2018.2792047>.

Appendix

Table 7.7 Arrangement of the hidden layers (hL), and number of neurons/nodes (nN), which illustrated with numbers (N) from 1 to 84 in Figures 5(e) and 6(e) for better visualization.

hL	nN	N	hL	nN	N	hL	nN	N	hL	nN	N	hL	nN	N	hL	nN	N
1	[5]	1	2	[5;5]	5	3	[5;5;5]	21	3	[10;5;5]	37	3	[15;5;5]	53	3	[20;5;5]	69
1	[10]	2	2	[5;10]	6	3	[5;5;10]	22	3	[10;5;10]	38	3	[15;5;10]	54	3	[20;5;10]	70
1	[15]	3	2	[5;15]	7	3	[5;5;15]	23	3	[10;5;15]	39	3	[15;5;15]	55	3	[20;5;15]	71
1	[20]	4	2	[5;20]	8	3	[5;5;20]	24	3	[10;5;20]	40	3	[15;5;20]	56	3	[20;5;20]	72
			2	[10;5]	9	3	[5;10;5]	25	3	[10;10;5]	41	3	[15;10;5]	57	3	[20;10;5]	73
			2	[10;10]	10	3	[5;10;10]	26	3	[10;10;10]	42	3	[15;10;10]	58	3	[20;10;10]	74
			2	[10;15]	11	3	[5;10;15]	27	3	[10;10;15]	43	3	[15;10;15]	59	3	[20;10;15]	75
			2	[10;20]	12	3	[5;10;20]	28	3	[10;10;20]	44	3	[15;10;20]	60	3	[20;10;20]	76
			2	[15;5]	13	3	[5;15;5]	29	3	[10;15;5]	45	3	[15;15;5]	61	3	[20;15;5]	77
			2	[15;10]	14	3	[5;15;10]	30	3	[10;15;10]	46	3	[15;15;10]	62	3	[20;15;10]	78
			2	[15;15]	15	3	[5;15;15]	31	3	[10;15;15]	47	3	[15;15;15]	63	3	[20;15;15]	79
			2	[15;20]	16	3	[5;15;20]	32	3	[10;15;20]	48	3	[15;15;20]	64	3	[20;15;20]	80
			2	[20;5]	17	3	[5;20;5]	33	3	[10;20;5]	49	3	[15;20;5]	65	3	[20;20;5]	81
			2	[20;10]	18	3	[5;20;10]	34	3	[10;20;10]	50	3	[15;20;10]	66	3	[20;20;10]	82
			2	[20;15]	19	3	[5;20;15]	35	3	[10;20;15]	51	3	[15;20;15]	67	3	[20;20;15]	83
			2	[20;20]	20	3	[5;20;20]	36	3	[10;20;20]	52	3	[15;20;20]	68	3	[20;20;20]	84

Table 7.8 Various levels of six critical factors to make new conditions for test dataset.

Level	Contamination Type	Pitch Distance (μm)	Voltage (V)	Temperature ($^{\circ}\text{C}$)	Humidity (%RH)	Contamination Level ($\mu\text{g}/\text{cm}^2$)
1	Adipic acid	300	2	25	78	35
2	Glutaric acid	600	3	35	88	50
3	Succinic acid	1000	5	40	90	75
4		2000	6	45	98	100
5			7	50		
6			10	55		

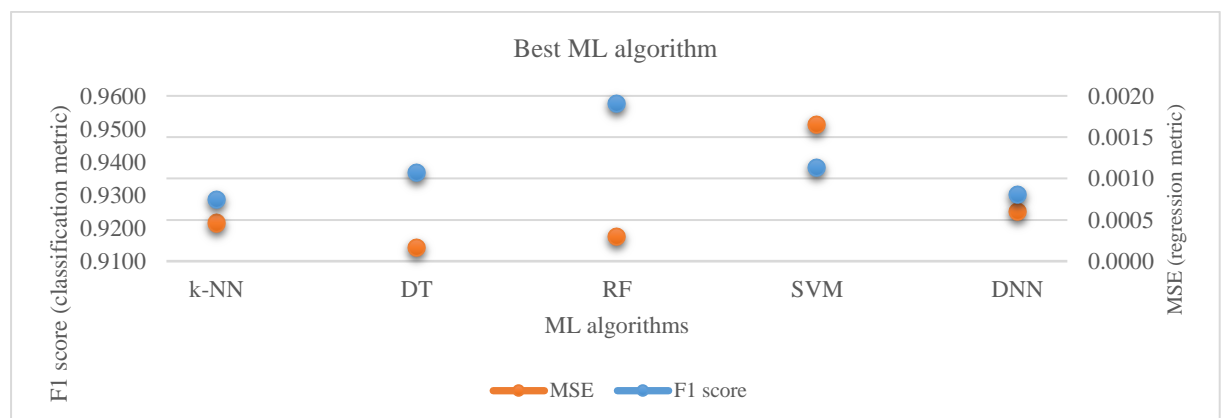


Figure 7.12 Overview of the best ML algorithm of the training dataset according to the F1 score and MSE metrics.





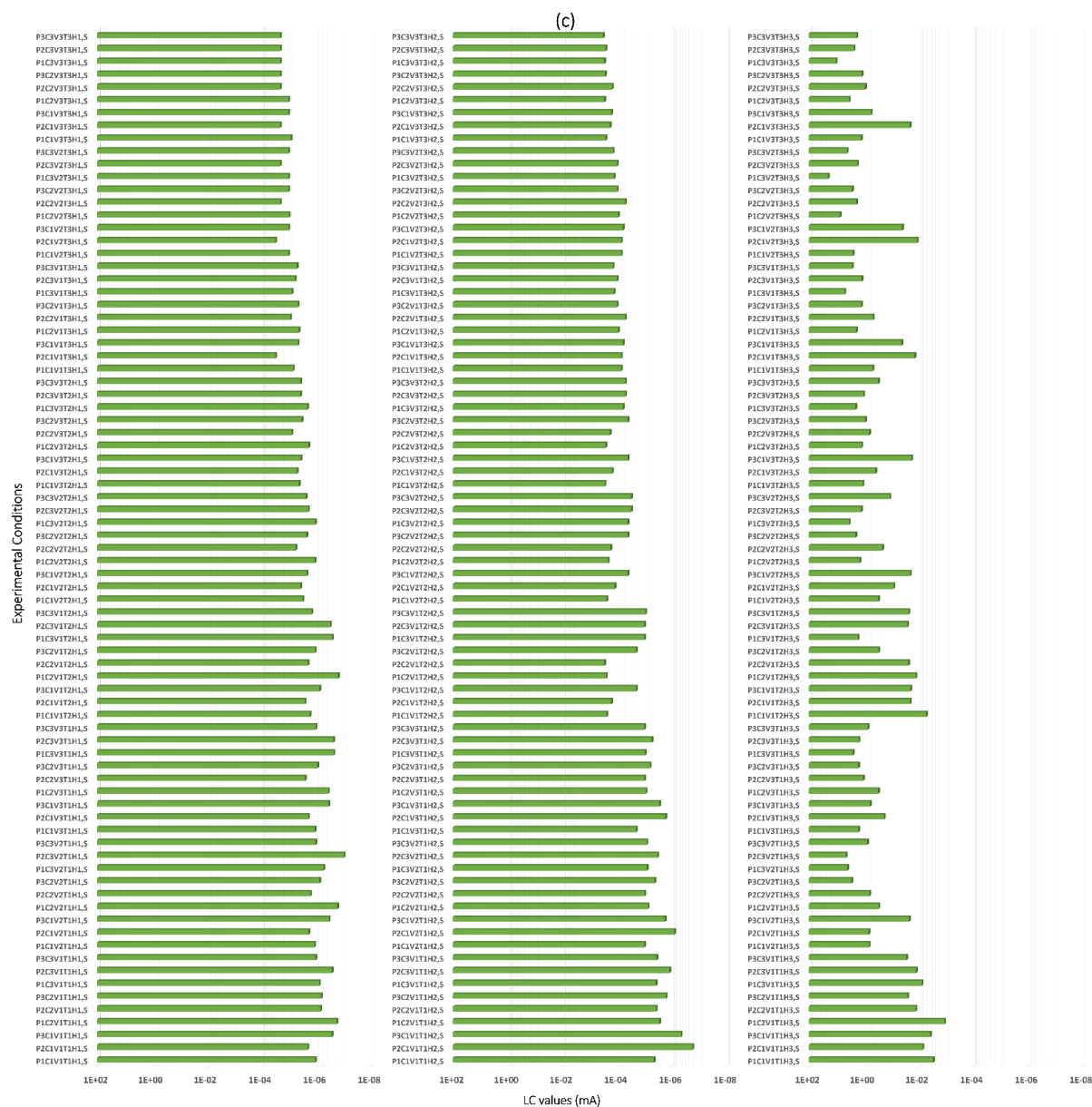


Figure 7.13 All experimental conditions combined P, C, V, T, and H factors, each at three levels (1, 2, and 3 based on Table 1) versus the average of LC values for (a) adipic acid (A), (b) glutaric acid (G), (C) succinic acid (S).

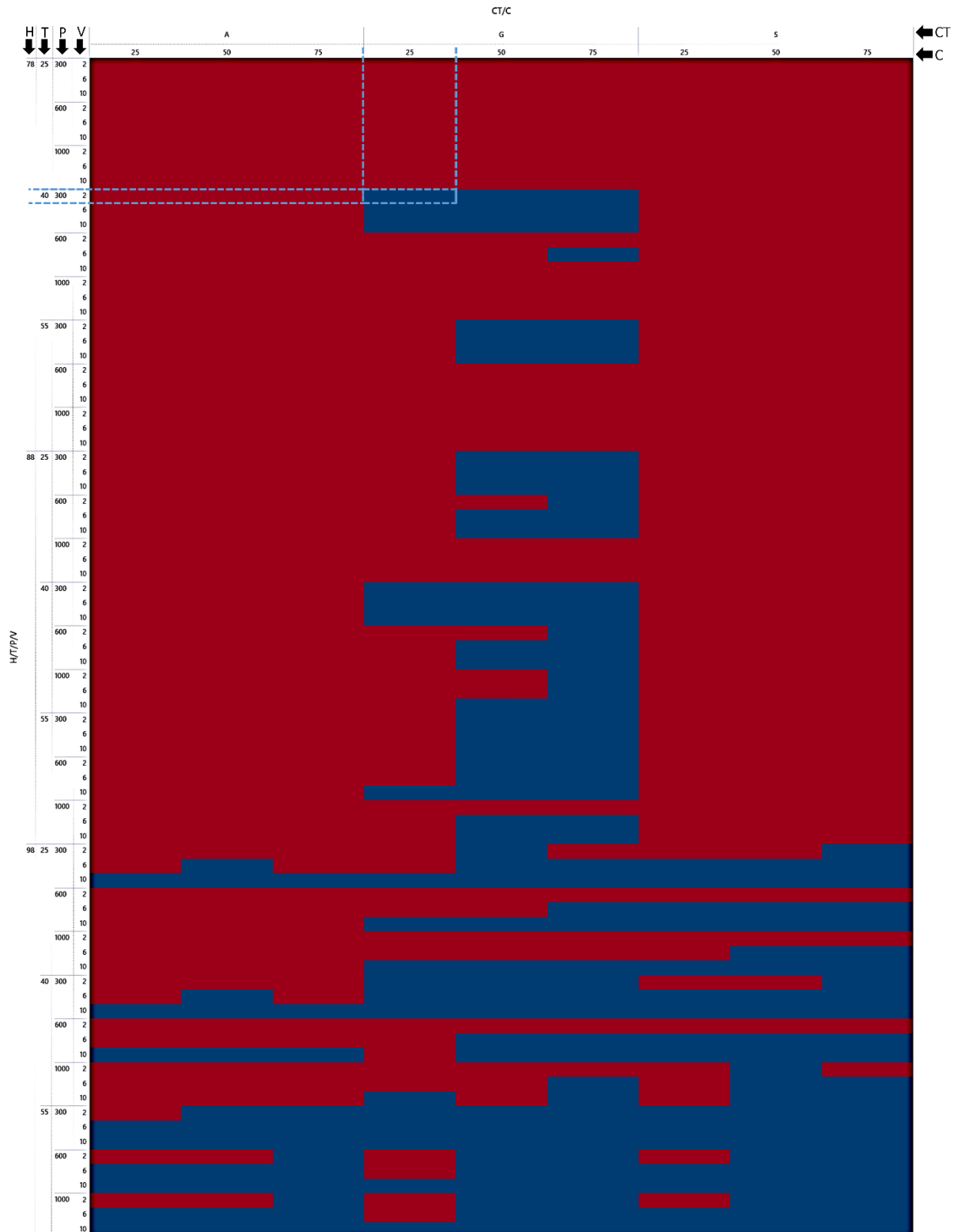


Figure 7.14 All PCB failure classification data results under various conditions combined with P, C, V, T, H, and CT factors, each at three levels. The red and blue colors present the Not-failure and Failure conditions, respectively. Each cell (box or rectangle) presents a condition merged of six factors at different levels. For instance, the cell marked with a light blue dotted line displayed a failure condition constructed of P1C1V1T2H1, G, i.e., low level of pitch distance (P1=300 μ m), low level of contamination level (C1=25 μ g/cm²), low level of voltage (V1=2V), medium level of temperature (T2=40°C), low level of humidity (H1=78%), and glutaric acid (G) as a contamination type.

8 Overall discussion

This chapter covers a brief discussion combining the investigations presented in the appended papers. Overall content in this thesis shows that predictive analytics involving proper data analytics process, from data gathering to make suitable decisions for improving actions based on appropriate and applicable prediction models can be developed for humidity related failures on electronics. Method provides better visualization of multiple parameters effect, which important to understand as the failure cause of combination of effects rather than single parameter. Presently the models developed in this thesis is based on testing using simple interdigitated PCBs without component, however similar methodology can be applied for more complex PCBs with components, which will be more useful. Finally, combining field failure data into analysis provide the possibility of correlating multi-parameter lab test data models to field failure models.

In this Ph.D. project, the SIR PCB surfaces were exposed to various conditions combined with different important and controllable factors, including; pitch distance (P), contamination level (C), temperature (T), voltage (V), humidity (H), and contamination type (CT), with different levels. This is performed inside the climatic chamber, and DC SIR testing measured current values as a main indicator by the potentiostat to investigate the failures on PCB surfaces such as SIR reduction and LC, as well as TTF due to ECM and dendrite formation, then predict them using predictive analytics approaches. Moreover, the role and sensitivity of each factor and their interactions with PCB failures have been studied using statistical investigations by applying DoE and OFAT design methodologies.

The combination of critical factors at different levels as well as evaluation of their interactions simultaneously on the SIR PCB surface, is shown a new understanding for carrying out proper design of experiment, simulation, and prediction model close to realistic conditions, to create a comprehensive understanding of the effects of different factors/levels on PCB failure once exposed to different conditions. The H factor significantly influences both classification analyses for failure status prediction due to ECM and short circuits, as well as regression analysis to predict the numerical value for LCs. H is an important factor in climatic conditions causing water layer formation on the PCBA surface. It is connected with CT effects as the hygroscopic nature of the activators in the flux ionic residue. The experimental results are indicated the proportionally

Overall discussion

combined impact of H and CT as a consequence of flux residues on PCBA surfaces. CT has a considerable impact on ECM failure indicating that more aggressive contamination caused more and quicker ECM failures on PCB surfaces because of increasing of the aggressiveness and acidity of solution owing to the high solubility.

The effect of the critical factors concerning the H and CT effects (under continuous humidity and using one WOAs as a contamination type) is clearly observable in the different experimental results and prediction models. For instance, P and T are illustrated as vital factors in CART analysis. As, they have presented the P and T as the preliminary splitters in the topmost of the trees, explaining in what way the important nodes could be subdivided. Furthermore, the ANOVA table has displayed the contribution percentage of P and T on the multivariate regression model in the high impact of these factors on PCB failure comparing to the C and V according to the experimental dataset. The P has shown a significant effect under humidity conditions on PCB failures (LC and TTF due to ECM). The significance of P is because of high component density and electronic miniaturization, which causes an increasing the electric field, therefore it is easier for dendrite formation during ECM and short circuits. The small pitch distance on the SIR PCB surface could create an electrochemical cell and connection very easier owing to water film formation between two electrical points. T also is an important factor leading to PCB failures. The T under the influence of humidity could effect in various forms, as follow: (i) it could increase the AH level in the environment to interact with PCB surface, (ii) It could decrease the DRH level for contaminations as well as to increase the solubility, (iii) It could also increase the electrochemical kinetics process containing the deposition process for ECM and dendrite formation. In addition, the C effect on PCB failures is not as vital as P and T effects. Nevertheless, the influence of C should be taken into account with other factors, especially T under H conditions. It is due to once the deliquescence happens, a near-saturated solution of contamination to the absorbed water layers that will consistently remain saturated regardless of the level of contamination unless the T is variant. Accordingly, whereas the C on the surface of the PCB is varied, the concentration in the water film will not alter considerably; therefore, it should not affect the failure remarkably at a constant T and H. Moreover, the V effect in correlation to humidity has shown to have a low effect on TTF. It might be because of this point that the extent of the leak current could be go through the narrow thickness of the water film on the PCB surface. Thus,

increasing of V will not considerably influence the SIR reduction and leak current for beginning metal ions dissolution and dendrite formation on PCB surface, unless further parameters for instance C , T , or P change.

For failure prediction purposes, three branches of predictive analytics included; statistical analysis, probabilistically approaches, and machine learning algorithms have been used, which are considered by different methods, i.e., multivariate regression analysis, ANOVA, probability distribution analysis, DT, RF, DNN, SVM, k-NN, and combination of them in all of this project. In addition, the correlation between PCB failures (i.e., LC and TTF due to ECM responses) is presented. It is useful before ECM happens (in several conditions, it takes more time until it happen) to reach and predict TTF. It means, based on the dataset presented, a suitable equation could be found to predict TTF according to LC changes. General current behavior at three parts (stable part, transient part, as well as unstable part) is given a new perception at various conditions, which looks like a sigmoid curve. The simulation of the whole leak current trend as well as its parameters is introduced by the Logistic function as a mathematical nonlinear growth function to predict future changes. This makes it possible to build a model to predict the entire current behavior at different conditions by mixture of logistic function and regression equation. Moreover, additional achievement of current study is classifying risky conditions based on the average of TTF, as well as PoF utilizing Weibull distribution for each condition, which is presented.

9 Overall conclusion

The conclusions are collected and categorized based on a combination of the different sets of experimental works and dataset investigations focusing on the branches of predictive analytics to predict three responses (PCB failures), and the key research objectives in this PhD project. To find all the details of the conclusions achieved from the experimental results, the reader is referred to individual paper appended in chapters (5-7).

Hierarchical failure mechanism on PCB surface, which result in a short circuit with interdependencies between the failures processes

1. Initial leakage current (LC) is the precursor for the electrochemical migration (ECM), although it is not a necessary condition that in each case LC leads to ECM.
2. LC is produced due to the electrochemical process, which also involves metal dissolution. Dissolved metals then migrate from the anode to the cathode and deposit in the form of the dendrite to create a permanent failure (short circuit).
3. LC itself could influence the functionality of the electronics depending on its sensitivity, and ECM leads to irreversible failure.
4. The limits of LC value allowed in an actual application depend on the sensitivity of the PCB, which can be down to 1 μA level, which is considered as the base level of leak current.
5. In corresponds to the general current behavior at three main states (stable, transient and unstable parts), the threshold of approximately 100 μA for the transient state is considered for this study, which is distinguished for the ECM and dendrite formation.
6. Normally, the LC value (stable part) larger than the ECM threshold (transient part) demonstrate the short circuit resulted from a permanent dendrite in the third state (unstable part).

Investigation of critical factors effect and their interactions to LC and TTF values besides failure status responses (based on three parts of the general current behavior)

Overall conclusion

1. For LC, based on the dataset collected from two levels full factorial design under a continuous relative humidity and a contamination type, and using ANOVA and regression analysis, the pitch distance, temperature, and contamination level had significant effect, while the voltage effect is not statistically significant. It could be because of the leak current limitation which is passing through the very thin thickness of created water layer on the PCB surface. However, voltage with other three factors has statistically significant effects on TTF.
2. Based on the dataset collected from three levels, complete crossed design and using the most appropriate selected machine learning algorithm, the humidity, temperature, pitch distance, contamination level, contamination type, and voltage factor presented significant effects on LC, respectively. However, on failure status classification, the two critical factors humidity with around 48%, and contamination type with 24% (the relative importance of these two factors together presented more than 70% effect on failure status response) have the most significant effect.
3. According to the dataset collected from three levels, and applied a one-factor-at-a-time design, and using four prediction models included; multivariate regression model, probabilistic distribution regression model, regression tree model, and classification tree model; the pitch distance, temperature, contamination level, and voltage factor have the highest percentage effects on TTF, respectively.

Predictive analytics, using combinations of statistical analysis, probabilistic approaches, and ML algorithms to predict LC, TTF, failure state, and high risky conditions

1. LC prediction could be utilized to guesstimate possibility of failure or even TTF if the appropriate correlation between LC and failure could be found in various usages.
2. The mathematical simulation of the general current behavior also provided the opportunity to build the prediction model of entire leak current at different conditions.
3. Predicting TTF and failure status is beneficial for pro-active design and improvement strategies for PCBA manufacturing process to increase reliability and

reduce failure risk in exposure to critical conditions. The reasonable prediction also provides situations to have more production with no interruption due to corrosion failure of electronic equipment.

4. From all regression prediction models that applied for TTF prediction, the multivariate regression analysis based on the number of factor/levels and limitation of experimental conditions have presented an efficient model with the highest accuracy and lowest error.
5. Compared to other methods, and based on experimental datasets and outputs (responses), machine learning algorithms provide more profound insights with remarkable accuracy and ease of interpretation, managing the big data with good speed, mapping the nonlinear relationships, performing well with messy data (outliers and missing values), and visualizing multiple and complex interactions (for tree-based machine learning algorithms).
6. From the most common machine learning algorithms for both classification and regression analysis in this study, the random forest algorithm has presented the most well organized in the training dataset, evaluation by appropriate metrics (validating dataset), and high performance in predicting PCB failures as the most suitable classifier and regressor model, correspondingly.

10 Suggestions for further work

The present Ph.D. work investigates the PCB failures using experimental works under various corrosive conditions combined different controllable factors and different levels. By focusing on prediction of the failures using predictive analytics approaches for purposes of more robustness and reliable design and reduce risk of electronics failures at different applications and climatic conditions. Some further investigations are suggested to be applied in continuation of the presented experimental and modelling outcomes where some of them are listed as follows:

- Continuing the experiments by adding more factors/levels e.g., different contamination types, distinct surface finished, diverse coating material at various thickness, different corrosive gas like H₂S, and SO₂ at different concentrations, and etc.
- Design more application oriented testing for example using more complex PCBAs and parameters or testing based on climatic conditions under user conditions.
- Using more predictive models that are not discussed in this project, for example from probabilistic approaches such as probabilistic graphical models (PGM) such as Bayesian networks etc., if proper data would be available.
- Data analysis and arrangement of different failure modes, failure mechanisms, failure causes, and failure effects of PCBAs for making precise and applicable prediction models to reduce their failure risk as much as possible.
- Failure mode and effect analysis (FMEA) of PCBAs focusing on corrosion factors as it is a significant step in the climatic reliability assessment of electronics. In this regard, design FMEA (D-FMEA) could be used, which focuses on product design and design-related deficiencies, with the focus on advancing the design and ensuring product operation. Moreover, the process FMEA (P-FMEA) could be used, which has focused on and emphasize of the manufacturing or assembly process, which can be modified to warrant as if a product is made to design prerequisite in a secure treatment, with at least downtime, scrap, and rework.
- Testing of more complex PCBAs with components etc., and building up more complicated models.